Three-Dimensional Four-Fermion Theories with Exact Chiral Symmetry on the Lattice

Dissertation

zur Erlangung des akademischen Grades
doctor rerum naturalium (Dr. rer. nat.)

vorgelegt dem Rat der
Physikalisch-Astronomischen Fakultät
der Friedrich-Schiller-Universität Jena

von M. Sc. Daniel Schmidt
geboren am 16. Mai 1988 in Hildesheim

Cover picture: Intersections of Binder cumulants for various lattice sizes indicating the critical coupling of the single-flavour Gross-Neveu model. For details see chapter 3 and figure 3.4.

Gutachter:

1. Prof. Dr. Andreas Wipf, Friedrich-Schiller-Universität Jena
2. Prof. Dr. Urs Wenger, Universität Bern, Schweiz
3. Prof. Dr. Simon Hands, Swansea University, Wales, UK

Tag der Disputation: 12.12.2017

Abstract

Four-fermion theories are a class of Quantum Field Theories that describe interactions between fermions via a fourth power of the field in the Lagrangian. Formulated in three spacetime dimensions, their purpose is twofold. On the one hand, they serve as low-energy descriptions of newly discovered materials like graphene. On the other hand, they are interesting as models for spontaneous symmetry breaking. Four-fermion theories allow various different realisations of chiral symmetry and the present work investigates the conditions of their spontaneous breaking.

A broken phase usually appears at strong couplings and requires non-perturbative methods for its analysis. In this work, four-fermion models are formulated on a discrete spacetime lattice, which allows computer simulations. Most previous lattice regularisations did not respect the full chiral symmetry of the corresponding continuum models. Here, we follow a superior approach using the SLAC derivative. Invented in 1976, it is less used because it cannot be applied to gauge theories. On the contrary, it allows an exact implementation of all internal symmetries of four-fermion theories on the lattice and is an ideal choice for these models.

We first study the well-known Gross-Neveu model (GN), where a second-order phase transition, related to the breaking of a $\mathbb{Z}_2$-symmetry, exists for any number of fermion flavours N_f. Here, new values for the critical exponents of this transition for $N_\mathrm{f} = 1, 2, 4$ and 8 are calculated in a finite size scaling analysis. Reasonable agreement with many previous calculations is found. For $N_\mathrm{f} = 1$ we provide the first values from a lattice field theory setup. They agree with other analytical estimates, but a discrepancy to results from Quantum Monte Carlo simulations is present.

The second model studied in this thesis is the Thirring model (Th). Contrary to GN, it has a continuous chiral symmetry. Most previous works only found a spontaneously broken phase for a small number of fermion flavours below a critical value N_f^cr. Various approaches to investigate chiral symmetry breaking for Th on the lattice are presented here. Apart from the conventional auxiliary field formulation, we apply Fierz transformations to Th and study a larger theory space of coupled four-fermion models. In summary, we never observe chiral symmetry breaking in our current simulations, not even for a single fermion flavour. Finally, a new formulation of four-fermion theories is introduced using dual variables acting as occupation numbers for the lattice points. It allows to identify regions of strong couplings where lattice artefacts occur. In future work, it may be used to simulate the irreducible single-flavour four-fermion model that currently suffers a strong sign problem.

Zusammenfassung

Vier-Fermion-Theorien sind eine Klasse von Quantenfeldtheorien, die eine Wechselwirkung zwischen Fermionen durch eine vierte Potenz des Feldes in der Lagrangedichte beschreiben. In drei Raumzeitdimensionen haben sie zwei unterschiedliche Nutzen. Einerseits können sie zur Beschreibung des Nieder-Energie-Verhaltens neu entdeckter Materialien wie Graphen benutzt werden. Andererseits sind sie interessante Modelle für spontane Symmetriebrechung. Vier-Fermion-Theorien erlauben verschiedene unterschiedliche Realisierungen von chiraler Symmetrie und die vorliegende Arbeit untersucht Bedingungen für deren spontane Brechung.

Eine gebrochene Phase tritt üblicherweise bei starken Kopplungen auf, sodass deren Untersuchung nicht-perturbative Methoden erfordert. In dieser Arbeit werden Vier-Fermion-Modelle auf einem diskreten Raumzeit-Gitter formuliert, sodass Computersimulationen möglich sind. Die meisten bisher untersuchten Gitterregularisierungen erfüllten aber nicht die vollständige chirale Symmetrie des zugehörigen Kontinuumsmodells. Hier benutzen wir mit der SLAC-Ableitung einen besseren Ansatz. Diese wurde zwar bereits 1976 erfunden, wird aber nur selten benutzt, da sie nicht für Eichtheorien angewendet werden kann. In Gegensatz dazu ist sie für Vier-Fermion-Theorien auf dem Gitter eine ideale Wahl, da sie eine exakte Umsetzung aller internen Symmetrien erlaubt.

Wir untersuchen hier zunächst das gut erforschte Gross-Neveu-Modell (GN), in dem es für eine beliebige Anzahl an Fermion-Flavours N_f einen Phasenübergang zweiter Ordnung gibt, der zu der Brechung einer $\mathbb{Z}_2$-Symmetrie gehört. Neue Werte für die kritischen Exponenten dieses Übergangs werden hier für $N_\mathrm{f} = 1, 2, 4$ und 8 durch eine Analyse des Skalierungsverhaltens bei endlichen Gittergrößen berechnet. Dabei liegt eine akzeptable Übereinstimmung mit bestehenden Rechnungen vor. Für $N_\mathrm{f} = 1$ präsentieren wir die ersten Werte aus einem Gitterfeldtheorie-Ansatz. Sie stimmen mit anderen analytischen Abschätzungen überein, es gibt allerdings eine Abweichung zu Ergebnissen aus Quanten-Monte-Carlo-Simulationen.

Das Thirring-Modell (Th) ist das zweite Modell, das in dieser Doktorarbeit untersucht wird. Im Gegensatz zu GN hat es eine kontinuierliche chirale Symmetrie. Eine spontan gebrochene Phase wurde in den meisten bestehenden Arbeiten nur für eine kleine Anzahl an Fermion-Flavours gefunden, solange diese kleiner als eine kritische Zahl N_f^cr ist. In der vorliegenden Arbeit werden zahlreiche Ansätze zur Untersuchung der chiralen Symmetriebrechung von Th auf dem Gitter vorgestellt. Neben der herkömmlichen Form mit einem Hilfsfeld wenden wir Fierz-Transformationen auf Th an und untersuchen einen größeren Theorie-Bereich mit gekoppelten Vier-Fermion-Modellen. Zusammenfassend müssen wir festhalten, dass wir nie chirale Symmetriebrechung in unseren Simulationen beobachten konnten, nicht einmal für einen einzelnen Fermion-Flavour. Abschließend führen wir eine

neue Formulierung von Vier-Fermion-Theorien mit dualen Variablen ein, die die Rolle von Besetzungszahlen der Gitterpunkte übernehmen. Diese Formulierung erlaubt eine bessere Identifizierung stark wechselwirkender Kopplungen, bei denen Gitterartefakte auftreten. In anschließenden Arbeiten könnte diese Formulierung verwendet werden, um das irreduzible Vier-Fermion-Modell mit einem Flavour zu simulieren, was gegenwärtig von einem starken Vorzeichenproblem verhindert wird.

Contents

1. Introduction

Symmetry is one of the most important concepts in modern physics. It is closely related to conserved quantities in nature like the total momentum of a system. Momentum conservation exists because the laws of physics do not depend on the absolute position of an experiment and allow to shift it with a symmetry transformation. Hence, models of theoretical physics are constructed to respect the symmetries of nature which we observe in experiments. The standard model of particle physics is currently the best theory to describe the fundamental forces of nature with the exception of gravitation. While its basic ingredients are *local* gauge symmetries, where the symmetry transformation can be varied across the spacetime, *global* symmetries also play an important role, transforming fields at all points of the spacetime in the same way. Chiral symmetry is such a global symmetry. It is important for the theory of Quantum Chromodynamics (QCD), which describes the strong interaction between quarks and gluons in the standard model. Chiral symmetry is necessary to understand physical effects like the small masses of pion particles [GL10]. QCD is studied very successfully with computer simulations using a discretised spacetime lattice and Monte Carlo algorithms [Par16]. This provides a motivation to investigate the correct implementation of chiral symmetry in lattice field theories.

Spontaneous breakdown of a symmetry is a concept tightly connected to symmetry itself. If a symmetry is spontaneously broken, the theoretical model still respects the symmetry, but the physical ground state violates at least a part of it. The most prominent example in particle physics is the Higgs-effect, where a spontaneously broken symmetry induces masses for W and Z bosons. Besides that, spontaneous symmetry breaking is also well-known in condensed matter physics where systems like magnets can show it. The easiest example, the Ising model, consists of regularly arranged spins s_i which can point either up or down and interact with their direct neighbours. The theoretical description does not change when we flip all spins $s_i \to -s_i$, which is an action of the mathematical group $\mathbb{Z}_2$. No alignment of the spins is present for high temperatures because thermal fluctuations lead to a random orientation. Measurements of the total magnetisation (the sum over all spins) would lead to an average close to zero, which does not change under a $\mathbb{Z}_2$ transformation. For low temperatures, all spins tend to align in the same direction. This breaks the symmetry of the system, and the dominating direction is chosen spontaneously while the system is cooled down. The alignment of spins leads to a non-zero magnetisation, which flips its sign with a $\mathbb{Z}_2$ transformation. Hence, the state of the system at low temperatures is no longer invariant and the symmetry is spontaneously broken. This is an example of a phase transition: depending on an external parameter like the temperature, the system shows a different behaviour. It can be either in a phase that respects the symmetry of the mathematical description or in a spontaneously broken

phase. The magnetisation indicates in which phase the system is. It is an example for an *order parameter* which is zero in the symmetric phase while it takes non-zero values if spontaneous symmetry breaking is present. The point where the system changes from one phase to the other is called a *critical point*. Astonishingly, many physical systems show similar macroscopic behaviour at their critical points, although they are microscopically completely different [Her07]. This important concept is known as *universality*. Only a few parameters like symmetries and the spacetime dimension determine the universality class of a model, allowing to share results on critical behaviour between physically very different applications. The renormalisation group provides an explanation for the universal behaviour. Starting from a microscopic model, small-scale fluctuations are integrated over, leading to an effective theory valid up to some momentum scale. This may change parameters like the coupling strength and can also introduce new interactions in the effective theory. Repeating this procedure, one may find fixed points where the effective theory is no longer changing. These fixed points of the renormalisation group equations are directly related to critical points. Models with very different microscopic descriptions can be attracted by the same fixed point, explaining the phenomenon of universality. All these concepts also exist with respect to chiral symmetry and critical points related to its spontaneous breaking are the main subject of study in the present work.

Theories of interacting fermions constitute a useful class of toy models that exhibit chiral symmetry. In particular, this work examines theories with an interaction of a fermion field raised to the fourth power. Here, a strong interaction of the fermions can lead to chiral symmetry breaking (χSB), which dynamically generates a mass for the fermions. Hence, these models can show a phase transition from a phase of massless fermions to a massive phase. This was the reason for Nambu & Jona-Lasinio [NJ61a; NJ61b] in 1961 to propose a four-fermion theory, the Nambu–Jona-Lasinio model (NJL) in four spacetime dimensions, to explain masses of nucleons before the advent of QCD. There is still active research on variations of this model [VR06].

The history of such four-fermion models reaches back to 1958, when Thirring [Thi58] proposed the Thirring model (Th) in two spacetime dimensions. This was the first Quantum Field Theory (QFT) of interacting fermions that could be solved analytically. The third important model is the Gross-Neveu model (GN), which was investigated in two dimensions by Gross & Neveu [GN74] for yet another purpose. It served as a toy model for asymptotic freedom, another property of QCD, where the interaction strength between quarks decreases with increasing energy. David Gross was awarded the Nobel prize of 2004 for his part in this discovery.

The main focus of the present work lies on GN and Th. Despite their original formulations, they are studied here in three spacetime dimensions. Then, GN can be used as a toy model for asymptotic safety [BGS11], a scenario that is currently discussed as a candidate for a quantum theory of gravity. Reviews on this topic are for example [NR06; Per09; RS12]. Additionally, there are applications outside the particle physics community for

three-dimensional incarnations of four-fermion models. Over the last years, new materials have been discovered where the low-energy spectrum of electronic excitations can be described by relativistic Dirac fermions as in particle physics [WBB14]. Therefore, they are called Dirac materials and encompass a wide range of substances like graphene [Cas09], high-temperature superconductors [BVZ06] and topological insulators [HK10; QZ11]. Especially the experimental realisation of graphene [Nov04], awarded with the Nobel prize of 2010, triggered many theoretical investigations to describe its electronic properties and is a main motivation to study three-dimensional fermionic QFTs. In this context, it was conjectured that the transition between semi-metallic and anti-ferromagnetic phases of graphene can be described by the chiral phase transition of GN [Her06]. But also Th can provide useful information [HS08; AHS10; HAS15]. This model is very similar to three-dimensional Quantum Electrodynamics (QED_3) [MZ03], describing the electronic properties of graphene [Sem84] or high temperature superconductors [AM96; FTV02]. In all these examples from condensed matter physics, the properties of a material can be related to the existence of spontaneous symmetry breaking. For example, it was argued that mechanical stress applied to a graphene sheet could tune it from a semi-metallic phase through a phase transition into an isolating phase [HJV09].

Theoretical considerations provide another reason to study four-fermion theories in three dimensions: here, fermions have mass dimension 1, so that the coupling of a four-fermion term has dimension -1, and the theory is perturbatively non-renormalisable. On the other hand, an expansion for a large number of fermion flavours is possible and allows a renormalisation [RWP89; Cal91]. This requirement of non-perturbative treatment makes four-fermion theories a good testing ground for calculations with methods that go beyond perturbation theory, for example by using Dyson-Schwinger-Equations (DSEs), the Functional Renormalisation Group (FRG), or lattice field theory. These approaches are often used to study the χSB of these models depending on the coupling strength and the flavour number N_f. But four-fermion models are also attractive to relatively new approaches like the conformal bootstrap [FGG73; Pol74; Mac77]. Very precise results for the critical exponents of the Ising model were obtained with this method [Kos16], but calculations for four-fermion theories started just recently. The first results for three-dimensional GN were published in 2017 by Iliesiu et al. [Ili17]. To check the accuracy of all these methods, precise calculations of critical properties on the lattice, as presented in the present work, are needed for comparison.

Moreover, cross-checks inside the lattice community are also necessary. In particular, lattice fermions with chiral symmetry are problematic. Simulations with a naive discretisation of the fermion action have the problem of *fermion doubling* [BB87], where the lattice model describes more fermion flavours than the original continuum theory. There is even the Nielsen-Ninomiya theorem, stating that no fermion discretisation exists that is local, free of doublers, preserves chiral symmetry, and has the correct continuum limit [NN81a; NN81b; NN81c]. Regarding four-fermion theories, chiral symmetry is an essen-

tial feature that should be respected by the lattice formulation. Thus, these models can serve as a testbed for simulations with chiral fermions in general. So far, most of the older simulations of GN[(a)] and Th[(b)] used so-called *staggered fermions* [KS75] that do not respect the full chiral symmetry of the continuum models. Additionally, they still have doublers, which only allows to simulate an even number of continuum flavours. Even more, the *sign problem* must be taken into account, one of the most urgent problems in lattice simulations with fermions [TW05]. Currently, a lot of effort is put into possible solutions to the sign problem because it prevents simulations of QCD at finite density [GL16]. Thus, previous lattice results for four-fermion theories must be confronted with more advanced simulations. Only recently, an investigation of four-fermion theories with correct lattice implementation of chiral symmetry and absence of the sign problem for any N_f was done [Han16b; Han17]. In the present work, we use a complementary approach and use the SLAC derivative [DWY76a; DWY76b], which is not local. It was already invented in 1976 but is seldom used in lattice field theory because it is not applicable for gauge theories like QCD and QED_3 [KS79]. On the other hand, chiral symmetry is implemented exactly at any finite lattice spacing, and we know that the SLAC derivative works well for Yukawa-type models[(c)]. Since four-fermion models possess no gauge symmetries and can be reformulated with Yukawa-type interactions, the SLAC derivative proved to be very beneficial in the present context.

Comparing the different non-perturbative methods, the situation for GN is quite clear. It shows χSB for any value of N_f with a phase transition of second order that can be classified by *critical exponents*. They are universal quantities that can be compared well between distinct approaches. The mostly analytical methods like DSE and FRG approaches are currently in good agreement, at least for $N_\mathrm{f} \geq 2$, but only few lattice simulations are available. The case $N_\mathrm{f} = 2$ is especially important because it corresponds to the physical situation in graphene. Here, a previous lattice simulation [Kär94] ignored the sign problem they had to expect, while the sign-problem-free approach with a *fermion bag* algorithm showed larger deviations from the analytical calculations [CL13]. For $N_\mathrm{f} = 1$, simulations with staggered fermions are not possible and Quantum Monte Carlo (QMC) algorithms were used so far [WCT14; LJY15; HW16]. No good agreement with the analytical calculations was found in this case. Thus, simulation results from a well-established algorithm without sign problem and with exactly chiral fermions are needed. In chapter 3, we provide these new calculations for the critical exponents of GN with $N_\mathrm{f} = 1, 2, 4$ and 8. They can serve as reference for future analytical and numerical calculations, but also show that simulations with SLAC fermions provide reliable results for four-fermion theories.

This reassurance is important because the situation is less clear for Th. It is expected here that χSB happens only for a small number of fermion flavours because no broken phase is

[(a)] See [HKK93; FJP96; Kär94; CS07; CL13].

[(b)] See [DH96; KK96; DHM97; DH99; HL99; CHS07; CL12a].

[(c)] Previous works using the SLAC derivative: [KLW05; Käs08; Ber08; Ber09; BBP09; Ber10; FSW12; WW12; Flo12].

present in the large-N_f expansion[(d)]. Only Hong & Park [HP94] found χSB for any N_f. The other works also present quite different results for the critical flavour number N_f^{cr}, below which χSB can happen. Earlier staggered lattice simulations[(e)] were roughly consistent with these findings. Together with an FRG study [GJ10; JG12], all predictions for a finite critical flavour number of Th were in the range $2 \leq N_f^{cr} < 7$. Considering more details of the phase transition, less agreement between the numerous works is left. For example, Kondo [Kon95] found a second-order phase transition, while also an infinite-order transition was proposed [Ito95; Sug97]. More recent lattice simulations with the correct symmetry do not show a phase transition at all [Han16b; Han17]. Thus, an alternative investigation with exactly chiral fermions on the lattice is useful to shed new light on the problem of χSB in Th. In order to solidify our findings, several different approaches to this problem are investigated in this work.

All these topics are presented with the following structure: In chapter 2, we collect general information about four-fermion theories and the simulation setup used in this work. We begin with definitions of the different models, putting emphasis on the distinction of reducible and irreducible models. Then, we apply a Hubbard-Stratonovich transformation (HS) to them, which is necessary to make the Lagrangians bilinear in the fermion fields. This is required by the rational Hybrid Monte Carlo (rHMC) algorithm we use. We also introduce Fierz identities and use them to replace the interaction term of Th by a GN interaction combined with a flavour-mixing term. Further details about the symmetries of the lattice models as well as chiral symmetry on the lattice and the SLAC derivative are given. The general simulation setup is summarised and we investigate our models with respect to a potential sign problem. In particular, the reducible versions of GN and Th are free of a sign problem for all N_f, whereas this is not the case for the irreducible models.

As a first example of χSB in four-fermion theories, we study GN in chapter 3. We present key points from the theory of finite size scaling which we employ to measure critical exponents. Different approaches are compared and evaluated with respect to systematic errors. New values for the critical exponents of GN with $N_f = 1, 2, 4$ and 8 in the reducible representation are given and constitute one of the main results of this work. This is the first lattice calculation of critical exponents of GN with exactly chiral fermions in a conventional lattice field theory approach. A detailed comparison with previous works and a section on the irreducible version of GN complete this chapter.

Having shown the successful application of the SLAC derivative in GN, the remaining chapters are devoted to the study of Th and its χSB. In chapter 4, we begin with direct simulations of the model after HS, where the Lagrangian of Th contains an auxiliary vector field. In this formulation, no order parameter is accessible and we cannot gain information about χSB in simulations with exact chiral symmetry. Also in simulations with a mass term, which explicitly breaks the symmetry, no evidence for χSB could be found.

[(d)] See [Gom91; HLY94; Ahn94; Ito95; Kon95; Sug97; AP98].
[(e)] See [KK96; DHM97; DH99; HL99; CHS07].

In chapter 5, we combine Th with two other models. Since χSB can be studied well in GN, a combination with Th is useful and we investigate the larger space of both interactions. A second attempt is made with a simplified version of NJL that preserves more of the original symmetry of Th. With both approaches, similar results were obtained. For $N_\mathrm{f} = 1$ no clear statement on the existence of χSB can be drawn, but it is very likely ruled out for $N_\mathrm{f} \geq 2$.

Finally, we present two reformulations of Th in chapter 6, where equivalent models with different degrees of freedom are investigated to overcome the problems encountered in the previous chapters. The first section presents simulations with Lagrangians that are equivalent to Th by the Fierz transformations introduced in chapter 2. In this setup, direct access to an order parameter for χSB is possible, but the models show very strong sign problems. Thus, the main result of this part is that Fierz identities can relate models with strong sign problem to equivalent formulations that are free of it. Finally, we give a description of four-fermion theories with dual variables. They carry the meaning of an occupation number and we present evidence that a transition to an unphysical phase occurs on the lattice when it is fully occupied by fermions. The attempt to overcome the sign problem of the models after Fierz transformation with the dual variables formulation was not yet successful. Only for a special case, we will point out a way to simulations without sign problem. Nevertheless, the combination of both approaches in this chapter with conventional simulations as in chapter 4 provided the foundations for our treatment of Th in [WSW17]. An overall conclusion is given in chapter 7.

The compilation of this thesis is solely due to the author. However, a large part of the work presented here was done in collaboration with Andreas Wipf and Björn Wellegehausen. Parts of the content of chapter 4, chapter 5 and section 6.1 were published in conference proceedings [SWW15; SWW16]. The work of chapter 6 built the basis for our publication [WSW17]. Except for section 6.2, all simulations were performed with a program mainly written by Björn Wellegehausen with contributions of Galstian Pour [Gal14] during his diploma thesis prior to the present work. The necessary computing power was mainly provided by the Theoretisch-Physikalisches Institut with nodes of the `Omega` *cluster at the University of Jena. Also local compute servers in the institute and the* `quadler` *cluster of the group of Prof. Brügmann were utilised. All $N_\mathrm{f} = 8$ simulations of GN were executed by Björn Wellegehausen on the LOEWE cluster at the University of Frankfurt. Hence, this work was indirectly supported by the Helmholtz International Center for FAIR within the LOEWE initiative of the State of Hesse.*

2. General Properties and Simulation Setup

In this work we consider QFTs in a three-dimensional, Euclidean spacetime, where the interaction is given by a fourth power of the fermion field ψ. Putting special emphasis on symmetries, we will introduce our notation and define our main four-fermion models in section 2.1 via their Lagrangians $\mathscr{L}[\bar{\psi},\psi]$. In the continuum, the latter are related to Euclidean actions $S[\bar{\psi},\psi]$ via integration over the spacetime. From an action, we can derive the partition sum as a path integral over the fields by

$$Z = \int \mathscr{D}\bar{\psi}\,\mathscr{D}\psi\, \mathrm{e}^{-S[\bar{\psi},\psi]}. \tag{2.1}$$

It can be used to calculate thermodynamic quantities and vacuum expectation values of observables $\mathscr{O}$ with

$$\langle \mathscr{O} \rangle = \frac{1}{Z} \int \mathscr{D}\bar{\psi}\,\mathscr{D}\psi\, \mathrm{e}^{-S[\bar{\psi},\psi]}\, \mathscr{O}[\bar{\psi},\psi]. \tag{2.2}$$

A well-established method to calculate the path integrals in these expressions are Monte Carlo simulations, where the spacetime is approximated by a lattice Λ of discrete, equally spaced points. Introductory textbooks on this area of research are for example [GL10; MM97; Rot05; Smi02]. We usually work with dimensionless quantities in the action obtained by an appropriate rescaling so that the spacing between adjacent points is $a = 1$. Consequently, the lattice volume V equals the total number of lattice sites. On the lattice, the measure of the path integral is a well-defined, finite product $\int \mathscr{D}\psi = \int \prod_{x\in\Lambda} \left(\mathrm{d}\psi(x)\right)$ and the Euclidean action is given by a summation over all lattice points:

$$S[\bar{\psi},\psi] = \sum_{x\in\Lambda} \mathscr{L}[\bar{\psi}(x),\psi(x)]. \tag{2.3}$$

In order to implement the action of a lattice model in a computer program, most algorithms require it to contain only second powers of the fermion fields, which allows an analytical integration over the fermions. A convenient transformation to turn four-fermion models into a bilinear form is presented in section 2.2 together with identities that will be used to transform different kinds of four-fermion interactions into each other. Afterwards, we give general information about algorithms and our simulation setup in section 2.3. This section also contains a discussion of chiral symmetry on the lattice and our approach to it. Finally, we consider the sign problem. Conventional simulation algorithms require the action to be real because $\mathrm{e}^{-S} \geq 0$ is used in a probability distribution to generate new configurations for the fields. If this assumption is not valid, the theory is said to suffer a sign problem. Details on this and an investigation of the relevant actions are given in section 2.4.

2.1. Four-Fermion Theories and Their Symmetries

In this section, we will define the four-fermion models treated in this work and classify them by their symmetries. As usual, the kinetic term of fermionic QFTs includes Dirac matrices γ_μ, where $\mu = 1,2,3$ labels the $d = 3$ Euclidean spacetime dimensions. The γ_μ satisfy the Euclidean Clifford algebra $\{\gamma_\mu, \gamma_\nu\} = 2\delta_{\mu\nu}\mathbb{1}$ and all three can be chosen Hermitian. Usually, QFTs use irreducible representations of this algebra, which are two-dimensional in three spacetime dimensions [WS86][(a)]. On the contrary, four-fermion theories are often discussed using a reducible representation with four-component spinors. These spinor indices are labelled with $i, j = 1, \ldots, d_\gamma$, where $d_\gamma = 2$ or 4 for irreducible and reducible representations respectively. We will begin the discussion of symmetries and the definition of our models in the reducible formulation in section 2.1.1. Only this formulation allows the definition of chiral symmetry, which is the main subject of our study. Afterwards, we decompose these models in section 2.1.2 into an irreducible formulation again putting special emphasis on symmetries.

2.1.1. Reducible Models

We begin with definitions of reducible four-fermion models that employ a four-dimensional representation of the Clifford algebra, denoted by γ_μ. Any of the usual representations of four-dimensional QFTs can be used. The reducible models are commonly studied in the literature, motivated by the applications in condensed matter systems mentioned in chapter 1. The corresponding four-component spinors are denoted by $\psi_a(x)$ with flavour index a running over N_f values. Only for a representation of dimension four, a non-trivial matrix $\gamma_5 := \gamma_1\gamma_2\gamma_3\gamma_4$ exists[(b)] that is necessary to define chiral symmetry because it can be used to construct projection operators on left- and right-handed spinors [GL10]. This handedness is called *chirality* and a *chiral tranformation*

$$\psi \to \mathrm{e}^{\mathrm{i}\theta\gamma_5}\psi, \qquad \bar{\psi} \to \bar{\psi}\,\mathrm{e}^{\mathrm{i}\theta\gamma_5}, \tag{2.4}$$

with a real parameter θ is closely linked to the projections. It defines a *chiral symmetry* of the action, which is invariant under (2.4), as long as the theory contains no terms like a bare mass that mix left- and right-handed spinors. Thus, the limit $m \to 0$ is commonly referred to as the *chiral limit*.

The general setup is the same with a reducible representation in three spacetime dimensions, but more transformations like (2.4) can be defined. Here, only the first three matrices are needed for the kinetic term, leaving both γ_4 and γ_5 free to define chiral symmetries. Additionally, also $\gamma_{45} := \mathrm{i}\gamma_4\gamma_5$ can be used to generate a chiral symmetry. This matrix is Hermitian because we take all other matrices to be Hermitian. In the following, we will

[(a)] In contrast to four spacetime dimensions, two inequivalent irreducible representations of the Clifford algebra exist.

[(b)] Similar definitions are possible for any representation of even dimension.

determine the largest possible symmetry group and Lagrangians that are invariant under it. Afterwards, models with less symmetry are presented.

Maximal Chiral Symmetry

A single-flavour theory of massless free fermions in three dimensions is invariant under transformations with all matrices given above, together with phase shifts generated by the identity. Since γ_μ commutes with $\mathbb{1}$ and γ_{45}, the single-flavour kinetic term $\bar{\psi}\gamma_\mu\partial^\mu\psi := \bar{\psi}\partial\!\!\!/\psi$ is invariant under the vector transformations

$$\psi \to \psi' = \mathrm{e}^{\mathrm{i}\alpha\mathbb{1}}\psi \qquad \bar{\psi} \to \bar{\psi}' = \bar{\psi}\,\mathrm{e}^{-\mathrm{i}\alpha\mathbb{1}} \tag{2.5a}$$

$$\psi \to \psi' = \mathrm{e}^{\mathrm{i}\beta\gamma_{45}}\psi \qquad \bar{\psi} \to \bar{\psi}' = \bar{\psi}\,\mathrm{e}^{-\mathrm{i}\beta\gamma_{45}}. \tag{2.5b}$$

This definition follows the conventions of Gies & Janssen [GJ10]. Additionally, γ_μ anti-commutes with γ_4 and γ_5. Therefore, the Lagrangian of massless free fermions is invariant under so-called axial transformations for $\bar{\psi}$ without minus sign in the exponent, similar to the four-dimensional case (2.4):

$$\psi \to \psi' = \mathrm{e}^{\mathrm{i}\varphi\gamma_4}\psi \qquad \bar{\psi} \to \bar{\psi}' = \bar{\psi}\,\mathrm{e}^{\mathrm{i}\varphi\gamma_4} \tag{2.5c}$$

$$\psi \to \psi' = \mathrm{e}^{\mathrm{i}\theta\gamma_5}\psi \qquad \bar{\psi} \to \bar{\psi}' = \bar{\psi}\,\mathrm{e}^{\mathrm{i}\theta\gamma_5}. \tag{2.5d}$$

Since the generating matrices $\Gamma \in \{\mathbb{1}, \gamma_4, \gamma_5, \gamma_{45}\}$ are Hermitian, their exponential $\mathrm{e}^{\mathrm{i}\phi\Gamma}$ is unitary. We have four real parameters $\alpha, \beta, \varphi, \theta$, leading to the symmetry group $U(2)$ for massless free fermions with a single flavour. Considering N_f fermion flavours, we can combine each of the transformations (2.5) with an independent flavour rotation by a unitary matrix $\psi \to U\psi$ and $\bar{\psi} \to \bar{\psi}U^\dagger$, with $U \in U(N_\mathrm{f})$ acting on the flavour indices. Together, the full symmetry group of massless free fermions in three dimensions is $U(2N_\mathrm{f})$[(c)]. Including a mass term explicitly breaks the chiral symmetries related to γ_4 and γ_5. The remaining matrices $\mathbb{1}$ and γ_{45} generate two independent $U(1)$ symmetries, leading to the multi-flavour breaking pattern

$$U(2N_\mathrm{f}) \to U(N_\mathrm{f}) \times U(N_\mathrm{f}). \tag{2.6}$$

So far, we only used the (anti-)commutation properties of γ_μ with the symmetry generators Γ. Obviously, also a current $j_\mu = \bar{\psi}_a\gamma_\mu\psi_a$ does not change under the transformations (2.5). Consequently, the reducible Lagrangian with a current-current interaction

$$\mathscr{L}_\mathrm{Th,red} = \bar{\psi}_a\,(\partial\!\!\!/ + m)\,\psi_a + \frac{g_\mathrm{Th}^2}{2N_\mathrm{f}}\left(\bar{\psi}_a\gamma_\mu\psi_a\right)^2 \tag{2.7}$$

also shares the full symmetry and breaking pattern (2.6) for $m = 0$. This defines Th. Its two-dimensional version was introduced by Thirring [Thi58] as the first analytically solvable field theory of interacting fermions. The main parameters of this model are the number

[(c)] With a different convention regarding signs and the i in the exponents, one may arrive at the non-compact group $U(N_\mathrm{f}, N_\mathrm{f})$.

of fermion flavours N_f, the coupling strength g^2_Th and a bare mass m. A summation over repeated flavour indices is always implied unless otherwise stated and the square in the interaction is outside the sum. We will see in section 2.2.2 that (2.7) can be rewritten with a vector field V_μ. This highlights the similarity to QED_3, which has a field A_μ, although this is a dynamical gauge field and not an auxiliary vector field as in Th.

The matrix γ_{45} also shares the (anti-)commutation properties with the generators Γ, making also $\bar{\psi}\gamma_{45}\psi$ invariant under (2.5). Hence the third model besides free fermions and Th with maximal chiral symmetry for $m = 0$ is

$$\mathscr{L}_\mathrm{G45,red} = \bar{\psi}_a \left(\partial\!\!\!/ + m\right) \psi_a - \frac{g^2_\mathrm{G45}}{2N_\mathrm{f}} \left(\bar{\psi}_a \gamma_{45} \psi_a\right)^2 , \tag{2.8}$$

which we will call the γ_{45}-model (G45). In addition, there are combinations of flavour-mixing interactions respecting the full symmetry [GJ10]. They are related to Th and G45-interactions by Fierz identities similar to the ones we will introduce in section 2.2.1.

Reduced Continuous Chiral Symmetry

A second model of historic importance will here be called NJL. Its four-dimensional version for a single flavour was suggested by Nambu & Jona-Lasinio [NJ61a] in order to describe mesons and nucleons as bound states of the bare fermions with dynamically generated mass, analogously to the BCS theory of superconductivity [BCS57a; BCS57b]. It is given by

$$\mathscr{L}_\mathrm{NJL,red} = \bar{\psi}_a \left(\partial\!\!\!/ + m\right) \psi_a - \frac{g^2_\mathrm{NJL}}{2N_\mathrm{f}} \left[\left(\bar{\psi}_a \psi_a\right)^2 - \left(\bar{\psi}_a \gamma_5 \psi_a\right)^2\right] . \tag{2.9}$$

The same idea was published around the same time by Vaks & Larkin [VL61]. Additionally, the Lagrangian (2.9) was also considered by Gross & Neveu [GN74]. It is therefore also called Gross-Neveu model in some publications (e.g. [CS07]).

Later on, in section 5.2, we will study a modification of (2.9) coupled with Th. This combination is interesting because (2.9) with $m = 0$ preserves three of the four symmetries generated by the matrices in Γ. This holds also for the joint model of (2.9) together with (2.7). Only the γ_4-symmetry (2.5c) is not compatible, while the transformation with γ_5 in (2.5d) leads to a $U(1)$-symmetry, similar to the vector transformations (2.5a) and (2.5b). They cannot be linked with each other to form a larger group. Including flavour rotations we get three factors of $U(N_\mathrm{f})$. A mass term breaks the symmetry corresponding to the transformation with γ_5 via

$$U(N_\mathrm{f}) \times U(N_\mathrm{f}) \times U(N_\mathrm{f}) \to U(N_\mathrm{f}) \times U(N_\mathrm{f}). \tag{2.10}$$

Discrete Chiral Symmetry

The simplest example of a four-fermion theory is GN, which has a scalar-scalar interaction. The Lagrangian density in Euclidean spacetime is given by

$$\mathscr{L}_\mathrm{GN,red} = \bar{\psi}_a \left(\partial\!\!\!/ + m\right) \psi_a - \frac{g^2_\mathrm{GN}}{2N_\mathrm{f}} \left(\bar{\psi}_a \psi_a\right)^2 . \tag{2.11}$$

The two-dimensional version of (2.11) was first introduced by Gross & Neveu [GN74] as a toy model to study dynamical symmetry breaking in asymptotically free field theories. In three dimensions, it serves as a model for electronic properties of Dirac materials like graphene as mentioned in chapter 1. Compared to NJL, it shows an even smaller subset of the maximal chiral symmetry. A full discussion of the symmetries of massless GN with Lagrangian (2.11) can be found in the work of Gehring et al. [GGJ15] including a physical explanation concerning graphene. Here, a short derivation of the main result is presented.

We note, that $(\bar{\psi}_a\psi_a)^2$ is still invariant under the vector transformations (2.5a) and (2.5b), but no longer under general axial transformations. Together with the flavour rotations, we can form a group of $U(N_\mathrm{f}) \times U(N_\mathrm{f})$. A closer look at the axial transformation (2.5d) leads to

$$\left(\bar{\psi}_a\psi_a\right)^2 \to \left(\bar{\psi}_a \mathrm{e}^{2\mathrm{i}\theta\gamma_5}\psi_a\right)^2 = \left(\bar{\psi}_a\left[\cos(2\theta)\mathbb{1} + \mathrm{i}\sin(2\theta)\gamma_5\right]\psi\right)^2, \tag{2.12}$$

which is invariant for $\theta = n\pi/2$ with $n \in \mathbb{Z}$. Thus, we have a transformation $\psi \to \left(\mathrm{i}\gamma_5\right)^n\psi$ and $\bar{\psi} \to \bar{\psi}\left(\mathrm{i}\gamma_5\right)^n$. The additional phase i^n and the cases with an even n can also be generated by (2.5a), but we find an independent discrete $\mathbb{Z}_2$-symmetry, which is usually written as

$$\psi \to \gamma_5\psi, \qquad \bar{\psi} \to -\bar{\psi}\gamma_5. \tag{2.13}$$

It can be explicitly broken by a mass term. The transformation (2.5c) with γ_4 does not lead to another independent symmetry of the form (2.13) because this transformation is equivalent to a combination of (2.13) with (2.5b) and fixed $\beta = \pi/2$. Concluding, GN has a symmetry with a possible breaking pattern

$$U(N_\mathrm{f}) \times U(N_\mathrm{f}) \times \mathbb{Z}_2 \to U(N_\mathrm{f}) \times U(N_\mathrm{f}) \tag{2.14}$$

and is the last of the four main models (Th and G45 with maximal chiral symmetry, NJL with a reduced continuous symmetry and GN with a discrete chiral symmetry) that we will need throughout this work. More general forms of four-fermion models are possible and we will encounter some in section 2.2.1, where flavour-mixing interactions appear. Beforehand, we will have a short look at further symmetry transformations of these models.

Parity and Mass Terms

Apart from the chiral symmetry discussed above, a short look at the *parity symmetry* is necessary to discuss our results for Th in section 4.2. A definition of time reversal and charge conjugation symmetries is also possible [Gom91], but not required here. Parity can be defined [GGJ15] by flipping the sign of a single spatial coordinate like $x = (x_1, x_2, x_3) \to x' = (x_1, -x_2, x_3)$, together with

$$\psi(x) \to \mathrm{i}\gamma_2\gamma_5\psi(x'), \qquad \bar{\psi}(x) \to \bar{\psi}(x')\,\mathrm{i}\gamma_2\gamma_5. \tag{2.15}$$

This choice is not unique because a similar definition with γ_4 is also possible [Gom91; GJ10]. The usual mass term $m\bar{\psi}\psi$ included in the Lagrangians above conserves parity. Also

$\mathrm{i}m_4\bar{\psi}\gamma_4\psi$ and $\mathrm{i}m_5\bar{\psi}\gamma_5\psi$ are possible parity-invariant mass terms and physically equivalent [Han16a; Han16b]. In contrast to this, a mass term including γ_{45} breaks the parity of the reducible models.

Spontaneous Symmetry Breaking

Even the symmetries of the massless models can be broken with the pattern (2.6) for Th and G45, (2.10) for NJL or (2.14) for GN because this breaking can happen spontaneously. A strong fermion interaction can form a non-vanishing chiral condensate

$$\langle\bar{\psi}\psi\rangle \neq 0 \tag{2.16}$$

that also breaks the chiral symmetries related to γ_4 and γ_5. It acts like a mass term and the fermions are said to acquire a dynamical mass. The chiral condensate is an order parameter for χSB, since it is non-zero in the broken phase, while it vanishes, when the symmetry is intact. Thus, it is of main importance for the rest of this work to show where χSB happens. Analogously to the parity-breaking mass term, we can define a parity-odd condensate $\langle\bar{\psi}\gamma_{45}\psi\rangle$, which is invariant under the full chiral symmetry of Th and G45, but induces spontaneous breaking of parity.

2.1.2. Irreducible Models

To derive Lagrangians in the irreducible representation from the reducible models in section 2.1.1 we choose a convenient representation of the $d_\gamma = 4$-dimensional Clifford algebra, where γ_μ is block-diagonal:

$$\begin{aligned} \gamma_\mu = \sigma_3 \otimes \sigma_\mu = \begin{pmatrix} \sigma_\mu & 0 \\ 0 & -\sigma_\mu \end{pmatrix}, \quad \gamma_4 = \sigma_1 \otimes \mathbb{1}_2 = \begin{pmatrix} 0 & \mathbb{1}_2 \\ \mathbb{1}_2 & 0 \end{pmatrix} \\ \Rightarrow \quad \gamma_5 = -\sigma_2 \otimes \mathbb{1}_2 = \begin{pmatrix} 0 & \mathrm{i}\mathbb{1}_2 \\ -\mathrm{i}\mathbb{1}_2 & 0 \end{pmatrix}, \quad \gamma_{45} = \sigma_3 \otimes \mathbb{1}_2 = \begin{pmatrix} \mathbb{1}_2 & 0 \\ 0 & -\mathbb{1}_2 \end{pmatrix}. \end{aligned} \tag{2.17}$$

Here, σ_μ and $-\sigma_\mu$ form two inequivalent irreducible representations for $d = 3$. Details can be found for example in the work of Pisarski [Pis91]. As suggested by the symbol σ_μ, a possible choice for an irreducible representation are the Pauli matrices. Keeping in mind that other possibilities exist, we will use σ_μ in general to refer to an irreducible representation of the Clifford algebra.

Splitting the four-component spinors into two two-component spinors $\chi_{a,r}$ numbered by $r = 1,2$ with

$$\psi_a = \begin{pmatrix} \chi_{a,1} \\ \chi_{a,2} \end{pmatrix} \qquad \text{and} \qquad \bar{\psi}_a = \begin{pmatrix} \bar{\chi}_{a,1} \\ -\bar{\chi}_{a,2} \end{pmatrix} \qquad \text{where} \qquad a = 1,\ldots,N_\mathrm{f}, \tag{2.18}$$

we introduced a minus sign in the second component of $\bar{\psi}$ to compensate the sign in

the second block of γ_μ. In this way, we get the usual kinetic term[(d)] $\bar{\chi}\partial\!\!\!/\chi = \bar{\chi}\sigma_\mu\partial^\mu\chi$ for all components, but the sign of a mass term is different for $r = 2$:

$$\begin{aligned}\sum_{a=1}^{N_\mathrm{f}}\left[\bar{\psi}_a\gamma^\mu\partial_\mu\psi_a + m\bar{\psi}_a\psi_a\right] &= \sum_{a=1}^{N_\mathrm{f}}\left[\bar{\chi}_{a,1}\sigma^\mu\partial_\mu\chi_{a,1} + \bar{\chi}_{a,2}\sigma^\mu\partial_\mu\chi_{a,2} + m\bar{\chi}_{a,1}\chi_{a,1} - m\bar{\chi}_{a,2}\chi_{a,2}\right] \\ &= \sum_{a=1}^{N_\mathrm{f}}\sum_{r=1}^{2}\left[\bar{\chi}_{a,r}\sigma^\mu\partial_\mu\chi_{a,r} - (-1)^r m\bar{\chi}_{a,r}\chi_{a,r}\right]. \end{aligned} \tag{2.19}$$

Here, we can introduce the irreducible flavour index $\alpha = 2a + r - 2 = 1, \ldots, N_{\mathrm{f,irr}}$ using Greek letters from the beginning of the alphabet as an abbreviation for the tuple (a, r). We denote the corresponding two-component spinors by $\chi_\alpha(x)$ and consider a variable number of $N_{\mathrm{f,irr}} := 2N_\mathrm{f}$ fermion flavours. In the following, we use $(-1)^r = (-1)^\alpha$ in the Lagrangians, where a summation over α in expressions like $\bar{\chi}_\alpha(-1)^\alpha\chi_\alpha$ is implied.

Lagrangians

After this derivation for free fermions, we can continue with our reducible four-fermion theories defined in section 2.1.1. NJL is not included here and will only be used in the reducible representation.

Th: Like the kinetic term, the decomposition (2.18) cancels the sign in the γ_μ of the interaction and we obtain a Lagrangian identical to (2.7) with ψ replaced by χ up to the sign in the mass term. It is given by

$$\mathscr{L}_{\mathrm{Th,irr}} = \bar{\chi}_\alpha\left(\partial\!\!\!/ - (-1)^\alpha m\right)\chi_\alpha + \frac{g_{\mathrm{Th}}^2}{2N_{\mathrm{f,irr}}}\left(\bar{\chi}_\alpha\gamma_\mu\chi_\alpha\right)^2. \tag{2.20}$$

G45: Due to the fact that $\gamma_{45} = \mathrm{diag}(\mathbb{1}_2, -\mathbb{1}_2)$ in our choice for the γ-matrices, the interaction in Lagrangian (2.8) reduces to the form of the reducible GN in (2.11) with ψ replaced by χ and can therefore be called *irreducible* Gross-Neveu model. It is given by

$$\mathscr{L}_{\mathrm{G45,irr}} = \bar{\chi}_\alpha\left(\partial\!\!\!/ - (-1)^\alpha m\right)\chi_\alpha - \frac{g_{\mathrm{G45}}^2}{2N_{\mathrm{f,irr}}}\left(\bar{\chi}_\alpha\chi_\alpha\right)^2. \tag{2.21}$$

GN: Like a mass term, the reduction leads to different signs in the interaction of half of the irreducible flavours and we do not recover the form of the reducible GN. Instead we have

$$\mathscr{L}_{\mathrm{GN,irr}} = \bar{\chi}_\alpha\left(\partial\!\!\!/ - (-1)^\alpha m\right)\chi_\alpha - \frac{g_{\mathrm{GN}}^2}{2N_{\mathrm{f,irr}}}\left((-1)^{\alpha-1}\bar{\chi}_\alpha\chi_\alpha\right)^2. \tag{2.22}$$

This result can also be found in the work of Gehring et al. [GGJ15], where in addition a projection onto four-component Weyl-spinors is given. Only in this form the action of massless GN decomposes into two independent parts for left- and right-handed spinors.

[(d)] We will use the notation $\partial\!\!\!/$ for both reducible and irreducible representation. It is a 2×2-matrix in spinor space when surrounded by spinors $\bar{\chi}, \chi$ and a 4×4-matrix when spinors $\bar{\psi}, \psi$ are used.

To be more general, we allow an odd number of flavours for the irreducible models, so that $\alpha = 1, \ldots, N_{\text{f,irr}}$ with $N_{\text{f,irr}} \in \mathbb{N}$. In these cases, there is no corresponding reducible model[(e)].

"Chiral" Symmetries

Now, we investigate the symmetries in the irreducible representation. To transform our chiral generators Γ given below equation (2.5), we use representation (2.17) of the γ-matrices. We can deduce from it that the transformations (2.5a) and (2.5b) with $\mathbb{1}$ and γ_{45} can be combined to give phase shifts for single two-component spinors, while (2.5c) and (2.5d) are rotations between different irreducible flavours. The $U(2N_\text{f})$ group of the reducible Th and G45 with N_f flavours is present in the corresponding irreducible model as rotations of the $N_{\text{f,irr}} = 2N_\text{f}$ irreducible flavours with group $U(N_{\text{f,irr}})$. Strictly speaking, the irreducible variants only have a flavour symmetry since no matrix like γ_5 exists that allows the definition of chirality.

Similarly, the symmetry group of $U(N_{\text{f,irr}}/2) \times U(N_{\text{f,irr}}/2)$ of the reducible GN can be seen directly in the Lagrangian of the irreducible version (2.22), where the flavours with an additional minus sign transform independently of the other half, because the generators $\mathbb{1}$ and γ_{45} are diagonal in the representation (2.17) used for the reduction. The $\mathbb{Z}_2$ transformation with γ_5 is an exchange of two corresponding flavours with different r, e.g. $\chi_{a,1}$ and $\chi_{a,2}$. Here, it is important to note that G45 can be seen as the irreducible version of GN. Hence, its critical behaviour is expected to be similar or identical to the one of GN [GGJ15], although G45 shares its symmetry group with Th and not GN. Simulations of both models are compared in section 3.4. A special case is the model with $N_{\text{f,irr}} = 1$. Obviously, GN and G45 coincide for this special case, and we will see in section 2.2.1 that also Th becomes equivalent to these models. They only have a $U(1)$-symmetry since no flavour rotations are possible.

Parity

We can also define parity in the irreducible representation, as before associated to a flip $x = (x_1, x_2, x_3) \to x' = (x_1, -x_2, x_3)$. Then, a possible parity transformation of the spinors is given by

$$\chi(x) \to \mathrm{i}\sigma_2 \chi(x'), \qquad \bar{\chi}(x) \to \bar{\chi}(x')\,\mathrm{i}\sigma_2, \tag{2.23}$$

but this is not equivalent to the reducible parity (2.15). An explicit calculation shows that (2.15) equals a transformation (2.23) together with an exchange of irreducible flavours [HP94; Ahn94]

$$\chi_{a,1}(x) \to \mathrm{i}\sigma_2 \chi_{a,2}(x'), \qquad \chi_{a,2}(x) \to \mathrm{i}\sigma_2 \chi_{a,1}(x'), \tag{2.24}$$

where $a = 1, \ldots, N_\text{f}$ as in (2.18). This is only well-defined for an even number of $N_{\text{f,irr}}$, while an irreducible parity transformation (2.23) is always possible and exists even in the $N_{\text{f,irr}} = 1$ model.

[(e)] One could think of these models as having half a reducible flavour. For example $N_{\text{f,irr}} = 5$ would correspond to $N_\text{f} = 2.5$.

Mass Terms and Condensates

Going to the irreducible representation, the parity-invariant mass term as well as the chiral condensate have a minus sign for flavours with $r = 2$ as in (2.19). Hence, for $N_{\text{f,irr}} = 2$ the statement equivalent to (2.16) is

$$\langle \bar{\chi}_1 \chi_1 \rangle - \langle \bar{\chi}_2 \chi_2 \rangle \neq 0. \tag{2.25}$$

Such a condensate or mass term is invariant under the extended parity with flavour exchange (2.24), but not under the irreducible parity (2.23). The opposite is true if we introduce a simple mass term $m_{\text{irr}} \bar{\chi} \chi$ in the irreducible representation. It can be derived from the γ_{45} mass term in the reducible representation. Similarly, the reducible parity-odd condensate $\langle \bar{\psi} \gamma_{45} \psi \rangle$ becomes $\sum_\alpha \langle \bar{\chi}_\alpha \chi_\alpha \rangle$ for irreducible flavours and corresponds to the naive definition of the chiral condensate in the irreducible representation. Contrary to (2.25), it can be extended easily to odd $N_{\text{f,irr}}$.

2.2. Rewriting the Lagrangians

In this section we introduce and apply two transformations that are often used in the context of four-fermion theories. We begin with Fierz identities in section 2.2.1, which relate the different four-fermion terms with each other. This allows to rewrite the Lagrangians of four-fermion models in terms of different interactions while the physics stays the same. Another exact relation can be obtained with the HS presented in section 2.2.2. It can be used to introduce auxiliary scalar fields replacing the four-fermion interaction by a Yukawa-type of interaction between fermions and bosons. This transformation is necessary for conventional lattice simulations because the resulting action is quadratic in the spinor fields and allows an analytical integration over the fermions.

2.2.1. Fierz Identities

The γ-matrices of a d_γ-dimensional representation of the Clifford algebra can be used to construct a complete basis of all $d_\gamma \times d_\gamma$-matrices [WS86]. Due to this fact, the different interaction terms of four-fermion theories are not all independent. The completeness relation allows the deduction of so-called *Fierz identities*. All relevant identities for three-dimensional four-fermion theories with both reducible and irreducible representations are given for example by Janssen [Jan12]. Also Ahn et al. [Ahn94] and Ahn & Park [AP98] used a Fierz identity to analytically study Th.

Here, we only work with Fierz identities in the irreducible representation, where calculations are much easier. We want to use them to reformulate the interaction term of Th, where no order parameter for χSB is accessible in our simulations of chapter 4. Since GN provides direct access to χSB (see chapter 3), a reformulated Lagrangian with a GN-like

interaction can be beneficial. There are several ways to achieve this. Using abbreviations of the form $|\bar{\chi}_\beta\chi_\alpha|^2 = (\bar{\chi}_\beta\chi_\alpha)(\bar{\chi}_\alpha\chi_\beta)$, we consider the following:

$$\left(\bar{\chi}_\alpha\sigma_\mu\chi_\alpha\right)^2 = -\left(\bar{\chi}_\alpha\chi_\alpha\right)^2 - 2\left|\bar{\chi}_\beta\chi_\alpha\right|^2, \tag{2.26a}$$

$$\left(\bar{\chi}_\alpha\sigma_\mu\chi_\alpha\right)^2 = 3\left(\bar{\chi}_\alpha\chi_\alpha\right)^2 + 2\left|\bar{\chi}_\beta\sigma_\nu\chi_\alpha\right|^2. \tag{2.26b}$$

A derivation of these identities and a more general form are given in appendix A. For $N_{\text{f,irr}} = 1$, both identities reduce to

$$\left(\bar{\chi}\sigma_\mu\chi\right)^2 = -3\left(\bar{\chi}\chi\right)^2, \tag{2.27}$$

which shows the equivalence of irreducible GN and Th with $g_{\text{GN}}^2 = 3g_{\text{Th}}^2$. For $N_{\text{f,irr}} \geq 2$, the equations in (2.26) show that Th can be replaced by GN only if we introduce additional flavour-mixing interactions. From (2.20) we get the resulting Lagrangians

$$\mathscr{L}_{\text{FM}} = \bar{\chi}_\alpha\left(\partial\!\!\!/ + m\right)\chi_\alpha - \frac{g_{\text{Th}}^2}{2N_{\text{f,irr}}}\left(\bar{\chi}_\alpha\chi_\alpha\right)^2 - \frac{g_{\text{Th}}^2}{N_{\text{f,irr}}}\left|\bar{\chi}_\beta\chi_\alpha\right|^2, \tag{2.28a}$$

$$\mathscr{L}_{\text{FVM}} = \bar{\chi}_\alpha\left(\partial\!\!\!/ + m\right)\chi_\alpha + \frac{3g_{\text{Th}}^2}{2N_{\text{f,irr}}}\left(\bar{\chi}_\alpha\chi_\alpha\right)^2 + \frac{g_{\text{Th}}^2}{N_{\text{f,irr}}}\left|\bar{\chi}_\beta\sigma_\nu\chi_\alpha\right|^2. \tag{2.28b}$$

$\bar{\chi}_\beta\chi_\alpha$ and $\bar{\chi}_\beta\sigma_\nu\chi_\alpha$ are a matrix in flavour space and a vector of matrices in the internal space respectively. In the following we will refer to the corresponding model with Lagrangian (2.28a) as the Fierz matrix formulation (FM) and call (2.28b) the Fierz vector-matrix formulation (FVM). A numerical investigation of these models is presented in section 6.1.

2.2.2. Hubbard-Stratonovich Transformations

All previously mentioned Lagrangians can be transformed to versions bilinear (instead of quartic) in the fermion fields by introducing auxiliary bosonic fields. This technique goes back at least to Hubbard [Hub59] and is usually called *HS*. Without it, Monte Carlo simulations with standard algorithms would not be possible. They require the fermions to be integrated out, which can only be done analytically when the action is bilinear in the fermion fields. See section 2.3 for further details on the algorithmic setup.

The transformation employs Gaussian integrals similarly to the well-known identities for real numbers p and q and $\alpha > 0$,

$$\mathrm{e}^{\alpha p^2} = \frac{1}{\sqrt{4\pi\alpha}}\int_{-\infty}^{\infty}\mathrm{d}q\,\mathrm{e}^{-\frac{1}{4\alpha}q^2 \pm pq} \qquad \text{and} \qquad \mathrm{e}^{-\alpha p^2} = \frac{1}{\sqrt{4\pi\alpha}}\int_{-\infty}^{\infty}\mathrm{d}q\,\mathrm{e}^{-\frac{1}{4\alpha}q^2 \pm \mathrm{i}pq}, \tag{2.29}$$

to introduce integrals over bosonic fields. As q^2 replaces p^2 in (2.29), the four-fermion term is replaced by a square of the new bosonic field, together with a Yukawa-type term analogous to pq. Regardless of the sign in the exponent on the left-hand side, the square of the bosonic field comes with a minus. For an originally negative exponent an additional i

appears in front of the Yukawa term. The sign of the latter is arbitrary. For convenience, we always take the sign such that the term is positive in the new Lagrangian. The parameter α occurs on the right-hand side in the denominator of the exponent. Therefore, all numerical results and plots in this work use an inverse coupling

$$\lambda_{\mathrm{X}} = \frac{N_{\mathrm{f}}}{g_{\mathrm{X}}^2} > 0, \tag{2.30}$$

where the strong coupling limit is found for $\lambda_{\mathrm{X}} \to 0$. We will now present the transformation for GN because it has the smallest number of degrees of freedom. The resulting Lagrangians for the other models are given afterwards. A distinction between reducible and irreducible models is not necessary since the transformations work analogously.

Transformation for GN

For GN with Lagrangian (2.11) we have an integral analogously to (2.29) for each lattice site, so that the full transformation is given by

$$\exp\left[\sum_x \frac{g_{\mathrm{GN}}^2}{2N_{\mathrm{f}}}\left(\bar{\psi}_a\psi_a\right)^2\right] = \left(\frac{N_{\mathrm{f}}}{2\pi g_{\mathrm{GN}}^2}\right)^{\frac{V}{2}} \int \mathscr{D}\sigma \exp\left[-\sum_x\left(\frac{N_{\mathrm{f}}}{2g_{\mathrm{GN}}^2}\sigma^2 + \bar{\psi}_a\sigma\psi_a\right)\right]. \tag{2.31}$$

Note, that the exponent on the left-hand side is positive due to the additional minus sign in the definition of the partition sum (2.1). Hence, the transformation leads to a real exponent on the right-hand side. The new auxiliary field σ enters the Lagrangian

$$\mathscr{L}_{\mathrm{GN,HS}} = \bar{\psi}_a\left(\partial\!\!\!/ + m + \sigma\right)\psi_a + \frac{1}{2}\lambda_{\mathrm{GN}}\sigma^2 \tag{2.32}$$

in the same way as a mass term. It has to transform non-trivially with $\sigma \to -\sigma$ under the $\mathbb{Z}_2$-symmetry to keep the new Lagrangian invariant. Similarly to the mass term, it does not change under parity transformations.

Transformation of the Other Main Models

For more involved Lagrangians, HS can induce multiple auxiliary fields which we will in general summarise by φ. For example, the current-current structure of the four-fermion term in Th requires the introduction of a scalar field for each spacetime dimension, equivalent to a vector field V_μ with $N_\varphi = 3$ components. In comparison with (2.31), we have an integral for each x and for each of the N_φ independent field components. Then, the factor in front of the integral has the exponent $VN_\varphi/2$. With these preliminaries, we give the resulting reducible Lagrangians for our main models.

Th: As mentioned before, HS introduces an auxiliary three-component vector field V_μ and we get

$$\mathscr{L}_{\mathrm{Th,HS}} = \bar{\psi}_a\left(\partial\!\!\!/ + m + \mathrm{i}V\!\!\!/\right)\psi_a + \frac{1}{2}\lambda_{\mathrm{Th}}V_\mu V^\mu. \tag{2.33}$$

The interaction in (2.7) comes with the sign opposite to GN, so that we now have an i in the Lagrangian. It is still invariant under all chiral transformations (2.5) and no

transformation of the vector field is required. On the contrary, the 2-component of the auxiliary field must change its sign under a parity transformation.

G45: Here, the transformation can be applied in the same way as for GN. We call the new scalar field ρ and get an interaction with the fermions through $\bar{\psi}_a \rho \gamma_{45} \psi_a$. The Lagrangian after the transformation reads

$$\mathscr{L}_{\mathrm{G45,HS}} = \bar{\psi}_a \left(\partial\!\!\!/ + m + \rho\gamma_{45}\right)\psi_a + \frac{1}{2}\lambda_{\mathrm{G45}}\rho^2. \tag{2.34}$$

Similarly to Th and in contrast to GN, the Lagrangian is invariant under the full chiral symmetry (2.5) without transforming the auxiliary field. Under parity, the scalar field transforms as $\rho \to -\rho$ because $\bar{\psi}\gamma_{45}\psi$ switches its sign.

NJL: For the Lagrangian (2.9), we can perform two transformations separately introducing fields σ and τ. Since the term with γ_5 comes with the opposite sign, it has an additional i after the transformation, so that the result reads

$$\mathscr{L}_{\mathrm{NJL,HS}} = \bar{\psi}_a \left(\partial\!\!\!/ + m + \sigma + \mathrm{i}\tau\gamma_5\right)\psi_a + \frac{1}{2}\lambda_{\mathrm{NJL}}\left(\sigma^2 + \tau^2\right). \tag{2.35}$$

In this form, the intact $U(1)$-symmetry from (2.5d) is evident because the scalar fields transform with

$$\sigma + \mathrm{i}\gamma_5\tau \to \mathrm{e}^{-2\mathrm{i}\theta\gamma_5}\left(\sigma + \mathrm{i}\gamma_5\tau\right) \quad \Leftrightarrow \quad \begin{pmatrix}\sigma\\ \tau\end{pmatrix} \to \begin{pmatrix}\cos 2\theta & \sin 2\theta\\ -\sin 2\theta & \cos 2\theta\end{pmatrix}\begin{pmatrix}\sigma\\ \tau\end{pmatrix}. \tag{2.36}$$

Thus, they also transform non-trivially under the $U(1)$ (or the equivalent $O(2)$ on the right-hand side) leaving the bosonic action invariant.

Transformation of Lagrangians After Fierz Transformation

Having completed the main four-fermion models of the present work, we now go on to perform HS on the reformulated versions of Th that we obtained in section 2.2.1 by Fierz transformations. The Lagrangians (2.28) include flavour-mixing terms, for which Hermitian matrix fields can be introduced. A short note on that was given by Janssen [Jan12] and a more detailed calculation of the necessary integrals can be found in appendix B. Here we present the resulting Lagrangians for both formulations we will investigate.

FM: Applying the transformations to the Lagrangian (2.28a) separately for each interaction term leads to

$$\mathscr{L}_{\mathrm{FM,HS}} = \bar{\chi}_\alpha \left[\left(\partial\!\!\!/ + m + \phi\right)\delta_{\alpha\beta} + T_{\alpha\beta}\right]\chi_\beta + \frac{1}{2}\lambda_{\mathrm{Th}}\phi^2 + \frac{1}{4}\lambda_{\mathrm{Th}}T_{\beta\alpha}T_{\alpha\beta}, \tag{2.37a}$$

with a Hermitian $N_{\mathrm{f,irr}} \times N_{\mathrm{f,irr}}$-matrix T and a GN-like scalar field ϕ.

FVM: For the Lagrangian (2.28b), we have to introduce a vector of Hermitian matrix fields $T^\mu_{\alpha\beta}$ with flavour and spacetime indices in addition to the GN-scalar ϕ. Both fields

come with an additional i due to the positive sign of the interaction in the original Lagrangian. We have

$$\mathscr{L}_{\text{FVM,HS}} = \bar{\chi}_\alpha \left[\left(\partial\!\!\!/ + m + \mathrm{i}\phi \right) \delta_{\alpha\beta} + \mathrm{i} T^\mu_{\alpha\beta} \sigma_\mu \right] \chi_\beta + \frac{1}{6}\lambda_{\text{Th}}\phi^2 + \frac{1}{4}\lambda_{\text{Th}} T^\mu_{\alpha\beta} T_{\beta\alpha,\mu}. \tag{2.37b}$$

Note, that these Lagrangians contain more degrees of freedom than necessary. For example, the field ϕ in (2.37a) and the trace of T can be exchanged by each other. Performing a shift of the diagonal elements $T_{\alpha\alpha} \to T_{\alpha\alpha} + \phi$ (no summation), we can eliminate ϕ by performing the resulting Gaussian path integral. This leads to

$$\begin{aligned} \mathscr{L}_{\text{FM}} &= \bar{\chi}_\alpha \left[(\partial\!\!\!/ + m)\, \delta_{\alpha\beta} + T_{\alpha\beta} \right] \chi_\beta + \frac{1}{4}\lambda_{\text{Th}} T_{\beta\alpha} T_{\alpha\beta} - \frac{\lambda_{\text{Th}}}{4(2+N_{\text{f,irr}})} (T_{\alpha\alpha})^2 \\ &\equiv \bar{\chi} \left[(\partial\!\!\!/ + m) + T \right] \chi + \frac{1}{4}\lambda_{\text{Th}} \operatorname{tr}\!\left(T^2\right) - \frac{\lambda_{\text{Th}}}{4(2+N_{\text{f,irr}})} (\operatorname{tr} T)^2, \end{aligned} \tag{2.38a}$$

which can be found in [Ahn94; AP98]. As a second possibility, T can be split into a traceless, Hermitian matrix $\hat{T}$ and a scalar field $\hat{\phi}$, where $\operatorname{tr} T = \hat{\phi} N_{\text{f,irr}}$. Then, the Lagrangian reads

$$\mathscr{L}_{\text{FM}} = \bar{\chi} \left[\left(\partial\!\!\!/ + m + \hat{\phi} \right) + \hat{T} \right] \chi + \frac{1}{4}\lambda_{\text{Th}} \operatorname{tr}\!\left(\hat{T}^2\right) + \frac{\lambda_{\text{Th}} N_{\text{f,irr}}}{2(2+N_{\text{f,irr}})} \hat{\phi}^2. \tag{2.38b}$$

The latter form was implemented for simulations as described in section 6.1.1. For $N_{\text{f,irr}} = 1$, both Lagrangians (2.38) have the form of GN, confirming the identity (2.27). Yet another Lagrangian, where no factors of N_{f} appear in the bosonic part, was used by Björn Wellegehausen to derive an effective potential for local condensates in our recent paper [WSW17].

Notation for General Discussions

To fix our notation, we give the general form of the action that all models share. We have

$$S[\bar{\Psi}, \Psi, \varphi] = \bar{\Psi}_I D_{IJ}[m, \varphi] \Psi_J + S_{\text{bos}}[\varphi], \tag{2.39}$$

where Ψ stands for either irreducible or reducible fermion fields, φ is a placeholder for all bosonic auxiliary fields and the general indices I, J run over spacetime, flavour and spin degrees of freedom. The Dirac operator $D[m, \varphi]$ always depends linearly on the bosons and describes their interaction with fermions, while the bosonic action $S_{\text{bos}}[\varphi]$ collects the terms quadratic in the auxiliaries.

2.3. Simulation Setup

This section summarises all details about our implementation of four-fermion theories on the lattice. Most of the simulations presented in this work were performed with a `C++` framework mainly developed by Björn Wellegehausen. Many details about the implementation can be found in his PhD-thesis [Wel12]. Like most lattice field theory simulations, we use a Markov Chain Monte Carlo algorithm to estimate expectation values of observables

defined via the path integral (2.2). Due to the HS in section 2.2.2, we have to include the auxiliary scalar degrees of freedom, which will be represented by φ in this section. In analogy to statistical mechanics, one usually interprets

$$P[\bar{\Psi},\Psi,\varphi] = \frac{1}{Z}\mathrm{e}^{-S[\bar{\Psi},\Psi,\varphi]} \tag{2.40}$$

as the probability to find the system in the state given by $\bar{\Psi},\Psi$ and φ. This requires $P[\bar{\Psi},\Psi,\varphi]$ to be non-negative. A violation of this is the origin of the *sign problem*, discussed in more detail in section 2.4. In this case, the algorithms presented here may not give correct results.

Assuming a non-negative probability distribution, expectation values of observables $\mathcal{O}$ can be calculated by the path integral over all possible field states

$$\langle\mathcal{O}\rangle = \int \mathcal{D}\bar{\Psi}\mathcal{D}\Psi\mathcal{D}\varphi\, P[\bar{\Psi},\Psi,\varphi]\mathcal{O}[\bar{\Psi},\Psi,\varphi]. \tag{2.41}$$

In a computer simulation, the program generates a finite sample of N configurations $(\bar{\Psi}_n,\Psi_n,\varphi_n)$ with $n = 1,\ldots,N$ which must be distributed according to (2.40). Then, an approximation for the expectation value (2.41) is given by

$$\langle\mathcal{O}\rangle \approx \frac{1}{N}\sum_{n=1}^{N}\mathcal{O}[\bar{\Psi}_n,\Psi_n,\varphi_n]. \tag{2.42}$$

The major difficulty is to efficiently obtain new configurations that are as statistically independent from the previous ones as possible.

We continue in section 2.3.1 with a summary of the algorithms used to generate new configurations. Afterwards, the problems related to chiral symmetry on the lattice are discussed in section 2.3.2, where we also present the SLAC derivative as a solution to them. Finally, we elaborate on the measurement of fermionic observable in our simulations in section 2.3.3.

2.3.1. Simulation Algorithms

Since the goal is to generate configurations distributed according to (2.40), all algorithms require the numerical evaluation of the action. The conventional approaches for simulations with fermions need actions bilinear in the fermion fields, as obtained in section 2.2.2. This allows to perform the path integral over Grassmann numbers in the partition sum analytically. For a Lagrangian of the general form (2.39), we get the *fermion determinant* $\det(D[m,\varphi])$ of the Dirac operator $D[m,\varphi]$, so that the probability distribution is given by

$$P[\varphi] = \frac{1}{Z}\det(D[m,\varphi])\mathrm{e}^{-S_{\mathrm{bos}}[\varphi]}. \tag{2.43}$$

For most of our models $D[m,\varphi]$ is diagonal in flavour space, so that the determinant factorises: $\det(D[m,\varphi]) = \det\big(D[m,\varphi]_{N_\mathrm{f}=1}\big)^{N_\mathrm{f}}$. Now, there are several ways to proceed with

the evaluation of the fermion determinant. We explain the efficient rHMC algorithm and an exact update algorithm that allows to study the sign problem (see section 2.4).

Rational Hybrid Monte Carlo (rHMC) Update

Most simulations in lattice field theory are performed with the Hybrid Monte Carlo (HMC) algorithm invented by Duane et al. [Dua87], which is explained in many textbooks [Wip13; GL10] and tutorials like [Sch09]. It generates a new configuration from the last one by an evolution through a fictitious molecular dynamics trajectory, which is then accepted or rejected in accordance with the probability distribution.

To evaluate the fermion determinant, so-called *pseudofermions* [Fuc81] are introduced, using the fact that a Gaussian path-integral over a bosonic field ϕ yields the inverse of a determinant. Hence, it is possible to write the determinant of a matrix M as

$$\det(M) = \frac{1}{\det\left(M^{-1}\right)} = \int \mathscr{D}\phi^\dagger \mathscr{D}\phi \, \mathrm{e}^{-\phi^\dagger M^{-1} \phi}, \tag{2.44}$$

assuming M to be positive definite. To derive the rHMC algorithm, which was first described by Horváth et al. [HKS99], we follow the more detailed descriptions of Kennedy [Ken06] and Wellegehausen [Wel12]. We define the explicitly positive definite matrix $M := D^\dagger D$ and introduce N_{pf} pseudofermions via

$$\det(D)^{N_{\mathrm{f}}} = \det(M)^{\frac{N_{\mathrm{f}}}{2}} = \left(\det(M)^q\right)^{N_{\mathrm{pf}}} = \prod_{p=1}^{N_{\mathrm{pf}}} \int \mathscr{D}\phi_p^\dagger \mathscr{D}\phi_p \exp\left(-\phi_p^\dagger M^{-q} \phi_p\right) \tag{2.45}$$

with $q = {}^{N_{\mathrm{f}}}/_{2N_{\mathrm{pf}}}$. The first equality requires $\det(D) \geq 0$. Our simulations typically use $N_{\mathrm{pf}} = N_{\mathrm{f}}$, leading to $q = {}^1/_2$. The matrix M^{-q} is estimated with N_{R} summands of a rational approximation

$$M^{-q} \approx \alpha_0 + \sum_{r=1}^{N_{\mathrm{R}}} \alpha_r \left(M + \beta_r \mathbb{1}\right)^{-1}, \tag{2.46}$$

where the coefficients α_0, α_r and β_r must be computed only once before starting simulations, for example with the Remez algorithm [Fra65]. The numerical accuracy of the coefficients, the interval on which the approximation is calculated and the number of summands N_{R} allow a fine tuning of the performance of the whole algorithm and different approximations can be used in distinct steps of the rHMC update.

The main numerical cost of a simulation consists of solving $(M + \beta_r \mathbb{1}) x_r = y$ for x_r with all parameters β_r. There are so-called *multi-shift* solvers extending the common iterative solvers to this kind of equations with shifts β_r. We use a multi-shift conjugate gradient (CG) solver [Jeg96], which can solve systems with many shifts simultaneously at small additional cost compared to solving a single system. Additionally, the integration in the fictitious molecular dynamics time is done on different time scales for fermions and bosons [Urb06]. This allows to decrease the number of expensive fermion action calculations while integrating the cheap bosonic part with higher accuracy. This is especially efficient if the main contribution to the molecular dynamics force comes from the bosonic part.

Exact Update

The rHMC algorithm works only for a positive definite D and does not allow to determine the possibly complex phase. However, it is possible to rewrite the fermion determinant as an *effective action*, so that (2.43) becomes

$$P[\varphi] = \frac{1}{Z} \mathrm{e}^{-S_{\mathrm{eff}}[\varphi] - S_{\mathrm{bos}}[\varphi]} \quad \text{with} \quad S_{\mathrm{eff}}[\varphi] = -\ln\det(D[m,\varphi]). \tag{2.47}$$

An explicit calculation of S_{eff} is possible and allows to access its imaginary part, but this is very expensive compared to a rHMC simulation. We only use this method on very small lattices to check if a model shows a sign problem. If this is the case, we measure the imaginary part as an observable and simulate the *phase-quenched* theory, meaning that we only take the real part of S_{eff} in the algorithm to generate new configurations. Further details how to proceed in case of a mild sign problem can be found in section 2.4.1.

2.3.2. Chiral Symmetry on the Lattice

This section is devoted to the lattice formulation of fermionic theories with chiral symmetry. A more detailed introduction is given in most textbooks, e.g. by Wipf [Wip13] or Gattringer & Lang [GL10]. Unfortunately, a naive discretisation with a forward or backward derivative in the action does not yield the desired result. One gets so-called *fermion doublers*, meaning that a lattice model in d spacetime dimensions actually describes $2^d N_{\mathrm{f}}$ fermion flavours instead of just N_{f}. They appear due to additional poles of the momentum space propagator at the edge of the Brillouin zone [GL10]. There have been many different attempts to solve this problem. The first one developed by Wilson can be found in any textbook on lattice field theory (e.g. [Wip13; GL10]) and introduces an additional momentum-dependent mass term, which decouples the doublers in the continuum limit by making them infinitely heavy. This solution to the doubling problem is not suitable for our models since the extra term explicitly breaks the chiral symmetry.

In fact, the implementation of chiral symmetry on the lattice is a long-standing problem in the community, and there is even a no-go theorem by Nielsen & Ninomiya [NN81a; NN81c; NN81b], built on earlier work [KS81; Kar81]. Assuming locality, Hermiticity and translational invariance, it states that there is no lattice Dirac operator with chiral symmetry and the correct continuum limit without doublers [Wip13]. In the following, some workarounds are presented.

SLAC Fermions

In this work, we use the very old and direct approach of SLAC fermions[(f)] introduced by Drell et al. [DWY76b; DWY76a]. It starts from the continuum momentum space propagator and simply replaces the continuous momentum vector by a finite number of discrete lattice

[(f)] SLAC is the abbreviation of the Stanford Linear Accelerator Center, where the authors worked when publishing their papers.

momenta. Here, the finite lattice volume leads to a discrete number of momenta, while the finite lattice spacing a induces a momentum cutoff π/a. Despite that, the behaviour is the same as in the continuum. Our discrete points follow the straight lines of the continuum dispersion relation up to the cutoff.

The application of the derivative in momentum space is just a multiplication with the lattice momenta. Doing a Fourier transformation back to position space, one can obtain the matrix elements of the derivative along a single spacetime direction as

$$\partial^{\mathrm{SLAC}}_{xx} = 0 \quad \text{and} \quad \partial^{\mathrm{SLAC}}_{xy}\Big|_{x\neq y} = \frac{\pi}{L}\frac{(-1)^{x-y}}{\sin\left(\frac{\pi}{L}(x-y)\right)}. \tag{2.48}$$

This derivative avoids the Nielsen-Ninomiya theorem by violating the assumption of locality, as the Dirac operator in momentum space is not a continuous function of the momenta[(g)]. Instead, there is a jump at the edge of the Brillouin zone. Apart from that, it is free of doublers[(h)] and implements the continuum chiral symmetry on the lattice in a straightforward way.

Nevertheless, it is seldom used in current simulations because Karsten & Smit [KS78; KS79] showed that the vacuum polarisation of QED is no longer Lorentz-covariant, preventing a renormalisation of the theory. Although there was some debate about the validity of the calculation [Rab81; KS81], it is in general believed not to work for gauge theories. On the other hand, the SLAC derivative can be used to solve the Schrödinger equation [FSW12] and to study two-dimensional Wess-Zumino models [KLW05]. The renormalisability for the latter was proven and simulations with the SLAC derivative showed fewer finite size effects than Wilson fermions [Ber09; Ber08; Käs08; Ber10; BBP09]. The proof of renormalisability works also for non-supersymmetric models with an interaction of Yukawa type, like our models have after the HS. Additionally, high-precision results were obtained already on moderate lattice sizes for the non-linear $O(3)$ sigma model [Flo12]. Thus, we are confident, that the SLAC derivative allows simulations of four-fermion theories without doublers, but with exact chiral symmetry.

Implementation of the SLAC Derivative

It is possible to implement the SLAC derivative using the position-space matrix elements (2.48), but it is advisable for computational efficiency to make use of its diagonal form in momentum space. Thus, we perform one-dimensional Fourier transformations of the lattice fields along all straight lines in all three directions. The resulting vectors are multiplied by $\mathrm{i}\gamma^\mu p_\mu$, and afterwards transformed back to position space. There, we apply the remaining parts of $D[m,\varphi]$, that are diagonal in position space, like a mass term or scalar fields. A first implementation and study of GN and Th was done in a diploma thesis [Gal14]. For the present work, the existing implementation was optimised and parallelised

(g) Campos & Tututi [CT02] show that the SLAC derivative is *ultralocal* up to a border matrix, which is non-zero only for matrix indices $I = J = 1$ or $I = J = N$.

(h) There were other non-local formulations for the derivative that still showed doublers [Pel88].

within the existing framework that uses a domain decomposition of the grid with `MPI` communication[(i)].

Using the SLAC derivative, one has to take special care of the boundary conditions. They are closely tied to the number of lattice points in the direction considered. For periodic boundary conditions, it is advisable to use an odd number of points because the resulting momenta can be arranged symmetrically around zero. For antiperiodic boundary conditions, there is an additional shift of $1/2$ in the wave numbers. In this way, there is no zero momentum and an even number of momenta can be chosen symmetrically. Other choices are in principle possible, but lead to an arbitrary decision if the additional unpaired momentum is put at the lower or the upper end of the spectrum. We use antiperiodic boundary conditions in the time direction and periodic ones otherwise. Thus, to avoid ambiguities, we always simulate with $V = L \times (L-1) \times (L-1)$ lattice points with even L and call this a *lattice of size L*.

Staggered Fermions

Since almost all previous lattice simulations of four-fermion theories were performed with staggered fermions, this section gives a short overview of their properties [GL10; Wip13]. Often, they are also named after Kogut & Susskind [KS75]. Starting from a naive discretisation of the kinetic term, a spacetime dependent similarity transformation of the spinors is applied that diagonalises the γ_μ. One ends up with d_γ copies of the same action (two or four in our cases). To reduce the number of doublers, only a single copy is kept as the staggered action, also reducing the computational cost of simulations. It is possible to rearrange this single-component staggered field into new Dirac fermions. They are formed from the eight neighbouring points of a cube, leading to a new lattice with doubled spacing. For the reducible representation, we now get two so-called *tastes* of fermions instead of the eight doublers of the naive theory. Unfortunately, the tastes do not have the full chiral symmetry of the original theory, and it is in general not clear if the full symmetry is recovered in the continuum limit. For GN, staggered fermions should reproduce the correct chiral behaviour. A discussion of previous results can be found in section 3.3.2. On the other hand, staggered simulations of Th have a breaking pattern which does not correspond to the continuum version (2.6). These results are summarised in section 4.2.2.

Ginsparg-Wilson Relation

Long after the first formulation of QCD on the lattice, and still a long time after the initial paper of Ginsparg & Wilson [GW82] in 1982, it was realised that solutions (lattice Dirac operators D) to the *Ginsparg-Wilson relation*

$$\{D, \gamma_5\} = aD\gamma_5 D \tag{2.49}$$

[(i)] This can require a large amount of communication since the Fourier transformations need lines of the whole linear lattice extend in any dimension. The investigation of parallel implementations more adapted to the problem at hand could be interesting, but was outside the scope of this project.

can be obtained and used to simulate QCD with a modified chiral symmetry. For lattice spacing $a \to 0$, the modified transformations reduce to the correct continuum expressions as in (2.4), while the Ginsparg-Wilson relation reproduces the definition of a chirally symmetric Dirac operator

$$\{D, \gamma_5\} = 0. \tag{2.50}$$

Nowadays, several lattice Dirac operators are known that allow exact chiral symmetry on the lattice via (2.49), see [GL10; Wip13] and references therein for some examples. Although these operators are commonly used to study QCD, they can be employed to investigate three-dimensional four-fermion theories. Pioneering work for using *domain wall fermions* in our setup was done by Hands [Han15; Han16a], who also presented first results on GN and Th [Han16b] that we will summarise in section 3.3.2 and section 4.2.2, respectively.

2.3.3. Calculation of Fermionic Observables

Having clarified our implementation of chiral symmetry on the lattice, the main goal is to investigate χSB. In section 2.1.1 it was already explained that the reducible chiral condensate $\langle \bar{\psi}\psi \rangle := \frac{1}{V}\sum_I \langle \bar{\psi}_I \psi_I \rangle$ is an order parameter for the expected phase transition between a symmetric and a broken phase. Thus, it is the main observable for all our simulations. With the notation of (2.39), it can be written as a derivative of the partition sum with respect to m:

$$\begin{aligned} \langle \bar{\psi}\psi \rangle &= \frac{1}{Z}\int \mathscr{D}\bar{\psi}\mathscr{D}\psi\mathscr{D}\varphi \, \frac{1}{V}\Big(\sum_I \bar{\psi}_I \psi_I\Big) \exp\Big(-\sum_{J,K} \bar{\psi}_J D_{JK}[m,\varphi]\psi_K + S_{\text{bos}}[\varphi]\Big) \\ &= -\frac{1}{V}\frac{\partial}{\partial m} \ln Z \quad \text{where} \quad D[m,\varphi] = \partial\!\!\!/ + m + D[\varphi]. \end{aligned} \tag{2.51}$$

On the other hand, the chiral condensate can be expressed through the propagator as

$$\frac{1}{V}\sum_I \langle \bar{\psi}_I \psi_I \rangle = \frac{1}{V} \operatorname{tr} D[m,\varphi]^{-1}, \tag{2.52}$$

where the matrix inverse is usually estimated by *stochastic estimator* methods [Bit89; DL94]. One introduces N_{SE} vectors η^α of random noise to obtain an approximation of

$$D^{-1}_{IJ} \approx \langle \eta^\dagger_J D^{-1}_{IK} \eta_K \rangle \quad \text{with} \quad \langle \eta^\dagger_I \eta_J \rangle = \frac{1}{N_{\text{SE}}}\sum_{\alpha=1}^{N_{\text{SE}}} \eta^\alpha_I \eta^\alpha_J = \delta_{IJ} \quad \text{and} \quad \langle \eta_I \rangle = 0. \tag{2.53}$$

This requires to solve the N_{SE} matrix equations $D_{KJ}\chi_J = \eta_K$, instead of a full inversion of the matrix. Usually, N_{SE} can be chosen much smaller than the matrix size and the error decreases with $1/\sqrt{N_{\text{SE}}}$.

A second observable, that is useful for all four-fermion theories, is the chiral susceptibility. In accordance with common practice for spin systems, it is given by the derivative of the order parameter with respect to the external field, which is the bare mass in our case. For continuum models, the susceptibility should show a divergence at the critical point where

the condensate is non-differentiable. As a remnant in a finite volume, we expect a finite peak on the lattice in our lattice susceptibility

$$\begin{aligned}\chi &:= \frac{1}{V}\frac{\partial}{\partial m}\langle\bar{\psi}\psi\rangle = \frac{1}{V}\frac{\partial^2}{\partial m^2}\ln Z = \frac{1}{V}\Big\langle\sum_{I,J}\big(\bar{\psi}_I\psi_I\big)\big(\bar{\psi}_J\psi_J\big)\Big\rangle \\ &= \frac{1}{V}\sum_{I,J}\big(D^{-1}_{II}D^{-1}_{JJ} - D^{-1}_{IJ}D^{-1}_{JI}\big).\end{aligned} \tag{2.54}$$

In our implementation, no average over J is present because the connected part $D^{-1}_{IJ}D^{-1}_{JI}$ is calculated with a matrix inversion on a *point source* at a randomly chosen lattice point. The disconnected parts are computed with the stochastic estimation described above. To get measurements of the susceptibility with small errors and to obtain accurate histograms of the chiral condensate, a large number of stochastic estimators is needed. We typically use $N_{\mathrm{SE}} = 1000$. Special algorithms are available to speed up the solution of linear equations with multiple right-hand sides. During the present work, the incremental `eigCG` algorithm of Stathopoulos & Orginos [SO10] was implemented. It gathers information about the eigensystem of D while performing a usual CG iteration. We can use this information for subsequent solutions with different right-hand sides to project out the lowest eigenvalues of the matrix. This leads to a better condition number and can drastically decrease the number of iterations needed in the CG.

During the investigation of the dual variables formulation in section 6.2, another observable, the *lattice filling factor* $\langle k\rangle$, proved to be useful. The field k will be introduced in section 6.2 and counts the fermions interacting locally with the auxiliary fields. Due to the Pauli principle, it takes integer values with $k \in [0, d_\gamma V N_{\mathrm{f}}]$, where the maximum is the total number of spinor degrees of freedom on the lattice. At the maximal value, the lattice is saturated with interacting fermions and free propagation is not possible. We will see, that this happens at very strong couplings and introduces lattice artefacts. Regardless of its origin, we can calculate the lattice filling factor in all formulations via

$$\langle k\rangle = \frac{1}{d_\gamma N_{\mathrm{f}}}\left(-\frac{\lambda}{V}\left\langle\frac{\mathrm{d}}{\mathrm{d}\lambda}\ln Z\right\rangle + N_\varphi\right) = \frac{1}{d_\gamma N_{\mathrm{f}}}\left(\frac{1}{V}\big\langle S_{\mathrm{bos}}[\varphi]\big\rangle - N_\varphi\right). \tag{2.55}$$

With this definition, it is normalised to $\langle k\rangle \in [0,1]$ and the number of auxiliary scalar fields N_φ appears to cancel contributions from the λ-dependent factor induced by HS in (2.31). In the conventional formulations it is the average value of the bosonic action or equivalently of the four-fermion terms.

2.4. Sign Problem

The rHMC algorithm described in section 2.3.1 requires a probability interpretation of expression (2.40). This implies that the action must be real. Otherwise, the action is said to suffer a sign problem, which obstructs simulations of many fermionic systems [TW05].

Most importantly, it also occurs in QCD at non-zero chemical potential, motivating various attempts to avoid or *solve* the sign problem, see for example the review by Forcrand [For10]. In section 2.4.1, we only present a few which are relevant for this work, while section 2.4.2 investigates the properties of our Dirac operators. Only for some models, we will be able to prove the absence of a sign problem.

2.4.1. Approaches to Solve the Sign Problem

In this section, we present two of various approaches to solve the sign problem. We begin with the easiest approach of *reweighting* and go on with the fermion bag approach that is useful for four-fermion theories.

Reweighting

A simple approach to circumvent the sign problem is *reweighting* [For10], which shifts the exponential of the imaginary part of S into the observables. We rewrite the partition sum (2.1) as

$$Z = \int \mathscr{D}\bar{\psi}\mathscr{D}\psi\mathscr{D}\varphi \, \mathrm{e}^{-\mathrm{Re}\, S[\bar{\psi},\psi,\varphi]} \mathrm{e}^{-\mathrm{i}\,\mathrm{Im}\, S[\bar{\psi},\psi,\varphi]} = Z_{\hat{P}} \left\langle \mathrm{e}^{-\mathrm{i}\,\mathrm{Im}\, S[\bar{\psi},\psi,\varphi]} \right\rangle_{\hat{P}}, \tag{2.56}$$

where the expectation value is now computed with respect to the non-negative probability

$$\hat{P} = \frac{1}{Z_{\hat{P}}} \mathrm{e}^{-\mathrm{Re}\, S[\bar{\psi},\psi,\varphi]} \quad \text{and} \quad Z_{\hat{P}} = \int \mathscr{D}\bar{\psi}\mathscr{D}\psi\mathscr{D}\varphi \, \mathrm{e}^{-\mathrm{Re}\, S[\bar{\psi},\psi,\varphi]}. \tag{2.57}$$

Then, we can write expectation values of general observables (2.2) as ratios

$$\langle \mathscr{O} \rangle = \frac{\left\langle \mathscr{O}\, \mathrm{e}^{-\mathrm{i}\,\mathrm{Im}\, S[\bar{\psi},\psi,\varphi]} \right\rangle_{\hat{P}}}{\left\langle \mathrm{e}^{-\mathrm{i}\,\mathrm{Im}\, S[\bar{\psi},\psi,\varphi]} \right\rangle_{\hat{P}}} := \frac{\langle \mathscr{O}\Omega \rangle_{\hat{P}}}{\langle \Omega \rangle_{\hat{P}}} \tag{2.58}$$

with weight $\Omega = \mathrm{e}^{-\mathrm{i}\,\mathrm{Im}\, S[\bar{\psi},\psi,\varphi]}$. Viewed this way, the sign problem is strong if the denominator of (2.58) becomes very small. In this case, a better estimate of $\langle \mathscr{O} \rangle$ requires an exponentially growing number of configurations [TW05]. Whenever we must expect a sign problem, we perform simulations with an exact calculation of the fermion determinant as described in section 2.3.1 and measure $\langle \Omega \rangle$. We take the real part $\langle w \rangle := \mathrm{Re}(\langle \Omega \rangle)$ as a measure for the strength of the sign problem. If it is close to one, the reweighting procedure can give good results. For $\langle w \rangle \approx 0$, different approaches are necessary.

Fermion Bag Approach

One possibility to overcome the sign problem is to introduce a different set of variables, like in the fermion bag approach. It was invented by Chandrasekharan [Cha08; Cha10] and extensively used to study four-fermion theories. A review can be found in [Cha13]. Results from the relevant papers for this thesis are discussed in more detail in section 3.3.2 for GN and in section 4.2.2 for Th. Most of these works use staggered fermions, so that they are possibly affected by the problems discussed in section 2.3.2. Using SLAC fermions instead, a similar approach inspired by the fermion bag formulation is presented in section 6.2.

Contrary to conventional HMC simulations, no HS is needed to introduce the fermion bags. Instead, the exponential of the four-fermion interaction in the partition sum (2.1) is expanded in the coupling. Due to the fermionic nature, the expansion contains only a single non-constant term. One can split up the path integral into configurations of new variables that take the value 1 if the interaction term is present and 0 otherwise. In the staggered formulation of [Cha10], the variables represent bonds between neighbouring lattice sites that can be either free or occupied. Then, the path integral can be evaluated analytically, again leading to a fermion determinant similar to (2.43). However, each row and column corresponding to an occupied bond must be dropped. What remains is a product of determinants, each describing a region where fermions are free. These regions are called *fermion bags*. Due to a duality, efficient simulations can be performed both at weak and strong couplings, when either the size of fermion bags or their dual is small [CL11b; CL12a].

The fermion bag approach allows to solve some sign problems that are present for example in the $N_\mathrm{f} = 2$ staggered formulation of GN [CL12b; Li13]. This is due to the fact that the sign problem only occurs for the free fermions inside the bags. Since the bags are much smaller than the whole lattice, it is easier to resum these configurations, yielding a reliable result. Simulations with Wilson fermions were also considered [Cha12; CL11a], with mixed success regarding the sign problem.

2.4.2. Analytical Properties of Our Dirac Operators

Some properties of Dirac operators can be used to prove the absence of a sign problem. For example, the free, massless operator $\partial\!\!\!/$ (equal to $\mathrm{i}\not{p}$ in momentum space) is anti-Hermitian so that its eigenvalues are purely imaginary. The same is true for $\partial\!\!\!/ + \mathrm{i}V\!\!\!/$, the Dirac operator of massless Th after HS in (2.33), and the model FVM in (2.37b) for $m = 0$. Since the matrix size is always a multiple of the even number d_γ, the determinant is purely real. It can still be negative so that this property is not sufficient to prove the absence of a sign problem. Nevertheless, one can show for the reducible Th that eigenvalues appear in complex conjugate pairs, but below we will use another proof together with GN. Introducing a mass term or a scalar field for GN as in (2.32) destroys the anti-Hermiticity. The Dirac operator of G45 also includes the Hermitian matrix γ_{45}, while NJL contains a mixture of Hermitian and anti-Hermitian parts. Regarding the model FM in (2.38), the operator also contains a mixture of Hermitian and anti-Hermitian parts.

Reducible Models

First, we show the absence of a sign problem in the reducible representation for the combination of GN and Th, simulated in section 5.1. Additionally, we include a possible mass term, showing the result to hold also for massive Th, studied in section 4.1.2. This operator has parts proportional to γ_μ and the identity. Using the representation of the Clifford algebra (2.17), we get a block diagonal form of the Dirac operator with an additional

minus sign for the lower block of γ_μ. We can write the determinant with an anti-Hermitian irreducible part $D_{\text{ah}} = \sigma_\mu(\partial^\mu + \mathrm{i}V^\mu) = -D_{\text{ah}}^\dagger$ and the Hermitian part $M = (m+\sigma)\mathbb{1} = M^\dagger$ as

$$\begin{aligned}\det(D_{\text{GN+Th}}) &= \begin{vmatrix} D_{\text{ah}} + M & 0 \\ 0 & -D_{\text{ah}} + M \end{vmatrix} = \det(D_{\text{ah}} + M)\det(-D_{\text{ah}} + M) \\ &= \det(D_{\text{ah}} + M)\det\big((D_{\text{ah}} + M)^\dagger\big) = |\det(D_{\text{ah}} + M)|^2 \geq 0,\end{aligned} \tag{2.59}$$

where we used $\det(D^\dagger) = (\det D)^*$. Similarly, one can use σ_2, the charge conjugation matrix of the irreducible representation, to show that the two blocks are the complex conjugate of each other.

This proof no longer works for G45 because γ_{45} introduces a sign flip in the Hermitian part that cannot be compensated by Hermitian conjugation. On the other hand, the model with a negative coupling $g_{\text{G45}}^2 < 0$ (or alternatively choosing a positive sign of the interaction in (2.8)) possesses an anti-Hermitian operator including $\mathrm{i}\gamma_{45}\rho$, that is free of a sign problem. We show in appendix D that this is not the right choice, so that we must use the version with potential sign problem. For NJL, an argument with the reducible charge conjugation matrix shows that eigenvalues come in complex conjugate pairs, turning the determinant real [GKN13]. Thus, the absence of a sign problem can only be proven for even N_{f}.

Irreducible Models

Now, we turn towards irreducible models. In the case of Th, the anti-Hermitian operator ensures purely imaginary eigenvalues. For the massless model, no sign problem is expected for even $N_{\text{f,irr}}$ due to the relation to the reducible model. This is no longer valid with an irreducible mass term, where we must expect a sign problem for any $N_{\text{f,irr}}$. For the irreducible G45 in (2.21) (the irreducible model with GN interaction), we have $D_{\text{G45,irr}} = \partial\!\!\!/ + m + \rho$ for a single irreducible flavour with general complex eigenvalues. If $N_{\text{f,irr}}$ is even, the resulting operator is similar to the reducible GN, but a sign is missing that is important to ensure non-negative eigenvalues via charge conjugation. For example, the irreducible two-flavour model has $\det\big(D_{\text{G45,irr}}\big)^2 = \det\big(\partial\!\!\!/ + \rho\mathbb{1}\big)^2$ while the reducible single-flavour model has $\det\big(D_{\text{GN,red}}\big) = \det(\partial\!\!\!/ + \sigma\mathbb{1})\det(-\partial\!\!\!/ + \sigma\mathbb{1}) = |\det(\partial\!\!\!/ + \sigma\mathbb{1})|^2$. We must expect a sign problem for any $N_{\text{f,irr}}$, but if we simulate the phase-quenched model with an exact update as described in section 2.3.1, we have

$$\big|\det D_{\text{G45,irr}}\big| = \big|\det\big(\partial\!\!\!/ + \rho\mathbb{1}\big)\big|^2 \equiv \det D_{\text{GN,red}}. \tag{2.60}$$

Thus, for any even $N_{\text{f,irr}}$, a phase-quenched simulation of the irreducible model should be identical to the reducible GN. Regarding the Fierz transformed versions of irreducible Th, no properties but the anti-Hermiticity of FVM are known, leading to a real determinant. For FM a complex determinant must be expected.

3. Gross-Neveu Model

We begin our numerical study with GN, knowing from previous investigations that a second-order χSB phase transition exists for all flavour numbers. It defines the *chiral Ising* universality class commonly discussed to be relevant for the physics of graphene [Her06; JH14]. The name originates from the $\mathbb{Z}_2$-symmetry breaking that our GN Lagrangian (2.11) shares with the Ising model, while the fermionic nature with chiral symmetry puts it in a distinct universality class.

To measure the critical exponents, we work with methods from the theory of *finite size scaling* that we introduce in section 3.1. Furthermore, it summarises our numerical methods to interpolate data points and to obtain error estimates. Simulating the reducible GN with the SLAC derivative introduced in section 2.3.2, we provide a general overview of observables in GN as well as new measurements of the critical exponents in section 3.2. We also study various different methods to obtain the critical exponents in order to find the optimal choice for the evaluation. Our findings are discussed and compared to previous results in section 3.3. Finally, in section 3.4, we compare the reducible GN with G45, which is equivalent to an irreducible formulation of GN.

3.1. Observables and Computational Methods

An order parameter for a second-order χSB phase transition is the chiral condensate $\langle\bar{\psi}\psi\rangle$ introduced in section 2.3.3. It is directly related to the expectation value of the GN scalar field σ in the Lagrangian (2.32) due to a DSE,

$$\int \mathscr{D}\bar{\psi}\mathscr{D}\psi\mathscr{D}\sigma\,\frac{\delta}{\delta\sigma(x)}\,\mathrm{e}^{-S[\bar{\psi},\psi,\sigma]} = 0 \quad \Leftrightarrow \quad \left\langle\bar{\psi}\psi\right\rangle = -\lambda_{\mathrm{GN}}\langle\sigma\rangle, \tag{3.1}$$

with $\sigma = \sum_x \sigma_x$. Thus, there is no need for a time-consuming computation of the chiral condensate on every configuration. We only calculate it on the smallest lattice size for a general overview. As in the Ising model, we expect tunnelling between the two minima of the effective potential at σ_{min} and $-\sigma_{\mathrm{min}}$, leading to $\langle\sigma\rangle \approx 0$. Hence, we take the absolute value and use $\Sigma := \langle|\sigma|\rangle$ as an order parameter. Similarly, we measured the susceptibility of the scalar field

$$\chi = V\left(\left\langle\sigma^2\right\rangle - \langle|\sigma|\rangle^2\right) \tag{3.2}$$

instead of the susceptibility of the chiral condensate. Both Σ and χ are expected to show a particular behaviour at a second-order phase transition that can be described by critical exponents. In section 3.1.1, we present methods to obtain them from lattice simulations. Furthermore, we combined results from simulations at different λ_{GN} with an interpolation algorithm described in section 3.1.2 together with our method to estimate statistical errors.

Table 3.1.: A common set of critical exponents and the corresponding physical quantity. The reduced coupling t is defined in (3.3), m is an external symmetry breaking parameter and k is the momentum. The column "Ising" refers to the standard mean field values for the Ising model with $\mathbb{Z}_2$-symmetry [Wip13]. The mean field calculation for GN is different, due to a different form of the effective potential. Values up to order $1/N_\mathrm{f}$ from Hands et al. [HKK93] are given in the column "GN". A more general calculation shows that these values depend on the dimension and only coincide with the Ising values for $d = 4$ [HKK91]. $\mathcal{O}\left(1/N_\mathrm{f}^2\right)$ results are given in (3.4).

Exponent	Quantity	Relation	Ising	GN
α	specific heat, $m = 0$	$C \propto \lvert t\rvert^{-\alpha}$	0	
β	order parameter, $m = 0$	$\Sigma \propto t^{\beta}$	$1/2$	$1 + \mathcal{O}\left(1/N_\mathrm{f}^2\right)$
γ	susceptibility, $m = 0$	$\chi \propto \lvert t\rvert^{-\gamma}$	1	$1 + \frac{8}{N_\mathrm{f}\pi^2}$
δ	order parameter at $t = 0, m \neq 0$	$\Sigma \propto m^{\frac{1}{\delta}}$	3	$2 + \frac{8}{N_\mathrm{f}\pi^2}$
ν	correlation length	$\xi \propto \lvert t\rvert^{-\nu}$	$1/2$	$1 + \frac{8}{3N_\mathrm{f}\pi^2}$
η	two-point correlation function	$D_\sigma \propto \frac{1}{k^{d-2+\eta}}$	0	$1 - \frac{16}{3N_\mathrm{f}\pi^2}$

3.1.1. Critical Exponents from Finite Size Scaling

For the definition of critical exponents, several observables are considered as a function of the reduced coupling

$$t = \frac{\lambda_\mathrm{GN}^\mathrm{cr} - \lambda_\mathrm{GN}}{\lambda_\mathrm{GN}^\mathrm{cr}}. \tag{3.3}$$

In table 3.1 the commonly used set of exponents and their definitions is given together with their values in $1/N_\mathrm{f}$-expansion up to first order from Hands et al. [HKK93]. With more sophisticated techniques, the critical exponents were obtained at least up to $\mathcal{O}\left(1/N_\mathrm{f}^2\right)$ [Gra92; Gra93; Gra94a; Vas93; Der93]. They are presented by Kärkkäinen et al. [Kär94] in a form convenient for comparison with lattice results as

$$\frac{1}{\nu} = 1 - \frac{32}{3\pi^2 n} + \frac{64\left(27\pi^2 + 632\right)}{27\pi^4 n^2} + \mathcal{O}(n^{-3}), \tag{3.4a}$$

$$\frac{\gamma}{\nu} = 1 + \frac{64}{3\pi^2 n} + \frac{64\left(27\pi^2 - 304\right)}{27\pi^4 n^2} + \mathcal{O}(n^{-3}), \tag{3.4b}$$

where $n = N_\mathrm{f} d_\gamma$ includes the number of spinor components d_γ additionally to N_f. Therefore, it is different for reducible and irreducible models. A closer look at the expansion (3.4a) shows that the large-N_f expansion may not be valid for the values of N_f considered here. For example, the second-order term is larger than the first-order term for $N_\mathrm{f} = 2$, where (3.4a) reads $1/\nu = 1 - 0.135 + 0.341$. For this reason, Janssen & Herbut [JH14] use a Padé approximation

$$[1/1]^{(1/\nu)}(N_\mathrm{f}) = \frac{584 + 27\pi^2 + 18\pi^2 N_\mathrm{f}}{632 + 27\pi^2 + 18\pi^2 N_\mathrm{f}} \tag{3.5}$$

for comparison. The notation $[1/1]^f$ stands for an approximation of the function f by the quotient of two polynomials each with degree 1. A series expansion of (3.5) leads back to (3.4a), but the rational function can provide better estimates for small values of N_f.

Only two critical exponents are given in (3.4) because the others are not independent and can be obtained from *hyperscaling relations*. Derivations for many of them are given in the book of Plischke & Bergersen [PB06]. Later, we will use for example

$$2\beta + \gamma = d\nu \quad \overset{d=3}{\Longrightarrow} \quad 2\frac{\beta}{\nu} + \frac{\gamma}{\nu} - 3 = 0, \tag{3.6}$$

where we restricted the expression to the spacetime dimension[(a)] $d = 3$. Another identity can be used to relate the exponent γ to the anomalous dimension η, which is often calculated in analytical work:

$$\frac{\gamma}{\nu} = 2 - \eta \quad \Rightarrow \quad \frac{\beta}{\nu} = \frac{1}{2}(1+\eta). \tag{3.7}$$

Further useful relations for GN are given by Hands et al. [HKK91] and proven to be satisfied up to $\mathcal{O}(1/N_\mathrm{f})$. Hands et al. [HKK93] also showed that the validity of hyperscaling is equivalent to the renormalisability of the model. Thus, it is important to check in our numerical results if these relations hold. We calculate γ/ν and β/ν independently and monitor the quality of our estimates with the identity (3.6). The third independent measurement is performed for $1/\nu$.

Finite Size Scaling and Critical Coupling

The ratios of critical exponents can be obtained by lattice simulations with methods from the theory of *finite size scaling*. Our setup is comparable to previous lattice studies of GN [Kär94; CS07] and similar models (e.g. [FJP96]). We calculate critical exponents from the scaling of thermodynamic observables with the size of the finite system, assuming that the correlation length ξ is the only relevant length scale. Good introductions can be found in the books of Landau & Binder [LB09], Plischke & Bergersen [PB06] or in more detail in the older work of Binder [Bin92]. The validity of hyperscaling relations is used when deriving the expressions cited in the following and gives another reason to check it numerically.

Before we are able to calculate critical exponents, we have to determine the critical coupling of the phase transition. Examining the fourth-order cumulant by Binder [Bin81],

$$U_\mathrm{B} = 1 - \frac{\langle \sigma^4 \rangle}{3\langle \sigma^2 \rangle^2}, \tag{3.8}$$

this can be done independently of critical exponents. Note, that the powers are taken after summation over the lattice since $\sigma = \sum_x \sigma_x$. In the symmetric phase, the distribution of the scalar field is expected to be Gaussian around zero, so that $U_\mathrm{B}(\lambda_\mathrm{GN} \gg \lambda_\mathrm{GN}^\mathrm{cr}) = 0$ for a theory with $\mathbb{Z}_2$-symmetry [CS07]. On the contrary, the value of $U_\mathrm{B}(\lambda_\mathrm{GN} \ll \lambda_\mathrm{GN}^\mathrm{cr}) = 2/3$ in the broken phase is independent of the symmetry. In a finite system, there is a smooth transition between these values. Only directly at the critical point, the value $U_\mathrm{B}(\lambda_\mathrm{GN}^\mathrm{cr})$ is independent of the system size. Thus, $\lambda_\mathrm{GN}^\mathrm{cr}$ can be obtained from the intersection points of

[(a)] In general, relations involving d are called *hyperscaling relations*, otherwise they are just called *scaling relations*.

$U_\mathrm{B}(\lambda_\mathrm{GN})$ for different lattice sizes. For very small sizes, corrections to the constant value are expected. According to Binder [Bin81], they can be described by

$$U_\mathrm{B}(L,b) = U_\mathrm{B}^\mathrm{cr}\left(1 + c\,L^{-w}\frac{1-b^{-w-\frac{1}{\nu}}}{1-b^{-\frac{1}{\nu}}}\right). \tag{3.9}$$

Here, $U_\mathrm{B}(L,b)$ is the value of the two Binder cumulants for the lattice sizes L and bL at their intersection, assuming $b > 1$. U_B^cr is the value of the Binder cumulant at the continuum critical point. We further introduced an arbitrary constant c and a correction exponent w that is a universal quantity like the critical exponents defined in table 3.1. It was recently calculated up to first order of the large-N_f expansion by Gracey [Gra17]. A similar form exists for the value of the critical coupling. Commonly, the term $1-b^{-1/\nu}$ is crudely approximated by $1/\nu \ln b$, so that plots of the data depending on $1/\ln b$ can be roughly fitted with the linear functions [Bin81; CS07]

$$U_\mathrm{B}(L,b) \approx U_\mathrm{B}^\mathrm{cr} + \frac{c_U}{\ln b} \tag{3.10}$$

$$\lambda_\mathrm{GN}^{-1}(L,b) \approx (\lambda_\mathrm{GN}^\mathrm{cr})^{-1} + \frac{c_\lambda}{\ln b}, \tag{3.11}$$

obtaining values for the coefficients c_U, c_λ as well as $U_\mathrm{B}^\mathrm{cr}, \lambda_\mathrm{GN}^\mathrm{cr}$, the continuum estimates for Binder cumulant and coupling at the critical point.

Here, a special problem arises due to the SLAC derivative because we do not simulate on cubic lattices. As mentioned in section 2.3.2, we have $V = L \times (L-1) \times (L-1)$ lattice points, making it uncertain, which value of L to take for the finite size scaling formulae. They require the validity of hyperscaling relations and the derivation of Binder [Bin81] assumes $V = L^d$. Thus, the most reasonable choice is

$$\tilde{L} = \sqrt[3]{V} = \sqrt[3]{L(L-1)^2}. \tag{3.12}$$

From a more physical point of view finite size scaling theory is based on the fact that the correlation length on the lattice is limited by the lattice size. Hence, taking $\tilde{L} = L-1$ as the smallest extent of the lattice could be a good choice. We will investigate both possibilities together with the naive choice $\tilde{L} = L$ in order to find systematic errors. In the following, we keep this problem in mind, but drop the tilde on L to make the notation clearer.

Critical Exponents from Finite Size Scaling

After obtaining $\lambda_\mathrm{GN}^\mathrm{cr}$ and U_B^cr, these values are used to evaluate Σ and its susceptibility χ. In the following, both variants are possible and we will compare results from using e.g. $\Sigma(\lambda_\mathrm{GN}^\mathrm{cr})$ and $\Sigma(U_\mathrm{B}^\mathrm{cr})$. Then, a dependence on the lattice size of the form

$$\Sigma := \langle|\sigma|\rangle \propto L^{-\frac{\beta}{\nu}} \quad \text{and} \quad \chi \propto L^{\frac{\gamma}{\nu}} \tag{3.13}$$

is expected from finite size scaling theory for sufficiently large L. In this way, we obtain the ratios β/ν and γ/ν that are related by the hyperscaling relation (3.6). As a second,

independent exponent, we measure ν because there are several possible observables that only scale with ν. One example is the slope of the Binder cumulant (3.8). It scales with

$$\frac{\partial U_\mathrm{B}}{\partial \lambda} \propto L^{\frac{1}{\nu}}. \tag{3.14}$$

The same scaling behaviour is expected for derivatives of the logarithm of the order parameter to some power. We use the particular form

$$\mathscr{D} \coloneqq \frac{\partial \ln\langle|\sigma|\rangle}{\partial \lambda} = \frac{\langle|\sigma| S_\mathrm{bos}\rangle}{\langle|\sigma|\rangle} - \langle S_\mathrm{bos}\rangle \propto L^{\frac{1}{\nu}}, \tag{3.15}$$

where S_bos is the purely bosonic part of the action corresponding to (2.32). Contrary to $\langle\sigma^2\rangle$, the scalar field is first squared and then averaged over the lattice. This observable only contains up to three powers of the scalar field and thus seems preferable to (3.14), where also higher powers must be calculated.

A similar method, sometimes called *phenomenological renormalisation* [EFM92], is to consider lattices of size L and bL and perform fits to

$$f_\lambda(\mathscr{O}) \coloneqq \ln\left(\frac{\mathscr{O}(bL, \lambda^\mathrm{cr}_\mathrm{GN})}{\mathscr{O}(L, \lambda^\mathrm{cr}_\mathrm{GN})}\right) = \omega \ln(b), \tag{3.16}$$

where $\mathscr{O} = \Sigma, \chi, \mathscr{D}$ and the corresponding exponents ω are $-\beta/\nu, \gamma/\nu$ and $1/\nu$. Corrections similar to (3.9) can be calculated. Additionally, we used (3.16) with values of the observables at fixed U^cr_B instead of $\lambda^\mathrm{cr}_\mathrm{GN}$ and call the corresponding function $f_U(\mathscr{O})$.

In the continuum theory, χ and $\mathscr{D}$ are divergent at the critical point. This is not possible in a finite volume, but both observables should have a peak which grows for increasing volume. Thus, fully independent of the estimate for $\lambda^\mathrm{cr}_\mathrm{GN}$ from the Binder cumulant, we can use the maximal values at the peaks in χ and $\mathscr{D}$ for $\mathscr{O}$ in (3.16). Similarly, we can estimate β directly from the scalar field expectation value by a fit to the defining equation

$$\Sigma \propto \left(\lambda^\mathrm{cr}_\mathrm{GN} - \lambda_\mathrm{GN}\right)^\beta. \tag{3.17}$$

This first requires an extrapolation to infinite volume. We perform this by a linear fit, checking if Σ is constant or tends to zero for $V \to \infty$. Then, we scan a range of $\lambda^\mathrm{cr}_\mathrm{GN}$ as a fixed parameter in the fit and chose the result with the smallest error in β.

In total, we can compare three different approaches, where the first two can be done either at fixed critical coupling or fixed value of U_B using a conversion from λ_GN to U_B with our measured function $U_\mathrm{B}(\lambda_\mathrm{GN})$. The methods are:

Fit λ/U_B**:** Direct linear fit to the size dependence (3.13) and (3.15) after taking the logarithm of the data points. This was used for example in [Kär94; CS07]

Ren λ/U_B**:** Phenomenological renormalisation by evaluation in terms of ratios of different lattice sizes L and bL and fits to (3.16). See for example [FJP96].

noBC: Estimation of the exponents without use of the Binder cumulant, where γ/ν and $1/\nu$ are obtained from the height of maxima in χ and $\mathscr{D}$. Σ is directly fitted to (3.17) to obtain β.

3.1.2. Interpolation and Error Estimates

With Monte Carlo simulations it is only possible to obtain values of observables at discrete couplings λ_p for $p = 1,\dots,N_\lambda$. The method of multi-histogram reweighting [FS89] allows to reuse the data from all N_λ simulations to calculate observables as a continuous function in λ, interpolating the discrete measurements. Like Kärkkäinen et al. [Kär94], we use a variation of this method, which does not need histograms. It was first described by Kajantie et al. [KKR91] and works as follows.

As input, we need measurements of the scalar field average $(1/V\sum_x \sigma_x)_{p,i}$ for all $p = 1,\dots,N_\lambda$ on every configuration $i = 1,\dots,N_p^{\text{conf}}$ as well as the part of the action that is proportional to the coupling. For GN, the latter is given by $H_{p,i} := (1/2\sum_x \sigma_x^2)_{p,i}$, the bosonic action divided by the coupling. Then, one solves the following system of equations for the free energy f_p at λ_p:

$$\mathrm{e}^{-f_p} = \sum_{q=1}^{N_\lambda} \sum_{i=1}^{N_q^{\text{conf}}} P\big(\lambda_p, H_{q,i}\big), \tag{3.18a}$$

$$P\big(\lambda, H_{q,i}\big) = \frac{\omega_q \mathrm{e}^{-\lambda H_{q,i}}}{\sum_r \omega_r N_r^{\text{conf}} \mathrm{e}^{-\lambda_r H_{q,i} + f_r}}. \tag{3.18b}$$

Here, additional weights $\omega_p = (1+2\tau_p)^{-1}$ can be used to take the autocorrelation time τ_p into account. We will introduce it in (3.21). Then, $\omega_p N_p^{\text{conf}}$ is an estimate for the number of uncorrelated configurations at coupling λ_p.

For any observable that is only a function of the scalar field, we can use (3.18b) to evaluate it at arbitrary λ. Once the f_p are determined, it is given by

$$\langle \mathscr{O} \rangle(\lambda) = \frac{\sum_{p,i} \mathscr{O}\big(\sigma_{p,i}\big) P\big(\lambda, H_{p,i}\big)}{\sum_{q,j} P\big(\lambda, H_{q,j}\big)}. \tag{3.19}$$

We use this procedure to calculate $\langle|\sigma|\rangle, \langle\sigma^2\rangle, \langle\sigma^4\rangle, \langle S_{\text{bos}}\rangle$ and $\langle|\sigma| S_{\text{bos}}\rangle$ as functions of λ. With these expectation values, we can calculate interpolations for the susceptibility χ (3.2), the Binder cumulant U_{B} (3.8) and the logarithmic derivative of the order parameter $\mathscr{D}$ (3.15).

Since the values $H_{q,i}$ can be very large and grow with the lattice volume, it is beneficial for the numerical evaluation to rewrite (3.18b) as

$$P\big(\lambda, H_{q,i}\big) = \omega_q \left[\sum_r \omega_r N_r^{\text{conf}} \mathrm{e}^{H_{q,i}(\lambda-\lambda_r)+f_r}\right]^{-1}. \tag{3.20}$$

The `C`-code[(b)] written to calculate interpolations evaluates the exponentials with data type `long double`, which has an extended precision and range using 80 bits[(c)]. This was sufficient to obtain interpolations over a reasonable range of λ for all lattice sizes studied here. In addition, the system of equations (3.18b) allows a constant shift in all f_p, allowing to fix one parameter (for example f_1) at an arbitrary value. This reduces the number of equations to solve by one. For the problem at hand, we perform a first run with $f_1 = 0$ to determine the full solution. For further solutions on resampled data, that we need in the next paragraph to obtain error estimates, we set $f_1 = -1/2 f_{N_\lambda}$, leading to a solution where the f_p are distributed symmetrically around zero. This slightly increases the performance and prevents numerical overflows in the exponentials, hence allowing interpolations over a longer range in λ. Besides that, a solution of the system can be obtained with a few ($\mathcal{O}(10)$) iterations of a standard solver for non-linear equations. The current implementation uses a multidimensional root finding algorithm of the freely available `GNU Scientific Library`.

Error Estimates

Common methods to estimate statistical errors in lattice field theory calculations are Jackknife- and Bootstrap-resampling together with a binning of the data. See the book of Gattringer & Lang [GL10] for a short introduction. All data points directly obtained from a simulation are given with a Jackknife error estimate of one standard deviation calculated in the simulation program.

For the calculation of the critical coupling and critical exponents, the whole procedure described above is performed within a binned Bootstrap process, allowing a greater flexibility than the Jackknife method. With a single set of lattice size and flavour, it proceeds as follows:

1. Divide the dataset of N_p^{conf} configurations for each λ_p into bins of size N_{bin}. This is done to reduce the correlation of configurations. In the following evaluation, we use $N_{\text{bin}} = 50$.

2. Create N_{boot} samples for each λ_p, where each sample has the original number of N_p^{conf} configurations but consists of randomly chosen bins.

3. Calculate N_{boot} interpolations, one for each set of samples.

Afterwards one can calculate a statistical error with the usual Bootstrap formula (see e.g. [GL10]) for every point of the interpolation, but we will continue with the interpolation samples on the randomly arranged bins. Performing the whole evaluation of critical exponents on a large set of resampled data allows us to obtain reliable estimates of the statistical errors for our final measurements. We repeat the three steps with each of the N_{lat} lattice

[(b)] The source code of the implementation can be obtained from `https://github.com/daniel-schmidt/HistogramReweighting`.

[(c)] This number of bits can depend on compiler implementation and system architecture.

sizes available for a given N_f. For a single run of the finite size scaling analysis, we now need a single interpolation from each lattice size. Building all possible combinations of samples from the different lattices gives a total of $N_\mathrm{tot} = N_\mathrm{boot}^{N_\mathrm{lat}}$ combinations of interpolations. Performing the evaluation on all of these samples is not feasible given our amount of data (usually $N_\mathrm{boot} = 1000$ and $N_\mathrm{lat} = 7$). We use another random choice, so that the implemented algorithm is:

1. Randomly select a combination of interpolations from the N_tot possible combinations, e.g. by generating N_lat random indices in the range from 1 to N_boot.

2. Obtain an estimate of $\left(\lambda_\mathrm{GN}^\mathrm{cr}, U_\mathrm{B}^\mathrm{cr}\right)$ by intersecting the interpolated Binder cumulants of the chosen combination.

3. Calculate an estimate of the critical exponents with the other observables Σ, χ and $\mathscr{D}$ of the same combination, possibly using either $\lambda_\mathrm{GN}^\mathrm{cr}$ or U_B^cr.

Repeating this $N_\mathrm{hist} = 10^4$ times[(d)], we get histograms of critical values and exponents. Then, the best estimate is given by the mean of all N_hist values with a statistical error given by the standard deviation of the data.

Integrated Autocorrelation Time

To include a weight for the different λ_p in the interpolation (3.18), we calculate the integrated autocorrelation time τ of $|\sigma|$ with an `octave` code from [Wol04; Wol07; SSV11]. It calculates τ from the autocorrelation function $\Gamma(t)$, which depends on the separation t between the configuration numbers. As usual it is defined by [GL10]

$$\tau = \frac{1}{2} + \sum_{t=1}^{W-1} \frac{\Gamma(t)}{\Gamma(0)}, \tag{3.21}$$

and the algorithm tries to find an optimal cutoff W to minimize systematic as well as statistical errors.

3.2. Simulation Results for the Reducible Model

In this section, we numerically explore the reducible GN and calculate critical exponents for $N_\mathrm{f} = 1, 2, 4$ and 8. Since there is no sign problem in this model (see section 2.4.2), we use the rHMC algorithm explained in section 2.3.1. A first run with an rHMC trajectory length of 0.6 showed large autocorrelations in σ, preventing reliable estimates for the critical coupling. An increase to 3.0 on smaller lattices ($L \leq 16$) and 5.0 on $L \geq 20$ was necessary to ensure independent configurations when performing 10 intermediate updates between measurements. We tuned the parameters of the algorithm to achieve an acceptance rate of more than 80%.

[(d)] Larger numbers like $N_\mathrm{hist} = 5 \cdot 10^4$ are possible but do not give better error estimates.

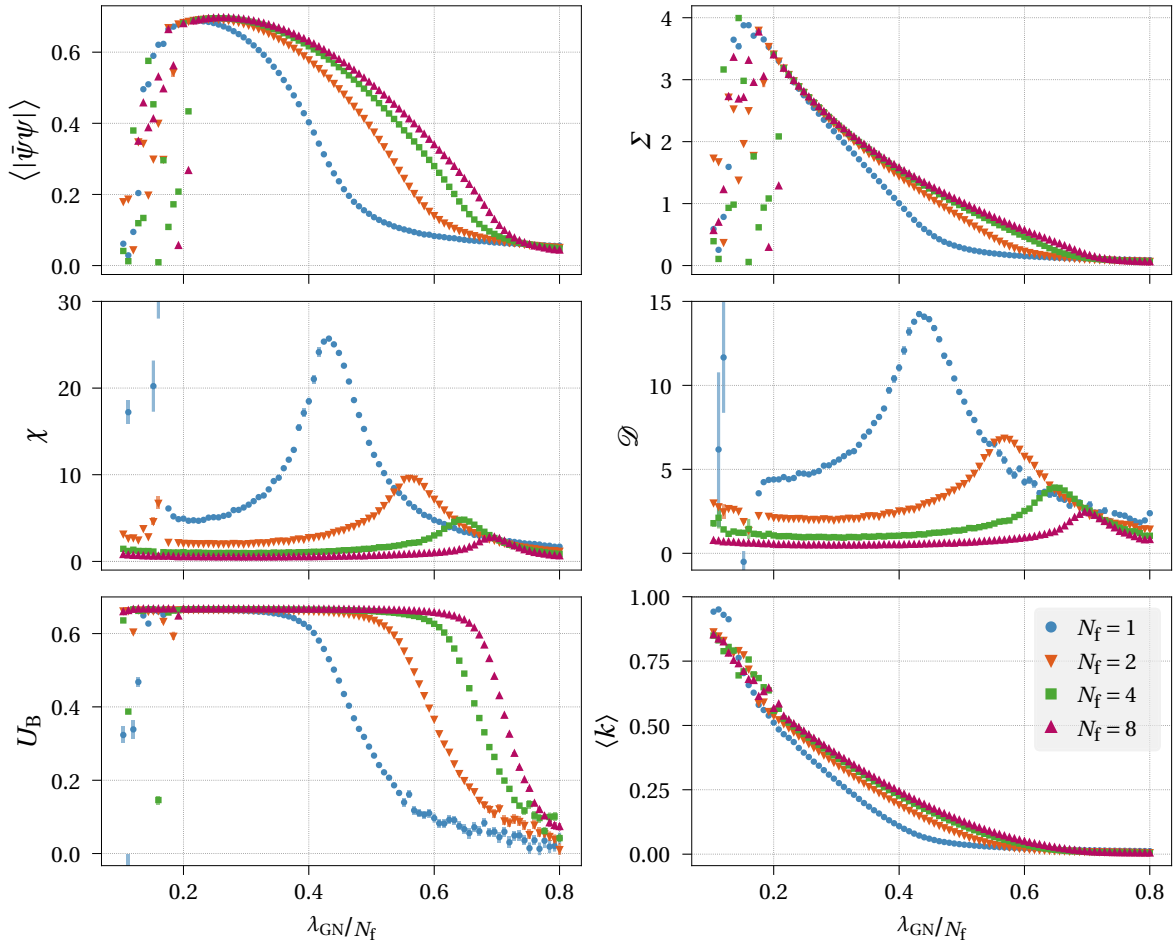

Figure 3.1.: Observables in GN as a function of λ_{GN} for various N_f on lattice size 8. The first row shows expectation values of absolute values of the chiral condensate $\langle|\bar{\psi}\psi|\rangle$ and the scalar field Σ. The second row displays the scalar field susceptibility χ from (3.2) and the derivative of the logarithm of the scalar field expectation value $\mathscr{D}$ from (3.15). The last row shows the Binder cumulant U_B from (3.8) and the lattice filling factor $\langle k\rangle$ defined in (2.55). Most errors are smaller than the symbol size. The large fluctuations for $\lambda_{GN} \lesssim 0.2N_f$ are due to insufficient thermalisation (see figure 3.2) and Pauli blocking on the lattice. Not all points in this region are visible in the plot range.

We begin with a general presentation of the observables in section 3.2.1, qualitatively investigating the general behaviour including dependence on flavour number and lattice size. Additionally, remarks about the interpolation procedure are given. Afterwards, section 3.2.2 compares different methods to calculate the critical coupling and gives estimates for all four flavour numbers we investigate. Quantitative results for the critical exponents are given in section 3.2.3, where different approaches are compared again. In the present section, we mainly focus on various evaluation methods. Later, in section 3.3, our best estimates are compared to literature values.

3.2.1. General Observations

We first present an overview of the observables for GN on lattice size 8, where it is easy to obtain a large number of configurations for many couplings. The results as a function of

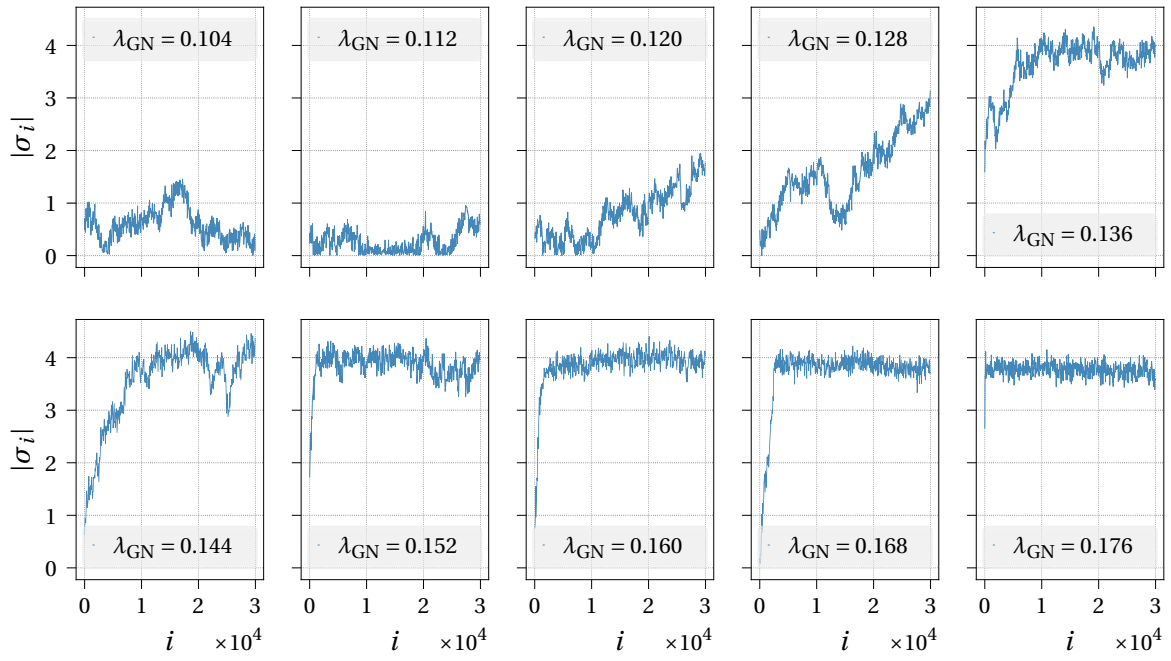

Figure 3.2.: HMC history of scalar field values at strong couplings. To make the images clearer, only every 50th measurement is shown.

λ_{GN} for varying N_f are given in figure 3.1. As expected, Σ, the absolute value of the scalar field, tends to zero for large λ_{GN} (weak coupling) and shows a region with non-zero expectation value for stronger coupling, signalling χSB. The value of Σ grows linearly with the interaction strength, but for very strong couplings ($\lambda_{GN} < 0.15$ for $N_f = 1$), large fluctuations and a sharp decrease are present. Looking at the scalar field values on single configurations of the ensembles in figure 3.2, we find a problem with the thermalisation of the system at very strong couplings. While only a few updates are needed to reach equilibrium for weak couplings, about 10^4 are necessary for $\lambda_{GN} = 0.136$ and $\lambda_{GN} = 0.144$ until the scalar field shows a fluctuation around an average value close to 4. Correspondingly, the integrated autocorrelation time (not shown here) is of order 10^3 for $N_f = 1$ and 2. There seems to be a saturation of the average value at these couplings and a linear growth is no longer observed. For even smaller couplings, there is still a tendency to grow at least for $\lambda_{GN} = 0.12$ and $\lambda_{GN} = 0.128$, but no thermalisation was reached within $3 \cdot 10^4$ updates. Since the chiral condensate is proportional to $\lambda_{GN}\langle\sigma\rangle$ by (3.1), the saturation of $\langle\sigma\rangle$ leads to a non-monotonic condensate approaching zero in the $\lambda_{GN} \to 0$ limit. All other observables show unreliable values in this region due to the insufficient thermalisation. Regarding the lattice filling factor defined in (2.55) and shown in the bottom right of figure 3.1, we find the onset of thermalisation problems above half filling around $\lambda_{GN} = 0.2N_f$. For larger λ_{GN}, the lattice filling decreases smoothly. It approaches zero in the region of the critical point, indicating that the symmetric phase is dominated by free fermions. In conclusion, the lattice filling factor suggests three phases: a phase of lattice artefacts with very long autocorrelations, when more than half of the fermions are interacting, a strongly interacting phase with broken chiral symmetry and a symmetric phase with almost no fermion interaction.

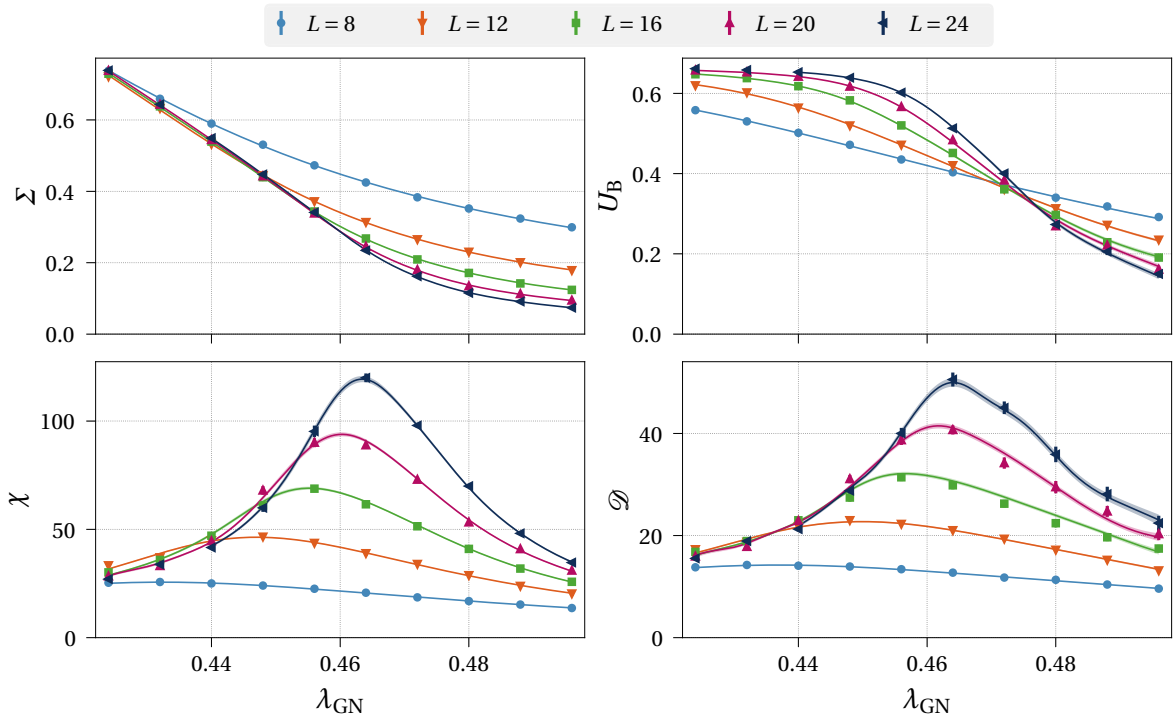

3.3(a) $N_f = 1$

Outside of the artefact phase, we find the expected behaviour in figure 3.1: The Binder cumulant approaches the values of $2/3$ in the broken and 0 in the symmetric phase with a transition in the critical region. This region is also marked by a peak in both susceptibility χ and logarithmic derivative of the scalar field expectation value $\mathscr{D}$. The integrated autocorrelation time is of $\mathcal{O}(1)$ for all couplings outside the problematic region.

Dependence on the Flavour Number

When increasing the flavour number, we observe a growing value of λ_{GN}^{cr}/N_f in figure 3.1, moving the critical point away from the artefact phase. The scalar field in the linear regime grows slower the larger the value of N_f, indicating a changing critical exponent β. This is consistent with smaller peaks in the susceptibility and the logarithmic derivative, also indicating a weaker phase transition for increasing N_f. A detailed analysis of the critical exponents can be found in section 3.2.3. Despite the change in the critical coupling, the saturation phase sets in around the same coupling. Independently of N_f, the observed scalar field averages for $\lambda_{GN} \lesssim 0.24 N_f$ are very close to each other if the ensemble was able to thermalise. Note, that the changes in Σ from $N_f = 4$ to $N_f = 8$ are already small, indicating that we approach the large-N_f regime. This is reasonable because the expansion (3.4) is done in $1/n$, counting all spinor components so that $n = 32$ for $N_f = 8$. Regarding the computational cost, the necessary simulation time for a fixed number of configurations increases approximately linearly with N_f.

Dependence on the Lattice Size, Statistical Errors and Interpolation

An overview of the finite size scaling behaviour of the observables near the critical point is given in figure 3.3 for $N_f = 1$ and 2. Similar graphics for $N_f = 4$ and 8 are given in figure C.1

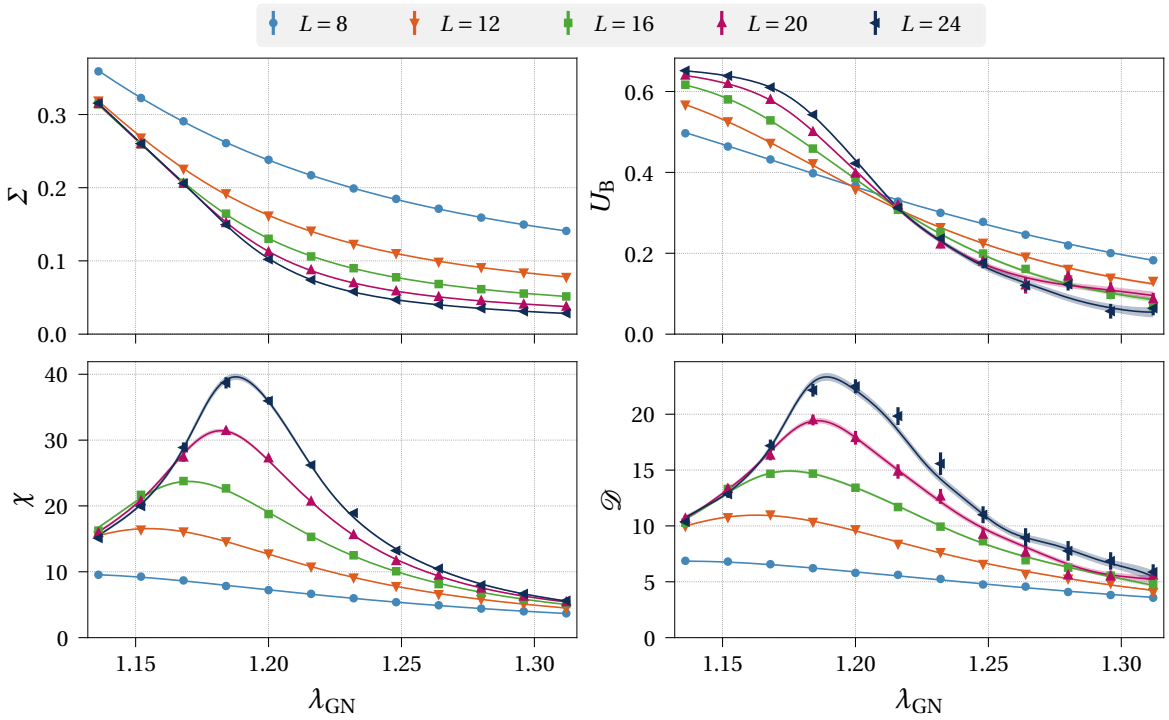

3.3(b) $N_f = 2$

Figure 3.3.: Raw data and interpolations for GN observables. Symbols indicate the measured data points with error bars, while lines denote the interpolation obtained with histogram reweighting. An error estimate for the interpolation is given by a shaded band around the main line.

of appendix C. Data points from simulations are shown together with an interpolation calculated by the algorithm described in section 3.1.2. Both have error estimates obtained by a resampling method. Here, we show simulations with evenly spaced lattice sizes $L = 8, 12, 16, 20$ and 24 for all flavours on a number of couplings near the critical point. Additional lattice sizes $L = 10$ and 14 will be included in section 3.2.2 and 3.2.3 to reduce errors when determining critical couplings and exponents. A simulation with $N_f = 1$ and $L = 32$ was also performed, but is too noisy to increase the quality of our exponent estimates. We mainly use it to check for systematic errors. The numbers of configurations we measured is given in detail in appendix C (see table C.1). It is usually 10^4 or larger for $L \leq 16$ and between $1.5 \cdot 10^3$ and 10^4 for $L \geq 20$.

Despite the changes in the critical coupling and the heights of peaks, the general behaviour is the same for all N_f investigated here. The absolute value of the scalar field shows a clear scaling region, where the value decreases to zero with increasing lattice size, while the different curves join for increasing coupling strength and are very similar for smaller λ_{GN}. Deviations from scaling are large for $L = 8$, but already $L = 12$ is much closer to the infinite volume limit.

We are able to find a small common region of intersection in the Binder cumulant, indicating the critical coupling. It is analysed in detail in section 3.2.2. The asymptotic value of $2/3$ for strong coupling is reached quickly for lattice sizes of 16 and larger, showing a good finite size scaling. On the other side of the intersection (in the symmetric phase),

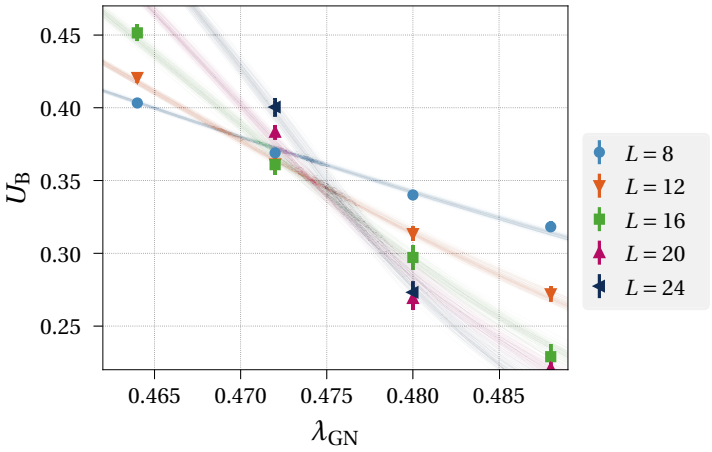

Figure 3.4.: Binder cumulant detail near the critical coupling for $N_f = 1$. Data points from simulations are shown together with interpolations (transparent, thin lines) of resampled data. Extrapolating the intersections to the continuum, the critical coupling is estimated by 0.4751(4), see figure 3.6(b) and table 3.2.

statistical errors in the Binder cumulant are much larger than in the broken regime. This can make it difficult to find a unique intersection between adjacent lattice sizes, especially for $L = 20$ and 24, where a smaller number of configurations is available. It also obscures the scaling and may even lead to negative average values of U_B. Nevertheless, we mostly observe the correct approach to zero when increasing L at fixed coupling.

The logarithmic derivative is also affected by larger errors in the symmetric phase on the largest lattice sizes. Both observables depend on higher powers of the scalar field (third power for $\mathscr{D}$ and fourth power for U_B), which can amplify fluctuations. On the contrary, the errors in the susceptibility are very small, but both χ and $\mathscr{D}$ show the expected qualitative behaviour. They both have a peak, which grows approximately constantly with increasing lattice size. The quantitative analysis in section 3.2.3 will lead to estimates for γ/ν and $1/\nu$. The position of the peak moves to weaker couplings when increasing the lattice size, in agreement with the intersection points in U_B and the roughly non-zero values in Σ. Likely, the critical inverse coupling on a finite lattice is always smaller than the infinite volume counterpart.

The interpolation with histogram reweighting tends to show undesirable oscillations in the symmetrical phase for U_B and $\mathscr{D}$, whenever we found large statistical errors in the data. Indeed, the oscillations can be decreased by interpolating ensembles with better statistics. This implies that we need a large number of configurations also on larger lattice sizes, where simulations are expensive. For example, more than 1000 configurations are necessary for $L = 24$ to obtain data with sufficient quality. Apart from this, the interpolation allows to obtain smooth curves that fit the data almost everywhere within the error bars. Especially the susceptibility is fitted well and the maximum of the peak in the interpolation seems reasonable, even if only a few data points are available.

3.2.2. Binder Cumulant and Critical Coupling

Now, we go on to a detailed evaluation of the lattice size dependence to calculate the critical coupling and the value of the Binder cumulant at criticality. A close-up of the critical region for $N_f = 1$ and a selection of L is given in figure 3.4, also showing a selection

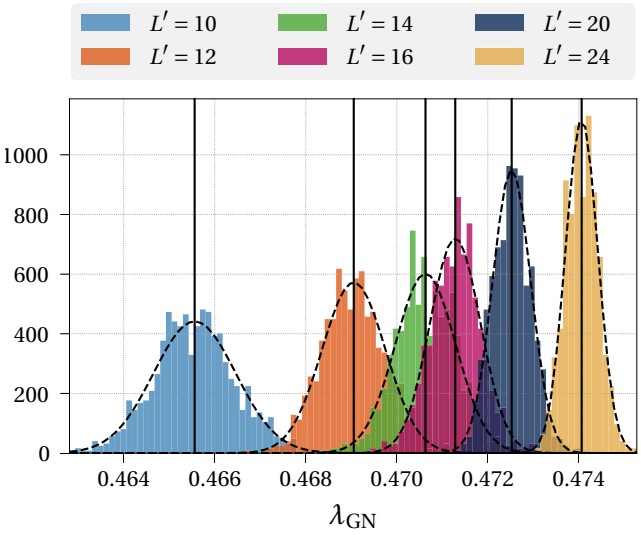

Figure 3.5.: Histograms of intersections of U_B for $N_f = 1$. Each interpolation of resampled data for lattice size $L = 8$ was intersected with all interpolations from each $L' > L$. The different colours represent different pairs L, L'. The dashed black lines give a normal distribution with mean and standard deviation of the data in each histogram. The mean value of each set of intersections gives an estimate for the critical coupling and is marked by a solid vertical line.

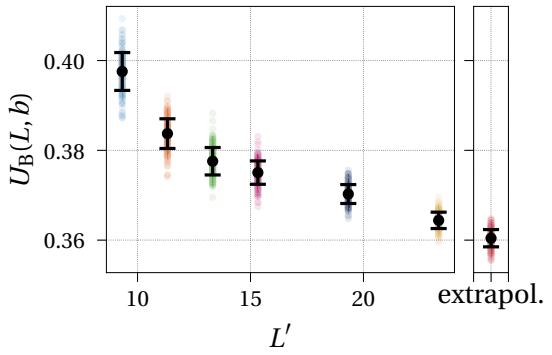

3.6(a) Critical value of the Binder cumulant.

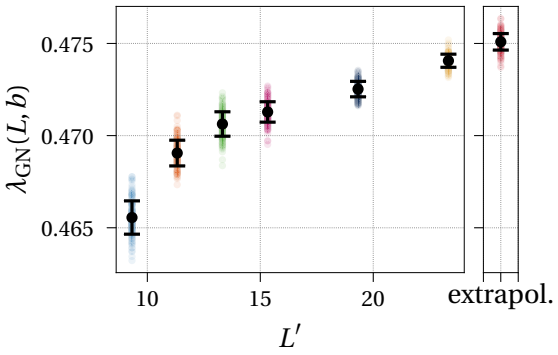

3.6(b) Critical coupling.

Figure 3.6.: Data from intersections of the Binder cumulant for $N_f = 1$ and $L = \sqrt[3]{8 \cdot 7^2}$. For each lattice size $L' = \sqrt[3]{V'}$ intersection points are shown together with mean and standard deviation similar to the histograms in figure 3.5. The extrapolations were obtained by fitting combinations of single points to (3.11).

of trajectories on the resampled data blocks. Clearly visible, the intersection of a curve with the one of the subsequent lattice size moves to larger λ_{GN} and smaller U_B. Keeping the smallest lattice size L fixed, we determine the intersection with every size $L' > L$. As described in section 3.1.2, we do this with a set of $N_{hist} = 10^4$ random combinations of single interpolations on resampled data sets. The resulting histograms for the critical inverse coupling are given in figure 3.5. Gaussian probability distributions fit well to the histograms and the mean indeed moves to larger λ_{GN} for increasing L'.

Next, we extrapolate each data set to infinite volume values for λ_{GN}^{cr} and U_B^{cr}. Varying also the smallest lattice size and trying to fit the scaling law with corrections (3.9) did not lead to reasonable and stable results, so that the rough approximation (3.11) of linear fits to $U_B(L, b)$ or $\lambda_{GN}(L, b)$ vs. $1/\ln b$ was used. Again, b is the ratio of two lattice sizes $L' = bL$, keeping L fixed. The result of the extrapolation is close to the intersection of the smallest with the largest lattice and can be found together with the data at various L' in figure 3.6. Numbers estimated with this procedure together with their statistical error are given in

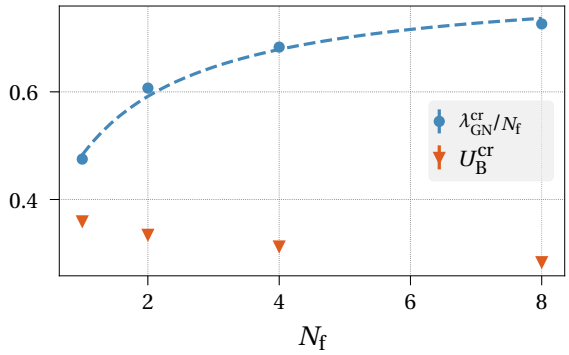

Figure 3.7.: Critical coupling and Binder cumulant value for various N_f. Errors are smaller than the symbol size and can be found in table 3.2. The dashed line shows the fit result (3.22) to the N_f-dependence expected for λ_{GN}^{cr} from the $1/N_f$ expansion.

figure 3.7 and table 3.2 for all four flavour numbers. It is known from the large-N_f expansion, that the inverse critical coupling should depend on N_f via $\lambda_{GN}^{cr} \propto N_f^2/N_f+1$ [HKK91]. Allowing an additive and a multiplicative renormalisation for our inverse critical lattice coupling, we indeed found a good fit of

$$\frac{\lambda_{GN}^{cr}(N_f)}{N_f} = 0.16(4) + \frac{0.65(5)N_f}{1+N_f} \xrightarrow{N_f\to\infty} 0.81(9) \tag{3.22}$$

to our data points. It is also shown as a dashed line in figure 3.7.

Systematic Errors

To investigate sources of systematic errors, we compared diverse methods to evaluate the data. No significant deviation was found testing the different possibilities to define the lattice size (see (3.12)). Hence, we use the third root of the volume for L and L'. Secondly, we can compare various evaluation methods. Estimates for λ_{GN}^{cr} and U_B^{cr} from the Binder cumulant intersection and from direct continuum extrapolations of Σ are shown in figure 3.8. To investigate a third source of systematic errors, the evaluation for both methods was also carried out without the smallest ($L = 8$) and the two smallest ($L = 8$ and $L = 10$) lattices. While the direct estimation does not depend much on the smallest lattice sizes, the Binder cumulant method does. The mean value moves to larger couplings and smaller U_B^{cr} when leaving out small lattices or adding $L = 32$ for $N_f = 1$. This shift of the intersection points can be seen directly in figure 3.4 and indicates deviations from the finite size scaling predictions. Corrections for the smaller lattices seem to be necessary, but fits to (3.9) were not successful. In general, the Binder cumulant method underestimates the continuum value of λ_{GN}^{cr} and overestimates the value of U_B^{cr}. Comparing the two different methods, results for $N_f = 1$ mostly agree well within the errors, while the lattice size dependence of λ_{GN}^{cr} is much stronger for $N_f \geq 2$. Figures for $N_f = 4$ and 8 can be found in figure C.2.

Table 3.2.: Results for λ_{GN}^{cr} and U_B^{cr} for $N_f = 1, 2, 4$ and 8. Values were obtained by a continuum extrapolation of intersections of the Binder cumulants on various lattice sizes as given in figure 3.6.

N_f	λ_{GN}^{cr}	λ_{GN}^{cr}/N_f	U_B^{cr}
1	0.4751(4)	0.4751(4)	0.3603(19)
2	1.2141(10)	0.6071(5)	0.3353(21)
4	2.7329(26)	0.6832(6)	0.3136(32)
8	5.810(4)	0.7263(5)	0.2844(34)

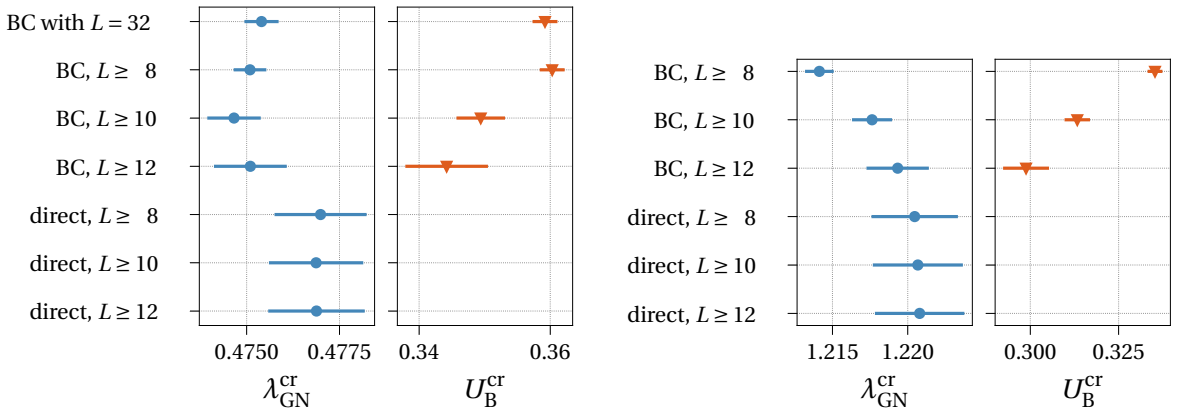

3.8(a) $N_f = 1$ **3.8(b)** $N_f = 2$

Figure 3.8.: Comparison of λ_{GN}^{cr} and U_B^{cr} for different methods. The critical coupling can be obtained from the intersection of Binder cumulants (BC), where also U_B^{cr} can be calculated, or by a direct extrapolation of Σ without using U_B. Results are given with the full set of L available and with smaller sets leaving out lattice size 8 or 8 and 10. For $N_f = 1$, we also show the resulting value for BC when including $L = 32$.

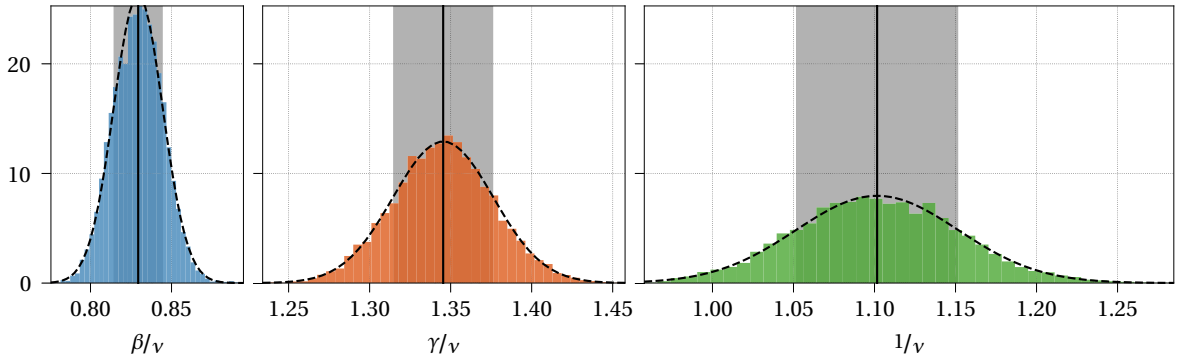

Figure 3.9.: Histograms of estimates for the critical exponents for $N_f = 1$. The dashed lines show Gaussian fits to the data having mean and standard deviation indicated by the vertical line and the shaded area. The resulting values for all N_f are given in table 3.3.

3.2.3. Critical Exponents

We first present results from the phenomenological renormalisation method **Ren**$_U$ (see section 3.1.1) with observables as a function of U_B, where we found the best fulfilment of the hyperscaling relation (3.6). A comparison with the other methods follows. Similarly to the evaluation of the critical coupling, we determine critical exponents on each of the $N_{hist} = 10^4$ samples of our resampled data and obtain histograms to estimate the statistical error in the exponents. As an example, results for $N_f = 1$ are given in figure 3.9. The distribution is Gaussian and the one for $1/\nu$ shows the largest standard deviation due to the fluctuations in $\mathscr{D}$ observed in section 3.2.1.

An example for one of the N_{hist} evaluations is shown in figure 3.10. We take as many values as possible for the smallest lattice size L, e.g. $L = 8, 10, 12$ and 14 so that enough larger lattices remain. For Σ, χ and $\mathscr{D}$ we perform linear fits with each given L to (3.16), obtaining the three critical exponents $-\beta/\nu, \gamma/\nu$ and $1/\nu$ from the slopes. As can be seen in

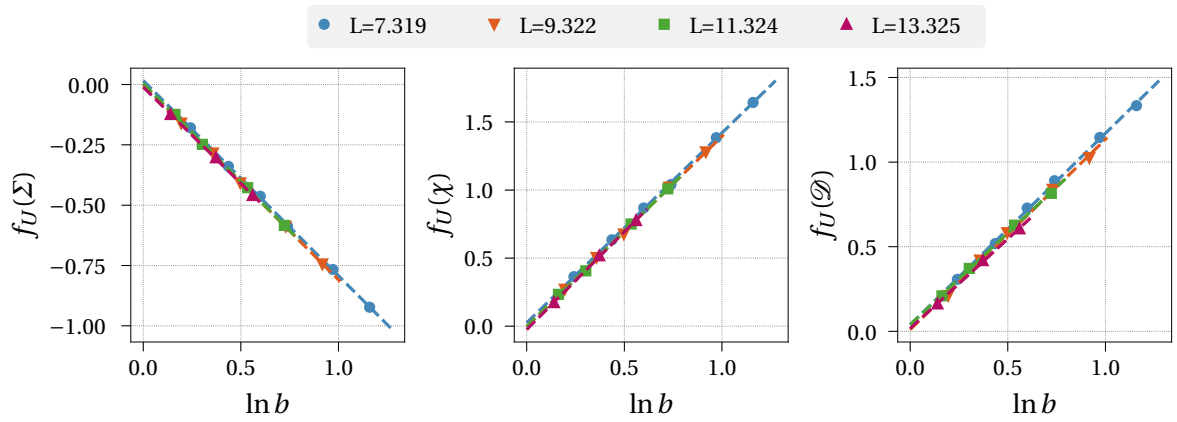

Figure 3.10.: Example for fits to obtain critical exponents for $N_f = 1$. Each figure shows the logarithm of observables at lattice size L and bL as a function of $\ln b$. The third root of the volume is used as lattice size. Different colours and symbols indicate different values for L. According to (3.16), the slope of the fits (dashed lines) gives the critical exponents $-\beta/\nu, \gamma/\nu$ and $1/\nu$ from left to right.

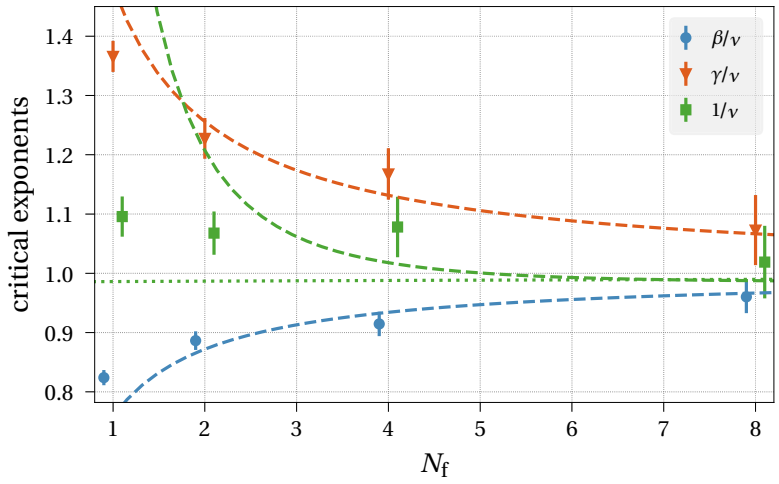

Figure 3.11.: Critical exponents for various N_f. The dashed lines represent the $1/N_f$-expansion results given in (3.4), whereas the dotted green line corresponds to the Padé approximation for $1/\nu$ given in (3.5). A small horizontal offset was added to the data points making them better distinguishable.

figure 3.10, the slopes of the fits are quite stable against variations of L. Thus, corrections to the finite size scaling behaviour are not necessary and we take the average value of the slopes for all L as estimate for the critical exponent. Repeating this with $N_{\text{hist}} = 10^4$ samples, we obtained the histograms in figure 3.9.

The results for our four values of N_f are presented in table 3.3 and figure 3.11. The latter also displays the second-order large-N_f formulae (3.4) with dashed lines and the Padé approximation for $1/\nu$ in (3.5) with a dotted line. We observe, that our results follow the general trend of the large-N_f expansion with decreasing γ/ν and $1/\nu$ for increasing N_f, while

Table 3.3.: Best estimates of critical exponents for various N_f. The last column gives the result of the hyperscaling relation (3.6) and should be zero. All values were obtained with the $\mathbf{Ren}_U$ method.

N_f	$1/\nu$	β/ν	γ/ν	$2\beta/\nu+\gamma/\nu-3$
1	1.096(34)	0.824(13)	1.366(26)	0.01(4)
2	1.07(4)	0.886(16)	1.228(34)	0.00(5)
4	1.08(5)	0.915(21)	1.17(4)	0.00(6)
8	1.02(6)	0.960(28)	1.07(6)	−0.01(8)

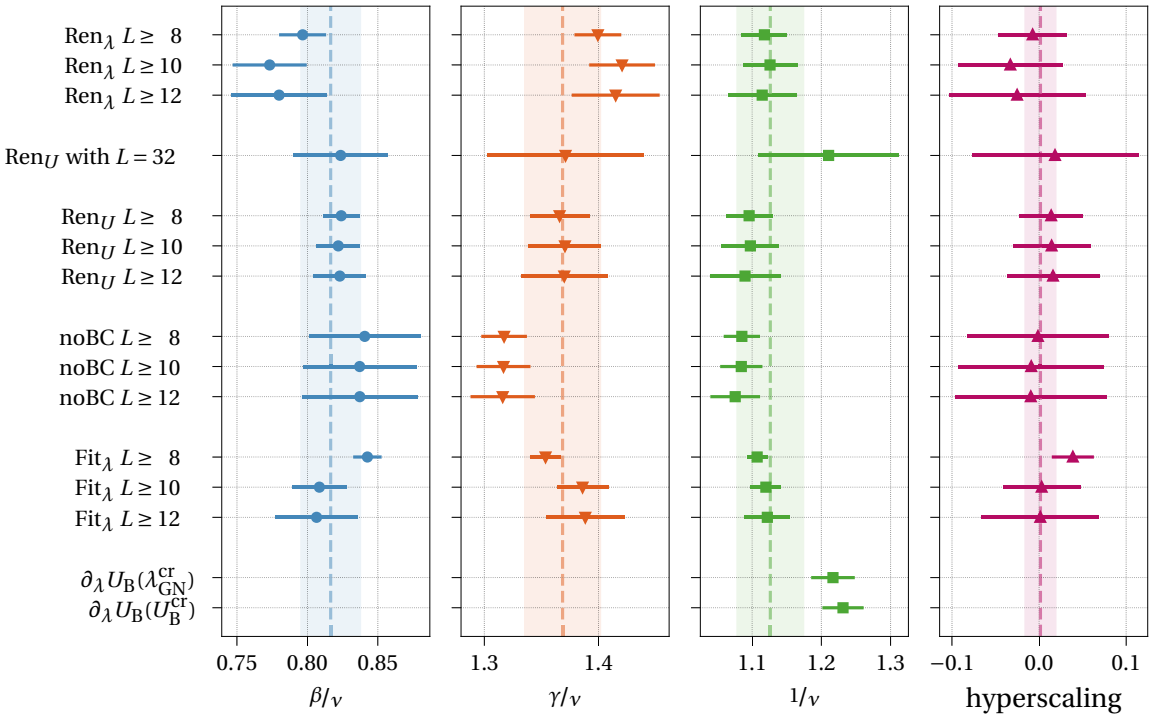

3.12(a) $N_f = 1$

Figure 3.12.: Comparison of different methods to evaluate critical exponents. For each method, evaluations excluding the smallest one or two lattice sizes are given. The last plot on the right shows the fulfilment of the hyperscaling relation (3.6) and should be zero. The data shown in these plots can be found in table C.2.

β/ν increases. Deviations from the dashed lines are large for $N_f = 1$ and still relevant for $N_f = 2$, especially for $1/\nu$. For $N_f = 4$, we are already near the expansion within our statistical errors and a good match is found for $N_f = 8$. The Padé approximation (3.5) does not fit well to our results for $N_f \leq 4$. In contrast to our data, it decreases for $N_f \to 1$ and is below 1. On the other hand, also the large-N_f prediction of $1/\nu$ with $N_f < 4$ seems not reliable, as it predicts much larger values than we found in our simulation. At $N_f = 8$, we are still able to resolve the small deviation of the large-N_f expansion from the limit $N_f \to \infty$, where all exponents have the value 1. At least our estimates for β/ν and γ/ν are more than one standard deviation away from this value.

Systematic errors

In figure 3.12(a), an overview of critical exponents for $N_f = 1$ obtained by the different methods explained in section 3.1.1 is given together with results omitting smaller lattice sizes. For the latter case, we only find larger changes for **Fit**$_\lambda$ when calculating the exponents without smaller lattices. This impairs the good results for the full data set, where the smallest statistical errors are present. Additionally, the hyperscaling relation is badly fulfilled when including all data, casting further doubt on this method. The other methods perform better when skipping smaller lattices because they depend on the factor $b = L'/L$ and already use multiple small lattices (see for example figure 3.10). Regarding our results

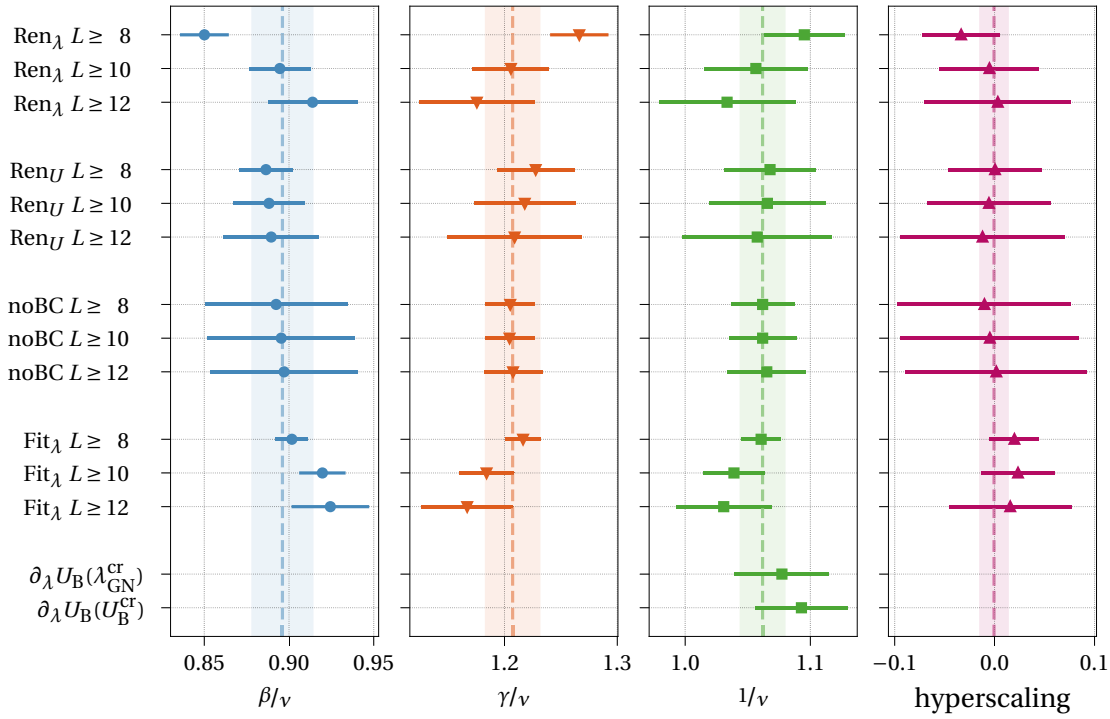

3.12(b) $N_f = 2$

for $N_f = 1$, the best choice is **Ren**$_U$, where statistical errors are comparably small and the hyperscaling relation is better fulfilled than for **Ren**$_\lambda$. The direct estimates of critical exponents without Binder cumulant (**noBC**) give slightly different results, especially for γ/ν. Likewise, the evaluation of the Binder cumulant slope (3.14) deviates from the other results for $N_f = 1$, leading to larger values. Including lattice size 32 for **Ren**$_U$, we only observe larger error bars for β/ν and γ/ν, while the mean value for $1/\nu$ is larger than without $L = 32$.

The situation is similar for larger N_f, see for example figure 3.12(b) for $N_f = 2$. Additional plots are given in the appendix, where $N_f = 4$ can be found in figure C.3(a) and $N_f = 8$ in figure C.3(b). In all cases, we find the smallest statistical errors in **Fit**$_\lambda$ accompanied by large lattice size dependence and slight violation of the hyperscaling relation. **Ren**$_U$, the phenomenological renormalisation depending on U_B, seems preferable, also over the same procedure depending on λ_{GN}, because it produces the most stable results with best accuracy of the hyperscaling relation. In contrast to $N_f = 1$, better agreement with the results from **noBC** and the Binder cumulant slope is found.

3.3. Discussion and Comparison With Previous Results

In this section we compare our findings of section 3.2 with previously obtained values for the critical exponents. They are universal quantities and can be compared directly to results from other calculations. There is a lot of literature available on the chiral Ising universality class of the $\mathbb{Z}_2$-symmetry-breaking transition of GN. While some authors discuss exactly

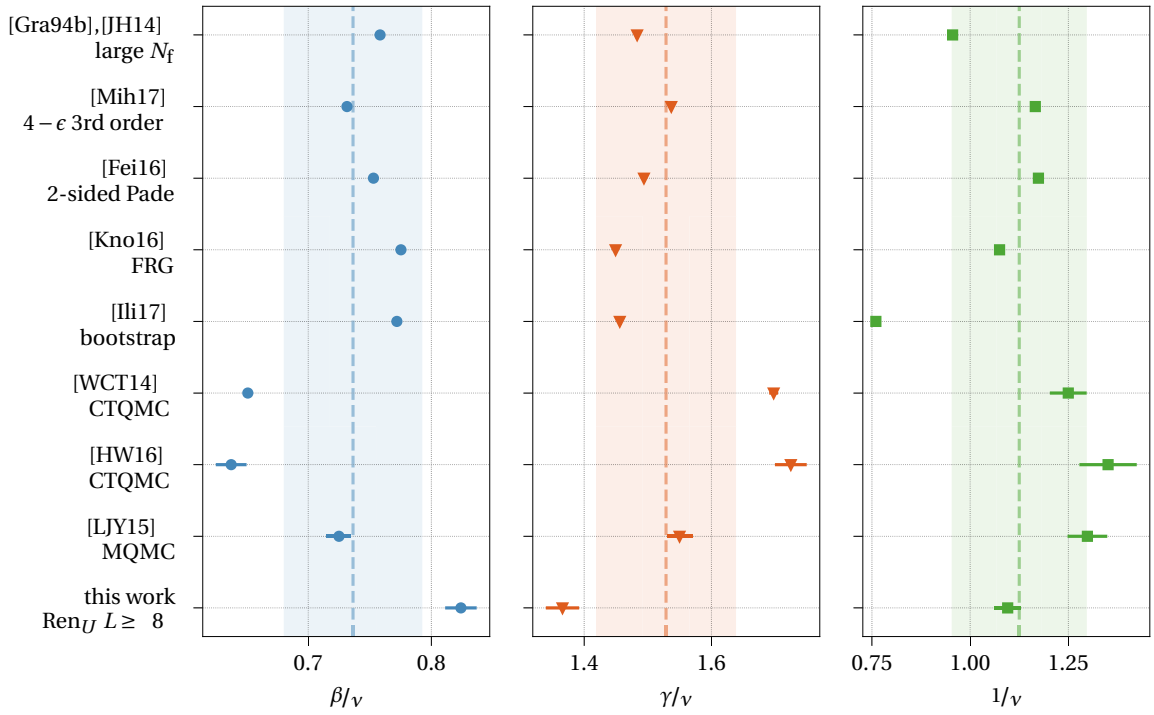

3.13(a) $N_f = 1$

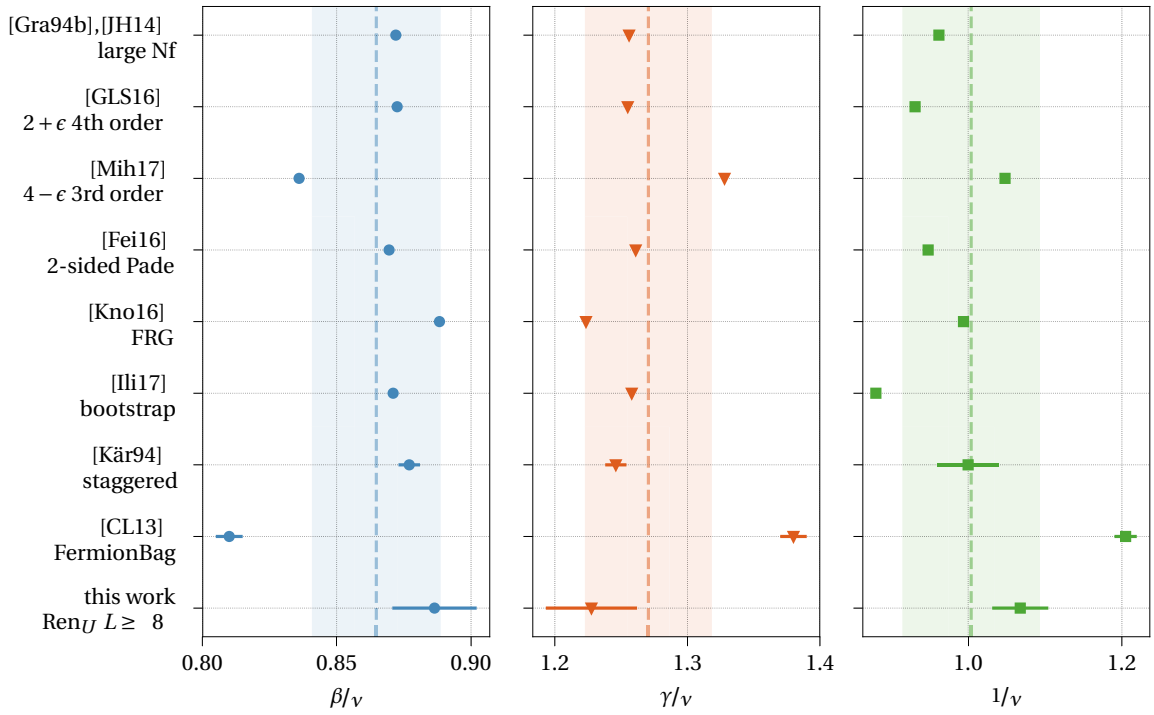

3.13(b) $N_f = 2$

Figure 3.13.: Comparison of our critical exponents with results from the literature. Only the most recent results are given for the analytical works. The vertical dashed lines give an overall average with a standard deviation indicated by the shaded area. No literature values for $N_f = 8$ are available. The data shown in these plots can be found in table C.2.

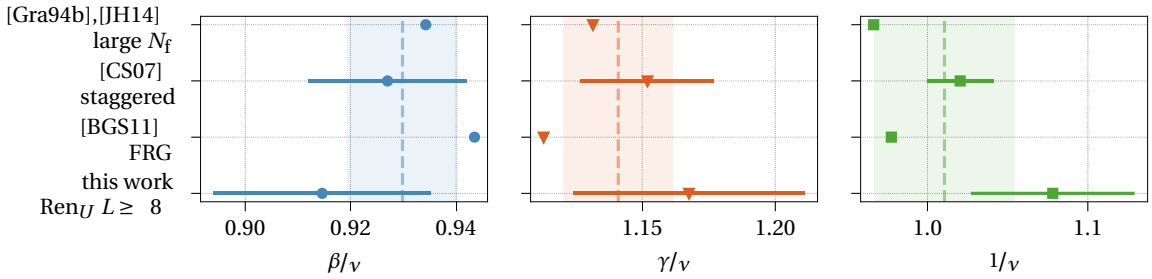

3.13(c) $N_f = 4$

the model we considered here, others give critical exponents for the Gross-Neveu-Yukawa model (GNY) that includes a kinetic term and a fourth-power interaction for the scalar field. Indeed, the additional terms are irrelevant in the continuum limit, so that the model yields the same large-distance physics [MZ03]. Additionally, some authors investigate a variant of GN with Majorana spinors and $O(N)$-symmetry that is also expected to be in the same universality class. We begin with a review of analytical results in section 3.3.1 and afterwards discuss older lattice simulations in section 3.3.2. Overview plots comparing our results with the most recent previous findings are given in figure 3.13. The data can be found in the appendix in table C.2. We finally give a summary in section 3.3.3.

3.3.1. Previous Analytical Results

We already presented the results from large-N_f expansion up to $\mathcal{O}\left(1/N_f^2\right)$ [Gra92; Gra93; Gra94a; Vas93; Der93] in (3.4) and a Padé resummation for $1/\nu$ [JH14] in (3.5). We compared them with our results in figure 3.11 and found both in good agreement for $N_f = 8$. Also $N_f = 4$ still seems to follow the analytical expansion. For all exponents with $N_f = 1$ and 2, deviations from 1 are smaller in our simulations than predicted by the large-N_f expansion, but a breakdown of it in this region is not surprising. The Padé approximation is not helpful and predicts a decrease in $1/\nu$ for decreasing N_f that our data does not support.

More involved calculations include expansions in the spacetime dimension as well as non-perturbative methods. All these methods commonly calculate the exponent $1/\nu$ and the anomalous dimensions $\eta_{\text{bos}}, \eta_{\text{ferm}}$ of bosons and fermions. Here, we use the hyperscaling relations (3.7) to obtain values for γ/ν as well as β/ν for better comparison.

ϵ-Expansions

Expansions were done both around lower $(2+\epsilon)$ and upper $(4-\epsilon)$ critical dimensions. In $2+\epsilon$ dimensions Gracey et al. [GLS16] recently extended previous works [Gra90; Gra91; LR91] to order ϵ^4 and gave critical exponents for $N_f = 2$. The expansion in $4-\epsilon$ was calculated by Mihaila et al. [Mih17] up to third order extending older work of Rosenstein et al. [RYK93]. The authors presented critical exponents for $N_f = 1$ and 2, obtained with Padé resummation like Gracey et al. [GLS16]. Lower-order results for both expansions around $2+\epsilon$ and $4-\epsilon$ were combined by Fei et al. [Fei16] with a two-sided Padé resummation to obtain values for $N_f = 1$ and 2 at $d = 3$.

For $N_\mathrm{f} = 1$, our result for $1/\nu$ agrees well with these results, while our value for β/ν is larger. In accordance with the hyperscaling relation, a deviation of γ/ν in the opposite direction is found. Taking the large systematic deviations in figure 3.12(a) into account, our result is still consistent with values of $\beta/\nu \approx 0.8$. Further studies generating more configurations on larger lattices would be necessary to examine if the estimate for β/ν approaches the previous calculations. For $N_\mathrm{f} = 2$, the discrepancy for $1/\nu$ is larger and only matches well with the result of Mihaila et al. [Mih17]. On the contrary, the deviations from his values for β/ν and γ/ν are the largest, while our results are in acceptable agreement with the other findings.

FRG Results

There were many investigations of GN variants with an FRG approach. Most recently, a high-precision study by Knorr [Kno16] employed pseudo-spectral methods and extended a first study [BK15] to next-to-leading order. Critical exponents with high accuracy were given for $N_\mathrm{f} = 1$ and 2. Older works in leading order include [RVW01; HNW02; JH14; VZ15] and [BGS11], which also gave values of critical exponents for $N_\mathrm{f} = 2, 4$ and 12. All these studies are in good agreement and the results seem to converge, so that we only use the values of Knorr [Kno16] for comparison in figure 3.13. For β/ν, we find a good fit with our values for $N_\mathrm{f} = 2$, opposed by larger disparity for $N_\mathrm{f} = 1$. Regarding $1/\nu$, a good match is found for $N_\mathrm{f} = 1$, but not for $N_\mathrm{f} = 2$. Comparing $N_\mathrm{f} = 4$ with [BGS11], we are more than a standard deviation off the FRG results.

Conformal Bootstrap

Lately, the conformal bootstrap showed great success determining the critical exponents of bosonic theories like the Ising model to very high precision (see e.g. [Kos16]). Starting in 2016, Iliesiu et al. [Ili16] began investigating fermionic theories in three dimensions with these methods, leading to the first results for GN in [Ili17]. Clearly visible in figure 3.13, their estimate for η (here converted to γ/ν and β/ν) agrees with the other analytical methods, as well as with our result for $N_\mathrm{f} = 2$. On the contrary, the accuracy of the $1/\nu$ result seems questionable, especially for $N_\mathrm{f} = 1$, where their values deviate from the overall average in figure 3.13(a) by more than two standard deviations.

3.3.2. Previous Lattice Results

Regarding previous lattice results, some works use approaches similar to ours, utilising lattice field theory implementations with HMC algorithm. They are presented in the next paragraph, while we also summarise alternative methods at the end of this section.

HMC simulations

There were a few previous lattice field theory studies calculating critical exponents of GN, all using staggered fermions. The first was performed by Hands et al. [HKK93]. They mainly

simulated $N_\mathrm{f} = 12$ flavours[(e)] to verify their results from the large-N_f expansion, which we already summarised in table 3.1. They determined the exponents β, γ and δ directly from fits to the relevant observables and were not able to resolve $\mathcal{O}(1/N_\mathrm{f})$ corrections. To obtain ν, they performed a finite temperature analysis and got $\nu = 0.94(13)$. They mentioned, that their lattice formulation is only free of a sign problem for even $N_\mathrm{f}/2$. This requirement was neither mentioned nor taken into account by Kärkkäinen et al. [Kär94], who did a similar simulation with $N_\mathrm{f} = 2$. They used finite size scaling techniques to obtain ratios of critical exponents similar to our approach given in section 3.1.1. Good agreement with the large-N_f formula for γ/ν (3.4b) was found, while there were slight deviations for ν. An independent measurement of β/ν fulfilled the hyperscaling relation (3.6) correctly to the three given decimal places. Despite the possible sign problem, our results for $N_\mathrm{f} = 2$ fit theirs within errors. The last study with this setup was done by Christofi & Strouthos [CS07] for $N_\mathrm{f} = 4$, where the same ratios of critical exponents were measured. We also find good agreement with our data.

An exploratory study of Hands [Han16b] successfully simulated GN with two flavours of domain wall fermions, but the author did not calculate critical exponents. These domain wall fermions are a solution to a generalised version of the Ginsparg-Wilson relation (2.49), that was adapted for three-dimensional four-fermion theories [Han15; Han16a]. The dependence on an additional parameter, the separation of the domain walls L_s, is studied. It must be chosen large enough because the full chiral symmetry on the lattice is only recovered for $L_s \to \infty$.

Non-HMC Simulations

Further results from simulations are available that did not use an HMC algorithm. Chandrasekharan & Li [CL13] employed the fermion bag approach shortly introduced in section 2.4.1. It allowed to simulate $N_\mathrm{f} = 2$ with staggered fermions, similarly to [Kär94], but the absence of the sign problem in this formulation could be shown [CL12b]. The susceptibility and ratios of correlation functions were used to obtain the critical exponents η, η_ψ and ν by a single fit. They were found to agree with values obtained for Th, contrary to the expectation for the continuum models. See section 4.2.2 for further discussion of these lattice results. Their exponents did not agree with the work of Kärkkäinen et al. [Kär94], which they believed to originate from the sign problem that was ignored there. By contrast, our new results are in better agreement with [Kär94] and the fermion bag data point is far off the overall average in figure 3.13(b).

Another approach are QMC algorithms that allowed to study quantum mechanical systems in analogy to GN for $N_\mathrm{f} = 1$ without sign problem. Wang et al. [WCT14; Wan15] used a Continuous-Time QMC to simulate spinless fermions on a honeycomb lattice at half filling that should share the chiral Ising universality class with GN and GNY. However, their critical exponents (see table C.2(a)) were not in agreement with previous analytical

[(e)] All values of N_f given here refer to continuum flavours, which is twice the number of staggered flavours for the reducible representation. See also section 2.3.2 for details about chiral fermions on the lattice.

results. They attributed this discrepancy to the fact that they used two-component spinors with opposite chirality, contrary to field theory calculations where the irreducible spinors have the same chirality. Results roughly consistent with these numerical findings were also reported by Hesselmann & Wessel [HW16]. Furthermore, Majorana QMC is also free of a sign problem and was used by Li et al. [LJY15], again giving numbers that are not in agreement with analytical calculations. Their value of ν was consistent with the other QMC approaches, but they found a larger value of η if (and only if) they included larger lattice sizes. With our new field-theoretical approach, we can confirm the discrepancy between the QMC simulations and other field theory methods, since our predictions in figure 3.13(a) are much closer to previous analytical calculations than the lattice QMC results. Possibly, also the lattice itself plays an important role because the QMC simulations were performed on a graphene-like honeycomb lattice, while ours is cubic.

3.3.3. Summary

We presented the first extensive study of GN with exactly chiral fermions in a lattice field theory approach and calculated critical exponents for $N_\mathrm{f} = 1, 2, 4$ and 8. The situation in the literature is clear for $N_\mathrm{f} = 2$ and our result fits well within the previous results, the only exception being the fermion bag simulation [CL13]. Oddly, we are in better agreement with the staggered simulation [Kär94] that possibly suffered a sign problem. For $N_\mathrm{f} = 1$ large discrepancies between analytical and QMC computations are present. Here, we can support the analytical results, although our own estimates for γ/ν and β/ν need more refinement. Also, simulations with other exactly chiral fermions could be useful to clean up the situation. In comparison with the few values explicitly given for $N_\mathrm{f} = 4$, our results fit within errors to the older simulation with staggered fermions [CS07], but more statistics would be required to improve our results. Then, a significant deviation from the large-N_f expansion could be found. No such deviation is present for $N_\mathrm{f} = 8$ in γ/ν, where we find a good match with (3.4b). We likely still see deviations for β/ν and γ/ν at $N_\mathrm{f} = 8$ from their infinite-N_f value of 1, opposed to the findings for $N_\mathrm{f} = 12$ [HKK93]. In general, our result for $1/\nu$ raises the question if the value of 1 is approached from below, as predicted by the large-N_f expansion and FRG calculations [BGS11]. Our plot figure 3.11 rather suggests, that it always stays above 1. This could be another starting point for refined studies or simulations with different lattice fermions.

3.4. The γ_{45}-Model (Irreducible Gross-Neveu Model)

After our extensive study of the reducible GN, we have a short look at its irreducible version, which is equivalent to G45 in the reducible representation (see section 2.1.2). Here, a non-vanishing scalar field expectation value Σ breaks the $\mathbb{Z}_2$ parity like the irreducible mass term discussed in section 2.1.2. Simulation results are given in section 3.4.1 and

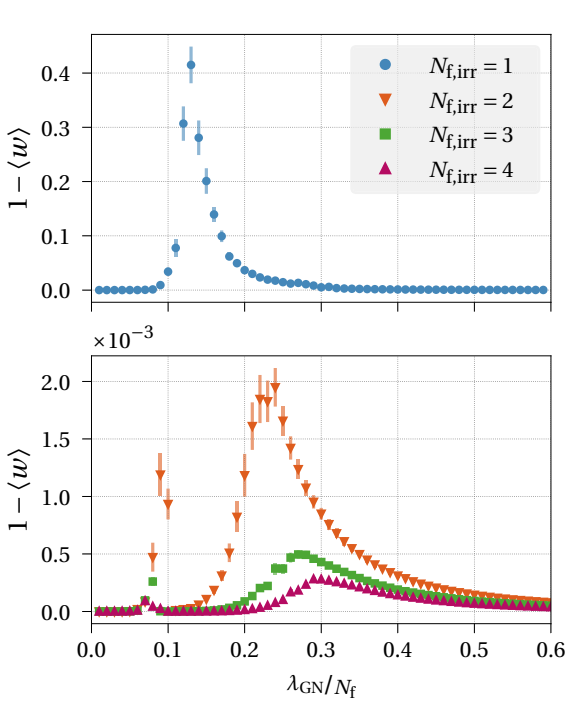

3.14(a) Weights for different $N_{\mathrm{f,irr}}$ with $L = 6$.

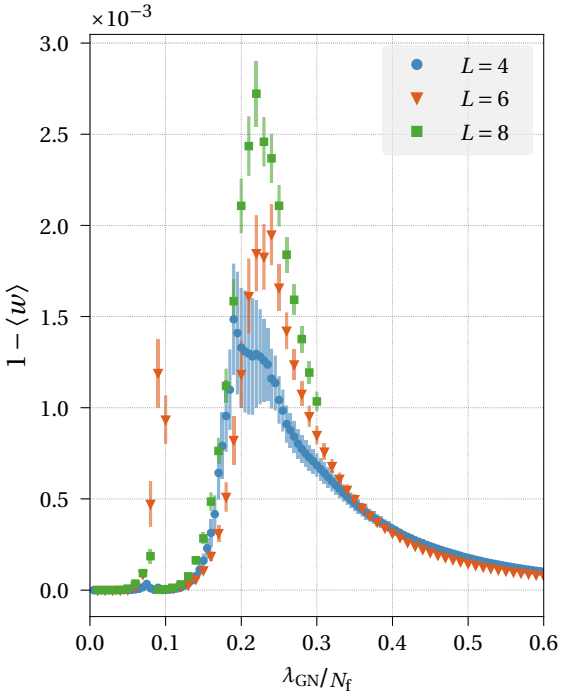

3.14(b) Weights for different L with $N_{\mathrm{f,irr}} = 2$

Figure 3.14.: Real parts of the expectation values of the weights for the irreducible GN with varying N_{f} and L. Due to the large difference in scale between $N_{\mathrm{f,irr}} = 1$ (where GN and Th are equivalent) and larger N_{f}, two plots are shown in figure 3.14(a).

discussed in section 3.4.2. Additionally, a calculation in appendix D shows that G45 with our choice of sign for the interaction in (2.11) has the same effective potential to first order as GN.

3.4.1. Simulation Results

Our code implements both the irreducible formulation of GN in (2.21) as well as the equivalent reducible G45 with γ_{45} as interaction matrix. Since both implementations showed good agreement in the observables for $N_{\mathrm{f,irr}} = 2N_{\mathrm{f}}$, only results with the irreducible formulation are shown here, were also odd $N_{\mathrm{f,irr}}$ can be simulated.

Due to the results of section 2.4.2, we must expect a sign problem[(f)] for any $N_{\mathrm{f,irr}}$. Hence, simulations with the phase-quenched model and the exact update algorithm were performed. As noted in section 2.4.2, the phase quenched irreducible formulation is identical to the reducible model, but it allows to measure the expectation value of the weight $\langle \Omega \rangle$ defined in (2.58). Its real part $\langle w \rangle$ takes the value of 1 if the action is real. The worse the sign problem is, the closer the weight gets to 0. The results in figure 3.14(a) show that the sign problem is much worse for $N_{\mathrm{f,irr}} = 1$ than for larger flavour numbers. The single flavour model is anyhow special due to its equivalence to Th (see (2.27)) and the simple combination of $\mathbb{Z}_2$-parity that is broken here, together with a $U(1)$-symmetry.

[(f)] Remarkably, the absence of a sign problem can be shown for G45 with *imaginary* couplings, but the potential calculated in appendix D is no longer stable.

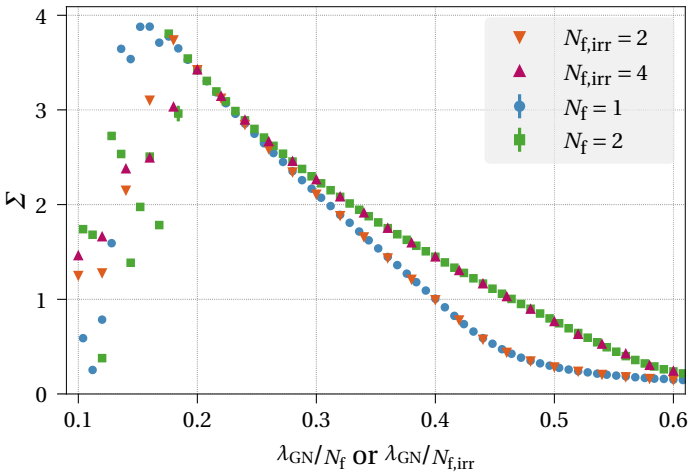

Figure 3.15.: Comparison of GN and its irreducible version. The expectation values of the absolute value of the scalar field are shown for GN with $N_f = 1,2$ as well as the corresponding irreducible model with $N_{f,irr} = 2,4$ on lattice size 8. Reweighting was used for the irreducible model, but corrections are very small (see figure 3.14).

For $N_{f,irr} > 1$ the deviation of the weight from 1 is very small on lattice size 6 and decreases further for larger $N_{f,irr}$. In figure 3.14(b) we see that the sign problem gets stronger for increasing lattice size, but is still of order 10^{-3} for $L = 8$.

We can use the measured weights to perform reweighting and calculate corrected expectation values of observables with equation (2.58). For $N_{f,irr} = 2$ and 4 for size $L = 8$, the corrections are of order 10^{-3} and smaller than the statistical errors in the scalar field. In figure 3.15, one can see that Σ is, up to the saturation phase, in very good agreement with the measurement of reducible GN for $N_f = 1$ and 2 on the same lattice size. Clearly, an evaluation of critical exponents for the irreducible GN would lead to very similar results as for the reducible version.

3.4.2. Discussion

Gehring et al. [GGJ15] studied G45 together with GN- and Th-interactions by methods of FRG. For $N_f = 1$, these interactions form a complete basis for the space of models with at least the symmetries of GN. For larger N_f also $\left(\bar{\psi}_a \gamma_{\mu\nu} \psi_a\right)^2$ had to be included in the investigation. They found the critical behaviour of GN only governed by the expected fixed point for $N_f \geq 2$. For $N_f = 1$ a different fixed point governs the phase transition, which may have different properties than the pure GN fixed point. Thus, the authors suspect that they found two fermionic theories (GN and G45 for $N_f = 1$), which show spontaneous breaking of a $\mathbb{Z}_2$-symmetry but potentially different critical behaviour.

On the contrary, our results in section 3.4.1 give evidence that this is not the case and that both GN and G45 share the same universality class for $N_{f,irr} = 2N_f$. This is also supported by the FRG calculation of Höfling et al. [HNW02] in the irreducible representation, where critical exponents for $N_{f,irr} = 4$ were found in agreement with later results for the reducible model with $N_f = 2$. At any currently accessible lattice size, we expect the sign problem for $N_{f,irr} \geq 2$ to be small enough, so that no relevant influence of reweighting on the critical exponents can be found. However, we cannot exclude that both models become fundamentally different for very large lattice sizes. For $N_{f,irr} = 1$, conventional simulations

are not possible due to the strong sign problem, but our dual-variables approach presented in section 6.2 can provide a way to solve it for this special case.

4. Thirring Model With Auxiliary Vector Field

This chapter is dedicated to Th in the original formulation (2.33), which contains an auxiliary vector field due to HS. In contrast to GN, where chapter 3 showed evidence that χSB can occur for any number of flavours with a second-order phase transition, Th is commonly expected to have a broken phase only for small N_f. Thus, the main question is: For which numbers of flavours can χSB happen in Th? Our answer to this question from simulations of the Lagrangian (2.33) with an auxiliary vector field is given in section 4.1. Remarkably, it is fundamentally different from most previous answers reviewed in section 4.2. This motivated further studies of coupled models in chapter 5 and alternative formulations of Th in chapter 6.

4.1. Simulation Setup and Results

This section presents new results from numerical simulations of the vector field formulation (2.33) with SLAC fermions and a conventional rHMC algorithm, as described in section 2.3. Necessary preliminary considerations are given in section 4.1.1, where a previously observed unphysical phase in lattice simulations of Th is discussed. We give our own results for Th with a small mass in section 4.1.2 to make contact with earlier lattice simulations. Afterwards, section 4.1.3 presents results from the first lattice simulation of massless Th with exactly chiral fermions.

4.1.1. Observables and Unphysical Phase

We mainly use the observables given in section 2.3.3, but use $\Sigma := \langle |\bar{\Psi}\Psi| \rangle$ instead of the chiral condensate (2.51), similar to our definition for GN. Additionally, we will show *Fisher plots* for simulations with non-zero mass as introduced in the next paragraph.

Fisher Plots

These plots are based on the definitions of critical exponents, as given in table 3.1 for GN. We use

$$\langle \bar{\psi}\psi \rangle \propto m^{\frac{1}{\delta}} \quad \text{and} \quad \langle \bar{\psi}\psi \rangle \propto t^{\beta}, \tag{4.1}$$

where t is the difference between λ_Th and the critical coupling as given in (3.3). Del Debbio & Hands [DH96] use a more general expansion in t

$$m = c_1 \langle \bar{\psi}\psi \rangle^{\delta} + c_2\, t \langle \bar{\psi}\psi \rangle^{\delta - \frac{1}{\beta}} + \ldots \tag{4.2}$$

which, using the mean field values of $\beta = 1/2$ and $\delta = 3$ in table 3.1, becomes

$$\left\langle \bar{\psi}\psi \right\rangle^2 = \tilde{c}_1 \frac{m}{\left\langle \bar{\psi}\psi \right\rangle} + c_2\, t. \tag{4.3}$$

The Fisher plot shows $\left\langle \bar{\psi}\psi \right\rangle^2$ as a function of $m/\langle \bar{\psi}\psi \rangle$. Thus, straight lines are expected in the plot if the mean field approximation is valid. Additionally, a fit to (4.2) with positive intercept on the vertical axis signals a non-vanishing chiral condensate in the limit $m \to 0$. We show Fisher plots of our own simulations in section 4.1.2.

Unphysical Phase

Before we go on to our lattice simulations, we have to take care of an issue that was reported by Del Debbio et al. [DHM97]. They found an unphysical phase, where the chiral condensate decreases and attributed this transition to a substantial difference between different regularisations. While the large-N_f expansion in the continuum [Han95] uses a current-conserving Pauli-Villars regulator, a lattice regularisation violates the current conservation. In this case, a divergent term appears that obstructs the transversality of the vacuum polarisation tensor. Del Debbio et al. [DHM97] compare this to the situation for QED$_3$, where a lattice perturbation theory calculation is given in the book of Rothe [Rot05]. In contrast to Th, *two* divergent contributions from different Feynman diagrams cancel each other, resulting in a finite expression for the vacuum polarisation as in the continuum. Only one of these diagrams occurs for Th because the interaction is $\bar{\psi}\,\mathrm{i}V_\mu\psi$ and not $\bar{\psi}\,\mathrm{e}^{\mathrm{i}eA_\mu}\psi$ as in lattice QED$_3$. Hence, there is only a single vertex with two fermions and a vector boson. To absorb the divergence of Th on the lattice, it is necessary to introduce a wave function renormalisation and a coupling constant renormalisation. They find

$$g^2_\mathrm{Th} \to g^2_\mathrm{R} = \frac{g^2_\mathrm{Th}}{1 - g^2_\mathrm{Th} J(m)} \quad \Rightarrow \quad \lambda_\mathrm{R} = \lambda_\mathrm{Th} - J(m), \tag{4.4}$$

where g^2_R and λ_R are renormalised (inverse) couplings and

$$J(m) = 2\int_{-\pi}^{\pi} \frac{\mathrm{d}^3 q}{(2\pi)^3} \frac{\sin^2 q_\mu}{\sum_\nu \sin^2 q_\nu + m^2} \xrightarrow{m\to 0} \frac{2}{3}. \tag{4.5}$$

Thus, in the chiral limit $m \to 0$, there is a limiting bare coupling of $\lambda^\mathrm{lim}_\mathrm{Th} = 2/3$ with $\lambda_\mathrm{R} < 0$ for $\lambda_\mathrm{Th} < \lambda^\mathrm{lim}_\mathrm{Th}$.

The authors interpret this as an unphysical phase and suggest that the model is no longer unitary for such strong bare couplings. In all their simulations with different flavour numbers, they find a sharp drop in the chiral condensate for couplings $1/g^2_\mathrm{Th} = \lambda_\mathrm{Th}/N_\mathrm{f} \leq 0.3$. Although the numerical value does not match $2/3$ well, they are drawn to the conclusion that this could be a sign of the onset of the unphysical phase. With this argument, a later study [CHS07] interprets the maximum of the chiral condensate as the point of infinite renormalised coupling.

Although this calculation depends on the use of Wilson fermions and a similar calculation

for the SLAC derivative is closer to the continuum expansion in [Han95], we must replace integrations over all momenta by corresponding sums over the Brillouin zone. A full calculation is difficult, but the requirement of an additive renormalisation (4.4) seems plausible. A different explanation of the unphysical phase is provided by our lattice filling factor $\langle k \rangle$ defined in (2.55). We saw in figure 3.1 that GN shows lattice artefacts and a decreasing condensate, when the value of $\langle k \rangle \gtrsim 0.5$ is exceeded. Thus, Pauli blocking may also be the reason for the unphysical behaviour for strong λ_{Th}.

Janssen & Gies [JG12] comment on this topic from the viewpoint of FRG. They do not find the transversality of the vector propagator necessary for the model to be non-perturbatively renormalisable if one studies a larger space of four-fermion theories. They suggest that the non-monotonic chiral condensate may be related to the Th fixed point not being on the axis of pure Th coupling, as described in section 4.2.1.

4.1.2. Explicit Symmetry Breaking With a Mass Term

We start our numerical investigations of massive Th with simulations in the reducible representation, where the model is free of a sign problem (see section 2.4.2). A particular lattice size is considered in the first part, while larger sizes and the irreducible representation are considered afterwards. For all data points in this section, we obtained 1000 configurations with 10 intermediate updates.

Reducible Model for Lattice Size 12

Results from a conventional rHMC simulation with lattice size 12 and $N_{\mathrm{f}} = 1, 2$ and 3 are given in figure 4.1. The first row of figure 4.1(a) presents curves of Σ for m in steps of 0.02 between 0.02 and 0.18 as a function of $\lambda_{\mathrm{Th}}/N_{\mathrm{f}}$. They all have a maximum around $\lambda_{\mathrm{Th}}^{\mathrm{max}} \approx 0.5 N_{\mathrm{f}}$ and show the non-monotonic behaviour attributed to a transition to an unphysical phase, as explained in section 4.1.1. Remarkably, the susceptibility shows a maximum approximately at the coupling, where Σ is maximal. Like in GN, the peak in the susceptibility corresponds to a transition in the lattice filling factor from small values at weak coupling to strongly growing values. On the other hand, the maximum of Σ in GN does not coincide with this point. Comparing to the form for GN in figure 3.1, the decrease for strong coupling is rather smooth and we did not find thermalisation problems in Σ for Th.

Weakening the explicit breaking, the values of Σ decrease roughly linearly, leaving no trace of a broken phase for any N_{f} in the chiral limit. For $N_{\mathrm{f}} = 1$ the curves are more pronounced around the maximum, but not qualitatively different. Only the maximum in χ moves to stronger couplings, an observation we cannot make for $N_{\mathrm{f}} \geq 2$. Thus, it looks like there is no χSB present for $N_{\mathrm{f}} = 1$ either. The Fisher plots in figure 4.1(b) solidify this outcome. No trajectory for any λ_{Th} has a positive intercept with the vertical axis that would indicate χSB. Increasing the coupling strength (decreasing λ_{Th}), the trajectories move to the left, up to the point where $\lambda_{\mathrm{Th}} \approx \lambda_{\mathrm{Th}}^{\mathrm{max}}$. For even stronger couplings, the trajectories

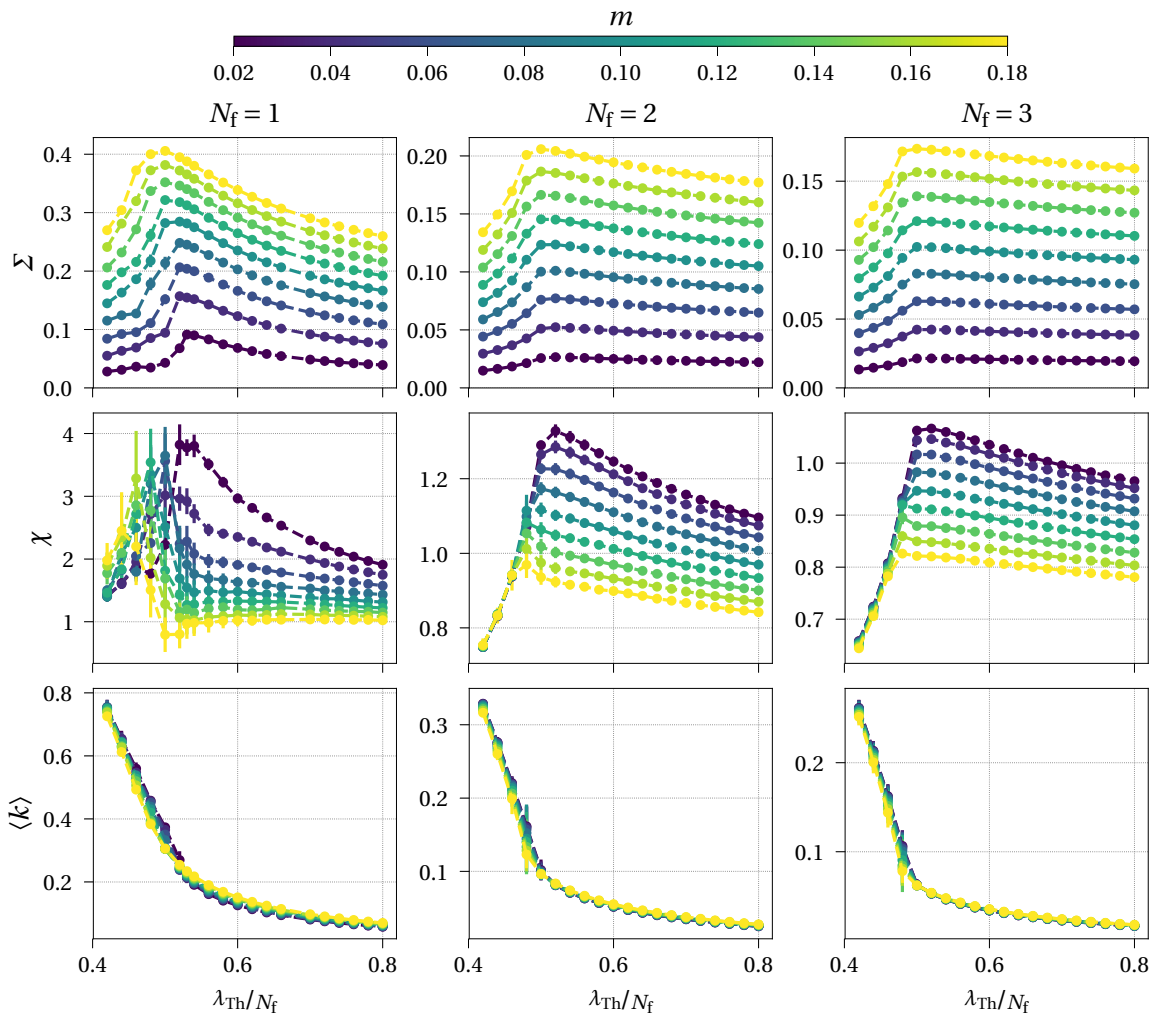

4.1(a) Chiral condensate, susceptibility and lattice filling factor. The colour indicates different masses.

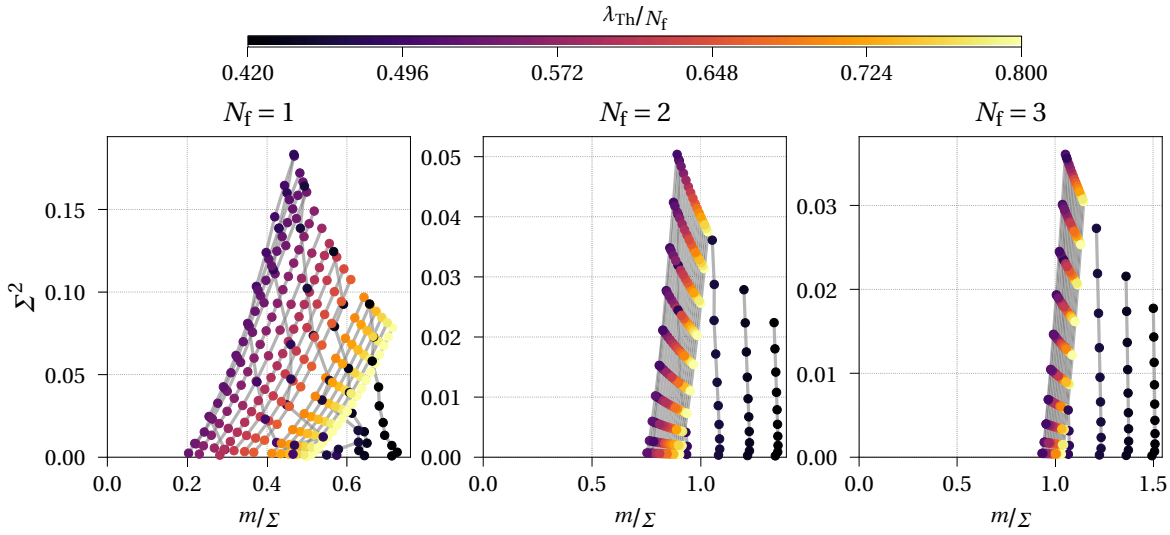

4.1(b) Fisher plots. The colour indicates different couplings. A line of constant inverse coupling (colour) intersecting the vertical axis would indicate χSB.

Figure 4.1.: Simulation results for reducible, massive Th on lattice size 12. The columns show different flavour numbers.

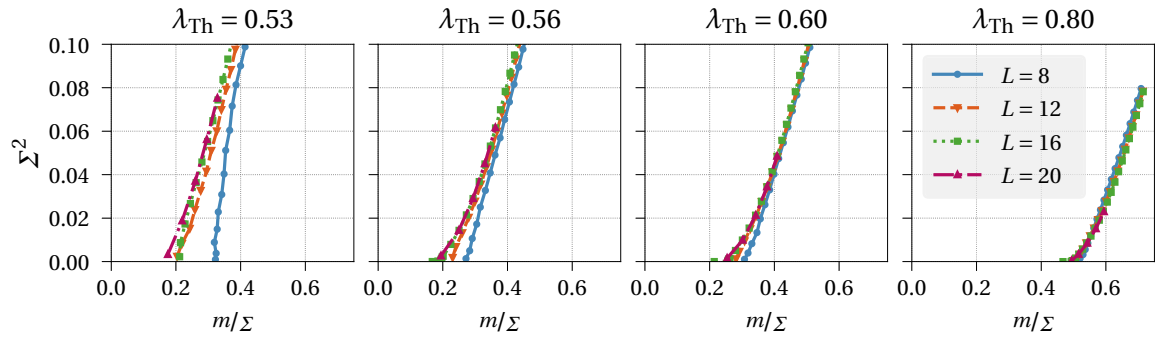

4.2(a) Fisher plots for $N_f = 1$ showing the dependence on the lattice size.

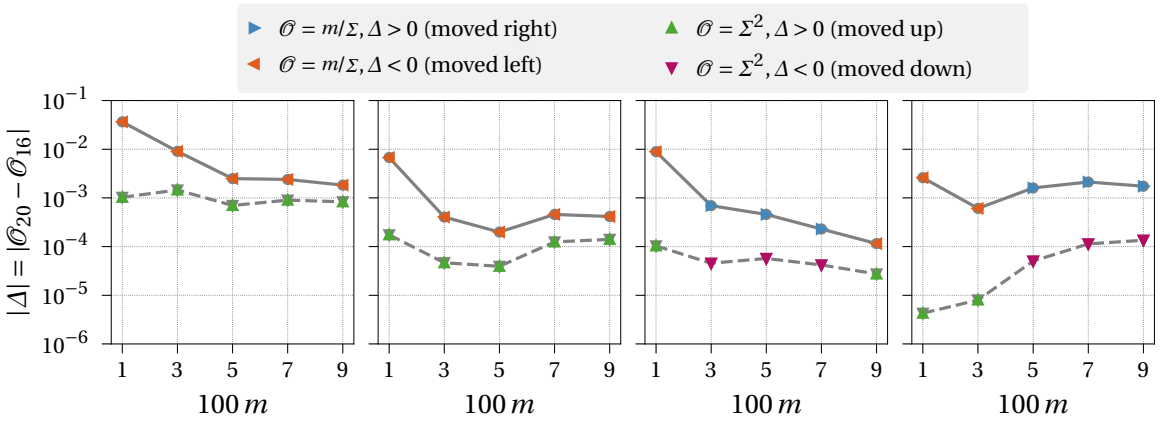

4.2(b) Differences between lattice size 16 and 20 in the $N_f = 1$ Fisher plot as a function of the bare mass. The couplings in each panel are the same as in 4.2(a). The two curves indicate changes on the horizontal axis in 4.2(a), as well as in the vertical direction. Different colours and symbols indicate the sign of the change. The orientation of the triangle signifies the direction of change when going from size 16 to 20, e.g. up and to the left for all masses in the leftmost plot.

Figure 4.2.: Lattice size dependence of the reducible massive Th for $N_f = 1$. Both parts show the same couplings. The values 0.53 and 0.56 are very close to the maximum in Σ on both sides, while 0.80 is in the weak coupling regime where no χSB is expected.

have a different shape. The slope is now negative and the curves move quickly to the right of the Fisher plot. Again, the behaviour is slightly different for $N_f = 1$, but without any significant impact on χSB.

Dependence on the Lattice Size

Simulations for $N_f = 1$ were also performed on lattice sizes 8, 16 and 20 to study finite volume effects. Fisher plots for a selection of couplings are shown in figure 4.2(a). While the curves for lattice size 8 show a visible deviation, there are only very small differences between larger lattices. For points with the same mass, figure 4.2(b) shows the difference between size 16 and 20 in both vertical and horizontal direction of the Fisher plots in figure 4.2(a).

For the couplings $\lambda_{\mathrm{Th}} = 0.53$ and 0.56 close to the maximum in the condensate at $\lambda_{\mathrm{Th}}^{\mathrm{max}}$, we can see that the points for all masses move up and to the left of the Fisher plot, when increasing the lattice size. This also happens for $\lambda_{\mathrm{Th}} = 0.6$ and 0.8 with small masses, but some points with larger mass move in the opposite direction. The changes are strongest

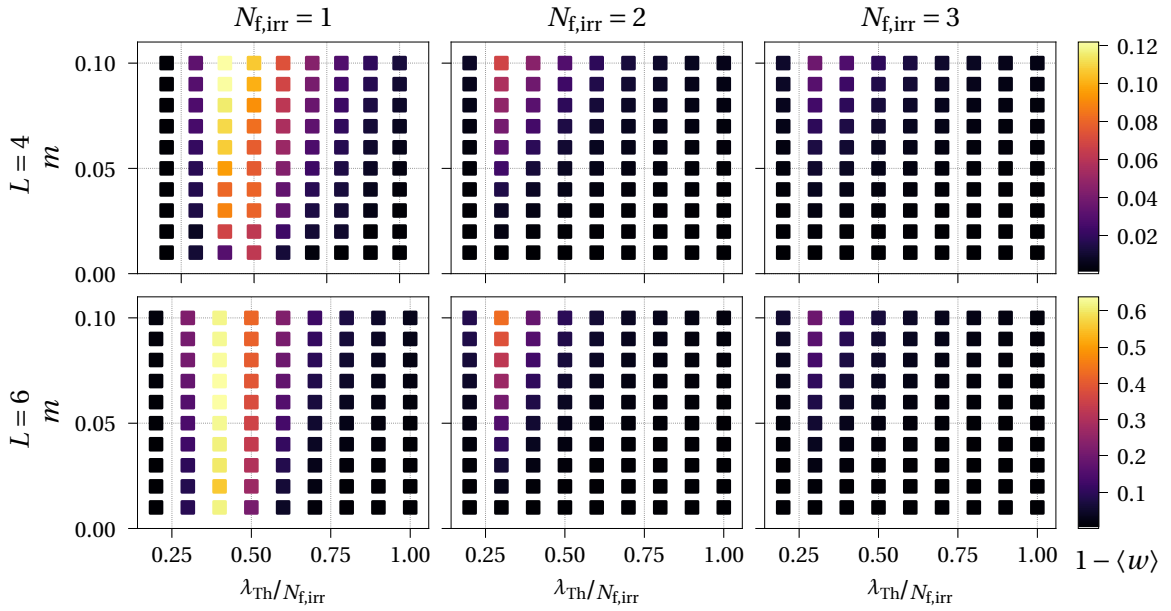

Figure 4.3.: Strength of the sign problem for irreducible Th with mass. Rows show results for different L, while columns have increasing N_{f} from left to right. Note the different scales of colour for $L = 4$ and $L = 6$.

for $\lambda_{\mathrm{Th}} = 0.53$, but they are rather small in total. Thus, we expect lines in the Fisher plots on larger lattices that are closer to the critical point (intersecting the origin) and we cannot fully exclude χSB. But to explicitly see this, lattice sizes far beyond currently possible simulations would be necessary.

Irreducible Model

We can contrast our previous findings with results from the irreducible model. Here, we use the naive mass term $m\bar{\chi}\chi$ and the corresponding condensate, associated to parity breaking (see section 2.1.2). Since a sign problem must be expected, we first look at the real part of the weight for $m = 0.01, \ldots, 0.1$ given in (2.58). In figure 4.3, we display $1 - \langle w \rangle$, which should be zero, but we find a non-zero region with growing values for increasing mass. Thus, the sign problem gets stronger with larger bare mass, at least in a region that correlates with large values of Σ. In the chiral limit, we expect and observe that the sign problem vanishes for even flavour numbers. Surprisingly, also odd $N_{\mathrm{f,irr}} > 1$ have a well-behaved sign for small masses with $1 - \langle w \rangle$ very close to 0. In general, taking a larger flavour number mitigates the sign problem, similar to irreducible GN in figure 3.14(a). Increasing the lattice size from 4 to 6, a huge increase of the maximum of $1 - \langle w \rangle$ is present in figure 4.3. We must expect a very strong sign problem for larger lattice sizes and masses.

Nevertheless neglecting it, we performed rHMC simulations on lattice size 12. The results for $N_{\mathrm{f,irr}} = 1, 2, 3$ are shown in figure 4.4. The different nature of the $N_{\mathrm{f,irr}} = 1$ model is clearly visible, showing signs of dynamical mass generation as expected, since the model is equivalent to GN. We find trajectories that tend to intersect the vertical axis, although the true behaviour might be obscured by insufficient knowledge about the curvature of the lines and the sign problem. Showing a behaviour similar to the simulations in the reducible

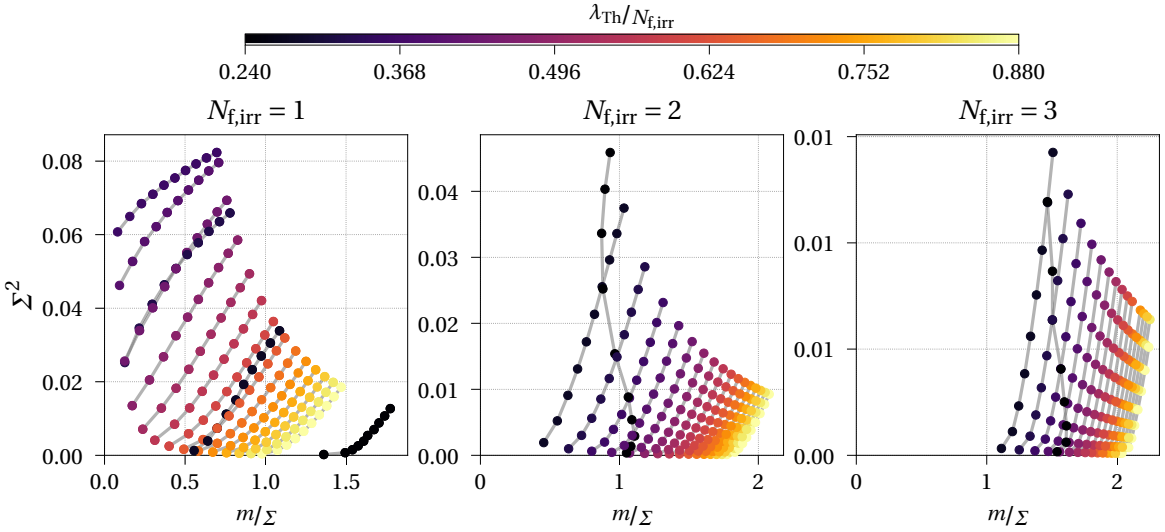

Figure 4.4.: Fisher plots for the irreducible Th. Note, that a potentially strong sign problem was ignored here.

representation, no hint for χSB can be found for $N_{\mathrm{f,irr}} = 2$ and also $N_{\mathrm{f,irr}} = 3$, where all lines are farther away from the origin. Hence, χSB seems to exist only for $N_{\mathrm{f,irr}} = 1$, but the present results are clearly not sufficient for a reliable conclusion.

4.1.3. Massless Model

This section presents new results for the reducible model with $m = 0$, which has the full chiral symmetry of the continuum model. 1000 configurations with 10 intermediate updates were calculated for massless Th with various numbers of flavours and lattice sizes from 8 to 20. The results for the absolute value of the chiral condensate Σ and the susceptibility χ are shown in figure 4.5. There is no signal of a non-vanishing chiral condensate in the large volume limit for any number of N_{f}, since the already small values of Σ decrease with increasing lattice size. They are artefacts of the stochastic estimator method used to obtain the chiral condensate, as explained in section 2.3.3. Remarkably, the noise has a form reminiscent of the curves for non-zero mass in figure 4.1(a) with a maximum around $\lambda_{\mathrm{Th}}/N_{\mathrm{f}} \approx 0.5$. We can indeed reduce the noise by a factor of $\sqrt{10}$ by taking 10 times more estimators, as expected. This can also be seen in figure 4.5, where all simulations were done with 1000 estimators, except $L = 20$ where only 100 estimators were used to reduce the computational costs. Therefore, the noise in Σ in the $L = 20$ simulation is larger by roughly a factor of $\sqrt{10}$ than for the other sizes.

We conclude, that there is no non-zero chiral condensate for Th in our simulations due to the exactly implemented chiral symmetry. Even looking at the individual configurations, we found Σ to be close to zero. Viewed in contrast to GN, we now do not have a scalar field, that transforms under chiral transformations with $\sigma \to -\sigma$. The auxiliary vector field of Th is invariant under any chiral transformation and fermions were integrated out to obtain the fermion determinant in (2.43), leaving no accessible order parameter.

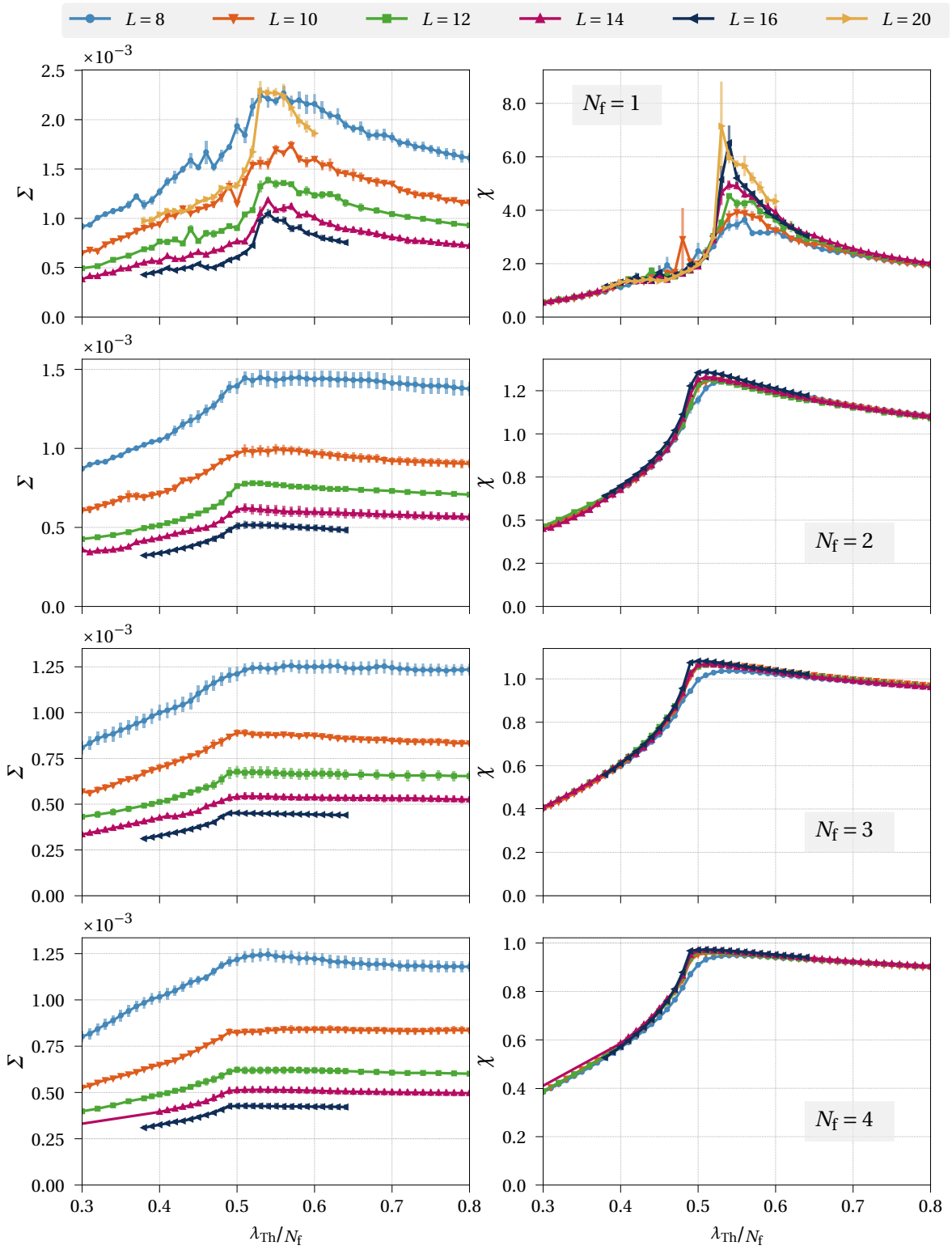

Figure 4.5.: Absolute value of the chiral condensate and susceptibility for the massless Th. The left column shows the dependence on the volume for Σ with N_f varying from 1 at the top to 4 at the bottom. The vertical axis is scaled by 10^{-3}, showing a very small value of the chiral condensate. The non-zero value is only due to numerical errors and decreases with increasing L. The number of stochastic estimators was decreased by a factor of 10 for $L = 20$, explaining the larger values in the top left image. The right column shows the corresponding susceptibilities. Note the large difference in scale for $N_f = 1$ and $N_f > 1$ and see also figure 4.6.

Susceptibility

The right column of figure 4.5 shows the susceptibility (2.54). A large difference in the shape exists for $N_\mathrm{f} = 1$ and $N_\mathrm{f} > 1$. In the latter cases, the susceptibility is a rather smooth curve, that increases up to a maximum around $\lambda_\mathrm{Th} = 0.5 N_\mathrm{f}$. For growing λ_Th (weak couplings) it decreases very slowly from the maximal value. Fluctuations are much larger for $N_\mathrm{f} = 1$ and there is a flat region at $\lambda_\mathrm{Th} \approx 0.45$. The main peak at $\lambda_\mathrm{Th} \approx 0.54$ is much more pronounced than for $N_\mathrm{f} > 1$ and grows strongly with the lattice size.

To compare the differences more easily, we investigated the maxima of the chiral susceptibility. Naively taking all points higher than their two neighbours on each side as local maxima, we obtained rough estimates for position and value of maxima in the susceptibility. They are plotted in figure 4.6 as a function of $\sqrt[3]{V}$, as defined for GN in (3.12). Only a single maximum was found for all curves with $N_\mathrm{f} \geq 2$, while several local maxima can be present for $N_\mathrm{f} = 1$. Regarding the values of the susceptibility at these maxima, we can clearly distinguish between the global maximum with the large peak and a second maximum around $\lambda_\mathrm{Th} \approx 0.45$ that occurs due to fluctuations around a roughly constant value in the flat region described earlier.

Increasing the lattice size, the maximum indicating the plateau range is quite stable in height, in contrast to the global maximum that grows for any flavour number. The remarkable difference between $N_\mathrm{f} = 1$ and more flavours is only seizable when comparing the amount of growth: The global maximum for $N_\mathrm{f} = 1$ is twice as high for $L = 20$ than for $L = 8$, while the increase for $N_\mathrm{f} = 2$ is 1.04 and decreases further to 1.02 for $N_\mathrm{f} = 4$. Thus, one might suspect that there is a remnant of a chiral symmetry breaking phase transition left for $N_\mathrm{f} = 1$ that does not persist for higher flavour numbers.

Comparing the susceptibility with the lattice filling factor in figure 4.7, the plateau for $N_\mathrm{f} = 1$ and a change in curvature for $N_\mathrm{f} = 2$ is observed, where $\langle k \rangle$ is well above half filling. We again find the main peak of χ near the transition from the weakly interacting phase to stronger interactions. This was also the case for the physical phase transition of GN in figure 3.1. But since the position of the susceptibility peak for the massive model in section 4.1.2 and figure 4.1(a) is at the maximum of Σ, it might be a sign of the transition to the lattice artefact phase. We will gain more insight into this in section 5.1, where the coupled GN and Th parameter space is investigated.

Irreducible model

A short investigation of the irreducible model with $m = 0$ confirmed the observations in figure 4.3 for non-zero mass. The sign problem only persists for $N_\mathrm{f,irr} = 1$, where the results are consistent with the equivalent GN-formulation presented in figure 3.14(b). Here, the same form of the weight as a function of the inverse coupling arises, although the fermion determinant only takes values ± 1 on a single configuration, while it is complex in the equivalent irreducible GN formulation. Thus, the real-valued fermion determinant of Th is not superior to the complex-valued determinant of GN. While the absence of

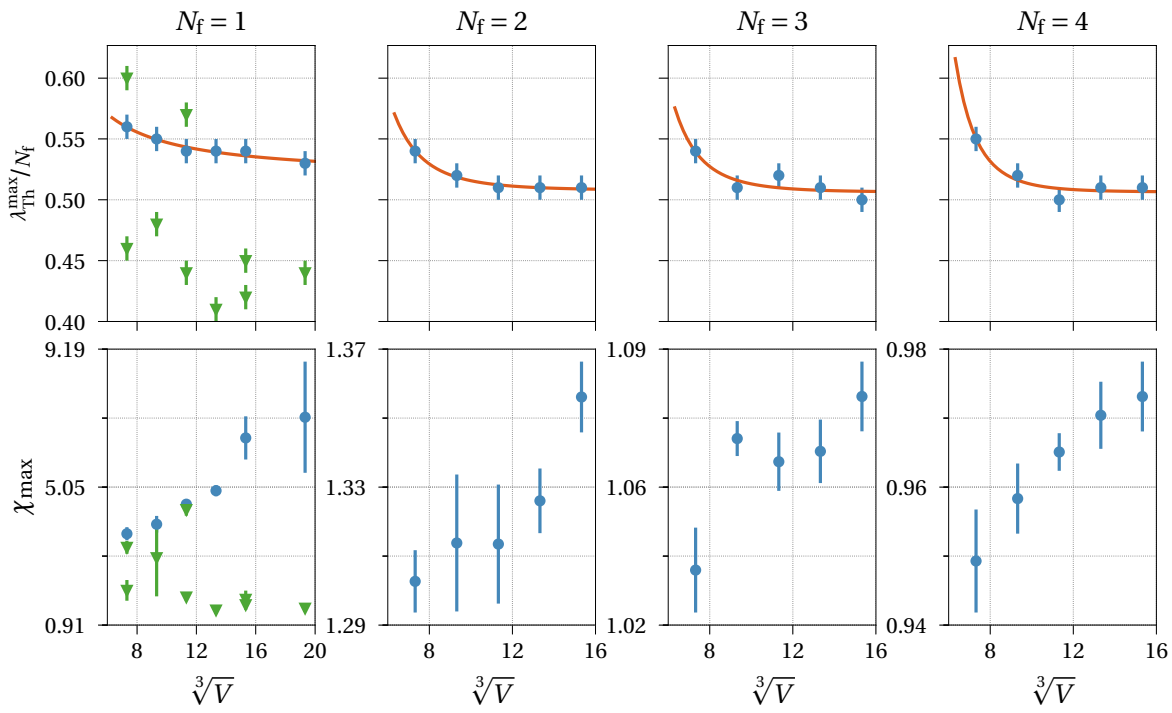

Figure 4.6.: Position and height of peaks in the chiral susceptibility of Th. The first row shows the position in λ_{Th} and the second row the value of the susceptibility at this coupling. The columns have increasing N_f from 1 (left) to 4 (right). As for GN, the values are plotted depending on $\sqrt[3]{V}$ instead of L. The plots in the first row have $\Delta\lambda_{Th} = 0.01$ as a rough error estimate. Only for $N_f = 1$, more than a single maximum was found. The ones with larger distance to the estimated critical coupling of $\lambda_{Th}^{max} \approx 0.54$ are shown in a different colour and with a distinct symbol. The smaller maxima at lower coupling correspond to the flat region in figure 4.5.

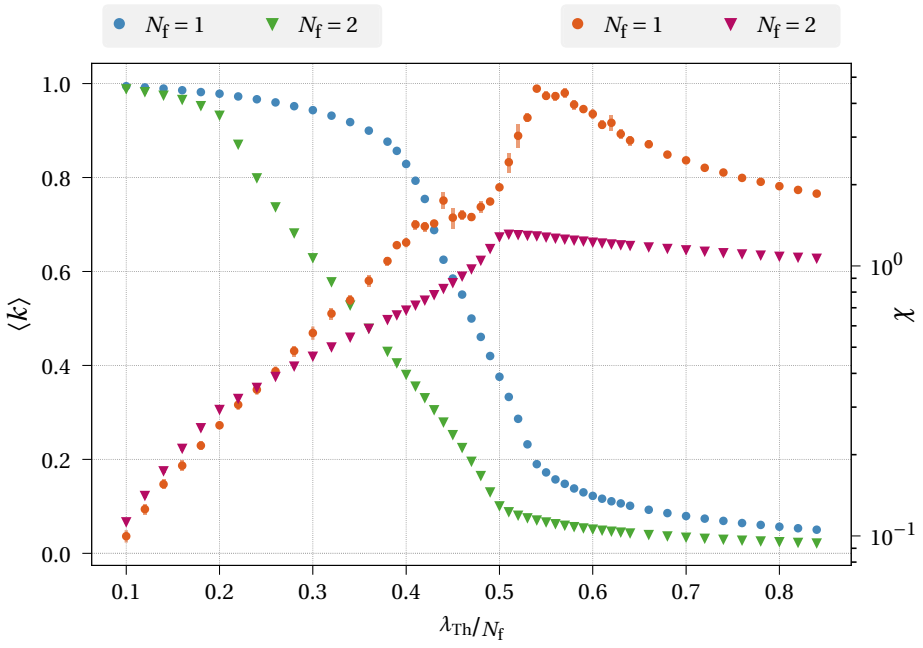

Figure 4.7.: Massless Th lattice filling factor (left axis) in comparison with susceptibility (right axis) for $N_f = 1$ (circles) and 2 (triangles). χ is shown on a logarithmic scale to highlight its curvature.

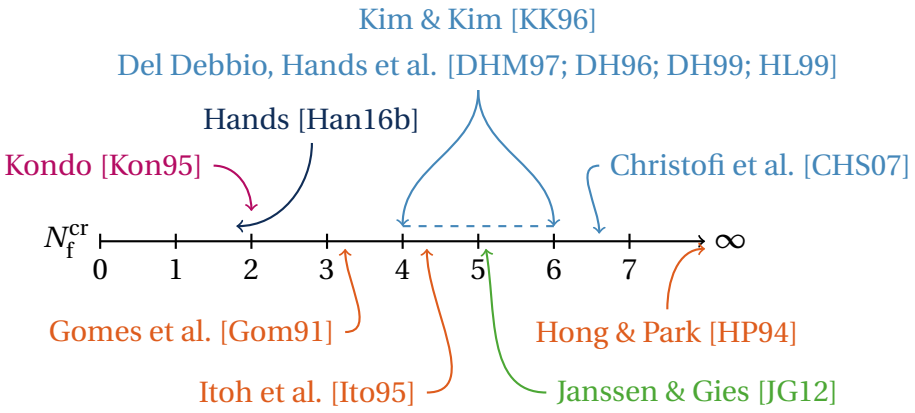

Figure 4.8.: Previous results for the critical flavour number in Th. The result of Kondo [Kon95] was obtained by large-N_f-expansion, the other sources above the line are different lattice results. Janssen & Gies [JG12] used FRG methods to obtain a value of N_f^{cr}, while the other works below the line employed DSEs. Further details are given in section 4.2.1 and section 4.2.2.

the sign problem for even $N_{f,irr}$ was expected from section 2.4.2, it is merely a numerical observation for odd $N_{f,irr}$. No configuration with negative sign was found for $N_{f,irr} = 3$ and $L = 8$ in a run generating 10000 configurations for a large range of λ_{Th}.

4.2. Discussion and Comparison With Previous Results

Contrary to our numerical results in the previous section, many older works found χSB for a small number of flavours in Th. Commonly, a critical flavour number N_f^{cr} is given, so that two phases (a broken and a symmetric one) exist for $N_f \leq N_f^{cr}$. For larger flavour numbers, the model is in the symmetric phase for any coupling. Although many estimates of N_f^{cr} are available, no agreement on a value exists. An overview of N_f^{cr} values for χSB in the reducible formulation calculated so far is given in figure 4.8.

Furthermore, the whole discussion in the literature is obscured by the subtle differences between reducible and irreducible representations. There are actually two mechanisms for dynamical mass generation: as an alternative to χSB in the reducible representation, the parity (2.23) of the irreducible model can break spontaneously. Building upon the work presented in this thesis, Björn Wellegehausen derived an effective potential for local condensates in our publication [WSW17]. Calculating coefficients of the potential with the simulation program also used here, he found no χSB for any even number of flavours in the irreducible model. This is in good agreement with our directly obtained data for the reducible model. However, a value of $N_{f,irr}^{cr} = 9$ was found for spontaneous *parity* breaking in models with an odd $N_{f,irr}$. This is not visible in figure 4.4 for $N_{f,irr} = 3$. In fact, the values of couplings where we observed χSB in [WSW17] are smaller than the ones shown in figure 4.4 and exhibit the possibly unphysical behaviour, moving to the right for increasing coupling strength. A partial explanation for the different behaviour with odd and even $N_{f,irr}$ and the

large discrepancies in the literature can be given by a parity breaking Chern-Simons-like term. It arises when integrating over an odd number of fermions, but cancels out for even numbers. The order of the limits $V \to \infty$ and $m \to 0$ determines if a cancellation happens, an issue that lead to some discussion in the literature [Gom91; Ahn94; RS94; Ito95]. Together with the potentially strong sign problem we ignored in figure 4.4, this may explain the different result we found here for Th with $N_{\mathrm{f,irr}} = 3$. More details on previous analytical results are summarised in section 4.2.1 and we compare our findings with other lattice simulations in section 4.2.2.

4.2.1. Previous Analytical Results

The oldest investigations of 3-dimensional Th were done using ingredients from a large-N_f expansion in DSE approaches. Gomes et al. [Gom91] did a first study and obtained a value of $N_\mathrm{f}^\mathrm{cr} = {}^{128}/_{\pi^2 d_\gamma}$, where $d_\gamma = 4$ for the reducible and $d_\gamma = 2$ for the irreducible model. In the first case, this leads to $N_\mathrm{f}^\mathrm{cr} \approx 3.24$. A different view on the irreducible Th was adopted by Hong & Park [HP94], leading to the conclusion that dynamical mass generation can happen for any $N_{\mathrm{f,irr}}$, so that no critical value exists. But the authors considered the breaking of the irreducible parity (2.23), for which the irreducible condensate $\langle \bar{\chi}\chi \rangle$ is an order parameter. Both papers were criticised by Itoh et al. [Ito95] for treating the auxiliary field as a gauge field, although their action was not gauge invariant. They themselves used a hidden local symmetry of Th and wrote it as a proper gauge theory with a particular gauge fixing. In a new DSE calculation for the reducible model, they found $N_\mathrm{f}^\mathrm{cr} = {}^{128}/_{3\pi^2} \approx 4.32$ for infinite coupling, the same value they had found for QED_3. This work was further extended and confirmed by Sugiura [Sug97]. Also Kondo [Kon95] used this gauge theory formulation of Th, but he constructed an effective potential for the chiral condensate in leading order of the large-N_f expansion and calculated N_f^cr as a function of the coupling, with $N_\mathrm{f}^\mathrm{cr} = 2$ for $g_\mathrm{Th}^2 \to \infty$. Employing Fierz identities when computing the effective potential, a different parity breaking pattern emerged in [Ahn94; AP98]: a dynamical mass generation for two and three irreducible flavours was seen, whereas the potential becomes unbounded from below for $N_\mathrm{f} \to \infty$. Similarly, in the functional Schrödinger picture no symmetry breaking in the large-N_f limit was found, while it appeared when higher-order corrections in ${}^1/_{N_\mathrm{f}}$ were included [HLY94]. These works mostly focused on reducible models conserving the reducible parity (2.15) [HP94; Ito95; Kon95; Sug97] or did not distinguish between irreducible and reducible models [Gom91; HLY94]. Thus, their predictions for N_f^cr should hold for χSB in the reducible representation, which we did not observe in our lattice simulations.

Recently, Janssen & Gies [JG12] did an extensive study of four-fermion theories with FRG methods, see also [GJ10; Jan12]. They only found the fixed point governing the critical behaviour of Th on the axis of pure Th interaction for $N_\mathrm{f} \to \infty$, while it was off the axis for any finite N_f. On the contrary, this fixed point was dominated by an NJL interaction for

small N_f, showing dynamical generation of a fermion mass. The latter did not exist for large N_f. Balancing this competition between scalar (NJL) and vector (Th) channels, they found $N_f^{cr} \approx 5.1(7)$.

4.2.2. Previous Lattice Results

During the 1990s, many lattice simulations of reducible Th with staggered fermions were performed, that we summarise in the first part of this section. The particular problems of this approach were already described in section 2.3.2. Only recently, other simulation methods were used to study Th, which are reviewed at the end of this section.

Conventional Algorithms with Staggered Fermions

All simulations with staggered fermions have an even number of N_f, since a single staggered flavour corresponds to two continuum flavours (see section 2.3.2). The symmetry breaking pattern for the lattice formulation of Th with N staggered flavours is [DH99]

$$U(N) \otimes U(N) \to U(N) \quad \text{with} \quad N_f = 2N, \tag{4.6}$$

and it is not clear if the correct pattern (2.6) is recovered in the continuum limit. Note, that $U(N) \otimes U(N)$ is the continuum chiral symmetry of GN in (2.14).

The first simulation results in 1996 were reported by Del Debbio & Hands [DH96] and Kim & Kim [KK96]. The latter used the hidden local symmetry of [Ito95] to simulate Th as a gauge theory. They included a small fermion mass and extrapolated the measured chiral condensate to the chiral limit. HMC simulations with lattice volumes 8^3 and 16^3 were performed for $N_f = 2, 4, 6$ and they always found a two-phase structure in the chiral condensate. Nevertheless, a qualitatively different behaviour of the phase transition for $N_f = 2$ and $N_f = 6$ was present. They concluded that the value of N_f^{cr} must be in between.

With similar parameters but with an action containing an auxiliary scalar field instead of a gauge field, Del Debbio & Hands [DH96] made use of Fisher plots to extrapolate their measured condensate to $m \to 0$. Together with the extensions [DHM97; DH99], the authors found $N_f^{cr} < 6$. The given Fisher plots clearly show χSB for $N_f = 2$ and 4 with a second-order phase transition. No clear signal appeared for $N_f = 6$, while evidence for a first-order transition with coexisting symmetric and broken phases was found. Due to this observation, they concluded that there is no possibility to perform a continuum limit for $N_f = 6$, resulting in

$$4 < N_f^{cr} < 6. \tag{4.7}$$

Their extensive study was accompanied by the investigation of susceptibilities and bound state masses as well as numerous conference proceedings [Han97; Del97b; Del97a]. It was complemented by Hands & Lucini [HL99] with simulations using a different algorithm allowing odd and non-integer flavour numbers. They mainly focused on $N_f = 3$ and 5. In the first case, a second-order phase transition was found with critical exponents fitting in

between the ones at $N_\mathrm{f} = 2$ and 4. For $N_\mathrm{f} = 5$, the order of the phase transition could not be determined. The behaviour of lines in the Fisher plot for this case [HL99, fig. 5], exhibiting an 'accumulation of the constant coupling trajectories around a line which if continued would intercept the horizontal axis', is actually similar to our observations near the transition to the unphysical phase in figure 4.1(b) and figure 4.4. Their conclusion was that the phase transition changes from second order at $N_\mathrm{f} = 4$ to first order at $N_\mathrm{f} = 6$, showing an intermediate behaviour in between. This did not allow a more precise statement than (4.7), but they gave a critical line in the (g, N_f)-plane.

Most recently, Christofi et al. [CHS07] repeated simulations with integer and non-integer values of $N_\mathrm{f} \in [2, 18]$ and various non-zero bare masses. They determined the limiting coupling, where the theory is suspected to change into an unphysical phase (see section 4.1.1), as the coupling g^{-2}_max of maximal chiral condensate. To obtain a value for N_f^cr in the strong coupling limit, they plotted both g^{-2}_max and the value of the condensate at this coupling as functions of N_f. They found some changes with the flavour number and concluded that

$$N_\mathrm{f}^\mathrm{cr} = 6.6(1). \tag{4.8}$$

Regarding details of the phase transition like critical exponents, their results disagree with the ones of the works presented in section 4.2.1 as well as our current simulations.

Fermion Bag Simulations

Another approach, also using staggered fermions and shortly introduced in section 2.4.1, are fermion bag simulations. The first example of the fermion bag algorithm already provided results for massless Th: Chandrasekharan [Cha10] found a second-order phase transition for a single staggered flavour (that would be $N_\mathrm{f} = 2$ in the reducible representation) and gave critical exponents. This study was extended to small couplings and lattice volumes up to 40^3 [CL11b; CL12a]. It was the first result with $m = 0$ and the authors noted that the chiral condensate was expected to be always zero. They studied the susceptibility instead, together with two other susceptibilities for conserved charges. Results for the critical exponents were obtained by a simultaneous fit to predictions from chiral perturbation theory. Since the fermion bag formulation also uses staggered fermions, their lattice action had the same symmetry (4.6), which may not have the correct continuum limit. Furthermore, a later paper [CL13] claimed that their lattice versions of GN and Th have the same symmetry and critical exponents. This was never observed in any other study of the two models and casts some doubt on the simulations regarding the question if the staggered lattice action successfully represents the continuum Th.

Domain Wall Fermions

The last numerical study of Th was started recently by Hands [Han16b] with exactly chiral fermions and a conventional HMC algorithm. He used domain wall fermions in a formulation presented earlier [Han15; Han16a] that are a solution to a generalised version of the Ginsparg-Wilson relation (2.49). While there was no ambiguity for GN in his setup, he

presented two versions of Th, differing in the treatment of the auxiliary vector field in the additional dimension introduced for the domain wall fermions.

Numerical simulations were performed on a lattice of volume 12^3 with a spacing of $L_s = 16$ between the domain walls. He presented results obtained with a bare mass of $m = 0.01$ for $N_\mathrm{f} = 2$. Similar to the observations with staggered fermions, he found a peak in the chiral condensate that could be related to a transition into the unphysical phase described in section 4.1.1. With domain wall fermions, the maximum was at $1/g^2 \approx 0.2$, compared to 0.3 for staggered fermions. Comparing the shape of our condensate for $m \neq 0$ in figure 4.1(a), we find qualitative agreement with these results [Han16b, fig. 10] and also the older results from staggered fermions in [DHM97, fig. 3] and [CHS07, fig. 2]. For both formulations of Th he found $\langle\bar{\psi}\psi\rangle/m$ to be constant, concluding that the chiral condensate vanishes in the limit $m \to 0$. Thus, no χSB was present for $N_\mathrm{f} = 2$ and

$$N_\mathrm{f}^\mathrm{cr} < 2. \tag{4.9}$$

The linear decrease with the mass is consistent with our observations for any N_f. Preliminary results for $N_\mathrm{f} = 1$ presented in a talk [Han17] also showed this behaviour, leading to the same conclusion as our simulations: No chiral symmetry breaking is present in simulations of reducible Th with exactly chiral fermions.

5. Coupled Models

This chapter presents simulations with an enlarged space of four-fermion interactions. The main focus is again on the chiral symmetry of Th, where the pure simulations in chapter 4 did not provide much insight. Motivated by the successful determination of critical properties for GN in chapter 3, we combine it with Th and present results for the whole two-dimensional coupling space in section 5.1. Another reason for this study are the FRG results for Th [GJ10; JG12; Jan12] (see section 4.2.1) that suggest to include more couplings in the space of four-fermion interactions.

The second model, presented in section 5.2, couples a simplified version of NJL to Th. Similar to GN, the auxiliary fields transform non-trivial under chiral transformations (see (2.36)) and we can measure the chiral condensate, but the coupled model still has a continuous $U(1)$ chiral symmetry generated by γ_5. Compared to the discrete chiral symmetry of GN, this coupled model is closer to the original formulation of Th. We can obtain histograms that directly show if the $U(1)$-symmetry is broken or not.

5.1. Thirring Model With Gross-Neveu Model

In chapter 3, we found useful results for GN with our numerical setup, where it is easy to study the scalar field expectation value as an order parameter of χSB. On the contrary, simulations of Th provided little new insight into its critical properties. Therefore, it is natural to study the combination of both models, which has the Lagrangian

$$\mathscr{L}_{\text{Th+GN}} = \bar{\psi}_a \left(\partial\!\!\!/ + \mathrm{i}V\!\!\!/ + \sigma\right) \psi_a + \frac{1}{2}\lambda_{\text{Th}} V_\mu V^\mu + \frac{1}{2}\lambda_{\text{GN}}\sigma^2. \tag{5.1}$$

A HS was already applied and introduced a vector field V_μ as well as a scalar field σ. We directly study the chiral limit $m = 0$ and always use the reducible representation, where we showed the absence of a sign problem in section 2.4.2. As usual, the couplings λ_{X} are the inverse of the original couplings in the four-fermion formulation and include a factor of N_{f}, see (2.30). Special emphasis is put on the behaviour in the limit of weak GN coupling when $\lambda_{\text{GN}} \to \infty$. In this limit we should recover the pure Th.

Our new simulations are presented in section 5.1.1 and found to be in surprisingly good agreement with the literature. Only a small number of previous works with analytical studies of the Lagrangian (5.1) are available and will be summarised and discussed in section 5.1.2.

5.1.1. Simulation Results

Numerically, the simulation of (5.1) is no more challenging than simulations of the single models. As a check for a sign problem, the model was simulated with the exact algorithm

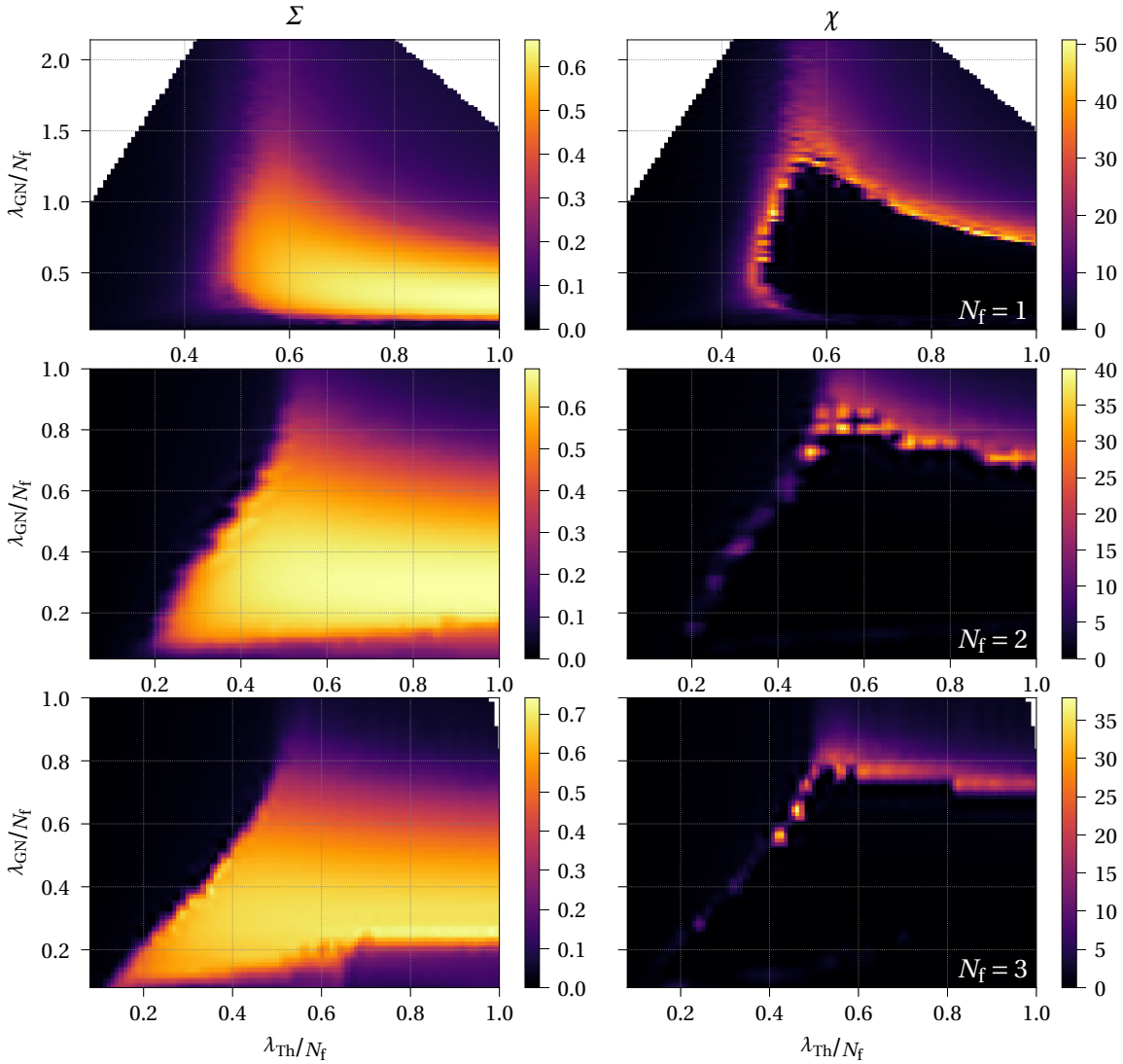

Figure 5.1.: The coupled GN and Th model for $N_f = 1,2,3$. The columns show the absolute value of the chiral condensate Σ and the susceptibility χ. The rows have $N_f = 1,2$ and 3 from top to bottom. Simulations were performed on lattice size 8 and an interpolation was used to obtain smooth images.

for $N_f = 1$, $\lambda_{GN} = 1.0, 1.2$ and various λ_{Th} on lattice size 6. No deviation from a positive determinant was found in agreement with the analytical prediction. The main additional cost comes from scanning a larger parameter space with two couplings for each N_f. For a quick overview, ensembles of 1000 configurations in the whole coupling plane were generated for lattice size 8 and $N_f = 1,2,3$. Results for Σ as defined in section 4.1.1 and its susceptibility χ are shown in figure 5.1. In all plots, we see a region of non-vanishing chiral condensate that extends to large λ_{Th}. This is expected, since the χSB of GN should be recovered in this limit. As figure 5.2(a) shows, its shape at constant λ_{Th} is already similar to the condensate of the pure GN, but the critical point is shifted to larger λ_{GN}.

Near the lower and near the left border, when at least one of the two couplings is strong, there is a connected region with small values of the condensate. We know from section 3.2.1, that thermalisation problems occur in the lower region, preventing reliable estimates of

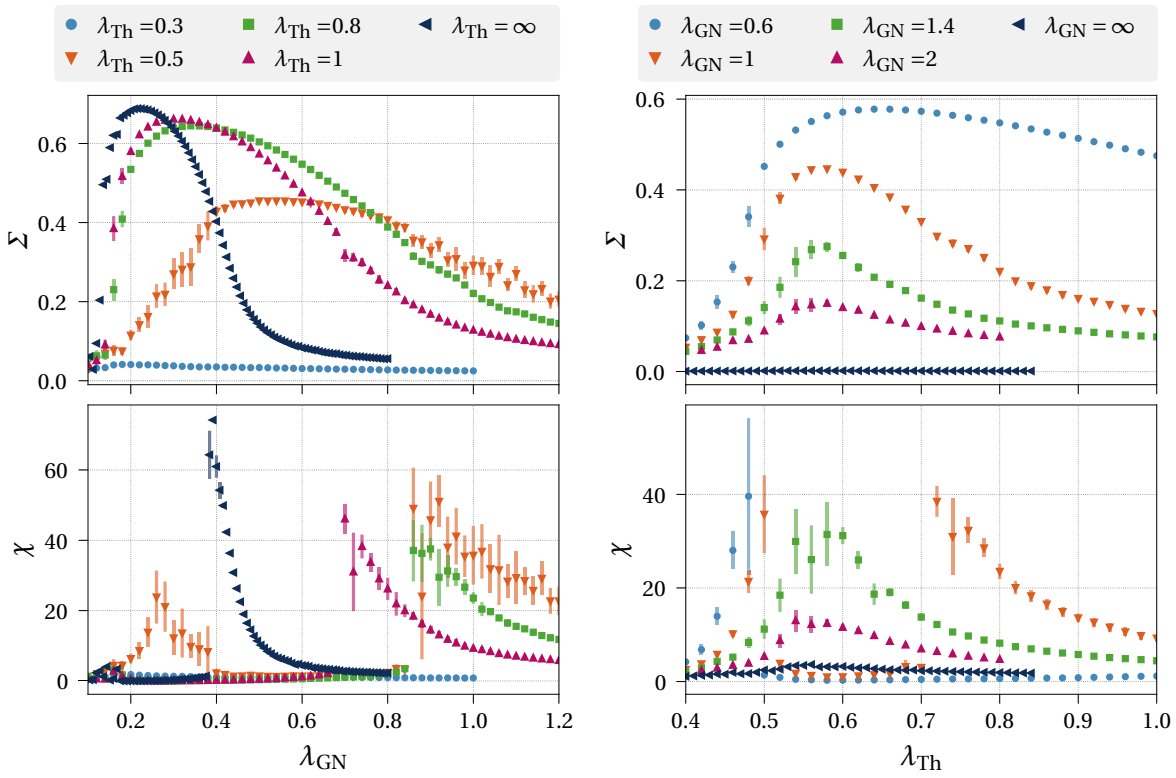

5.2(a) Cuts with constant Th coupling.

5.2(b) Cuts with constant GN coupling.

Figure 5.2.: Comparison of Σ and χ in the space of coupled GN and Th with the single models for $N_{\mathrm{f}} = 1$.

the chiral condensate. It is interesting to see that this region is connected to the left border, where the Th interaction is strong. Here, the proposed lattice artefact phase of Th from section 4.1.1 is approached in the pure Th limit $\lambda_{\mathrm{GN}} \to \infty$ (upper left corner). In the upper right region, the low value of the chiral condensate is clearly present due to the intact symmetry, since it is connected to this phase of GN. The main question is if this region is directly in contact with the unphysical phase to the left for the limit of vanishing GN coupling strength. This is difficult to tell from the data in figure 5.1 for any N_{f}.

The susceptibility also reflects this phase structure and provides a little more insight. We can identify the peak of GN which ends at the right border. Furthermore, there is a second peak, signalling the transition to the unphysical phase of Th, similar to our observations with a mass term in figure 4.1(a). Near the lower border, this second peak vanishes and only artefacts of the badly thermalised scalar field are present. Most interestingly, the physical peak merges with the other one when approaching the upper border of the pure Th, leading to the signal in figure 4.5. This fusion of the peaks can also be seen in cuts at fixed λ_{GN} as in figure 5.2(b), where the non-vanishing chiral condensate is enclosed by both peaks and decreases as the peaks join. Comparing the different flavour numbers, we can see a significant difference between $N_{\mathrm{f}} = 1$ and larger flavour numbers. While the physical phase boundary is curved upwards for $N_{\mathrm{f}} = 1$ and the condensate extends towards larger λ_{GN}, the curvature for $N_{\mathrm{f}} \geq 2$ is much smaller.

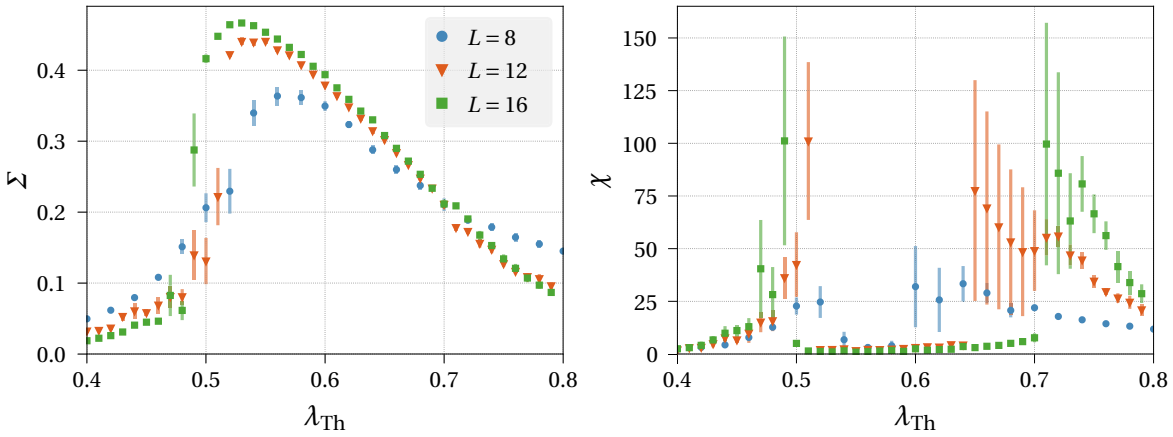

Figure 5.3.: Volume scaling of chiral condensate and susceptibility for the coupled GN and Th with $N_\mathrm{f} = 1$ at $\lambda_{\mathrm{GN}} = 1.2$.

Dependence on the Lattice Size

Simulations on larger lattice sizes were performed at a fixed value of $\lambda_{\mathrm{GN}} = 1.2$. The results can be found in figure 5.3. One can see that lattice size 8 is rather small, since the value of the chiral condensate increases and becomes more pronounced on larger lattices. From the GN simulations in chapter 3, we would expect an almost constant value of the condensate in the broken phase, as for the scalar field in figure 3.3. For $L = 12$ and $L = 16$ the lines are already in good agreement up to the transition to the unphysical phase, while the peaks in the susceptibility still move farther apart. Due to the limited statistics, the signal is noisy and further simulations would be necessary for a detailed analysis of the finite size scaling behaviour.

5.1.2. Discussion and Comparison With Previous Results

We now go on to compare our findings with the few results available from previous publications and discuss possible implications for the critical flavour number of Th.

Previous Analytical Results

Dateki [Dat97] studied the Lagrangian (5.1) with methods similar to the investigation of Th by Kondo [Kon95] (see section 4.2.1). He used the hidden local symmetry of the latter to write the coupled theory as a gauge theory with gauge field V_μ and constructed an effective potential for the order parameter by an inversion method. His main result was a critical surface in the space spanned by both couplings and N_f given by

$$g^2_{\mathrm{GN}} = 1 + \frac{1}{N_\mathrm{f}} \left(\frac{2}{g^2_{\mathrm{Th}}} \log\left(1 + g^2_{\mathrm{Th}}\right) - 1 \right). \tag{5.2}$$

In his notation, the phase transition of pure GN is at $g^2_{\mathrm{GN}} = 1 + 1/N_\mathrm{f}$ in the large-N_f expansion, in agreement with [HKK91]. He found that this point also determines the critical behaviour for the full space. If the model is in the broken phase of GN with $g^2_{\mathrm{GN}} \gtrsim 1$, this phase dominates and there is always χSB. For $g^2_{\mathrm{GN}} \lesssim 1$ (symmetric phase of GN) the coupled

model is dominated by Th, showing χSB only if the flavour number is lower than a critical one. Performing the limit $g_{\mathrm{Th}}^2 \to \infty$ in (5.2), it is given by

$$N_{\mathrm{f}} = \left(1 - g_{\mathrm{GN}}^2\right)^{-1}. \tag{5.3}$$

Approaching the critical coupling of GN, $g_{\mathrm{GN}}^2 \to 1$, we see that $N_{\mathrm{f}}^{\mathrm{cr}} \to \infty$, as expected for pure GN. Possible implications for the critical flavour number of Th were not discussed by the author, but we can recover the pure Th for $g_{\mathrm{GN}}^2 \to 0$, which obviously gives $N_{\mathrm{f}}^{\mathrm{cr}} = 1$. Thus, (5.2) implies the existence of χSB in pure Th for $N_{\mathrm{f}}^{\mathrm{cr}} = 1$, but only at infinitely strong Th coupling. First setting $g_{\mathrm{GN}}^2 = 0$ in (5.2), we get an expression for the critical flavour number of Th:

$$N_{\mathrm{f}} = 1 - \frac{2}{g_{\mathrm{Th}}^2} \log\left(1 + g_{\mathrm{Th}}^2\right). \tag{5.4}$$

This also exhibits a phase transition for $N_{\mathrm{f}}^{\mathrm{cr}} = 1$ at infinite coupling, while no χSB exists for larger N_{f} or at any finite value of Th coupling if we only consider integer numbers of (reducible) flavours. However, note that $N_{\mathrm{f}} = 1$ is not *large*. The expansion in $1/N_{\mathrm{f}}$ is likely not valid for this value!

Results in qualitative agreement with Dateki [Dat97] were already found before by Kim et al. [KKK95] using DSEs. But similar to the first works for Th, they added a gauge fixing term to the Lagrangian without physical motivation. These results were used by a few works [DGM98; MS00] using the combined interaction of Th and GN to model the low energy behaviour of superconductors. From a FRG perspective, it is natural to study a whole theory space with different interaction channels. As mentioned earlier, Janssen & Gies [JG12] studied a complete basis of four-fermion interactions, a part of which are GN and Th. Since the fixed point dominating the critical behaviour of Th was found to have non-vanishing λ_{GN} for finite N_{f}, this is another motivation to study a space of more than a single four-fermion interaction.

Comparison with Our Numerical Results

The result of Dateki [Dat97] is plotted in figure 5.4 and bears a resemblance to our lattice simulations in figure 5.1. He observed a similar difference between $N_{\mathrm{f}} = 1$ and larger flavour numbers because the critical line only diverges for $N_{\mathrm{f}}^{\mathrm{cr}} = 1$ and reaches the pure Th ($\lambda_{\mathrm{Th}} \to 0$). The situation in our lattice simulations is complicated by the lattice artefact phase of Th. If we stick to the interpretation that this phase starts where the renormalised coupling λ_{R} from (4.4) turns zero and that this point corresponds to the second peak in the susceptibility (or the decrease of the chiral condensate), the question about a critical flavour number can be formulated in terms of the susceptibility peaks in the $(\lambda_{\mathrm{GN}}, \lambda_{\mathrm{Th}})$-plane. There are three different possibilities: The two peak lines ...

1. intersect at finite λ_{GN};
2. stay apart for all λ_{GN}; or
3. merge in the $\lambda_{\mathrm{GN}} \to \infty$ limit.

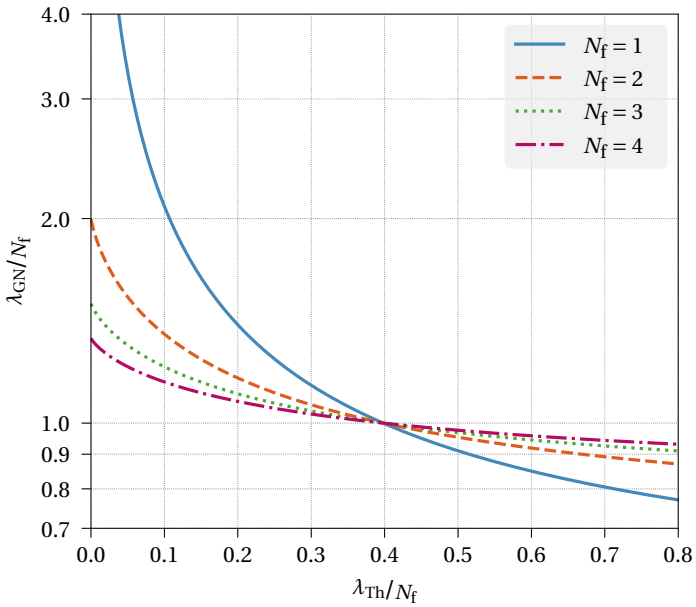

Figure 5.4.: Critical lines calculated by Dateki [Dat97] in the GN and Th plane for various flavour numbers. The blue line for $N_f = 1$ diverges when $\lambda_{Th} \to 0$, indicating χSB in the strong coupling limit. In the other cases, the finite value of $\lambda_{GN} = {}^{N_f^2}/_{N_f-1}$ is reached according to (5.3). These cases do not show χSB in the pure Th limit. Although not visible in the plot, the lines approach ${}^{N_f}/_{N_f+1}$ for large λ_{Th}, as required by the large-N_f expansion of the pure GN.

In the first case, there would be no χSB for this flavour number, while it would be clearly present in the second case. For the last possibility, we would have found N_f^{cr} in the limit $\lambda_{Th} \to 0$ as commonly given by the analytical works in section 4.2.1. In the scenario of Dateki [Dat97], we have the third case for $N_f = 1$ and the first one for all other integer values of N_f. Our simulation results are consistent with this scenario, since the peaks only seem to merge for $N_f = 1$ and there is still a single peak left in pure Th. Only a very small signal remains for $N_f \geq 2$ making the case 1 most likely. Thus, our simulations favour $N_f^{cr} < 2$. It is not possible to tell with the available amount of data if we really have χSB for $N_f = 1$. Besides a merged peak, the signal for pure Th could be only the unphysical peak, while the physical phase transition vanished in the artefact phase. Also the second scenario is still feasible, since the peaks move apart for larger volumes. A careful study of the infinite volume limit together with the limit of $\lambda_{GN} \to \infty$ would be necessary to exclude it. We present a more detailed study in the next section for a combined model that preserves a larger symmetry group.

5.2. Thirring Model With a Global $U(1)$ Model

The study of coupled GN and Th in section 5.1 already provided some insight into χSB in the plane spanned by both couplings and in the limit of pure Th. But this approach breaks a part of the large chiral symmetry group of Th down to the symmetry of GN with a discrete $\mathbb{Z}_2$ group. In order to study a coupled model with a continuous symmetry, we chose a version of NJL, where the chiral symmetry (2.5d) generated by γ_5 is intact and the auxiliary fields transform under a group of $U(1)$ as given in (2.36). To keep it as simple as possible, the new fields are taken to be *global*, in the sense that they are constant in spacetime. They can vary from one configuration to another, but the field values are the same for all lattice points.

5.2.1. Model Definition and Observables

Here, we present the Lagrangian of the model that we simulated together with special observables adapted to the $U(1)$-symmetry of the coupled model.

Model Definition

We use an action that is based on a sum of the Lagrangians for Th in (2.33) and NJL in (2.35). Together with the partition function, it is given by

$$S = \sum_x \bar{\psi}\left(\partial\!\!\!/ + \mathrm{i}V\!\!\!/ - \frac{1}{\sqrt{V}}\left(\sigma + \mathrm{i}\gamma_5\tau\right)\right)\psi + \frac{1}{2}\lambda_{\mathrm{Th}}\sum_x V_\mu V^\mu + \frac{1}{2}V\lambda_{\mathrm{g}}\left(\sigma^2+\tau^2\right) \tag{5.5}$$

$$:= S_{\mathrm{D}} + S_{\mathrm{Th}} + S_{\mathrm{g}}, \tag{5.6}$$

$$Z \propto \int \mathscr{D}\bar{\psi}\mathscr{D}\psi\mathscr{D}V_\mu \,\mathrm{d}\sigma\,\mathrm{d}\tau\,\mathrm{e}^{-S}. \tag{5.7}$$

Note, that there is no summation over the lattice in S_{g} because the fields are constant in spacetime. This is also the reason for the volume factor of $1/\sqrt{V}$ in the Dirac operator. After a rescaling of the fields like $\sigma \to \sqrt{V}\sigma$, we can integrate them out and obtain a four-fermion action similar to (2.9). But due to the global fields, the action

$$\mathrm{e}^{-S_{\mathrm{g}}} = \exp\left(\frac{1}{2\lambda_{\mathrm{g}}N_{\mathrm{f}}}\left(\Sigma^2 - T^2\right)\right) \tag{5.8}$$

contains averages over the lattice in $\Sigma := \frac{1}{V}\sum_x \bar{\psi}_x\psi_x$ and $T := \frac{1}{V}\sum_x \bar{\psi}_x\gamma_5\psi_x$, that can be interpreted as real and imaginary part of the chiral condensate. In the limit $\lambda_{\mathrm{g}} \to \infty$, the action gives a trivial contribution of 1 to the partition function and we recover Th. Similarly, we can switch off the Thirring coupling to perform a simulation of the global NJL part.

For the definition of observables, it is convenient to transform the fields to a polar coordinate form with $\sigma = r\cos\phi$ and $\tau = r\sin\phi$, adapted to the $U(1)$-symmetry of the global model. In the following, we will use a partition sum $Z(r)$ dependent on the radial direction r and defined via

$$Z := \int_0^\infty \mathrm{d}r\, r\,\mathrm{e}^{-S_{\mathrm{g}}(r)}Z(r). \tag{5.9}$$

Observables

We can use $Z(r)$ to get a formula for the absolute value of the chiral condensate by

$$\bar{\Sigma} = \frac{1}{V}\sum_x \langle\bar{\psi}\mathrm{e}^{\mathrm{i}\gamma_5\phi}\psi\rangle = \int_0^\infty \mathrm{d}r\; r\mathrm{e}^{-\lambda_{\mathrm{g}}r^2}\Sigma_r. \tag{5.10}$$

Here, Σ_r is defined as

$$\Sigma_r = \frac{1}{\sqrt{V}}\frac{\partial \ln Z(r)}{\partial r} = \frac{1}{VZ(r)}\int \mathscr{D}\bar{\psi}\mathscr{D}\psi\mathscr{D}V_\mu \int_0^{2\pi}\mathrm{d}\phi\sum_x \bar{\psi}\,\mathrm{e}^{\mathrm{i}\gamma_5\phi}\psi\,\mathrm{e}^{-S_{\mathrm{D}}-S_{\mathrm{Th}}}. \tag{5.11}$$

In addition, we define a corresponding rotated susceptibility $\bar{\chi}$ by using $\frac{\partial^2 \ln Z(r)}{\partial r^2}$ in the expressions above. A direct measurement of the chiral condensate is also possible. Additionally, we can obtain histograms in the (Σ, T) plane, but it proved to be more beneficial

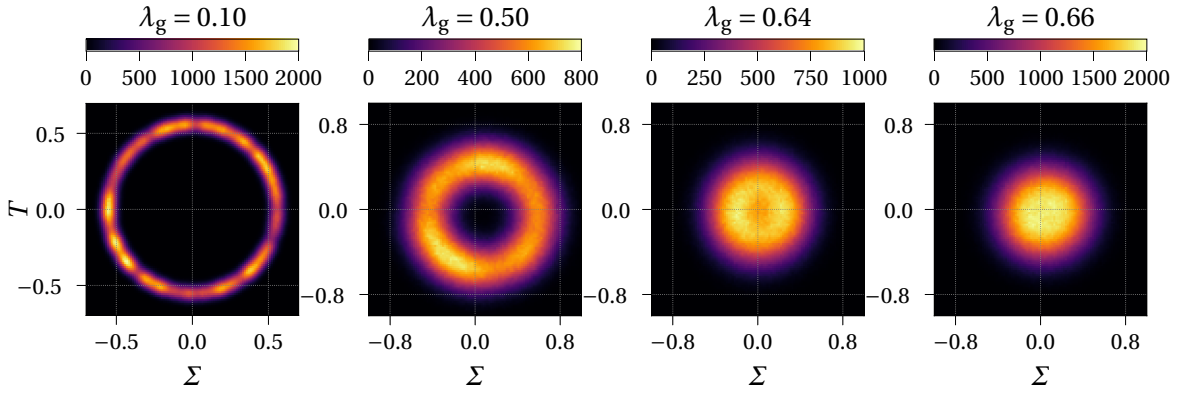

Figure 5.5.: Histograms of the chiral condensate for the pure global model with $N_f = 2$ and $L = 16$. The given couplings are in the unphysical phase ($\lambda_g = 0.10$), in the broken phase ($\lambda_g = 0.50$), close to the critical coupling ($\lambda_g = 0.64$) and in the symmetric phase ($\lambda_g = 0.66$).

to make histograms of $\Sigma(x) := (\bar{\psi}\psi)(x)$ and $T(x) := (\bar{\psi}\gamma_5\psi)(x)$ at each point x on the lattice. The remaining $U(1)$-symmetry leads to rotationally invariant two-dimensional histograms and the observed forms are either rings or disks. To analyse this data, we calculate another one-dimensional local histogram in the radial direction by computing $r = \sqrt{\sigma^2 + \tau^2}$ and binning the r-values. Since we choose the bins of the radial histogram of equal width Δr, we have to include a correction because the area in the original histogram grows with the radius. The area of the ring corresponding to bin k is

$$\pi\left(r_{k+1}^2 - r_k^2\right) = \pi\left((r_k + \Delta r)^2 - r_k^2\right) = \pi\Delta r\,(2r_k + \Delta r) = 2\pi\Delta r\,\bar{r}_k, \tag{5.12}$$

where $\bar{r}_k = \frac{1}{2}(r_{k+1} + r_k)$ is the midpoint of each bin. Since $2\pi\Delta r$ is constant, we divide each value in a bin by $\bar{r}_k$ to obtain a correct histogram. We use a cubic spline interpolation of the radial histogram to obtain the radius with the maximal value, which should correspond to the absolute value of the chiral condensate. In the following, we call this condensate Σ_{hist}.

5.2.2. Simulation Results for the Pure Global Model

At first, we study the pure global model without Th interaction. As mentioned earlier, we can make histograms for real and imaginary parts of the condensate. Examples for $N_f = 2$ on lattice size 16 are shown in figure 5.5. The corresponding observables introduced in section 5.2.1 are shown in figure 5.6. At very strong global couplings, we find rings with small width as in the first image of figure 5.5. The radius, corresponding to the absolute value of the chiral condensate, increases with λ_g up to a maximum. Around this maximum, the width of the rings grows, so that the rings look like in the example in the second image of figure 5.5. Following the previous interpretations, the physical phase with χSB is to the right of the maximum in figure 5.6. In this phase, the radius of the rings decreases with decreasing coupling strength up to a point of phase transition. Around this point, the rings no longer show a clear hole in the origin as in the third image. Finally, we get small disks centred around the origin when we arrive in the symmetric phase.

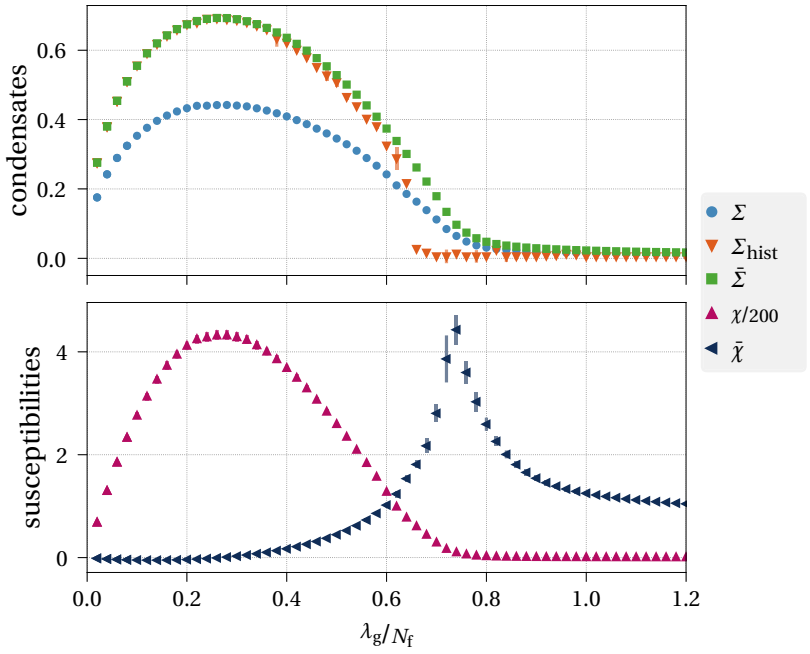

Figure 5.6.: Comparison of observables for the pure global model with $N_f = 2$ and $L = 16$. The upper part shows the three different versions of the absolute value of the chiral condensate. The lower part shows the common and the radial susceptibility defined below equation (5.11). Note, that χ is rescaled by an arbitrary factor of 200 to fit it into the plot.

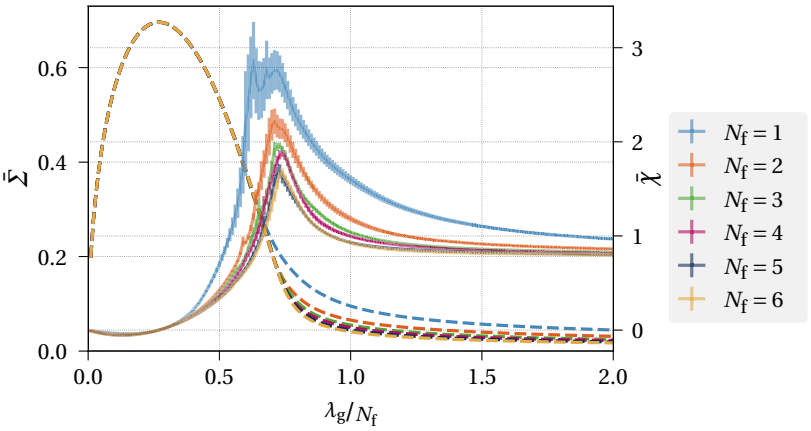

Figure 5.7.: The rotated observables for varying N_f in the pure global model. The left vertical axis gives the range for $\bar{\Sigma}$ (dashed lines), while the right vertical axis measures $\bar{\chi}$ (solid lines).

In figure 5.6, the data points labelled with Σ_{hist} are obtained from these histograms. The fluctuations and errors around the critical point result from the difficulty to distinguish rings and disks at these couplings. The rotated chiral condensate $\bar{\Sigma}$ defined in (5.11) is indeed a good definition to describe the radius of the histograms. In the broken phase it agrees well with Σ_{hist} and does not suffer from the problems around the phase transition. On the other hand, it shows no sharp transition at this point due to finite-size effects like the condensate of GN (see figure 3.1 and figure 3.3). Thus, Σ_{hist} is more reliable to indicate a symmetric phase. The usual definition of the absolute value of the chiral condensate Σ shows a behaviour similar to $\bar{\Sigma}$ but has a smaller scale. The lower part of figure 5.6 shows, that the peak of the ordinary susceptibility χ is *not* at the physical transition. Its form follows the shape of the chiral condensate. On the contrary, the rotated susceptibility $\bar{\chi}$ has a peak at the critical point and serves as a good observable for it.

Regarding the dependence on N_f, only little variation is found in figure 5.7. The peak in $\bar{\chi}$ is less pronounced for larger N_f and the finite size effects in $\bar{\Sigma}$ are smaller. Most importantly, the physical phase transition stays at constant $\lambda_g/N_f \approx 0.75$ and the position of the maximal

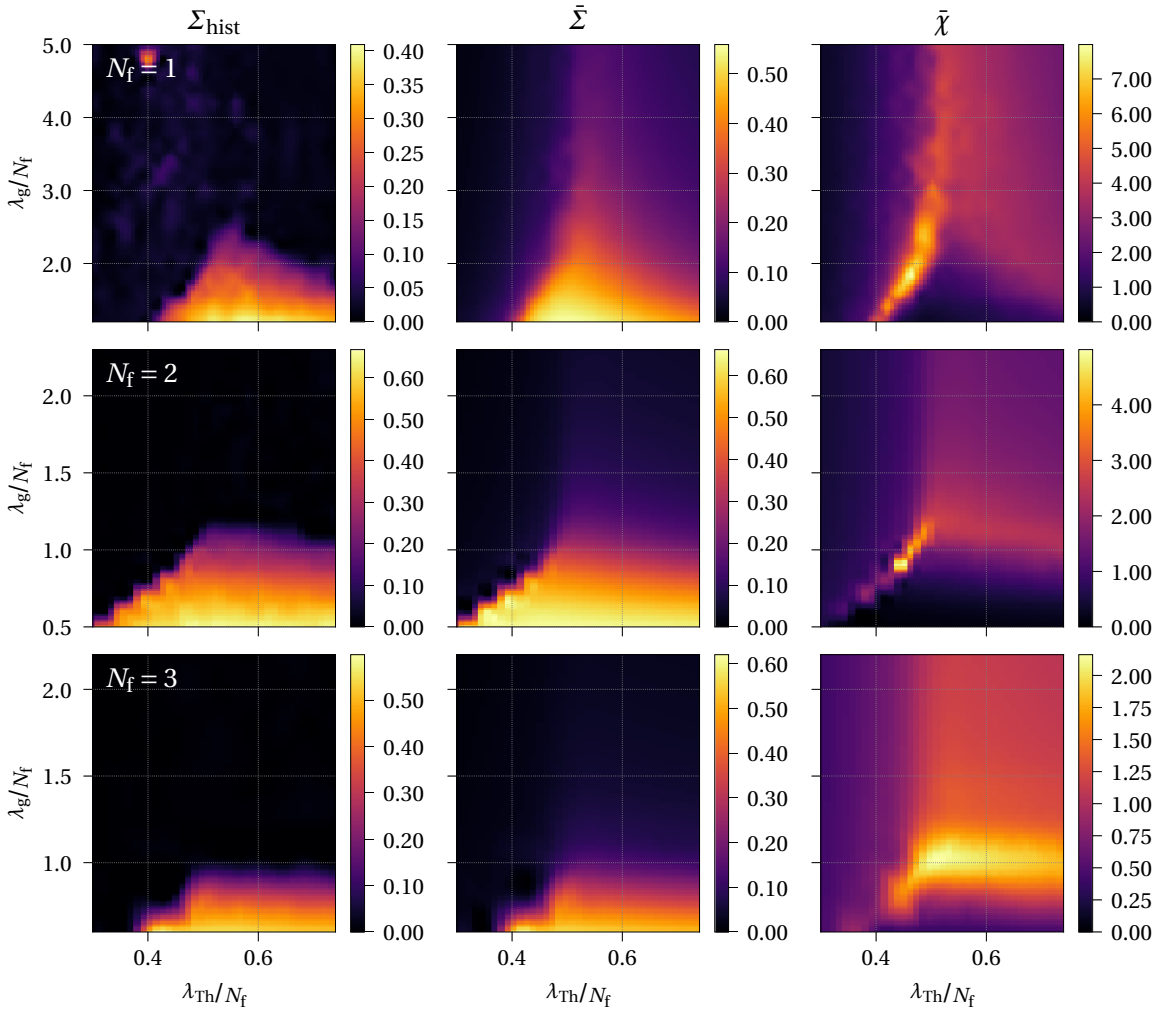

Figure 5.8.: Coupled Th with global NJL for various flavours on $L = 8$. An interpolation was used to obtain smooth images.

condensate is also constant. Comparing the simulations on lattice size 8 in figure 5.7 with size 16 in figure 5.6, the rotated susceptibility grows with increasing lattice size, as expected. The observables related to the chiral condensate are more pronounced on the larger lattice, but the phase transition stays roughly at the same coupling.

5.2.3. Simulation Results for the Coupled Model

We now turn towards simulations in the full two-dimensional coupling space of the model (5.7). For various couplings on lattice size 6 with $N_f = 1$, the determinant showed no negative sign in a simulation with 1000 updates that were performed with an exact calculation of it. Thus, we can be assured that rHMC simulations are feasible. A first overview of the full coupling space is given in figure 5.8 for lattice size 8. Due to the observations in section 5.2.2, we show the rotated observables $\bar{\Sigma}$ and $\bar{\chi}$ together with the chiral condensate from the radial histogram Σ_{hist}. The general behaviour is similar to the coupled GN and Th described in section 5.1 (see in particular figure 5.1). For $N_f \geq 2$, the condensate extends only shortly into the region of $\lambda_g/N_f \gtrsim 0.75$, where the pure global model is in the symmetric

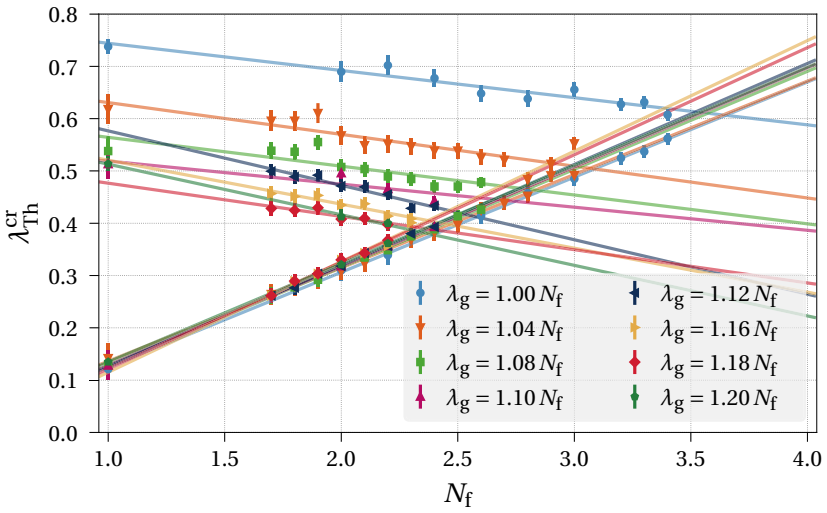

Figure 5.9.: The two critical points from Σ_{hist} for $L = 12$ as a function of N_{f}. The larger value of λ_{Th} corresponds to the physical transition and the smaller one to the unphysical transition. Data is shown together with linear extrapolations in N_{f}.

phase. Again, this non-zero region is more pronounced for $N_{\mathrm{f}} = 1$. Comparing the two versions of the chiral condensate, we can see here that the smeared extension of $\bar{\Sigma}$ to large λ_{g} does not occur for Σ_{hist}. It is only an artefact of the stochastic estimation.

The susceptibility shows two peaks, where the one to the right (for $\lambda_{\mathrm{Th}} \to \infty$) belongs to the physical transition of our global NJL model. One more time, we observe a second peak, that we can attribute to the unphysical phase transition of Th. It merges with the physical peak in the limit $\lambda_{\mathrm{g}} \to \infty$, where we recover the pure Th. Thus, we are faced with the same problem described in section 5.1.2.

Extrapolation of $N_{\mathrm{f}}^{\mathrm{cr}}$ as a Function of λ_{g}

We now investigate the extrapolation $\lambda_{\mathrm{g}} \to \infty$ in more detail on larger lattices. To determine a critical flavour number at a fixed λ_{g}, we performed simulations with many non-integer $N_{\mathrm{f}} \in [1.7, 4.0]$, which is possible in the rHMC algorithm as long as an integer number of pseudofermions is used, see (2.45). We obtained values of $\lambda_{\mathrm{Th}}^{\mathrm{cr}}$ for the artefact transition as the point of steepest increase in Σ_{hist} for increasing λ_{Th}. For the physical transition, we use the point, where the condensate falls below a threshold of 0.03. Plotting both critical points for $L = 12$ as a function of N_{f} for various global couplings, we obtain figure 5.9. We find a good agreement with linear fits of $\lambda_{\mathrm{Th}}^{\mathrm{cr}}(N_{\mathrm{f}})$ for both transitions. Chiral symmetry breaking is present for a given λ_{g} in the triangular region between the two lines of the corresponding colour. An estimate for $N_{\mathrm{f}}^{\mathrm{cr}}$ at the given λ_{g} can be obtained by the intersection of the two lines, indicating the point, where the physical transition moves into the artefact phase. Increasing λ_{g}, the position of the unphysical transition is quite stable, while the $\lambda_{\mathrm{Th}}^{\mathrm{cr}}$ of the physical point decreases. This narrows down the region of non-zero chiral condensate and reduces $N_{\mathrm{f}}^{\mathrm{cr}}$. Simulations with $\lambda_{\mathrm{g}}/N_{\mathrm{f}} = 1.0$ on $L = 16$ showed a similar trend when increasing the lattice size. Extrapolating $N_{\mathrm{f}}^{\mathrm{cr}}(\lambda_{\mathrm{g}})$ in the global coupling, we obtained figure 5.10 and a good fit with a rational function

$$N_{\mathrm{f}}^{\mathrm{cr}}(\lambda_{\mathrm{g}}) = 2.15(4) + 1.44(4)\left(\frac{\lambda_{\mathrm{g}}}{N_{\mathrm{f}}}\right)^{-12.0(9)}. \tag{5.13}$$

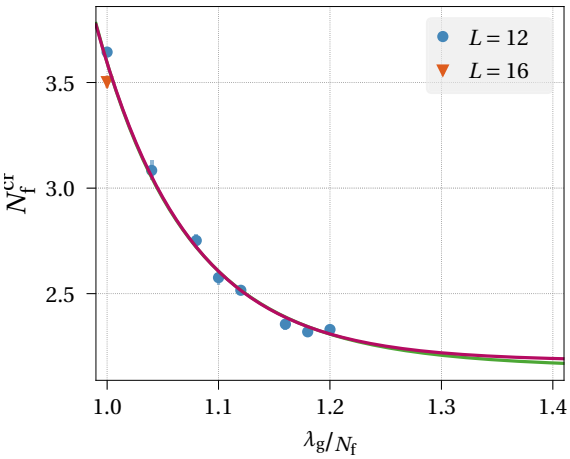

Figure 5.10.: Extrapolation of N_f^{cr} as a function of the global coupling. The values for N_f^{cr} are obtained by intersecting the two lines for each λ_g in figure 5.9. Two fits with the rational function (5.13) and an exponential form are shown, but only small deviations near $\lambda_g = 1.4\,N_f$ are visible.

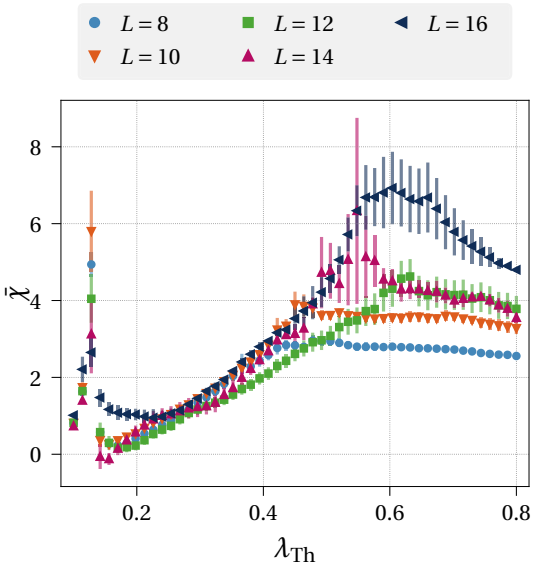

5.11(a) $\lambda_g = 1.0\,N_f$

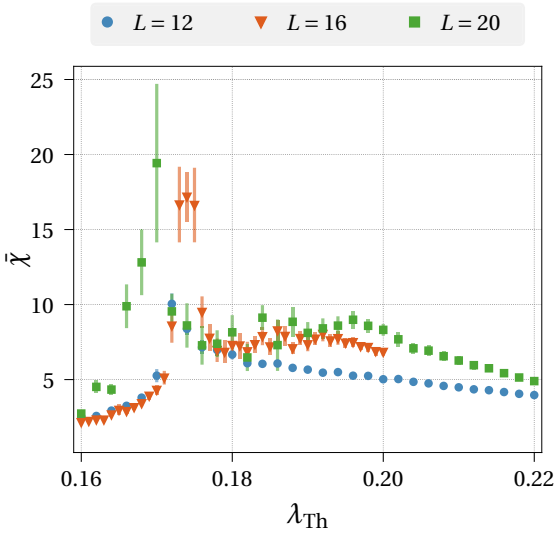

5.11(b) $\lambda_g = 4.0\,N_f$

Figure 5.11.: Rotated susceptibility $\bar{\chi}$ for $N_f = 1$ and fixed λ_g as a function of Th coupling. Note the different scales on both axes.

This leads to a value of $N_f^{cr} = 2.15(4)$ for the pure Th. A fit with an exponential ansatz found a similar result of $N_f^{cr} = 2.18(3)$.

Extrapolation for $N_f = 1$

Additional simulations for $N_f = 1$ were performed to probe the result at weaker global coupling and with more lattice sizes. Since values of Σ_{hist} become too small for reliable estimates of the critical points, we now use peaks in the rotated susceptibility $\bar{\chi}$. An overview for two global couplings is given in figure 5.11. With $\lambda_g = 1.0\,N_f$ close to the critical coupling of the pure global model, we find a sharp peak at the unphysical transition and a well-separated, wide maximum at larger λ_{Th} that grows with increasing lattice size. For $\lambda_g = 4.0\,N_f$ and $L = 12$, we do not find a second maximum related to a physical transition, casting doubt on our previously obtained critical flavour number. A small maximum appears again for $L = 16$ and 20, very close to the sharp peak of the unphysical transition.

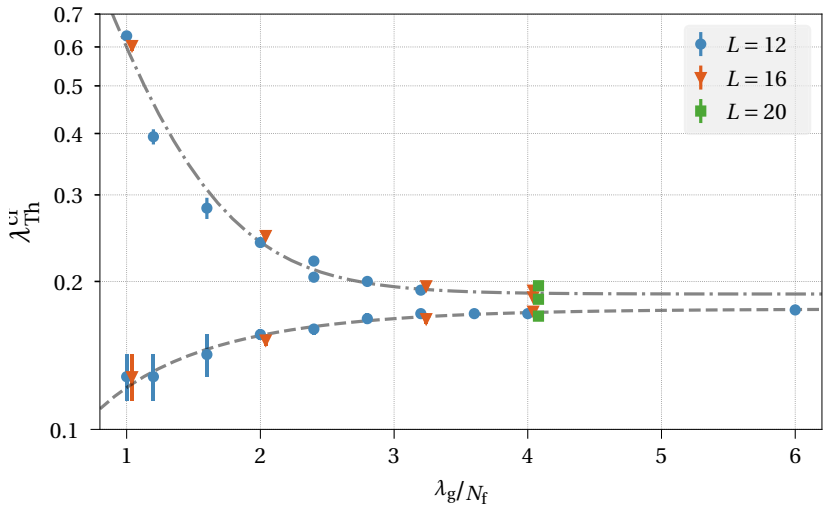

Figure 5.12.: All maxima of the rotated susceptibility $\tilde{\chi}$ for $N_{\mathrm{f}} = 1$. The error bars represent the resolution in λ_{Th} used in the simulations. Note the logarithmic scale on the vertical axis and the small offset added to λ_{g} for $L = 16$ and 20 to increase visibility of the data points.

The positions of all maxima we found are indicated in figure 5.12. Here, rational fits did not work well, but we were able to model the λ_{g}-dependence by an exponential ansatz with $\lambda_{\mathrm{Th}}^{\mathrm{cr}} = a\,\mathrm{e}^{-b\lambda_{\mathrm{g}}} + c$. We found $c = 0.176(1)$ for the unphysical transition and $c = 0.189(1)$ for the physical one, suggesting that the peaks stay apart for $\lambda_{\mathrm{g}} \to \infty$. However, we must admit that simulations with larger λ_{g} likely do not show separate peaks unless larger lattices are used. This delicate handling of the two limits $\lambda_{\mathrm{g}} \to \infty$ and $V \to \infty$ prevents more reliable results.

6. Reformulations

After the direct simulation of Th in the common vector field formulation in chapter 4 and the studies of Th coupled with other models in chapter 5, this section presents another alternative approach to χSB for Th. We abandon the vector field formulation, where no order parameter of χSB is accessible, and reformulate Th with other degrees of freedom. Fierz identities, already introduced in section 2.2.1, provide means to do this in various ways. Results of simulations with these transformed Lagrangians are reported in section 6.1.

The second part in section 6.2 is closely related to this since it was originally invented by Björn Wellegehausen to overcome the sign problem that we will find in section 6.1. It is an adaption of the fermion bag idea of Chandrasekharan [Cha08; Cha10], that we reviewed in section 2.4.1, to our setup with the SLAC derivative. We re-express the partition sum of our four-fermion models in terms of a new dual field that can be interpreted as an occupation number for the lattice degrees of freedom.

6.1. Fierz Identities

In this section, we study Th after the application of Fierz identities, as described in section 2.2.1. To our knowledge, no previous lattice simulations with this setup were published, but Fierz identities have been used for large-N_f [Ahn94; AP98] and FRG studies [GJ10; Jan12; JG12] of Th. Results of these works were already reviewed in section 4.2.1. We will present details about the implemented actions in section 6.1.1. Since it was not possible to show the absence of a sign problem in section 2.4, we investigate its occurrence and severity in section 6.1.2.

6.1.1. Implementation Details

Starting point for the implementation are the Lagrangians after HS in (2.37) and the variants in (2.38). Here, we show an example for the formulation (2.38b), which has the fewest number of degrees of freedom. It contains a Hermitian, traceless matrix $\hat{T}$ of dimension $N_\mathrm{f,irr}$, which has $N_\mathrm{f,irr}^2 - 1$ independent real entries. As a basis for such matrices, we can take generalisations of the Gell-Mann matrices λ_s as given by Stover [Sto] and use the decomposition $\hat{T}_{\alpha\beta} = t_s(\lambda_{\alpha\beta})_s$ with $s = 1, \dots, N_\mathrm{f,irr}^2 - 1$. Together with the trace degree of freedom ϕ, the reformulated model includes $N_\mathrm{f,irr}^2$ real scalar fields, while Th contains three, independently of $N_\mathrm{f,irr}$. With the trace of the generalised Gell-Mann matrices in flavour space given by $(\lambda_{\alpha\beta})_s(\lambda_{\beta\alpha})_r = 2\delta_{sr}$, we can write

$$\hat{T}_{\alpha\beta}\hat{T}_{\beta\alpha} = t_s t_r (\lambda_{\beta\alpha})_s (\lambda_{\alpha\beta})_r = 2\sum_s t_s^2. \tag{6.1}$$

Now, the Lagrangian reads

$$\mathscr{L}_{\mathrm{FM}} = \bar{\chi}_\alpha \left[\left(\partial\!\!\!/ + m + \phi \right) \delta_{\alpha\beta} + t_s (\lambda_{\alpha\beta})_s \right] \chi_\beta + \frac{1}{2} \lambda_{\mathrm{Th}} \sum_s t_s^2 + \frac{\lambda_{\mathrm{Th}} N_{\mathrm{f,irr}}}{2\,(2 + N_{\mathrm{f,irr}})} \phi^2 . \tag{6.2}$$

We can finally rescale the field $\phi \to \sqrt{\frac{2+N_{\mathrm{f,irr}}}{N_{\mathrm{f,irr}}}}\phi$ and obtain the implemented Lagrangian

$$\mathscr{L}_{\mathrm{FM}} = \bar{\chi}_\alpha \left[\left(\partial\!\!\!/ + m + \sqrt{\frac{2 + N_{\mathrm{f,irr}}}{N_{\mathrm{f,irr}}}} \phi \right) \delta_{\alpha\beta} + t_s (\lambda_{\alpha\beta})_s \right] \chi_\beta + \frac{1}{2} \lambda_{\mathrm{Th}} \left(\sum_s t_s^2 + \phi^2 \right). \tag{6.3}$$

The same procedure can be applied for the other reformulations.

Contrary to the models studied in chapter 3, 4 and 5, the Lagrangians resulting from (2.37) have Dirac operators which are non-diagonal in flavour space. Therefore, it is not possible to write the fermion determinant as a power of the single-flavour operator as in (2.45). We have to use the full operator with flavour indices, so that the matrix size grows with $N_{\mathrm{f,irr}}$. This largely increases the computational costs for larger flavour numbers. Since we must expect a sign problem (see section 2.4.2), we use conventional simulations with the exact update algorithm described in section 2.3.1 to study it.

6.1.2. Simulation Results

In figure 6.1(a), we compare the different formulations of Th for $N_{\mathrm{f,irr}} = 2$ and $L = 4$. This figure confirms the absence of a sign problem for Th in the usual vector field formulation for even $N_{\mathrm{f,irr}}$ that was already discussed together with the massive model in figure 4.3. Furthermore, results for the first Fierz identity (2.26a), leading to FM, and the second identity (2.26b), leading to FVM, are given. The corresponding Lagrangians were given in (2.37a) and (2.37b). For the first Lagrangian with a GN-like term and a matrix field in flavour space, no restrictions on the sign of the determinant were found in section 2.4.2 and a complex phase is indeed present in our simulations. The deviations from a real weight are strongest in a region of $\lambda_{\mathrm{Th}}/N_{\mathrm{f}} \in [0.2, 0.4]$ and decrease for both stronger and weaker couplings. Since the weights are not close to zero, reweighting as in (2.58) is possible and was performed for Σ in figure 6.2. The region of imaginary weights is accompanied by a maximum in the chiral condensate that could be a sign of χSB. Reweighting is clearly necessary and alters the mean values in a significant way. Unfortunately, an increase in lattice size dramatically worsens the sign problem. Results for the still very small size $L = 6$ are shown in figure 6.1(b). There, we find a region with complex determinant, where the real part of the average weight $\langle w \rangle$ is close to zero, rendering reweighting impossible. When increasing $N_{\mathrm{f,irr}}$, this behaviour does not change except that the sign problem also seems to be present for small λ_{Th}. Note, that only very few configurations could be obtained for larger N_{f} because the computational cost drastically increases as the number of degrees of freedom grows with $N_{\mathrm{f,irr}}^2$. By any account, conventional simulations with Lagrangian

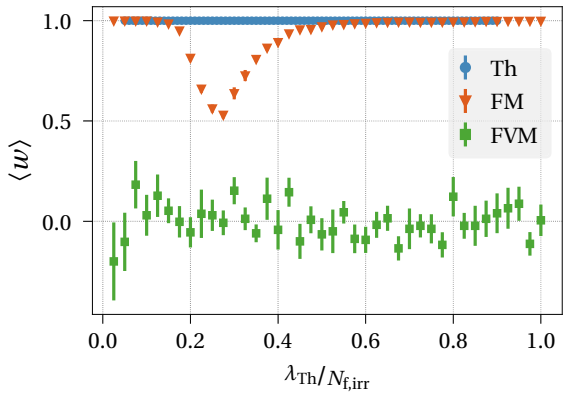

6.1(a) Different formulations of Th for $N_{\text{f,irr}} = 2$ and $L = 4$. A sign problem is present for both Lagrangians after Fierz transformations.

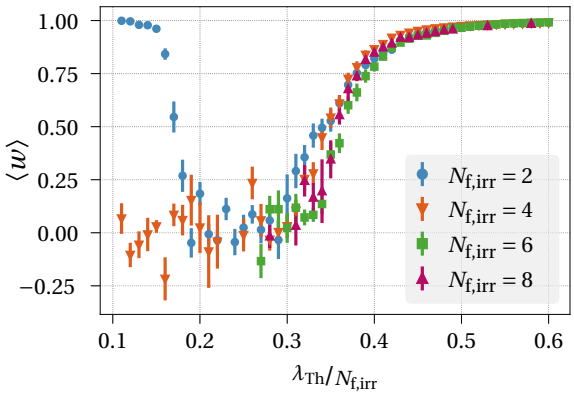

6.1(b) FM with different $N_{\text{f,irr}}$ and $L = 6$. There is a region with $\lambda \lesssim 0.35 N_{\text{f,irr}}$ for any $N_{\text{f,irr}}$, where the sign problem is very severe.

Figure 6.1.: Study of the sign problem of Th after Fierz transformations were applied. Both plots show the real part of average values of the weight defined in (2.58) that is 1 if the determinant of the Dirac operator is real and positive.

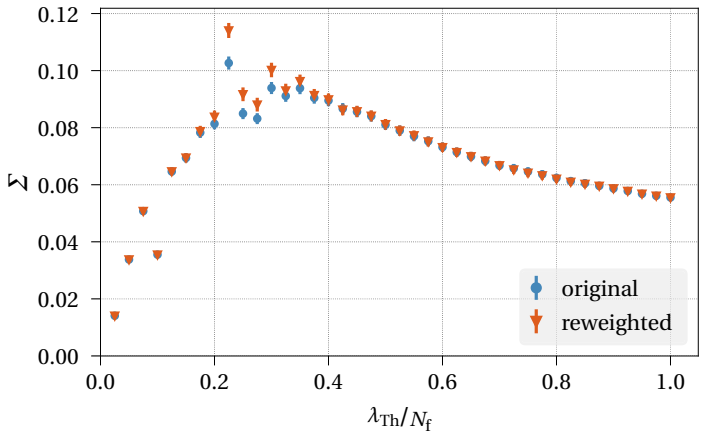

Figure 6.2.: Reweighted absolute value of the chiral condensate Σ for FM with $N_{\text{f,irr}} = 2$ and $L = 4$. In comparison with the original average values (circles), we find large deviations around the maximum of Σ.

FM in (2.37a) are not possible. In section 6.2, we investigate an alternative approach to simulate this model.

Although the Dirac operator of FVM with Lagrangian (2.37b) has real eigenvalues (see section 2.4.2), the sign problem in figure 6.1(a) is even worse. The sign jumps on nearly every update in the HMC, leading to an average value close to zero. This behaviour is already present on lattice size 4 and prevents any data evaluation. Therefore, no further simulations where performed with this reformulation.

We conclude that Fierz identities can relate four-fermion models without a sign problem to equivalent models with a sign problem. The sign problem arises in different ways for the two Fierz identities, but it is always too strong to obtain meaningful results regarding χSB. Conversely, this may be a great benefit for models that *originally* suffer from a sign problem and allow a reformulation in a sign-problem-free manner. Unfortunately, the situation is reversed for Th, which is free of a sign problem in the common vector field formulation, but allows no access to χSB. Note, that an investigation of NJL in $d = 4$ found a similar trade-off between χSB and a sign problem when using Fierz identities [GKN13].

Although the very strong sign problems could not be solved here, our recent work [WSW17] bridged the gap between a sign-problem-free simulation in the vector formulation and explicit order parameters after Fierz transformations by the construction of an effective potential. This required the introduction of dual variables as presented in the next section.

6.2. Dual Variables Formulation

This section investigates a dual-variables formulation of four-fermion theories with SLAC fermions. It was originally proposed by Björn Wellegehausen to solve the sign problem of Th after Fierz transformations, as presented in section 6.1. Based on the fermion bag idea of Chandrasekharan [Cha08; Cha10] introduced in section 2.4.1, we integrate out the interaction part of the partition sum to obtain new variables k_{IJ} that can be interpreted as lattice occupation numbers. A detailed calculation is shown in section 6.2.1, while section 6.2.2 presents first numerical results.

6.2.1. Derivation

We start from a general Lagrangian similar to (2.39) for irreducible four-fermion models after HS. Abbreviating the scalar fields in the Dirac operator with a matrix H, we write

$$\mathscr{L} = \bar{\chi}\left(\partial\!\!\!/ + H[\varphi]\right)\chi + S_{\text{bos}}[\varphi](\lambda), \tag{6.4}$$

where $S_{\text{bos}}[\varphi]$ contains quadratic terms in the bosonic fields φ. In general, H has lattice, spin and flavour indices, which we collect in a single index I. Assuming implicit summation over these indices, the partition sum is given by

$$Z(\lambda) = C_{\text{HS}} \int \mathscr{D}\bar{\chi}\mathscr{D}\chi\mathscr{D}\varphi\, \mathrm{e}^{-\bar{\chi}_I\left(\partial\!\!\!/_{IJ} + H_{IJ}[\varphi]\right)\chi_J - S_{\text{bos}}[\varphi](\lambda)} := C_{\text{HS}} \int \mathscr{D}\varphi\, W[\varphi]\, \mathrm{e}^{-S_{\text{bos}}[\varphi](\lambda)}. \tag{6.5}$$

Here, $C_{\text{HS}} = (\lambda/2\pi)^{VN_\varphi/2}$ is the pre-factor induced by HS in (2.31) and depends on N_φ, the number of bosonic degrees of freedom per lattice site, e.g. $N_\varphi = 1$ for GN or $N_\varphi = 3$ for Th. Splitting the exponential of sums into a product, the fermionic part becomes

$$W[\varphi] = \int \mathscr{D}\bar{\chi}\mathscr{D}\chi\, \mathrm{e}^{-\bar{\chi}_I \partial\!\!\!/_{IJ}\chi_J} \prod_{M,N} \mathrm{e}^{-\bar{\chi}_M H_{MN}\chi_N}. \tag{6.6}$$

There is still a summation over I and J implied, while the sum over M and N was replaced by the product. Since $\bar{\chi}, \chi$ are Grassmann variables we have $\chi_M\chi_M = \bar{\chi}_M\bar{\chi}_M = 0$. Hence, the exponential function contains only two terms in its series expansion. We have

$$W[\varphi] = \int \mathscr{D}\bar{\chi}\mathscr{D}\chi\, \mathrm{e}^{-\bar{\chi}_I \partial\!\!\!/_{IJ}\chi_J} \prod_{M,N} \left(1 - \bar{\chi}_M H_{MN}\chi_N\right). \tag{6.7}$$

With the introduction of dual variables $k_{MN} \in \{0,1\}$, acting as occupation numbers, we can use $1 - \bar{\chi}_M H_{MN}\chi_N = \sum_{k_{MN}=0}^{1} \left(-\bar{\chi}_M H_{MN}\chi_N\right)^{k_{MN}}$. Whenever a k_{MN} is set to one, the

corresponding fermionic degree of freedom participates in the interaction. Now, we expand the product of sums to a sum over all possible configurations of k_{MN}:

$$W[\varphi] = \sum_{\{k_{MN}\}} \int \mathscr{D}\bar{\chi}\mathscr{D}\chi \, \mathrm{e}^{-\bar{\chi}_I \partial\!\!\!/_{IJ} \chi_J} \prod_{M,N} \left(-\bar{\chi}_M H_{MN} \chi_N\right)^{k_{MN}}. \tag{6.8}$$

Here, we can restrict k_{MN} to a matrix with maximal one non-zero entry per row *and* column. The contribution of all other configurations is zero, due to the Grassmann nature of $\bar{\chi}, \chi$. For example, $k_{11} = 1$ and $k_{21} = 1$ would lead to a product involving $\chi_1 \chi_1 = 0$. Thus, we have the constraints

$$\sum_M k_{MN} \in \{0,1\} \quad \text{and} \quad \sum_N k_{MN} \in \{0,1\}. \tag{6.9}$$

Integrating over the fermions in (6.8), we get the usual determinant of the derivative operator, but the contribution of the first exponential is cancelled by the second factor every time a $k_{MN} = 1$ is set. This leads to the determinant of a free Dirac operator, where each row M and column N is deleted, whenever a k_{MN} is set. We denote this matrix by $\partial\!\!\!/[k]$ and obtain

$$W[\varphi] = \sum_{\{k_{MN}\}} \det(\partial\!\!\!/[k]) \prod_{MN} (-H_{MN})^{k_{MN}}. \tag{6.10}$$

To proceed, we need to specify the form of H and S_{bos}. In the following, we present the calculation for GN, which has the simplest form. The more involved derivations for Th and FM can be found in appendix E.

Irreducible GN / G45

The irreducible version of Lagrangian (2.32) has $H_{MN} = \sigma_x \delta_{xy} \delta_{ij} \delta_{\alpha\beta}$ (no summation over x), where the field contribution σ_x is diagonal in the spacetime-index x and independent of spinor (i, j) and flavour (α, β) indices. Thus, the dual-variables field only depends on the lattice position and we can write

$$W[\sigma] = \sum_{\{k_x\}} \det(\partial\!\!\!/[k]) \prod_x (-\sigma_x)^{k_x}, \tag{6.11}$$

where $k_x := \sum_{i,\alpha} k_{xi\alpha} \in \{0, 1, \ldots, 2N_{\text{f,irr}}\}$ includes a sum over spinor and flavour indices. The constraint (6.9) is trivially fulfilled because k_{MN} must be diagonal.

Going back to the partition sum, it can be factorised in local weights $w(k_x)$ that are given by the Gaussian integrals in

$$Z(\lambda_{\text{GN}}) = C_{\text{HS}} \sum_{\{k_x\}} \det(\partial\!\!\!/[k]) \int_{-\infty}^{\infty} \prod_x \mathrm{d}\sigma_x (-\sigma_x)^{k_x} \mathrm{e}^{-\frac{1}{2}\lambda_{\text{GN}}\sigma_x^2} := C_{\text{HS}} \sum_{\{k_x\}} \det(\partial\!\!\!/[k]) \prod_x w(k_x). \tag{6.12}$$

The remaining one-dimensional integration can be performed easily. Since the integrand in w is odd for odd values of k_x, the integral vanishes in these cases[(a)] and we can restrict the configurations to those with even k_x. With the usual Γ-function that extends the

[(a)] With non-zero mass also contributions from odd k_x arise.

factorial function to non-integer numbers, they have a local weight of

$$w(k_x) = \int_{-\infty}^{\infty} \mathrm{d}\sigma\, (-\sigma)^{k_x} \mathrm{e}^{-\frac{1}{2}\lambda_{\mathrm{GN}}\sigma^2} = \left(\frac{2}{\lambda_{\mathrm{GN}}}\right)^{\frac{k_x+1}{2}} \Gamma\left(\frac{k_x+1}{2}\right) \quad \text{for even } k_x. \tag{6.13}$$

Now, the product over x in (6.12) can be simplified by introducing $k = \sum_x k_x$. Additionally, we define occupation numbers n_s for $s = 0, 1, \ldots, N_{\mathrm{f,irr}}$, counting how many k_x of a given configuration have the value $2s$. They are related to the lattice volume by $\sum_{s=0}^{N_{\mathrm{f,irr}}} n_s = V$, since every lattice site must be occupied exactly once. After pulling out a common factor $C_{\mathrm{GN}} = C_{\mathrm{HS}} \cdot (2/\lambda_{\mathrm{GN}})^{\frac{V}{2}} = \pi^{-\frac{V}{2}}$, the full partition sum is given by

$$Z(\lambda_{\mathrm{GN}}) = C_{\mathrm{GN}} \sum_{\{k_x\}} \det(\partial\!\!\!/[k]) \left(\frac{2}{\lambda_{\mathrm{GN}}}\right)^{\frac{k}{2}} \prod_{s=0}^{N_{\mathrm{f,irr}}} \Gamma\left(\frac{2s+1}{2}\right)^{n_s}. \tag{6.14}$$

In this form, the meaning of $\langle k \rangle$ as a lattice filling factor as well as the definition (2.55) become apparent. Indeed, we can obtain an expression containing the expectation value of our dual-variables field by $-\frac{\lambda}{V}\frac{\mathrm{d}}{\mathrm{d}\lambda_{\mathrm{GN}}} \ln Z$. A shift by $-1/2$ is necessary to compensate the additional contribution from C_{GN} and we divide by $k_x^{\max} = d_\gamma N_{\mathrm{f,irr}}$ for a normalisation such that $\langle k \rangle \in [0, 1]$.

Other Formulations

In the formulation FM, we obtain a field $k_{xi}^{\alpha\beta}$. As before, we use the abbreviations k and $k_x^{\alpha\beta}$ for the sums over the missing indices. Contrary to the previous paragraph, we must count diagonal and off-diagonal values of $k_x^{\alpha\beta}$ separately. Here, $n_{s,x}$ with $s = 1, 2$ gives the number of diagonal elements $k_x^{\alpha\alpha}$ (no summation) that equal s at a given x, $n_s = \sum_x n_{s,x}$, and $\tilde{n}_2$ counts how many $k_x^{\alpha\beta}$ take the value 2 for $\alpha < \beta$ on the whole lattice. With these definitions, the result of the computation for FM in appendix E is

$$Z(\lambda_{\mathrm{Th}}) = C \sum_{\left\{k_{xi}^{\alpha\beta}\right\}} \det(\partial\!\!\!/[k])(-1)^k 2^{\tilde{n}_2} \left(\frac{2}{\lambda_{\mathrm{Th}}}\right)^{\frac{k}{2}} \prod_x \Gamma\left(\frac{n_{1,x}+1}{2}\right) U\left(\frac{n_{1,x}+1}{2}, \frac{n_{1,x}+3}{2} + n_{2,x}, 1\right). \tag{6.15}$$

All coefficients independent of k are collected in $C = 2^{V(N_{\mathrm{f,irr}}-1)}\pi^{-\frac{V}{2}}$. The confluent hypergeometric function of the second kind $U(a, b, z)$ is well-known in mathematics [Wei] and its values can be calculated for example with `Mathematica`. The local constraints on $k_{xi}^{\alpha\beta}$ are

$$k_x^{\alpha\beta} = k_x^{\beta\alpha}, \quad \sum_{\alpha=1}^{N_{\mathrm{f,irr}}} k_{xi}^{\alpha\beta} \in \{0, 1\}, \quad \sum_{\beta=1}^{N_{\mathrm{f,irr}}} k_{xi}^{\alpha\beta} \in \{0, 1\}, \quad n_{1,x} \text{ even}. \tag{6.16}$$

In appendix E, we also derived a partition function for Th with dual variables $k_{x\alpha}^{ij}$ and similar constraints. Here, the action of the Fierz transformation is clear: It interchanges spin degrees of freedom by flavour degrees of freedom. In the FM formulation, we have $d_\gamma = 2$ matrices $k_{xi}^{\alpha\beta}$ of size $N_{\mathrm{f}} \times N_{\mathrm{f}}$, while we have $N_{\mathrm{f}}\, d_\gamma \times d_\gamma$-matrices in the Th formulation. Both versions are fully equivalent with respect to the rows and columns that are deleted in the free Dirac operator $\partial\!\!\!/[k]$. Also the difference between any formulation of Th and GN

becomes apparent. In GN, we must always delete the row and the column with the same index because k_x is diagonal. This preserves the anti-Hermiticity of the operator and leads to real determinants of $\partial\!\!\!/[k]$. For Th, we have additional interactions between different spinor components that are not present in GN. They can be realised by interactions of different spins as in Th or between different flavours as in FM.

In general, the range of interactions on the lattice depends on the fermion derivative, while the derivation of the partition sums in the dual variables formulation is independent of the choice of the lattice derivative. In our investigation with SLAC fermions, a lattice site x interacts with all other points along the straight lines in all three spacetime directions that pass through x. In comparison, the interaction in the approach of Chandrasekharan & Li [CL13] is only between the corners of a cube. Their formulation of GN has interactions across the edges, the diagonals on the surfaces, and through the body of the cube. Opposed to our formulation, there is less interaction for Th, where only edge bonds are allowed.

6.2.2. Implementation and Results

For lattices with only $4 \times 1 \times 1$ points and $N_\mathrm{f} = 1$ or 2, it is possible to confirm the equivalence of the partition sums before and after introduction of the dual variables in an exact calculation with `Mathematica`. In the dual-variables approach, we can also compute $Z(\lambda)$ for quasi-two-dimensional lattice sizes like $2 \times 3 \times 1$, but larger lattices require a Monte Carlo algorithm to sample configurations.

Implementation

An implementation[(b)] with a simple Metropolis algorithm was used to perform updates. In the beginning, the program generates a list of allowed local configurations k_{IJ} either for FM or GN. For a single update, the resulting weight is always zero when choosing a new random configuration at a single random lattice point. Hence, new random configurations are placed at two different random lattice sites. Afterwards, an accept/reject-step is performed, where we have to calculate the change of the action from the old configuration k_1 to the new k_2. For this, an efficient update of the determinant is done with the formula [Bro]

$$\det(\partial\!\!\!/[k_2]) = \det\big(\partial\!\!\!/[k_1] + AB^\dagger\big) = \det(\partial\!\!\!/[k_1]) \det\big(\mathbb{1} + B^\dagger \partial\!\!\!/[k_1]^{-1} A\big), \tag{6.17}$$

where $\det(\partial\!\!\!/[k_1])$ is the fermion determinant before the update. A and B are matrices of shape $(\operatorname{rank}\partial\!\!\!/) \times n$ where $n \ll \operatorname{rank}\partial\!\!\!/$ is the number of rows and columns that need to be updated. Hence, the matrix in the last factor of (6.17) is of size $n \times n$ and its determinant can be computed at low cost. A full calculation of the determinant and the inverse of the free Dirac operator is only necessary for the initial configuration. If the new configuration was accepted, we also have to update the inverse of $\partial\!\!\!/[k_1]$. This can be done similarly to the

[(b)] Source code can be found on `https://github.com/daniel-schmidt/FermiOwn`.

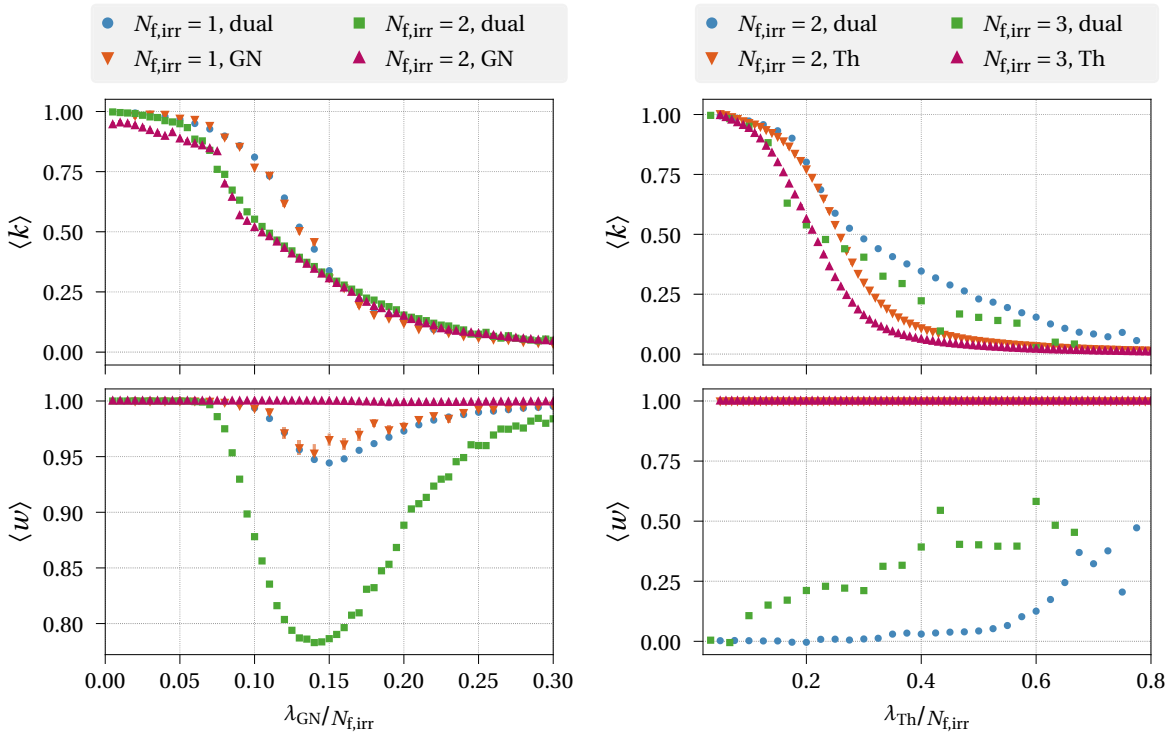

6.3(a) GN with scalar field and its dual variables formulation given by (6.14).

6.3(b) Th in the vector field formulation and the dual variables form of FM given in (6.15).

Figure 6.3.: Comparison of observables for the dual variables formulation. Results with $L = 4$ from a conventional simulation with exact update are compared to their equivalent dual variables formulation simulated with a Metropolis algorithm.

determinant update (6.17) with a simplified version of Woodbury's formula [Lie]

$$\partial[k_2]^{-1} = \left(\partial[k_1] + AB^\dagger\right)^{-1} = \partial[k_1]^{-1} - \partial[k_1]^{-1} A\left(\mathbb{1} + B^\dagger \partial[k_1]^{-1} A\right)^{-1} B^\dagger \partial[k_1]^{-1}. \tag{6.18}$$

For the simulations presented in the following, we used $10V$ updates between measurements to decrease correlations. As with the exact algorithm, we have direct access to the complex phase of the determinant and can obtain the weight as defined in (2.58). Likewise, we also simulate phase-quenched if the determinant is not positive.

Irreducible GN

As a first step, we present the single-flavour case, where all formulations given above are equivalent to the irreducible GN and a strong sign problem was found in section 3.4. The field k_x can take the values 0 or 2 and due to $n_0 + n_1 = V$ and $n_1 = k/2$, we only need n_1 to rewrite the partition sum (6.14). The prefactor cancels due to $\Gamma(1/2) = \sqrt{\pi}$ and $\Gamma(3/2) = \sqrt{\pi}/2$ and we find

$$Z(\lambda_{\mathrm{GN}}) = \sum_{\{n_{1,x}\}} \det(\partial[n_1])\lambda_{\mathrm{GN}}^{-n_1}. \tag{6.19}$$

Whenever an $n_{1,x}$ is set, we delete the whole contribution (two rows and two columns) at that point in ∂. In appendix E, we also showed that the FM partition sum (6.15) becomes identical to (6.19) for $N_{\mathrm{f,irr}} = 1$ when considering $\lambda_{\mathrm{Th}} = 3\lambda_{\mathrm{GN}}$ from the Fierz identity (2.27).

We show in figure 6.3(a) that a naive simulation of (6.19) reproduces the sign problem of the scalar field formulation as previously given in figure 3.14(a). In contrast to GN, the determinant is no longer complex, since $\partial\!\!\!/[n_1]$ is anti-Hermitian for all n_1 as in the vector field (Th) formulation of the $N_{\mathrm{f,irr}} = 1$ model. Our numerical investigation showed that exactly all configurations with a negative determinant are those with an odd n_1. This can provide a solution to the sign problem: we only sample the configurations with even n_1, which always have a positive determinant and allow a probability interpretation of their weights. Given such a configuration, we can add the contribution from all odd configurations with $n_1 + 1$ employing a reweighting procedure as in (2.58). Here, it does not matter that the weights are negative. For every configuration with even n_1, there are $V - n_1$ configurations with odd $n_1 + 1$, each with a previously unset $n_{x,1}$ set to 1. Thus, there seems to be no need to sample the configurations with odd n_1. With further investigations, e.g. regarding algorithmic properties like ergodicity and efficient update schemes, this approach should allow sign-problem-free simulations of the $N_{\mathrm{f,irr}} = 1$ four-fermion model, which are not possible at the moment.

For the GN-equivalent with $N_{\mathrm{f,irr}} = 2$, the sign problem in the dual variables approach is worse than in the original scalar field formulation, see figure 6.3(a). So far, no systematic analysis to identify possible resummations was done for this model. Regarding the lattice filling factor $\langle k \rangle$, the results from our two different approaches are in reasonable agreement for GN, even in the region where the sign problem is strongest. For very strong couplings, where GN showed an unphysical phase with thermalisation problems, we even get a smoother curve from the dual variable approach.

Multi-Flavour FM

In figure 6.3(b), we compare the vector field formulation of Th, where no sign problem was found, with the dual-variables version of FM. As in the previous paragraph, $\langle k \rangle$ is also in agreement for both formulations of Th at strong couplings, but deviations become large for $\langle k \rangle \lesssim 0.5$. For a wide range of λ_{Th}, we already find an average weight close to zero on lattice size $L = 4$. This must be compared to figure 6.1(a), where the sign problem for FM in a conventional simulation was shown. It is worse in the dual variables formulation, again preventing a successful calculation of observables.

Various attempts to classify and resum local configuration were not yet successful in obtaining positive weights. Nevertheless, we shortly discuss the local configurations of $k_{xi}^{\alpha\beta}$ with $N_{\mathrm{f,irr}} = 2$ as an example. In this case, i, α as well as β take the values 1 or 2, leading to $2^8 = 256$ possible configurations for a fixed x. Selecting only those that are allowed by the constraints (6.16), we are left with 15 configurations. They are given in table 6.1 together with the matrix $k_x^{\alpha\beta}$ including a sum over spins, the values of n_1, n_2 and $\tilde{n}_2$ and the resulting local weight

$$w_{\mathrm{loc}}\big(n_{1,x}, n_{2,x}, \tilde{n}_{2,x}\big) \coloneqq \frac{2^{\tilde{n}_{2,x}}}{\sqrt{\pi}} \Gamma\left(\frac{n_{1,x}+1}{2}\right) U\left(\frac{n_{1,x}+1}{2}, \frac{n_{1,x}+3}{2} + n_{2,x}, 1\right). \tag{6.20}$$

Table 6.1.: Allowed local configurations for the dual variables formulation of FM with $N_{\mathrm{f,irr}} = 2$. The matrix $k_x^{\alpha\beta}$ in the third row is the sum of the matrices $k_{xi}^{\alpha\beta}$ in the first two rows. In the fourth row, n_1 and n_2 count the number of ones and twos on the diagonal of $k_x^{\alpha\beta}$, while $\tilde{n}_{2,x}$ counts the twos in the upper right corner. $\tilde{n}_{1,x}$ is not given here because it is not needed in the partition sum (6.15).

number	1	2	3	4	5	6	7	8
$k_{x1}^{\alpha\beta}$	$\begin{pmatrix}0&0\\0&0\end{pmatrix}$	$\begin{pmatrix}0&0\\0&0\end{pmatrix}$	$\begin{pmatrix}0&0\\0&0\end{pmatrix}$	$\begin{pmatrix}0&0\\0&1\end{pmatrix}$	$\begin{pmatrix}0&0\\0&1\end{pmatrix}$	$\begin{pmatrix}0&0\\1&0\end{pmatrix}$	$\begin{pmatrix}0&1\\0&0\end{pmatrix}$	$\begin{pmatrix}0&1\\1&0\end{pmatrix}$
$k_{x2}^{\alpha\beta}$	$\begin{pmatrix}0&0\\0&0\end{pmatrix}$	$\begin{pmatrix}0&1\\1&0\end{pmatrix}$	$\begin{pmatrix}1&0\\0&1\end{pmatrix}$	$\begin{pmatrix}0&0\\0&1\end{pmatrix}$	$\begin{pmatrix}1&0\\0&0\end{pmatrix}$	$\begin{pmatrix}0&1\\0&0\end{pmatrix}$	$\begin{pmatrix}0&0\\1&0\end{pmatrix}$	$\begin{pmatrix}0&0\\0&0\end{pmatrix}$
$k_x^{\alpha\beta}$	$\begin{pmatrix}0&0\\0&0\end{pmatrix}$	$\begin{pmatrix}0&1\\1&0\end{pmatrix}$	$\begin{pmatrix}1&0\\0&1\end{pmatrix}$	$\begin{pmatrix}0&0\\0&2\end{pmatrix}$	$\begin{pmatrix}1&0\\0&1\end{pmatrix}$	$\begin{pmatrix}0&1\\1&0\end{pmatrix}$	$\begin{pmatrix}0&1\\1&0\end{pmatrix}$	$\begin{pmatrix}0&1\\1&0\end{pmatrix}$
$n_{1,x}, n_{2,x}, \tilde{n}_{2,x}$	0, 0, 0	0, 0, 0	2, 0, 0	0, 1, 0	2, 0, 0	0, 0, 0	0, 0, 0	0, 0, 0
w_{loc}	1	1	1/2	3/2	1/2	1	1	1

number	9	10	11	12	13	14	15
$k_{x1}^{\alpha\beta}$	$\begin{pmatrix}0&1\\1&0\end{pmatrix}$	$\begin{pmatrix}0&1\\1&0\end{pmatrix}$	$\begin{pmatrix}1&0\\0&0\end{pmatrix}$	$\begin{pmatrix}1&0\\0&0\end{pmatrix}$	$\begin{pmatrix}1&0\\0&1\end{pmatrix}$	$\begin{pmatrix}1&0\\0&1\end{pmatrix}$	$\begin{pmatrix}1&0\\0&1\end{pmatrix}$
$k_{x2}^{\alpha\beta}$	$\begin{pmatrix}0&1\\1&0\end{pmatrix}$	$\begin{pmatrix}1&0\\0&1\end{pmatrix}$	$\begin{pmatrix}0&0\\0&1\end{pmatrix}$	$\begin{pmatrix}1&0\\0&0\end{pmatrix}$	$\begin{pmatrix}0&0\\0&0\end{pmatrix}$	$\begin{pmatrix}0&1\\1&0\end{pmatrix}$	$\begin{pmatrix}1&0\\0&1\end{pmatrix}$
$k_x^{\alpha\beta}$	$\begin{pmatrix}0&2\\2&0\end{pmatrix}$	$\begin{pmatrix}1&1\\1&1\end{pmatrix}$	$\begin{pmatrix}1&0\\0&1\end{pmatrix}$	$\begin{pmatrix}2&0\\0&0\end{pmatrix}$	$\begin{pmatrix}1&0\\0&1\end{pmatrix}$	$\begin{pmatrix}1&1\\1&1\end{pmatrix}$	$\begin{pmatrix}2&0\\0&2\end{pmatrix}$
$n_{1,x}, n_{2,x}, \tilde{n}_{2,x}$	0, 0, 1	2, 0, 0	2, 0, 0	0, 1, 0	2, 0, 0	2, 0, 0	0, 2, 0
w_{loc}	2	1/2	1/2	3/2	1/2	1/2	11/4

We can reduce the number of necessary configurations from 15 to 10 because some of them lead to the same global weight $\det(\partial[k])$. For example, configurations 10 and 14 are identical because the first can be obtained from the second by an exchange of spin. Also 9 and 15 delete the same rows and columns in $\partial[k]$. Additionally, only the sign of the determinant changes when switching from a flavour-singlet interaction to a flavour-mixing one. In the matrix form of table 6.1, this amounts to moving the ones from the diagonal entries to the off-diagonal elements. The configuration pairs $(2,3)$, $(8,13)$, and $(14,15)$ are related in this way. Finally, two such changes identify 9 with 15, which both lead to the same determinant. In total, the local weight of the sum over configurations 9, 10, 14, and 15 (all those with $k_x = 4$) is $2 - 2 \cdot 1/2 + 11/4 = 15/4$ and it is sufficient to include only one configuration, e.g. number 15, with this local weight into the calculation of the partition sum. The remaining 10 configurations are given in table 6.2 together with their local weights. For $N_{\mathrm{f,irr}} = 3$, all 118 allowed configurations can be filtered out of the total 2^{18} configurations. This is no longer possible for $N_{\mathrm{f}} \geq 4$, where a more constructive approach would be necessary that directly leads to allowed configurations. Another possibility to investigate is the dual-variables formulation of Th given in appendix E, where one can

Table 6.2.: Reduced set of configurations for the dual variables formulation of FM with $N_{\mathrm{f,irr}} = 2$. A resummation of configurations $(2,3)$, $(8,13)$ and $(9,10,14,15)$ was performed.

number	1	3	4	5	6	7	11	12	13	15
w_{loc}	1	$-1/2$	$3/2$	$1/2$	1	1	$1/2$	$3/2$	$-1/2$	$15/4$

obtain the same configurations in table 6.1 for $N_{\mathrm{f,irr}} = 2$ with $k_{xi}^{\alpha\beta}$ replaced by $k_{x\alpha}^{ij}$. This has the advantage for simulations that $\partial\!\!\!/$ can be split into independent single-flavour blocks, contrary to the formulation presented here.

The resummations performed here are not sufficient to obtain a set of configurations with positive weights as for the single-flavour model. The complex phase of the fermion determinant is not predictable so far and the sign problem for FM remains unsolved. Nevertheless, the dual variables formulation in terms of the fields k_{IJ} provided new insights into four-fermion theories and allowed a definition of the lattice filling factor that is also useful for conventional simulations with auxiliary fields.

7. Conclusions

In this work, we investigated a previously unused approach to four-fermion theories on the lattice. We performed the first simulations of three-dimensional fermionic QFTs with the SLAC derivative, allowing an exact implementation of all internal symmetries at any finite lattice spacing. Its dispersion relation is as close to the continuum form as possible and no ambiguities arise due to its use in lattice formulations. Hence, it is a very good choice to study effects like χSB in strongly interacting QFTs without gauge symmetries. Prime examples for such theories are three-dimensional four-fermion models. Keeping possible applications in condensed matter physics in mind, we used them as toy models to learn more about spontaneous χSB.

Our main objects of study were GN with a scalar-scalar interaction and Th with a vector-vector interaction. Many previous works exist for GN, calculating critical exponents with various numerical as well as analytical methods. Therefore, GN provided a good testing ground to explore the performance of the SLAC derivative and our simulation setup for investigations of χSB in three-dimensional four-fermion theories. We were able to confirm the common belief that χSB exists for any number of fermion flavours. To study the phase transition quantitatively, well-known methods from the theory of finite sizes scaling were successfully employed. Furthermore, an algorithm was implemented that uses all physical information from the ensembles at various couplings to calculate a smooth interpolation. Using these methods, critical exponents for the phase transitions with $N_\mathrm{f} = 1, 2, 4$ and 8 were calculated. For $N_\mathrm{f} = 4$ and 8, we found good agreement with the large-N_f expansion. In comparison with previous lattice field theory simulations employing staggered fermions for $N_\mathrm{f} = 2$ and 4, our new results match well with the older estimates. Remarkably, our results for $N_\mathrm{f} = 2$ support the findings of Kärkkäinen et al. [Kär94], where a possible sign problem of their lattice formulation was ignored, but they are not in good accord with estimates from the fermion bag approach of Chandrasekharan & Li [CL13]. For $N_\mathrm{f} = 1$, large discrepancies exist in the literature between analytical calculations and QMC simulations. Our work provides the first calculation of critical exponents in a lattice field theory approach and agrees reasonably well with the results from FRG methods and ϵ-expansions around 2 and 4 dimensions. Therefore, it is questionable if the works with QMC algorithms actually simulate models in the same universality class. Further work in this area seems to be necessary to find the origin of the disparity. Note, that the calculation of the exponent ν in the conformal bootstrap approach also shows a large deviation from our result. In general, our approach with the SLAC derivative works well for χSB in GN and it is competitive to other lattice simulations. In a short study, we also provided evidence that GN in the irreducible representation as well as the equivalent G45 are in the same chiral Ising universality class as GN.

The situation for Th is less clear in the literature and our results propose a radically different picture, contrary to the common belief. Previously, almost all investigations, either on the lattice, using DSEs or FRG methods, found a critical flavour number N_f^cr such that χSB is present for $N_\mathrm{f} \leq N_\mathrm{f}^\mathrm{cr}$. Though the values given for N_f^cr vary in the literature, its very existence seemed to be established. Only the most recent lattice simulations of Hands [Han16b; Han17] with a different approach to exact chiral symmetry raised doubt on this. Spontaneous symmetry breaking was neither found for $N_\mathrm{f} = 2$ [Han16b] nor for $N_\mathrm{f} = 1$ [Han17]. This is consistent with our own simulations, where also no trace of spontaneous χSB is present. In the conventional formulation of massless Th with an auxiliary vector field, a clear statement was hampered by the exact implementation of chiral symmetry because no order parameter for its breaking is accessible on the lattice. With an external breaking by a mass term, we found no evidence for χSB for any flavour number.

Our effort to study a larger space of couplings, combining Th either with a GN interaction or a global NJL term, is also consistent with the absence of χSB in Th for any N_f. We always found a three-phase structure in the coupling plane with a region of lattice artefacts, a symmetric regime, and a phase of spontaneous symmetry breaking. Whenever we approached the pure Th by reducing the second coupling, indications for χSB vanished and we were left with a symmetric phase in direct contact with the unphysical region. For both coupled models, the region of broken symmetry for $N_\mathrm{f} = 1$ was found to exhibit a different shape than for $N_\mathrm{f} \geq 2$ with a larger extension in the direction of the pure Th. In a more detailed study of Th coupled to the global NJL for $N_\mathrm{f} = 1$, it was difficult to perform the two limits of pure Th and infinite volume. On larger lattices, the region of χSB extends closer to the pure Th. Although a rough extrapolation showed a very small region of broken symmetry for pure Th, this result may change when including larger lattices and weaker couplings of the global model.

Alternative approaches to Th using Fierz identities to reformulate the model with different degrees of freedom were not successful in direct simulations. For both identities used here, we found a very strong sign problem preventing the investigation of χSB, although an order parameter is accessible in these formulations. Here, the main conclusion is that the sign problem can appear with very different characteristics for Lagrangians that are physically equivalent due to Fierz identities. In general, also the introduction of dual variables was not yet successful to eliminate the sign problem. Nevertheless, it provided an insight into the unphysical phases, which we found for GN and Th. In the case of GN, we found a saturation of the scalar field and thermalisation problems as soon as more than half of the lattice is filled. For Th, the peak in the chiral susceptibility as well as the position of the maximum in the condensate for massive fermions appear where the lattice filling factor has a transition between low filling and a region of linear increase. The reformulations in this work also paved the way for our work [WSW17], combining simulations in the sign-problem-free vector field formulation of Th with effective potentials for local order parameters that Björn Wellegehausen derived from a Lagrangian after Fierz transformation.

The dual variables formulation may also be used to study the irreducible four-fermion model with $N_{\mathrm{f,irr}} = 1$, where GN and Th are equivalent. In conventional simulations of this model with a mass term, we found indications of parity breaking but also a strong sign problem. Remarkably, always the same dependence of the weight on the coupling arises in different formulations, although the determinant of the Dirac operator is complex for GN and real for Th. In the dual variables formulation, we also find arbitrary real weights, but the negative contributions only come from configurations where an odd number of lattice sites participates in the interaction. This should allow sign-problem-free simulations which could be a topic for new studies.

In conclusion, we record that no reliable evidence for χSB in Th was found in this work, although our approach worked well to calculate the critical exponents of GN for different N_{f}. Only for $N_{\mathrm{f}} = 1$, our simulations for Th seem to show remnants of χSB. A reason for this is provided by the effective potentials calculated in [WSW17]. For all couplings, the one for $N_{\mathrm{f}} = 1$ is very flat at the origin, but the small curvature is positive, making the theory always symmetric. Our paper also showed that χSB is only absent for all N_{f} in the reducible representation. A critical flavour number with a value of $N_{\mathrm{f,irr}}^{\mathrm{cr}} = 9$ only exists for odd $N_{\mathrm{f,irr}}$ and is related to a spontaneous breaking of parity. This can provide a possible explanation for the values found in earlier simulations with staggered fermions, together with the differences in the symmetry that the lattice theory preserves. The discrepancies in DSE and FRG results are harder to explain and further investigations are needed to achieve overall consensus on the answer of the critical flavour number in Th. Our current approach with SLAC fermions strongly suggests that there is no χSB in the reducible model, in agreement with other simulations using chiral fermions [Han16b; Han17]. It also shows that exact chiral symmetry on the lattice is necessary to capture the correct behaviour of four-fermion theories in three dimensions. The older works with staggered fermions seem to be reliable for GN but not for Th. Thus, also other previous lattice results for four-fermion models should be checked with exactly chiral fermions. For example, investigations of NJL and a larger space of multiple four-fermion interactions could be done with our setup. Additionally, future simulations with SLAC fermions could also provide new estimates for the critical exponents of the chiral Heisenberg universality class with a study of the $U(1)$-invariant GN.

A. Derivation of Fierz Identities

Here we give a derivation of some Fierz identities that are useful to rewrite the Th interaction of the irreducible model. In this setup, a complete set of matrices is given by $\{\mathbb{1}, \sigma_1, \sigma_2, \sigma_3\}$, where the σ_μ are the usual Pauli matrices. Any 2×2-matrix M_{jk} can be expressed as

$$M_{jk} = \tfrac{1}{2}\operatorname{tr}(M)\delta_{jk} + \tfrac{1}{2}\operatorname{tr}(M\sigma_\mu)(\sigma^\mu)_{jk}. \tag{A.1}$$

We set $M_{jk} = B_{ji}\chi_i^\alpha \bar\chi_l^\beta C_{lk} \equiv B\chi^\alpha\bar\chi^\beta C$ with arbitrary matrices B and C. The lower indices $i, j, \ldots$ label the two-spinor components, while the upper Greek indices from the beginning of the alphabet $\alpha, \beta, \ldots$ label the $N_{\text{f,irr}}$ flavours. Spacetime indices μ, ν run over $d = 3$ directions. Inserting this in the completeness relation, we get

$$B_{ji}\chi_i^\alpha\bar\chi_l^\beta C_{lk} = \tfrac{1}{2}B_{mi}\chi_i^\alpha\bar\chi_l^\beta C_{lm}\delta_{jk} + \tfrac{1}{2}B_{mi}\chi_i^\alpha\bar\chi_l^\beta C_{ln}(\sigma_\mu)_{nm}(\sigma^\mu)_{jk}, \tag{A.2}$$

$$\Leftrightarrow \quad B\chi^\alpha\bar\chi^\beta C = -\tfrac{1}{2}\left(\bar\chi^\beta CB\chi^\alpha\right)\mathbb{1} - \tfrac{1}{2}\left(\bar\chi^\beta C\sigma_\mu B\chi^\alpha\right)\sigma^\mu. \tag{A.3}$$

In the second line we switched to a matrix notation, took care of the anti-commuting nature of spinors and used the cyclic property of the trace. Taking general matrices A, B and performing a multiplication with $\bar\chi^\gamma A$ from the left and $D\chi^\delta$ from the right leads to the general identity

$$\left(\bar\chi^\gamma AB\chi^\alpha\right)\left(\bar\chi^\beta CD\chi^\delta\right) = -\tfrac{1}{2}\left(\bar\chi^\beta CB\chi^\alpha\right)\left(\bar\chi^\gamma AD\chi^\delta\right) - \tfrac{1}{2}\left(\bar\chi^\beta C\sigma_\mu B\chi^\alpha\right)\left(\bar\chi^\gamma A\sigma^\mu D\chi^\delta\right). \tag{A.4}$$

Now, there are several options to obtain a Th interaction term. It appears on the right-hand side of (A.4) for $A = B = C = D = \mathbb{1}$ if we contract the flavour indices of the equation with $\delta^{\alpha\beta}$ and $\delta^{\gamma\delta}$. We obtain

$$\left(\bar\chi^\gamma\chi^\alpha\right)^2 = -\tfrac{1}{2}\left(\bar\chi^\alpha\chi^\alpha\right)^2 - \tfrac{1}{2}\left(\bar\chi^\alpha\sigma_\mu\chi^\alpha\right)^2, \tag{A.5}$$

where we use the abbreviation $\left|\bar\chi^\gamma\chi^\alpha\right|^2 = \left(\bar\chi^\gamma\chi^\alpha\right)\left(\bar\chi^\alpha\chi^\gamma\right)$. Thus, we can replace the Th interaction by a GN-term and another flavour-mixing interaction. For a single irreducible flavour, this establishes the identity of GN and Th via

$$\left(\bar\chi^\alpha\sigma_\mu\chi^\alpha\right)^2 = -3\left(\bar\chi^\alpha\chi^\alpha\right)^2. \tag{A.6}$$

Another possibility is to take $B = \sigma_\nu, C = \sigma_\rho$ and $A = D = \mathbb{1}$, leading to the Th-interaction term on the left-hand side of (A.4). Now using the Clifford algebra we can derive

$$\begin{aligned}\left(\bar\chi^\gamma\sigma_\nu\chi^\alpha\right)\left(\bar\chi^\beta\sigma_\rho\chi^\delta\right) &= -\tfrac{1}{2}\left(\bar\chi^\beta\sigma_\rho\sigma_\nu\chi^\alpha\right)\left(\bar\chi^\gamma\chi^\delta\right) - \tfrac{1}{2}\left(\bar\chi^\beta\sigma_\rho\sigma_\mu\sigma_\nu\chi^\alpha\right)\left(\bar\chi^\gamma\sigma^\mu\chi^\delta\right) \\ &= -\tfrac{1}{2}\left(\bar\chi^\beta\sigma_\rho\sigma_\nu\chi^\alpha\right)\left(\bar\chi^\gamma\chi^\delta\right) - \tfrac{1}{2}\left(\bar\chi^\beta\sigma_\rho\left(2\delta_{\mu\nu} - \sigma_\nu\sigma_\mu\right)\chi^\alpha\right)\left(\bar\chi^\gamma\sigma^\mu\chi^\delta\right)\end{aligned} \tag{A.7}$$

and contract this equation with $\delta^{\nu\rho}$. This gives a factor of 3 (the spacetime dimension) for

the first term on the right-hand side due to $\delta^{\nu\rho}\sigma_\nu\sigma_\rho = \sigma_\nu\sigma^\nu = 3\cdot\mathbb{1}$, while the second term contains $2\sigma_\mu - 3\sigma_\mu = -\sigma_\mu$. On the left, there is no matrix multiplication between σ_ν and σ_ρ, so that we get a term similar to the Th interaction. Now, the equation reads

$$\left(\bar{\chi}^\gamma\sigma_\nu\chi^\alpha\right)\left(\bar{\chi}^\beta\sigma^\nu\chi^\delta\right) = -\tfrac{3}{2}\left(\bar{\chi}^\beta\chi^\alpha\right)\left(\bar{\chi}^\gamma\chi^\delta\right) + \tfrac{1}{2}\left(\bar{\chi}^\beta\sigma_\mu\chi^\alpha\right)\left(\bar{\chi}^\gamma\sigma^\mu\chi^\delta\right). \tag{A.8}$$

This identity can be contracted in two different ways to obtain the Th interaction: On the one hand, a contraction with $\delta_{\alpha\gamma}$ and $\delta_{\delta\beta}$ generates the term on the left-hand side, on the other hand, the term appears on the right-hand side after a contraction with $\delta_{\alpha\beta}$ and $\delta_{\gamma\delta}$. The results are

$$\left(\bar{\chi}^\alpha\sigma_\nu\chi^\alpha\right)^2 = -\tfrac{3}{2}\left(\bar{\chi}^\beta\chi^\alpha\right)^2 + \tfrac{1}{2}\left(\bar{\chi}^\beta\sigma_\mu\chi^\alpha\right)^2, \tag{A.9}$$

$$\left(\bar{\chi}^\gamma\sigma_\nu\chi^\alpha\right)^2 = -\tfrac{3}{2}\left(\bar{\chi}^\alpha\chi^\alpha\right)^2 + \tfrac{1}{2}\left(\bar{\chi}^\alpha\sigma_\mu\chi^\alpha\right)^2. \tag{A.10}$$

In the first case, the Th interaction is replaced by two flavour-mixing terms, which include both $\mathbb{1}$ and the Pauli matrices. In the second case, the GN interaction appears again, but we also have a flavour-mixing term with σ_ν. For the single-flavour case, these identities lead back to the relation between Th and GN in (A.6).

Further identities including products of Pauli matrices can be calculated from the general form (A.4), but only the most basic identities derived above were used for simulations in this work. See [Jan12; GGJ15] for a more comprehensive treatment of the topic.

B. General Hubbard-Stratonovich Transformations

This section contains derivations of the necessary formulae for the HS of flavour-mixing interactions, needed in section 2.2.2 to transform the Lagrangians after application of Fierz identities. We want to transform exponentials with flavour-mixing terms of the form

$$\exp\left[\pm\alpha^2\left|\bar{\chi}_\alpha \Gamma \chi_\beta\right|^2\right], \tag{B.1}$$

where Γ is either the identity or σ_μ and $\alpha \in \mathbb{R}$. A summation over all lattice points in the exponent is implied. Here, we do the calculation for $\Gamma = \mathbb{1}$, which carries over to $\Gamma = \sigma_\mu$, since this is only a matrix in spinor space, not interfering with the flavour structure. We present the calculation for a positive sign in the exponent of (B.1), which is needed for the Lagrangian (2.28a) of FM.

In the following, it is important to distinguish between Hermitian conjugation with respect to spin degrees of freedom, denoted by the usual †, and Hermitian conjugation regarding the flavour indices, written here with the superscript $^{\mathrm{hc}}$. Regarding spinor products , we use the convention $\bar{\chi} = \chi^\dagger$ of Wipf [Wip13; Wip16] and have

$$\left(\bar{\chi}_\beta \chi_\alpha\right)^\dagger = \chi_\alpha^\dagger \bar{\chi}_\beta^\dagger = \bar{\chi}_\alpha \chi_\beta. \tag{B.2}$$

This expression is not Hermitian in spinor space, in contrast to the Hermitian *flavour-space* matrix $X_{\alpha\beta} = \bar{\chi}_\alpha \chi_\beta$:

$$\left(X^{\mathrm{hc}}\right)_{\alpha\beta} = X^*_{\beta\alpha} = \left(\bar{\chi}_\beta \chi_\alpha\right)^* = \left(\left(\bar{\chi}_\beta \chi_\alpha\right)^\dagger\right)^T = \left(\bar{\chi}_\alpha \chi_\beta\right)^T = \bar{\chi}_\alpha \chi_\beta = X_{\alpha\beta}. \tag{B.3}$$

The transposition with ^{T} is with respect to the spin indices and can be dropped in the next-to-last equation because the expression includes an implicit summation over the spin index and is a scalar. Hence, we can introduce a Hermitian matrix field $T_{\beta\alpha} = T^*_{\alpha\beta} = \left(T^{\mathrm{hc}}\right)_{\beta\alpha}$ and define a shifted Hermitian matrix in flavour space

$$M_{\beta\alpha} = (2\alpha)^{-1} T_{\beta\alpha} + \alpha \bar{\chi}_\alpha \chi_\beta = \left(M^{\mathrm{hc}}\right)_{\beta\alpha}. \tag{B.4}$$

The following expression

$$-\operatorname{tr}\left(M \cdot M^{\mathrm{hc}}\right) = -\operatorname{tr}\left(M^2\right) = -M_{\beta\alpha}\left(M^{\mathrm{hc}}\right)_{\alpha\beta} = -\left(\frac{1}{4\alpha^2} T_{\beta\alpha} T_{\alpha\beta} + \alpha^2 \bar{\chi}_\alpha \chi_\beta \bar{\chi}_\beta \chi_\alpha + \bar{\chi}_\beta T_{\beta\alpha} \chi_\alpha\right) \tag{B.5}$$

yields the necessary term to compensate the four-fermion interaction in the exponential (B.1). Thus, we multiply with the Hubbard-Stratonovich factor $\exp\left[-\operatorname{tr}\left(M \cdot M^{\mathrm{hc}}\right)\right]$. In the resulting Lagrangian, the last term gives a Hermitian contribution to the Dirac operator.

To obtain the additional factors that appear after the transformation, we integrate the exponential over M. Since this matrix is Hermitian, we can split it into real and imaginary part using a symmetric matrix S and an antisymmetric matrix A with

$$M_{\beta\alpha} = S_{\beta\alpha} + \mathrm{i}A_{\beta\alpha}, \tag{B.6}$$

where $S_{\beta\alpha} = S_{\beta\alpha}, A_{\beta\alpha} = -A_{\beta\alpha}$ and $S_{\beta\alpha}, A_{\beta\alpha} \in \mathbb{R}$. This leads to

$$-\sum_{\alpha,\beta=1}^{N_{\mathrm{f,irr}}} M_{\beta\alpha}M_{\alpha\beta} = -\sum_{\alpha,\beta=1}^{N_{\mathrm{f,irr}}} \left(S_{\beta\alpha}^2 + A_{\beta\alpha}^2\right) = -\sum_{\alpha=1}^{N_{\mathrm{f,irr}}} S_{\alpha\alpha} - 2\sum_{\alpha<\beta} \left(S_{\beta\alpha}^2 + A_{\beta\alpha}^2\right), \tag{B.7}$$

where we have a total of $N_{\mathrm{f,irr}} + 2\cdot\frac{N_{\mathrm{f,irr}}(N_{\mathrm{f,irr}}-1)}{2} = N_{\mathrm{f,irr}}^2$ Gaussian integrals, but the $N_{\mathrm{f,irr}}$ integrals over the diagonal components do not have a factor of 2 in the exponent. We get in total

$$\int \mathscr{D}M \exp\left[-\mathrm{tr}\left(M\cdot M^\dagger\right)\right] = \left(\sqrt{\pi}\right)^{N_{\mathrm{f,irr}}} \left(\sqrt{\frac{\pi}{2}}\right)^{N_{\mathrm{f,irr}}(N_{\mathrm{f,irr}}-1)} = 2^{-\frac{N_{\mathrm{f,irr}}}{2}(N_{\mathrm{f,irr}}-1)} \left(\sqrt{\pi}\right)^{N_{\mathrm{f,irr}}^2}. \tag{B.8}$$

For the HS we divide by this factor to normalise the integral to one. Rewriting the integral in terms of the new auxiliary field $T_{\alpha\beta}$, we get an additional factor of $(2\alpha)^{-N_{\mathrm{f,irr}}^2}$ from the integration measure. Hence, the resulting overall factor for a fixed lattice site is

$$C_{x,\mathrm{HS}} = 2^{-\frac{N_{\mathrm{f,irr}}}{2}(N_{\mathrm{f,irr}}-1)} \left(2\alpha\sqrt{\pi}\right)^{-N_{\mathrm{f,irr}}^2} = \sqrt{2}^{N_{\mathrm{f,irr}}} \left(\alpha\sqrt{2\pi}\right)^{-N_{\mathrm{f,irr}}^2}. \tag{B.9}$$

In the Lagrangian (2.28a), we have $\alpha^2 = \lambda^{-1}$ and an additional scalar field ϕ that comes with its own prefactor of $\sqrt{\frac{\lambda}{2\pi}}^V$. The total prefactor for the whole partition function is

$$C_{\mathrm{HS}} = 2^{\frac{V}{2}N_{\mathrm{f,irr}}} \left(\frac{\lambda}{2\pi}\right)^{\frac{V}{2}\left(N_{\mathrm{f,irr}}^2+1\right)}. \tag{B.10}$$

We will use this expression to compare the partition sums calculated in the dual variables formulation of section 6.2.

C. Additional Material for the Gross-Neveu Model

In this appendix, we collect additional material for GN as presented in section 3.2 and section 3.3.

Table C.1.: Number of configurations obtained for GN. All numbers are given in units of 10^3 and additional 10 updates between measurements were performed. The first 100 configurations were not used in order to ensure thermalisation. If two numbers are given, e.g. 10,30, the larger number was obtained for couplings near the critical point. If a range is given, e.g. 7.5–10, simulations did not reach their goal and were evaluated with the amount of configurations that could be obtained.

L	$N_f = 1$	$N_f = 2$	$N_f = 4$	$N_f = 8$
8	10,30	10,30	10,30	10,30
10	10,30	10,20	10	10
12	20	20	10	7.5–10
14	10,12	12	10	1.3–5.8
16	10	10	10	8–10
20	2,10	5	2	1.45–2
24	2–10	2,5	1.8–2	1.6–2
32	1–2			

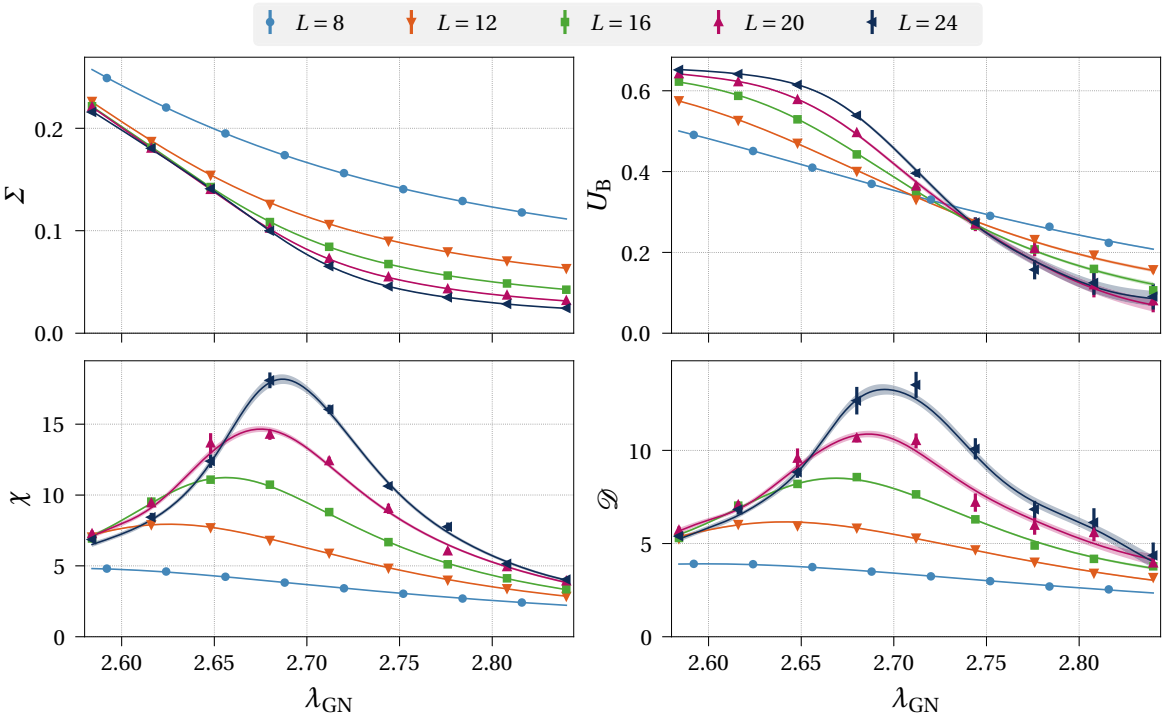

C.1(a) $N_f = 4$

Figure C.1.: Raw data and interpolations for GN observables in addition to figure 3.3. Symbols indicate the measured data points with error bars, while lines denote the interpolation obtained with histogram reweighting. An error estimate for the interpolation is given by a shaded band around the main line.

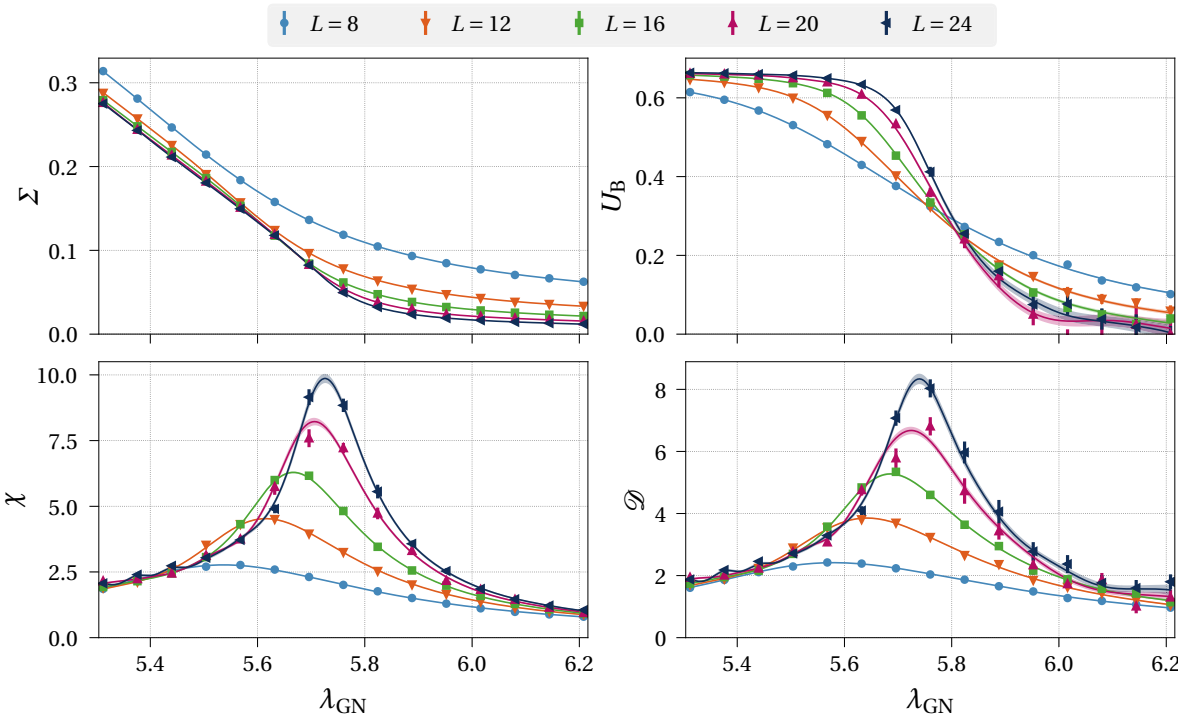

C.1(b) $N_f = 8$

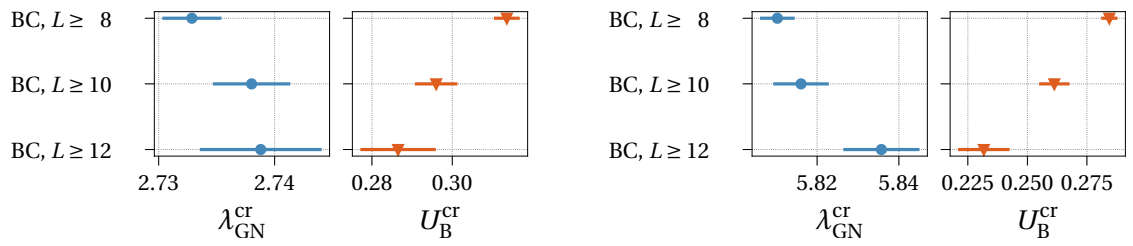

C.2(a) $N_f = 4$ **C.2(b)** $N_f = 8$

Figure C.2.: Comparison of λ_{GN}^{cr} and U_B^{cr} for different methods as in figure 3.8. The critical couplings were obtained from the intersection of Binder cumulants (BC), where also U_B^{cr} can be calculated. Results are given with the full set of L available and with smaller sets leaving out lattice size 8 or 8 and 10.

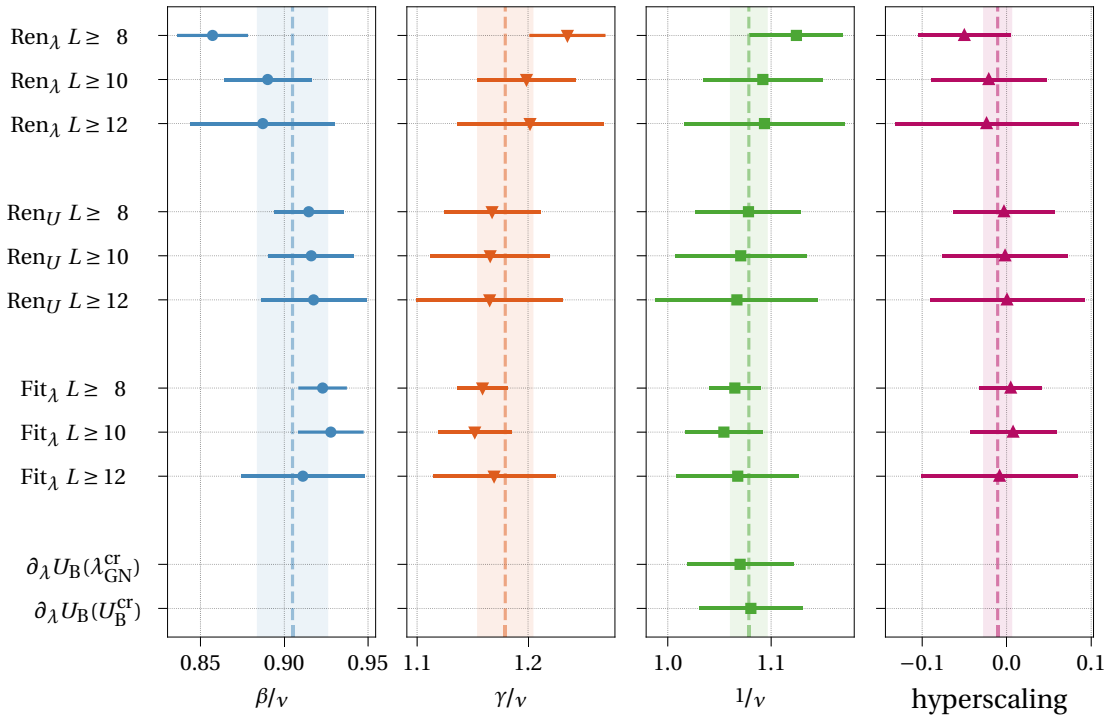

C.3(a) $N_\mathrm{f} = 4$

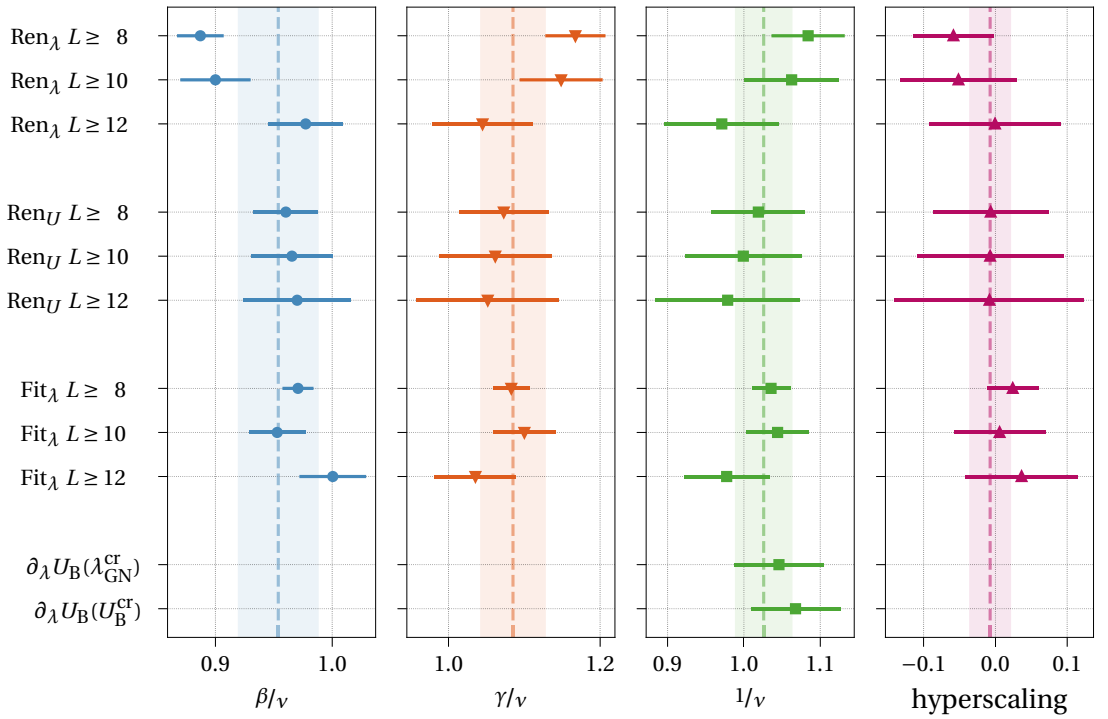

C.3(b) $N_\mathrm{f} = 8$

Figure C.3.: Comparison of different methods to evaluate critical exponents as in figure 3.12. For each method, evaluations excluding the smallest one or two lattice sizes are given. The last plot on the right shows the fulfilment of the hyperscaling relation (3.6) and should be zero.

Table C.2.: Comparison of critical exponents for GN. The most recent analytical results, all available lattice results and our own results from various evaluation methods as described in section 3.1.1 are shown. The data is also plotted in figure 3.12, C.3(b) and 3.13

C.2(a) $N_\mathrm{f} = 1$

Method	Paper	$1/\nu$	β/ν	γ/ν
large N_f, Padé	[Gra94b],[JH14]	0.955[a]	0.758	1.483
$4-\epsilon$ 3rd order	[Mih17]	1.166	0.732	1.537
2-sided Padé	[Fei16]	1.174	0.753	1.494
FRG	[Kno16]	1.075(4)	0.775	1.449
conf. bootstrap	[Ili17]	0.760	0.772	1.456
CTQMC	[WCT14]	1.25(5)	0.651(4)	1.698(7)
CTQMC	[HW16]	1.35(7)	0.637(13)	1.725(25)
MQMC	[LJY15]	1.30(5)	0.725(10)	1.550(20)
Ren_λ $L \geq 8$	this work	1.118(33)	0.797(17)	1.399(21)
Ren_λ $L \geq 10$	this work	1.13(4)	0.773(26)	1.421(29)
Ren_λ $L \geq 12$	this work	1.11(5)	0.780(34)	1.42(4)
Ren_U with $L = 32$	this work	1.21(10)	0.824(33)	1.37(7)
Ren_U $L \geq 8$	this work	1.096(34)	0.824(13)	1.366(26)
Ren_U $L \geq 10$	this work	1.10(4)	0.822(16)	1.371(32)
Ren_U $L \geq 12$	this work	1.09(5)	0.823(18)	1.37(4)
noBC $L \geq 8$	this work	1.085(26)	0.84(4)	1.317(20)
noBC $L \geq 10$	this work	1.084(30)	0.84(4)	1.317(24)
noBC $L \geq 12$	this work	1.08(4)	0.84(4)	1.316(28)
Fit_λ $L \geq 8$	this work	1.107(15)	0.843(10)	1.354(13)
Fit_λ $L \geq 10$	this work	1.120(22)	0.808(19)	1.386(22)
Fit_λ $L \geq 12$	this work	1.122(33)	0.806(29)	1.388(34)
$\partial_\lambda U_\mathrm{B}(\lambda_\mathrm{GN}^\mathrm{cr})$	this work	1.217(32)	–	–
$\partial_\lambda U_\mathrm{B}(U_\mathrm{B}^\mathrm{cr})$	this work	1.231(30)	–	–

[a] Note, that a wrong value for this was stated by Vacca & Zambelli [VZ15] which is also given in [Kno16].

C.2(b) $N_\mathrm{f} = 2$

Method	Paper	$1/\nu$	β/ν	γ/ν
large N_f, Padé	[Gra94b],[JH14]	0.962	0.872	1.256
$2+\epsilon$ 4th order	[GLS16]	0.931	0.873	1.255
$4-\epsilon$ 3rd order	[Mih17]	1.048	0.836	1.328
2-sided Padé	[Fei16]	0.948	0.869	1.261
FRG	[Kno16]	0.994(2)	0.888	1.224
conf. bootstrap	[Ili17]	0.880	0.871	1.258
staggered	[Kär94]	1.00(4)	0.877(4)	1.246(8)
fermion bag	[CL13]	1.205(15)	0.810(5)	1.38(1)
Ren_λ $L \geq 8$	this work	1.095(32)	0.850(14)	1.266(26)
Ren_λ $L \geq 10$	this work	1.056(41)	0.895(18)	1.206(34)
Ren_λ $L \geq 12$	this work	1.034(55)	0.914(26)	1.175(51)
Ren_U $L \geq 8$	this work	1.068(36)	0.886(16)	1.228(34)
Ren_U $L \geq 10$	this work	1.066(46)	0.888(21)	1.218(45)
Ren_U $L \geq 12$	this work	1.058(60)	0.889(28)	1.209(60)
noBC $L \geq 8$	this work	1.062(25)	0.892(42)	1.205(22)
noBC $L \geq 10$	this work	1.062(27)	0.895(43)	1.204(22)
noBC $L \geq 12$	this work	1.065(31)	0.897(43)	1.208(26)
Fit_λ $L \geq 8$	this work	1.061(16)	0.902(10)	1.216(16)
Fit_λ $L \geq 10$	this work	1.039(25)	0.920(14)	1.184(24)
Fit_λ $L \geq 12$	this work	1.031(38)	0.924(23)	1.167(41)
$\partial_\lambda U_\mathrm{B}(\lambda_\mathrm{GN}^\mathrm{cr})$	this work	1.077(38)	–	–
$\partial_\lambda U_\mathrm{B}(U_\mathrm{B}^\mathrm{cr})$	this work	1.093(37)	–	–

C.2(c) $N_\mathrm{f} = 4$

Method	Paper	$1/\nu$	β/ν	γ/ν
large N_f, Padé	[Gra94b],[JH14]	0.967	0.934	1.131
FRG	[BGS11]	0.978	0.944	1.113
staggered	[CS07]	1.020(21)	0.927(15)	1.152(25)
Ren_λ $L \geq 8$	this work	1.125(45)	0.857(21)	1.236(34)
Ren_λ $L \geq 10$	this work	1.092(58)	0.890(26)	1.199(45)
Ren_λ $L \geq 12$	this work	1.094(78)	0.887(43)	1.202(66)
Ren_U $L \geq 8$	this work	1.078(51)	0.915(21)	1.168(43)
Ren_U $L \geq 10$	this work	1.071(64)	0.916(26)	1.166(54)
Ren_U $L \geq 12$	this work	1.067(79)	0.917(31)	1.165(66)
Fit_λ $L \geq 8$	this work	1.065(25)	0.923(15)	1.159(23)
Fit_λ $L \geq 10$	this work	1.054(37)	0.928(20)	1.152(33)
Fit_λ $L \geq 12$	this work	1.068(59)	0.911(37)	1.169(55)
$\partial_\lambda U_\mathrm{B}(\lambda_\mathrm{GN}^\mathrm{cr})$	this work	1.070(51)	–	–
$\partial_\lambda U_\mathrm{B}(U_\mathrm{B}^\mathrm{cr})$	this work	1.080(50)	–	–

C.2(d) $N_\mathrm{f} = 8$

Method	Paper	$1/\nu$	β/ν	γ/ν
large N_f, Padé	[Gra94b],[JH14]	0.979	0.967	1.067
Ren_λ $L \geq 8$	this work	1.084(48)	0.887(20)	1.167(40)
Ren_λ $L \geq 10$	this work	1.062(62)	0.900(30)	1.149(55)
Ren_λ $L \geq 12$	this work	0.971(75)	0.977(32)	1.045(66)
Ren_U $L \geq 8$	this work	1.019(61)	0.960(28)	1.073(59)
Ren_U $L \geq 10$	this work	0.999(76)	0.966(35)	1.062(74)
Ren_U $L \geq 12$	this work	0.979(94)	0.970(46)	1.052(94)
Fit_λ $L \geq 8$	this work	1.036(25)	0.971(13)	1.083(24)
Fit_λ $L \geq 10$	this work	1.044(41)	0.953(24)	1.100(41)
Fit_λ $L \geq 12$	this work	0.977(56)	1.000(29)	1.036(54)
$\partial_\lambda U_\mathrm{B}(\lambda_\mathrm{GN}^\mathrm{cr})$	this work	1.046(58)	–	–
$\partial_\lambda U_\mathrm{B}(U_\mathrm{B}^\mathrm{cr})$	this work	1.068(59)	–	–

D. Mean Field Calculation for the γ_{45}-Model

Here, we present a first-order mean field calculation for G45 to show that the well-known effective potential of GN appears and to confirm that we use the model with the correct sign of interaction. Similar calculations for GN and NJL can be found for example in the textbooks of Coleman [Col85] and Miransky [Mir94] and in the paper of Scherer et al. [SBG13].

We begin with the Dirac operator of the Lagrangian (2.34), which can be split in two blocks similarly to (2.59). Due to the minus sign in the second block of γ_{45} in (2.17), we have

$$D[\rho] = \begin{pmatrix} \sigma_\mu \partial_\mu + \alpha\rho & 0 \\ 0 & -\sigma_\mu \partial_\mu - \alpha\rho \end{pmatrix} := \begin{pmatrix} D_2[\rho] & 0 \\ 0 & -D_2[\rho] \end{pmatrix}. \tag{D.1}$$

Here, we introduced the irreducible Dirac operator $D_2[\rho]$ and the constant $\alpha = 1$ for our choice of interaction sign in (2.8). If we had chosen the other sign (or $g^2_{\mathrm{G45}} < 0$), we would get $\alpha = \mathrm{i}$ and the full operator would be anti-Hermitian.

The minus sign in front of the second operator is irrelevant for the determinant in spinor space, since it is 2-dimensional. The general form of the eigenvalues for the operator $D_2[\rho]$ is

$$\lambda_\pm = \alpha\rho \pm \mathrm{i}\left|p_\mu\right| \qquad \Rightarrow \qquad \lambda_+\lambda_- = (\alpha\rho)^2 + \left|p_\mu\right|^2. \tag{D.2}$$

The second operator has $\lambda^{(2)}_\mp = -\lambda_\pm = -\alpha\rho \mp \mathrm{i}\left|p_\mu\right|$ leading to complex conjugate pairs for $\alpha = \mathrm{i}$ from $\lambda^*_+ = \lambda^{(2)}_-$ and $\lambda^*_- = \lambda^{(2)}_+$, while no relation exists for $\alpha = 1$. This agrees with the fact given in 2.4.2 that the operator with $\alpha = \mathrm{i}$ is free of a sign problem, while this is not the case for the second possibility.

To calculate a mean field approximation, we ignore fluctuations of ρ. Then, the theory is described by the effective action obtained after integration over the fermions as in (2.47). With $P[\rho] \propto \mathrm{e}^{-S}$ we have

$$S = S_{\mathrm{eff}}[\rho] + S_{\mathrm{bos}}[\rho] = -\ln\det(D[\rho]) + S_{\mathrm{bos}}[\rho] = -\operatorname{tr}\ln(D[\rho]) + S_{\mathrm{bos}}[\rho]. \tag{D.3}$$

The trace of logarithms is the sum over all logarithms of the eigenvalues. Our D in the irreducible representation has two distinct eigenvalues from the spinor matrix structure and infinitely many from the differential operator parametrised by p_μ, where the trace is given by the integration over d^3p. The sum over the spin-eigenvalues gives $\ln\lambda_- + \ln\lambda_+ = \ln(\lambda_+\lambda_-)$, and the whole action is given by

$$S = S_{\mathrm{bos}}[\rho] - N_{\mathrm{f}} \int \frac{\mathrm{d}^3p}{(2\pi)^3} \ln(-\lambda_+(p)\lambda_-(p)) = S_{\mathrm{bos}}[\rho] - \frac{N_{\mathrm{f}}}{2\pi^2} \int_0^\Lambda \mathrm{d}p\, p^2 \ln\left[(p^2 + \alpha^2\rho^2)^2\right]. \tag{D.4}$$

In the last step, we performed the integration over the angular coordinates and introduced a momentum cutoff Λ. The factor of N_f comes in since the multi-flavour Dirac operator contains N_f identical diagonal copies of the single-flavour operator. The remaining integral can be performed and we get

$$\frac{S}{N_\mathrm{f}} = \frac{\lambda_{\mathrm{G45}}\rho^2}{2} - \frac{2\alpha^2\Lambda\rho^2}{3\pi^2} + \frac{2\alpha^3\rho^3}{3\pi^2}\arctan\left(\frac{\Lambda}{\alpha\rho}\right) - \frac{\Lambda^3}{6\pi^2}\log\left(\left(\alpha^2\rho^2+\Lambda^2\right)^2\right) + \frac{2\Lambda^3}{9\pi^2}, \tag{D.5}$$

which can be expanded for $\Lambda \to \infty$ to

$$\frac{S_\mathrm{eff}}{N_\mathrm{f}} \approx \frac{\alpha\left|\rho\right|^3}{3\pi} + \rho^2\left(\frac{\lambda_{\mathrm{G45}}}{2N_\mathrm{f}} - \frac{\alpha^2\Lambda}{\pi^2}\right) + \frac{2\Lambda^3}{9\pi^2} - \frac{2\Lambda^3\log(\Lambda)}{3\pi^2}. \tag{D.6}$$

Dropping the term without field dependence and introducing the renormalised coupling $\lambda_\mathrm{ren} = \left(\frac{\lambda_{\mathrm{G45}}}{2N_\mathrm{f}} - \frac{\alpha^2\Lambda}{\pi^2}\right)$, we obtain

$$\frac{S_\mathrm{eff}}{N_\mathrm{f}} \approx \rho^2\lambda_\mathrm{ren} + \frac{\alpha\left|\rho\right|^3}{3\pi}. \tag{D.7}$$

For G45 with $\alpha = 1$, this is the same result commonly presented for GN, but we find an imaginary term $\sim \mathrm{i}\left|\rho\right|^3$ for the modified version of G45 without sign problem and $\lambda_{\mathrm{G45}} < 0$. The derivative is given by

$$\frac{\mathrm{d}S_\mathrm{eff}}{\mathrm{d}\rho} = \rho\left(2\lambda_\mathrm{ren} + \frac{\alpha\left|\rho\right|}{\pi}\right), \tag{D.8}$$

which has an extremum at $\rho = 0$ and two additional extrema at $\rho = \pm 2\pi\alpha\lambda_\mathrm{ren}$ if $\lambda_\mathrm{ren} < 0$. The latter are indeed minima of the effective potential, which takes the values of $\frac{4\pi^2}{3}\lambda_\mathrm{ren}^3 < 0$ below the value of the potential at the origin. This shows that χSB for our definition of G45 with $\alpha = 1$ should happen for any N_f as in GN.

E. Derivation of Dual-Variable Formulations

Here, we calculate the dual-variables formulation of the partition sum for FM, where we found a very strong sign problem in section 6.1.2. This was the main motivation to study this formulation. Additionally, we explore a direct derivation from the vector-field formulation of Th.

Derivation for FM

Contrary to the direct implementation described in section 6.1.1, we use the Lagrangian (2.37a) with a redundant scalar field ϕ and a Hermitian matrix T in flavour space. In total we have $N_\varphi = N_\mathrm{f}^2 + 1$ real degrees of freedom. This version is easier to treat than the form with a traceless matrix used in section 6.1.1. The interaction term is given by

$$H_x^{\alpha\beta} = T_x^{\alpha\beta} + \phi_x \delta^{\alpha\beta}. \tag{E.1}$$

Due to its index structure, our dual variable $k_{xi}^{\alpha\beta}$ also has two flavour indices, one spinor index and a spacetime index, but the expression (6.10) for W only contains $k_x^{\alpha\beta} = \sum_i k_{xi}^{\alpha\beta}$ explicitly. It takes the values 0, 1 or 2 since there are two spinor components.

As in (6.12), we can introduce local weights $w(k_x)$ and write the partition sum as

$$Z(\lambda_\mathrm{Th}) = C_\mathrm{HS} \sum_{\left\{k_{xi}^{\alpha\beta}\right\}} \det(\partial[k])(-1)^k \prod_x w(k_x), \tag{E.2}$$

where C_HS was calculated in (B.10). The weight at a fixed lattice site x is

$$w(k_x) = \int_{-\infty}^{\infty} \mathrm{d}\phi \int_{-\infty}^{\infty} \mathrm{d}T \left(T^{\alpha\beta} + \phi\,\delta^{\alpha\beta}\right)^{k_x^{\alpha\beta}} \exp\!\left(-\frac{1}{2}\lambda_\mathrm{Th}\phi^2 - \frac{1}{4}\lambda_\mathrm{Th}\sum_{\gamma\delta} T^{\delta\gamma}T^{\gamma\delta}\right). \tag{E.3}$$

The integration measure over the Hermitian matrices $\int \mathrm{d}T = \prod_{\alpha\le\beta} \int \mathrm{d}T^{\alpha\beta}$ is given such that we can use $T^{\beta\alpha} = (T^{\alpha\beta})^*$ and only count independent degrees of freedom. In a similar way, we can factorise the exponential function and write

$$\exp\!\left(-\frac{1}{4}\lambda_\mathrm{Th}\sum_{\alpha\beta} T^{\alpha\beta}T^{\beta\alpha}\right) = \prod_{\alpha\beta} \mathrm{e}^{-\frac{1}{4}\lambda_\mathrm{Th}T^{\alpha\beta}T^{\beta\alpha}} = \left(\prod_\alpha \mathrm{e}^{-\frac{1}{4}\lambda_\mathrm{Th}(T^{\alpha\alpha})^2}\right)\left(\prod_{\alpha<\beta} \mathrm{e}^{-\frac{1}{2}\lambda_\mathrm{Th}\left|T^{\alpha\beta}\right|^2}\right). \tag{E.4}$$

Now, we can split the local weight into factors only containing either diagonal or non-diagonal elements of T. We obtain

$$w(k_x) = \int_{-\infty}^{\infty} \mathrm{d}\phi\, \mathrm{e}^{-\frac{1}{2}\lambda_\mathrm{Th}\phi^2} \prod_\alpha w_\mathrm{diag}\left(\phi, k^{\alpha\alpha}\right) \prod_{\alpha<\beta} w_\mathrm{nd}\left(k^{\alpha\beta}, k^{\beta\alpha}\right). \tag{E.5}$$

The integrals over the non-diagonal fields are given by the complex Gaussian integral

$$w_{\mathrm{nd}}(k,k') = \int \mathrm{d}z\, \mathrm{e}^{-\frac{1}{2}\lambda_{\mathrm{Th}}|z|^2} z^k (z^*)^{k'} = \frac{2\pi}{\lambda_{\mathrm{Th}}} k! \left(\frac{2}{\lambda_{\mathrm{Th}}}\right)^k \delta_{kk'} \tag{E.6}$$

leading to the additional constraint $k_x^{\alpha\beta} = k_x^{\beta\alpha}$. Including the product over flavours and lattice points for configurations with non-zero weight, we get a sum over the off-diagonal variables $\tilde{k} = \sum_x \sum_{\alpha<\beta} k_x^{\alpha\beta}$ in the exponent. Whenever a $k_x^{\alpha\beta}$ has the value 2, we have to include an additional factor of 2 from $k!$. Hence, we introduce $\tilde{n}_2$, counting the number of $k_x^{\alpha\beta} = 2$ for $\alpha < \beta$. In conclusion, we have

$$\prod_x \prod_{\alpha<\beta} w_{\mathrm{nd}}\left(k^{\alpha\beta}, k^{\beta\alpha}\right) = \left(\frac{2\pi}{\lambda_{\mathrm{Th}}}\right)^{V\tilde{N}} 2^{\tilde{n}_2} \left(\frac{2}{\lambda_{\mathrm{Th}}}\right)^{\tilde{k}} \quad \text{with} \quad \tilde{N} = \frac{1}{2} N_{\mathrm{f,irr}}(N_{\mathrm{f,irr}} - 1). \tag{E.7}$$

The diagonal contribution is given by a real integration

$$w_{\mathrm{diag}}(\phi,k) = \int_{-\infty}^{\infty} \mathrm{d}t\, \mathrm{e}^{-\frac{1}{4}\lambda_{\mathrm{Th}} t^2} \left(t+\phi\right)^k = 2\sqrt{\frac{\pi}{\lambda_{\mathrm{Th}}}} \begin{cases} 1 & k=0, \\ \phi & k=1, \\ \frac{2}{\lambda_{\mathrm{Th}}} + \phi^2 & k=2. \end{cases} \tag{E.8}$$

To put the products over x and α together, we introduce numbers $n_{i,x}$ for $i = 0,1,2$ that count, how many $k_x^{\alpha\alpha}$ equal i (no summation over α). At each x they can take the values $n_{i,x} \in \{0,1,\ldots,N_{\mathrm{f,irr}}\}$ and must sum up to $N_{\mathrm{f,irr}}$ in total. With this notation, we obtain

$$\prod_x \prod_\alpha w_{\mathrm{diag}}(\phi,k) = 2^{VN_{\mathrm{f,irr}}} \left(\frac{\pi}{\lambda_{\mathrm{Th}}}\right)^{\frac{VN_{\mathrm{f,irr}}}{2}} \prod_x \phi_x^{n_{1,x}} \left(\frac{2}{\lambda_{\mathrm{Th}}} + \phi_x^2\right)^{n_{2,x}}. \tag{E.9}$$

Finally, we can perform the remaining integral over ϕ in (E.5). At each lattice point it is

$$I(n_1,n_2) \coloneqq \int_{-\infty}^{\infty} \mathrm{d}\phi\, \mathrm{e}^{-\frac{1}{2}\lambda_{\mathrm{Th}}\phi^2} \phi^{n_1} \left(\frac{2}{\lambda_{\mathrm{Th}}} + \phi^2\right)^{n_2} = C_I \int_{-\infty}^{\infty} \mathrm{d}\varphi\, \mathrm{e}^{-\varphi^2} \varphi^{n_1} \left(1+\varphi^2\right)^{n_2}, \tag{E.10}$$

where a redefinition of the field with $\varphi \coloneqq \sqrt{\frac{\lambda_{\mathrm{Th}}}{2}}\phi$ was used and we defined $C_I(n_1,n_2) \coloneqq \left(\sqrt{\frac{2}{\lambda_{\mathrm{Th}}}}\right)^{(1+n_1+2n_2)}$. We can directly see that the integral vanishes if n_1 is odd. Then, the integrand is an odd function which is integrated over a symmetric interval. For even n_1, the integrand is a function of φ^2, allowing us to restrict the integration to the positive real numbers. We substitute $\varphi = \sqrt{y}$ and obtain

$$I(n_1,n_2) = C_I \int_0^{\infty} \mathrm{d}y\, \mathrm{e}^{-y} y^{\frac{n_1-1}{2}} \left(1+y\right)^{n_2} \quad \text{with} \quad n_1 \text{ even}. \tag{E.11}$$

This integral is proportional to an integral representation of the confluent hypergeometric function of the second kind [Wei]

$$U(a,b,z) = \frac{1}{\Gamma(a)} \int_0^{\infty} \mathrm{d}y\, \mathrm{e}^{-zy} y^{a-1} (1+y)^{b-a-1}. \tag{E.12}$$

Reading off $a = {}^{(n_1+1)}/_2$, $b = n_2 + {}^{(n_1+3)}/_2$ and $z = 1$ we are lead to the solution

$$I(n_1, n_2) = \begin{cases} C_I\, \Gamma\left(\frac{n_1+1}{2}\right) U\left(\frac{n_1+1}{2}, \frac{n_1+3}{2} + n_2, 1\right) & n_1 \text{ even}, \\ 0 & n_1 \text{ odd}. \end{cases} \tag{E.13}$$

For the integer values of n_1, n_2 that are relevant here, it can be analytically evaluated with computer algebra systems like `Mathematica`.

We now evaluated all parts of the local weights in (E.5) together with the product over all lattice sites. This enables us to write down the partition sum

$$Z(\lambda_{\mathrm{Th}}) = \underbrace{2^{\frac{VN_{\mathrm{f,irr}}}{2}} \left(\frac{\lambda_{\mathrm{Th}}}{2\pi}\right)^{\frac{V}{2}\left(N_{\mathrm{f,irr}}^2+1\right)} \sum_{\left\{k_{xi}^{\alpha\beta}\right\}} \det(\partial[k])(-1)^k}_{\text{from (E.2)}} \underbrace{\left(\frac{2\pi}{\lambda_{\mathrm{Th}}}\right)^{V\tilde{N}} 2^{\tilde{n}_2} \left(\frac{2}{\lambda_{\mathrm{Th}}}\right)^{\tilde{k}}}_{\text{from (E.7)}}$$
$$\underbrace{\cdot 2^{\frac{VN_{\mathrm{f,irr}}}{2}} \left(\frac{2\pi}{\lambda_{\mathrm{Th}}}\right)^{\frac{VN_{\mathrm{f,irr}}}{2}}}_{\text{from (E.9)}} \prod_x \underbrace{C_I(n_{1,x}, n_{2,x}) \Gamma\left(\frac{n_{1,x}+1}{2}\right) U\left(\frac{n_{1,x}+1}{2}, \frac{n_{1,x}+3}{2} + n_{2,x}, 1\right)}_{\text{from (E.13)}}. \tag{E.14}$$

Using $n_i = \sum_x n_{i,x}$, we get an overall factor ${}^{(2/\lambda_{\mathrm{Th}})^{\frac{1}{2}(V+n_1+2n_2)}}$ by pulling C_I out of the product. Together with ${}^{(2/\lambda_{\mathrm{Th}})^{\tilde{k}}}$, the exponent combines to $\frac{1}{2}(V + n_1 + 2n_2 + 2\tilde{k}) = \frac{1}{2}(V + k)$. The powers of ${}^{2\pi/\lambda_{\mathrm{Th}}}$ in the sum partially cancel with the prefactor from HS. Collecting all remaining coefficients independent of k in $C = 2^{VN_{\mathrm{f,irr}}-V} \pi^{-\frac{V}{2}}$ we arrive at the final form

$$Z(\lambda_{\mathrm{Th}}) = C \sum_{\left\{k_{xi}^{\alpha\beta}\right\}} \det(\partial[k])(-1)^k 2^{\tilde{n}_2} \left(\frac{2}{\lambda_{\mathrm{Th}}}\right)^{\frac{k}{2}} \prod_x \Gamma\left(\frac{n_{1,x}+1}{2}\right) U\left(\frac{n_{1,x}+1}{2}, \frac{n_{1,x}+3}{2} + n_{2,x}, 1\right). \tag{E.15}$$

The local constraints on the field $k_{xi}^{\alpha\beta}$ are

$$k_x^{\alpha\beta} = k_x^{\beta\alpha}, \quad \sum_{\alpha=1}^{N_{\mathrm{f,irr}}} k_{xi}^{\alpha\beta} \in \{0,1\}, \quad \sum_{\beta=1}^{N_{\mathrm{f,irr}}} k_{xi}^{\alpha\beta} \in \{0,1\}, \quad n_{1,x} \text{ even}. \tag{E.16}$$

Single-Flavour Model

For $N_{\mathrm{f,irr}} = 1$, the possible local configurations are $k_{xi}^{11} \in \{(0,0), (0,1), (1,0), (1,1)\}$. Summed over the spin, only the first and the last configuration are allowed by the constraints because they have $k_x^{11} \in \{0,2\}$. The corresponding value for $n_{1,x}$ is always 0, which leads to $\Gamma({}^1/_2)^V = \pi^{\frac{V}{2}}$ in the partition function and cancels the factor C. Furthermore, we find $n_{2,x} = 0$ for the first and $n_{2,x} = 1$ for the second possibility, so that $n_2 = \frac{k}{2}$ is the only remaining variable. The confluent hypergeometric function evaluates to $U({}^1/_2, {}^3/_2, 1) = 1$ and $U({}^1/_2, {}^5/_2, 1) = {}^3/_2$ respectively. This contributes a total factor of ${}^{(3/2)^{n_2}}$. Since there is only one flavour, $\tilde{n}_2$ is always zero. Finally, we arrive at the following partition sum for $N_{\mathrm{f,irr}} = 1$:

$$Z(\lambda_{\mathrm{Th}}) = \sum_{n_{2,x}} \det(\partial[n_2]) \left(\frac{3}{\lambda_{\mathrm{Th}}}\right)^{n_2}. \tag{E.17}$$

This is identical to the single-flavour partition sum for the irreducible GN in (6.19) and confirms the identity $\lambda_{\mathrm{Th}} = 3\lambda_{\mathrm{GN}}$ given below equation (2.27).

Derivation for the Irreducible Th

The interaction term in the irreducible version of (2.33) is independent of flavour indices, but has a contribution in spin-space. With $H_{MN} = V_{x,\mu}\delta_{xy}\sigma^{\mu}_{ij}\delta_{\alpha\beta}$ (summation only over μ) we get

$$Z(\lambda_{\mathrm{Th}}) = C_{\mathrm{HS}} \sum_{\left\{k_x^{ij}\right\}} \det(\partial[k]) \prod_x \int_{-\infty}^{\infty} \mathrm{d}V_{x,\mu} \left(-V_{x,\mu}\sigma^{\mu}_{ij}\right)^{k_x^{ij}} := C_{\mathrm{HS}} \sum_{\left\{k_x^{ij}\right\}} \det(\partial[k])(-1)^k \prod_x w(k_x), \tag{E.18}$$

where $k_x^{ij} = \sum_{\alpha=1}^{N_{\mathrm{f,irr}}} k_{x\alpha}^{ij} \in \{0,1,\ldots,N_{\mathrm{f,irr}}\}$. To proceed with the integration of the vector field, we use the Pauli matrices as a specific representation of σ_μ. Then, the local weights are given by

$$w(k_x) = \int \mathrm{d}V_\mu \exp\left(-\frac{1}{2}\lambda V_\mu^2\right)(V_1 - \mathrm{i}V_2)^{k_x^{12}}(V_1 + \mathrm{i}V_2)^{k_x^{21}} V_3^{k_x^{11}+k_x^{22}}(-1)^{k_x^{22}}. \tag{E.19}$$

The integration over V_3 is given by a Gaussian integral similar to (E.8), but k_x^{ij} now takes $N_{\mathrm{f}}+1$ values. The integral vanishes for odd $\bar{k}_x = k_x^{11} + k_x^{22} \in \{0,1,\ldots,2N_{\mathrm{f,irr}}\}$, otherwise it is

$$w_3(\bar{k}_x) := \int_{-\infty}^{\infty} \mathrm{d}V_3\, \mathrm{e}^{-\frac{1}{2}\lambda_{\mathrm{Th}}V_3^2} V_3^{\bar{k}_x} = \left(\frac{2}{\lambda}\right)^{\frac{1}{2}(\bar{k}_x+1)} \Gamma\left(\frac{\bar{k}_x+1}{2}\right) \quad \text{for} \quad \bar{k}_x \text{ even}. \tag{E.20}$$

As for GN in (6.14), we can introduce occupation numbers n_s for $s = 0,1,\ldots,N_{\mathrm{f,irr}}$, counting how many configurations have the trace $\bar{k}_x = 2s$, and write

$$\prod_x w_3(\bar{k}_x) = \left(\frac{2}{\lambda_{\mathrm{Th}}}\right)^{\frac{1}{2}(\bar{k}+V)} \prod_{s=0}^{N_{\mathrm{f,irr}}} \Gamma\left(\frac{2s+1}{2}\right)^{n_s}. \tag{E.21}$$

For the integration over V_1 and V_2 we introduce a complex notation $z = V_1 + \mathrm{i}V_2$ and obtain an integral identical to (E.6) with the constraint $k_x^{12} = k_x^{21}$. With $\sum_x k_x^{12} = k^{12}$, the product over the lattice volume is given by

$$\prod_x w_{12}(k_x^{12}, k_x^{21}) = \left(\frac{2\pi}{\lambda_{\mathrm{Th}}}\right)^V \left(\frac{2}{\lambda_{\mathrm{Th}}}\right)^{k^{12}} \prod_x k_x^{12}!. \tag{E.22}$$

Again, the exponents of $2/\lambda_{\mathrm{Th}}$ combine to the total k. Introducing $\tilde{n}_s$, which counts how many k_x^{12} have the value s, and $C = \pi^{-\frac{V}{2}}$, we can write the resulting partition sum as

$$Z(\lambda_{\mathrm{Th}}) = C \sum_{\left\{k_{x\alpha}^{ij}\right\}} \det(\partial[k])(-1)^{k+k^{22}} \left(\frac{2}{\lambda_{\mathrm{Th}}}\right)^k \prod_{s=0}^{N_{\mathrm{f,irr}}} (s!)^{\tilde{n}_s} \Gamma\left(\frac{2s+1}{2}\right)^{n_s}. \tag{E.23}$$

Bibliography

[Ahn94] Y. M. Ahn, B. K. Chung, J.-M. Chung & Q.-H. Park. “Spontaneous Breaking of Parity in 2+1-Dimensional Thirring Model”. Apr. 29, 1994. arXiv: hep-th/9404181 (cit. on pp. 7, 16, 17, 21, 70, 87).

[AP98] Y. M. Ahn & Q. H. Park. “Spontaneous Breaking of Generalized Parity in 2+1-Dimensional Four-Fermi Interactions”. In: *Journal of the Korean Physical Society* 33.6 (Dec. 1, 1998), pp. 655–658. URL: http://www.jkps.or.kr/journal/list.html?pn=vol&TG=vol&s_v=33&s_n=6&year=1998 (visited on 06/01/2017) (cit. on pp. 7, 17, 21, 70, 87).

[AM96] I. J. R. Aitchison & N. E. Mavromatos. “Deviations from Fermi-liquid behavior in (2+1)-dimensional quantum electrodynamics and the normal phase of high-T_c superconductors”. In: *Physical Review B* 53.14 (Apr. 1, 1996), pp. 9321–9336. arXiv: hep-th/9510058. DOI: 10.1103/PhysRevB.53.9321 (cit. on p. 5).

[AHS10] W. Armour, S. Hands & C. Strouthos. “Monte Carlo Simulation of the Semimetal-Insulator Phase Transition in Monolayer Graphene”. In: *Physical Review B* 81.12 (Mar. 4, 2010). arXiv: 0910.5646. DOI: 10.1103/PhysRevB.81.125105 (cit. on p. 5).

[BVZ06] A. V. Balatsky, I. Vekhter & J.-X. Zhu. “Impurity-Induced States in Conventional and Unconventional Superconductors”. In: *Reviews of Modern Physics* 78.2 (May 9, 2006), pp. 373–433. arXiv: cond-mat/0411318. DOI: 10.1103/RevModPhys.78.373 (cit. on p. 5).

[BCS57a] J. Bardeen, L. N. Cooper & J. R. Schrieffer. “Microscopic Theory of Superconductivity”. In: *Physical Review* 106.1 (Apr. 1, 1957), pp. 162–164. DOI: 10.1103/PhysRev.106.162 (cit. on p. 12).

[BCS57b] J. Bardeen, L. N. Cooper & J. R. Schrieffer. “Theory of Superconductivity”. In: *Physical Review* 108.5 (Dec. 1, 1957), pp. 1175–1204. DOI: 10.1103/PhysRev.108.1175 (cit. on p. 12).

[BTW02] J. Berges, N. Tetradis & C. Wetterich. “Non-Perturbative Renormalization Flow in Quantum Field Theory and Statistical Physics”. In: *Physics Reports* 363 (4-6 June 2002), pp. 223–386. arXiv: hep-ph/0005122. DOI: 10.1016/S0370-1573(01)00098-9 (cit. on p. 133).

[Ber09] G. Bergner. “Symmetries and the methods of quantum field theory : supersymmetry on a space-time lattice”. PhD Thesis. Jena: Friedrich-Schiller-Universität, 2009. URL: http://www.tpi.uni-jena.de/qfphysics/homepage/wipf/abschlussarbeiten/bergner_diss.pdf (cit. on pp. 6, 25).

[Ber10] G. Bergner. “Complete Supersymmetry on the Lattice and a No-Go Theorem: A Simulation with Intact Supersymmetries on the Lattice”. In: *Journal of High Energy Physics* 2010.1 (Jan. 2010). arXiv: 0909.4791. DOI: 10.1007/JHEP01(2010)024 (cit. on pp. 6, 25).

[BBP09] G. Bergner, F. Bruckmann & J. M. Pawlowski. “Generalising the Ginsparg-Wilson Relation: Lattice Supersymmetry from Blocking Transformations”. In: *Physical Review D* 79.11 (June 12, 2009). arXiv: 0807.1110. DOI: 10.1103/PhysRevD.79.115007 (cit. on pp. 6, 25).

[Ber08] G. Bergner, T. Kästner, S. Uhlmann & A. Wipf. “Low-dimensional Supersymmetric Lattice Models”. In: *Annals of Physics* 323.4 (Apr. 2008), pp. 946–988. arXiv: 0705.2212. DOI: 10.1016/j.aop.2007.06.010 (cit. on pp. 6, 25).

[Bin81] K. Binder. “Finite size scaling analysis of Ising model block distribution functions”. In: *Zeitschrift für Physik B Condensed Matter* 43.2 (June 1, 1981), 119 bibrangedash /140. DOI: 10.1007/BF01293604 (cit. on pp. 34, 35).

[Bin92] K. Binder. “Finite size effects at phase transitions”. In: *Computational Methods in Field Theory*. Berlin, Heidelberg: Springer, 1992, pp. 59–125. DOI: 10.1007/3-540-55997-3_31 (cit. on p. 34).

[Bit89] K. Bitar, A. D. Kennedy, R. Horsley, S. Meyer & P. Rossi. “The QCD finite temperature transition and hybrid Monte Carlo”. In: *Nuclear Physics B* 313.2 (Feb. 6, 1989), pp. 348–376. DOI: 10.1016/0550-3213(89)90323-4 (cit. on p. 27).

[BK15] J. Borchardt & B. Knorr. “Global solutions of functional fixed point equations via pseudo-spectral methods”. In: *Physical Review D* 91.10 (May 14, 2015). arXiv: 1502.07511. DOI: 10.1103/PhysRevD.91.105011 (cit. on p. 53).

[BGS11] J. Braun, H. Gies & D. D. Scherer. “Asymptotic Safety: A Simple Example”. In: *Physical Review D* 83.8 (Apr. 11, 2011), p. 085012. arXiv: 1011.1456. DOI: 10.1103/PhysRevD.83.085012 (cit. on pp. 4, 52, 53, 55, 110).

[Bro] M. Brookes. *Matrix Manual: Matrix Property Proofs*. URL: http://www.ee.ic.ac.uk/hp/staff/dmb/matrix/proof003.html#DetSum_p (visited on 08/29/2017) (cit. on p. 93).

[BB87] C. Burden & A. N. Burkitt. “Lattice Fermions in Odd Dimensions”. In: *Europhysics Letters* 3.5 (Mar. 1, 1987), p. 545. DOI: 10.1209/0295-5075/3/5/006 (cit. on p. 5).

[Cal91] C. de Calan, P. A. Faria da Veiga, J. Magnen & R. Sénéor. “Constructing the three-dimensional Gross-Neveu model with a large number of flavor components”. In: *Physical Review Letters* 66.25 (June 24, 1991), pp. 3233–3236. DOI: 10.1103/PhysRevLett.66.3233 (cit. on p. 5).

[CT02] R. G. Campos & E. S. Tututi. “Ultralocality on the lattice”. Aug. 26, 2002. arXiv: hep-lat/0208053 (cit. on p. 25).

[Cas09] A. Castro Neto, F. Guinea, N. Peres, K. Novoselov & A. Geim. “The electronic properties of graphene”. In: *Reviews of Modern Physics* 81.1 (Jan. 14, 2009), pp. 109–162. DOI: 10.1103/RevModPhys.81.109 (cit. on p. 5).

[Cha08] S. Chandrasekharan. “A New Computational Approach to Lattice Quantum Field Theories”. In: *PoS(LATTICE 2008)003*. 26th International Symposium on Lattice Field Theory. Williamsburg, Virginia, USA: Proceedings of Science, 2008. arXiv: 0810.2419 (cit. on pp. 29, 87, 90).

[Cha10] S. Chandrasekharan. “The fermion bag approach to lattice field theories”. In: *Physical Review D* 82.2 (July 14, 2010). arXiv: 0910.5736. DOI: 10.1103/PhysRevD.82.025007 (cit. on pp. 29, 30, 72, 87, 90).

[Cha12] S. Chandrasekharan. “Solutions to sign problems in lattice Yukawa models”. In: *Physical Review D* 86.2 (July 3, 2012). arXiv: 1205.0084. DOI: 10.1103/PhysRevD.86.021701 (cit. on p. 30).

[Cha13] S. Chandrasekharan. “Fermion bag approach to fermion sign problems”. In: *The European Physical Journal A* 49.7 (July 17, 2013), pp. 1–12. DOI: 10.1140/epja/i2013-13090-y (cit. on p. 29).

[CL11a] S. Chandrasekharan & A. Li. “Fermion bag approach to the sign problem in strongly coupled lattice QED with Wilson fermions”. In: *Journal of High Energy Physics* 2011.1 (Jan. 2011). arXiv: 1008.5146. DOI: 10.1007/JHEP01(2011)018 (cit. on p. 30).

[CL11b] S. Chandrasekharan & A. Li. “The generalized fermion-bag approach”. In: *PoS(Lattice 2011)058*. 29th International Symposium on Lattice Field Theory. Squaw Valley, Lake Tahoe, California, USA: Proceedings of Science, Nov. 22, 2011. arXiv: 1111.5276 (cit. on pp. 30, 72).

[CL12a] S. Chandrasekharan & A. Li. “Fermion Bags, Duality, and the Three Dimensional Massless Lattice Thirring Model”. In: *Physical Review Letters* 108.14 (Apr. 5, 2012), p. 140404. arXiv: 1111.7204. DOI: 10.1103/PhysRevLett.108.140404 (cit. on pp. 6, 30, 72).

[CL12b] S. Chandrasekharan & A. Li. “Fermion bag solutions to some sign problems in four-fermion field theories”. In: *Physical Review D* 85.9 (May 22, 2012), p. 091502. arXiv: 1202.6572. DOI: 10.1103/PhysRevD.85.091502 (cit. on pp. 30, 54).

[CL13] S. Chandrasekharan & A. Li. “Quantum critical behavior in three dimensional lattice Gross-Neveu models”. In: *Physical Review D* 88.2 (July 31, 2013), p. 021701. arXiv: 1304.7761. DOI: 10.1103/PhysRevD.88.021701 (cit. on pp. 6, 51, 54, 55, 72, 93, 98, 110).

[CHS07] S. Christofi, S. Hands & C. Strouthos. “Critical flavor number in the three dimensional Thirring model”. In: *Physical Review D* 75.10 (May 21, 2007), p. 101701. arXiv: hep-lat/0701016. DOI: 10.1103/PhysRevD.75.101701 (cit. on pp. 6, 7, 60, 69, 72, 73).

[CS07] S. Christofi & C. Strouthos. “Three dimensional four-fermion models - A Monte Carlo study”. In: *Journal of High Energy Physics* 2007 (05 May 29, 2007), p. 088. arXiv: hep-lat/0612031. DOI: 10.1088/1126-6708/2007/05/088 (cit. on pp. 6, 12, 34–36, 52, 54, 55, 110).

[Col85] S. Coleman. *Aspects of Symmetry: Selected Erice Lectures*. Cambridge: Cambridge University Press, 1985. ISBN: 978-0-511-56504-5. DOI: 10.1017/CBO9780511565045 (cit. on p. 112).

[Dat97] T. Dateki. “The Phase Structure of the Gross-Neveu Model with Thirring Interaction at the Next to Leading Order of $1/N$ Expansion”. In: *Progress of Theoretical Physics* 97.6 (June 1, 1997), pp. 921–937. arXiv: hep-th/9701183. DOI: 10.1143/PTP.97.921 (cit. on pp. 77–79).

[Del97a] L. Del Debbio. “The phase structure of the 3-d Thirring model”. In: *Nuclear Physics B - Proceedings Supplements 53*. Lattice 96. Lattice 96. Washington University, St. Louis, USA: Elsevier, Feb. 1997, pp. 699–701. arXiv: hep-lat/9608003. DOI: 10.1016/S0920-5632(96)00758-X (cit. on p. 71).

[Del97b] L. Del Debbio. “Chiral symmetry breaking in the 3-d Thirring model for small N_f”. In: *Nuclear Physics B - Proceedings Supplements 63*. 15th International Symposium on Lattice Field Theory. Edinburgh, UK: Elsevier, Sept. 12, 1997. arXiv: hep-lat/9709034 (cit. on p. 71).

[DH99] L. Del Debbio & S. J. Hands. “The three-dimensional Thirring model for $N_f = 4$ and $N_f = 6$”. In: *Nuclear Physics B* 552 (1–2 July 12, 1999), pp. 339–362. arXiv: hep-lat/9902014. DOI: 10.1016/S0550-3213(99)00258-8 (cit. on pp. 6, 7, 69, 71).

[DHM97] L. Del Debbio, S. J. Hands & J. C. Mehegan. “The Three Dimensional Thirring Model for Small N_f”. In: *Nuclear Physics B* 502 (1-2 Sept. 1997), pp. 269–308. arXiv: hep-lat/9701016. DOI: 10.1016/S0550-3213(97)00435-5 (cit. on pp. 6, 7, 60, 69, 71, 73).

[DH96] L. Del Debbio & S. Hands. “Monte Carlo Simulation of the Three Dimensional Thirring Model”. In: *Physics Letters B* 373 (1-3 Apr. 1996), pp. 171–177. arXiv: hep-lat/9512013. DOI: 10.1016/0370-2693(96)00137-2 (cit. on pp. 6, 59, 69, 71).

[Der93] S. E. Derkachov, N. A. Kivel, A. S. Stepanenko & A. N. Vasiliev. “On Calculation of $1/n$ Expansions of Critical Exponents in the Gross-Neveu Model with the Conformal Technique”. Feb. 9, 1993. arXiv: hep-th/9302034 (cit. on pp. 33, 52).

[DGM98] G. A. Diamandis, B. C. Georgalas & N. E. Mavromatos. “$N = 1$ Supersymmetric Spin-Charge Separation in effective gauge theories of planar magnetic superconductors”. In: *Modern Physics Letters A* 13 (05 Feb. 20, 1998), pp. 387–404. arXiv: cond-mat/9711257. DOI: 10.1142/S0217732398000449 (cit. on p. 78).

[DL94] S. J. Dong & K. F. Liu. “Stochastic Estimation with $\mathbb{Z}_2$ Noise”. In: *Physics Letters B* 328 (1-2 May 1994), pp. 130–136. arXiv: hep-lat/9308015. DOI: 10.1016/0370-2693(94)90440-5 (cit. on p. 27).

[DWY76a] S. D. Drell, M. Weinstein & S. Yankielowicz. “Strong-coupling field theory. I. Variational approach to φ^4 theory”. In: *Physical Review D* 14.2 (July 15, 1976), pp. 487–516. DOI: 10.1103/PhysRevD.14.487 (cit. on pp. iii, iv, 6, 24).

[DWY76b] S. D. Drell, M. Weinstein & S. Yankielowicz. “Strong-coupling field theories. II. Fermions and gauge fields on a lattice”. In: *Physical Review D* 14.6 (Sept. 15, 1976), pp. 1627–1647. DOI: 10.1103/PhysRevD.14.1627 (cit. on pp. 6, 24).

[Dua87] S. Duane, A. D. Kennedy, B. J. Pendleton & D. Roweth. “Hybrid Monte Carlo”. In: *Physics Letters B* 195.2 (Sept. 3, 1987), pp. 216–222. DOI: 10.1016/0370-2693(87)91197-X (cit. on p. 23).

[Dys49] F. J. Dyson. “The S Matrix in Quantum Electrodynamics”. In: *Physical Review* 75.11 (June 1, 1949), pp. 1736–1755. DOI: 10.1103/PhysRev.75.1736 (cit. on p. 133).

[EFM92] J. Engels, J. Fingberg & D. E. Miller. “Phenomenological renormalization and scaling behaviour of SU(2) lattice gauge theory”. In: *Nuclear Physics B* 387.2 (Nov. 30, 1992), pp. 501–519. DOI: 10.1016/0550-3213(92)90171-7 (cit. on p. 36).

[Fei16] L. Fei, S. Giombi, I. R. Klebanov & G. Tarnopolsky. “Yukawa Conformal Field Theories and Emergent Supersymmetry”. In: *Progress of Theoretical and Experimental Physics* 2016.12 (Dec. 1, 2016). arXiv: 1607.05316. DOI: 10.1093/ptep/ptw120 (cit. on pp. 51, 52, 109, 110).

[FGG73] S. Ferrara, A. F. Grillo & R. Gatto. “Tensor Representations of Conformal Algebra and Conformally Covariant Operator Product Expansion”. In: *Annals Phys.* 76 (1973), pp. 161–188. DOI: 10.1016/0003-4916(73)90446-6 (cit. on p. 5).

[FS89] A. M. Ferrenberg & R. H. Swendsen. “Optimized Monte Carlo data analysis”. In: *Physical Review Letters* 63.12 (Sept. 18, 1989), pp. 1195–1198. DOI: 10.1103/PhysRevLett.63.1195 (cit. on p. 37).

[Flo12] R. Flore, D. Körner, A. Wipf & C. Wozar. “Supersymmetric Nonlinear O(3) Sigma Model on the Lattice”. In: *Journal of High Energy Physics* 2012.11 (Nov. 2012). arXiv: 1207.6947. DOI: 10.1007/JHEP11(2012)159 (cit. on pp. 6, 25).

[FJP96] E. Focht, J. Jersák & J. Paul. “Interplay of universality classes in a three-dimensional Yukawa model”. In: *Physical Review D* 53.8 (Apr. 15, 1996), pp. 4616–4627. arXiv: hep-lat/9511005. DOI: 10.1103/PhysRevD.53.4616 (cit. on pp. 6, 34, 36).

[For10] P. de Forcrand. “Simulating QCD at finite density”. In: *PoS(LAT2009)010*. 27th International Symposium on Lattice Field Theory. Beijing, China: Proceedings of Science, May 4, 2010. arXiv: 1005.0539 (cit. on p. 29).

[FSW12] J. Förster, A. Saenz & U. Wolff. “Matrix Algorithm for Solving Schrödinger Equations with Position-Dependent Mass or Complex Optical Potentials”. In: *Physical Review E* 86.1 (July 11, 2012), p. 016701. arXiv: 1112.5294. DOI: 10.1103/PhysRevE.86.016701 (cit. on pp. 6, 25).

[FTV02] M. Franz, Z. Tesanovic & O. Vafek. “QED_3 theory of pairing pseudogap in cuprates: From d-wave superconductor to antiferromagnet via "algebraic" Fermi liquid”. In: *Physical Review B* 66.5 (Aug. 29, 2002). arXiv: cond-mat/0203333. DOI: 10.1103/PhysRevB.66.054535 (cit. on p. 5).

[Fra65] W. Fraser. “A Survey of Methods of Computing Minimax and Near-Minimax Polynomial Approximations for Functions of a Single Independent Variable”. In: *J. ACM* 12.3 (July 1965), pp. 295–314. DOI: 10.1145/321281.321282 (cit. on p. 23).

[Fuc81] F. Fucito, E. Marinari, G. Parisi & C. Rebbi. “A proposal for Monte Carlo simulations of fermionic systems”. In: *Nuclear Physics B* 180.3 (May 25, 1981), pp. 369–377. DOI: 10.1016/0550-3213(81)90055-9 (cit. on p. 23).

[Gal14] D. Galstian Pour. “Kritisches Verhalten des dreidimensionalen Gross-Neveu- und Thirring-Modells”. Diplomarbeit. Jena: Friedrich-Schiller-Universität, Apr. 2014. 54 pp. URL: http://www.tpi.uni-jena.de/qfphysics/homepage/wipf/abschlussarbeiten/galstian_diplom_14.pdf (visited on 03/16/2017) (cit. on pp. 8, 25).

[GL10] C. Gattringer & C. B. Lang. *Quantum Chromodynamics on the Lattice*. Vol. 788. Lecture Notes in Physics. Berlin, Heidelberg: Springer, 2010. ISBN: 978-3-642-01849-7. DOI: 10.1007/978-3-642-01850-3 (cit. on pp. 3, 9, 10, 23, 24, 26, 27, 38, 39, 134).

[GL16] C. Gattringer & K. Langfeld. “Approaches to the sign problem in lattice field theory”. In: *International Journal of Modern Physics A* 31.22 (Aug. 9, 2016), p. 1643007. arXiv: 1603.09517. DOI: 10.1142/S0217751X16430077 (cit. on p. 6).

[GGJ15] F. Gehring, H. Gies & L. Janssen. “Fixed-point structure of low-dimensional relativistic fermion field theories: Universality classes and emergent symmetry”. In: *Physical Review D* 92.8 (Oct. 29, 2015). arXiv: 1506.07570. DOI: 10.1103/PhysRevD.92.085046 (cit. on pp. 13, 15, 16, 57, 103).

[Gie12] H. Gies. “Introduction to the Functional RG and Applications to Gauge Theories”. In: 852 (2012), pp. 287–348. arXiv: hep-ph/0611146. DOI: 10.1007/978-3-642-27320-9_6 (cit. on p. 133).

[GJ10] H. Gies & L. Janssen. “UV fixed-point structure of the three-dimensional Thirring model”. In: *Physical Review D* 82.8 (Oct. 2010). arXiv: 1006.3747. DOI: 10.1103/PhysRevD.82.085018 (cit. on pp. 7, 11–13, 70, 74, 87).

[GW82] P. H. Ginsparg & K. G. Wilson. “A Remnant of Chiral Symmetry on the Lattice”. In: *Physical Review D* 25.10 (May 15, 1982), pp. 2649–2657. DOI: 10.1103/PhysRevD.25.2649 (cit. on p. 26).

[Gom91] M. Gomes, R. S. Mendes, R. F. Ribeiro & A. J. da Silva. “Gauge structure, anomalies, and mass generation in a three-dimensional Thirring model”. In: *Physical Review D* 43.10 (May 15, 1991), pp. 3516–3523. DOI: 10.1103/PhysRevD.43.3516 (cit. on pp. 7, 13, 69, 70).

[GKN13] D. Grabowska, D. B. Kaplan & A. N. Nicholson. “Sign Problems, Noise, and Chiral Symmetry Breaking in a QCD-like Theory”. In: *Physical Review D* 87.1 (Jan. 22, 2013). arXiv: 1208.5760. DOI: 10.1103/PhysRevD.87.014504 (cit. on pp. 31, 89).

[Gra90] J. A. Gracey. “Three-loop calculations in the $O(N)$ Gross-Neveu model”. In: *Nuclear Physics B* 341.2 (Sept. 10, 1990), pp. 403–418. DOI: 10.1016/0550-3213(90)90186-H (cit. on p. 52).

[Gra91] J. A. Gracey. “Computation of the three-loop β-function of the $O(N)$ Gross-Neveu model in minimal subtraction”. In: *Nuclear Physics B* 367.3 (Dec. 30, 1991), pp. 657–674. DOI: 10.1016/0550-3213(91)90012-M (cit. on p. 52).

[Gra92] J. A. Gracey. “Anomalous mass dimension at $O(1/N^2)$ in the $O(N)$ Gross-Neveu model”. In: *Physics Letters B* 297.3 (Dec. 31, 1992), pp. 293–297. DOI: 10.1016/0370-2693(92)91265-B (cit. on pp. 33, 52).

[Gra93] J. A. Gracey. “The conformal bootstrap equations for the four fermi interaction in arbitrary dimensions”. In: *Zeitschrift für Physik C Particles and Fields* 59.2 (June 1, 1993), pp. 243–249. DOI: 10.1007/BF01566688 (cit. on pp. 33, 52).

[Gra94a] J. A. Gracey. “Computation of $\beta(g_c)$ at $O(1/N^2)$ in the $O(N)$ Gross Neveu Model in Arbitrary Dimensions”. In: *International Journal of Modern Physics A* 09 (04 Feb. 10, 1994), pp. 567–589. arXiv: hep-th/9306106. DOI: 10.1142/S0217751X94000285 (cit. on pp. 33, 52).

[Gra94b] J. A. Gracey. “Computation of Critical Exponent η at $O(1/N^3)$ in the Four Fermi Model in Arbitrary Dimensions”. In: *International Journal of Modern Physics A* 09 (05 Feb. 20, 1994), pp. 727–744. arXiv: hep-th/9306107. DOI: 10.1142/S0217751X94000340 (cit. on pp. 51, 52, 109–111).

[Gra17] J. A. Gracey. "Critical exponent ω in the Gross-Neveu-Yukawa model at $O(1/N)$". July 17, 2017. arXiv: 1707.05275 (cit. on p. 35).

[GLS16] J. A. Gracey, T. Luthe & Y. Schroder. "Four Loop Renormalization of the Gross-Neveu Model". In: *Physical Review D* 94.12 (Dec. 30, 2016). arXiv: 1609.05071. DOI: 10.1103/PhysRevD.94.125028 (cit. on pp. 51, 52, 110).

[GN74] D. J. Gross & A. Neveu. "Dynamical symmetry breaking in asymptotically free field theories". In: *Physical Review D* 10.10 (Nov. 15, 1974), pp. 3235–3253. DOI: 10.1103/PhysRevD.10.3235 (cit. on pp. 4, 12, 13).

[Han95] S. Hands. "$O(1/N_f)$ corrections to the Thirring model in $2 < d < 4$". In: *Physical Review D* 51.10 (May 15, 1995), pp. 5816–5826. arXiv: hep-th/9411016. DOI: 10.1103/PhysRevD.51.5816 (cit. on pp. 60, 61).

[Han97] S. Hands. "Fixed Point Four-Fermi Theories". In: *Recent developments in nonperturbative quantum field theory*. APCTP-ICTP Joint International Conference. Seoul, Korea, June 24, 1997. URL: http://arxiv.org/abs/hep-lat/9706018 (visited on 05/23/2014) (cit. on p. 71).

[Han15] S. Hands. "Domain Wall Fermions for Planar Physics". In: *Journal of High Energy Physics* 2015.9 (Sept. 1, 2015), p. 47. arXiv: 1507.07717. DOI: 10.1007/JHEP09(2015)047 (cit. on pp. 27, 54, 72).

[Han16a] S. Hands. "From Domain Wall to Overlap in $2+1d$". In: *Physics Letters B* 754 (Mar. 10, 2016), pp. 264–269. arXiv: 1512.05885. DOI: 10.1016/j.physletb.2016.01.037 (cit. on pp. 14, 27, 54, 72).

[Han16b] S. Hands. "Towards Critical Physics in $2+1d$ with $U(2N)$-Invariant Fermions". In: *Journal of High Energy Physics* 2016.11 (Nov. 2016). arXiv: 1610.04394. DOI: 10.1007/JHEP11(2016)015 (cit. on pp. 6, 7, 14, 27, 54, 69, 72, 73, 99, 100).

[Han17] S. Hands. "Numerical study of the $2+1d$ Thirring model with $U(2N)$-invariant fermions". In: 35th International Symposium on Lattice Field Theory. Granada, Spain, Aug. 25, 2017. arXiv: 1708.07686 (cit. on pp. 6, 7, 73, 99, 100).

[HAS15] S. Hands, W. Armour & C. Strouthos. "Graphene as a Lattice Field Theory". In: *PoS(CPOD2014)016*. 9th International Workshop on Critical Point and Onset of Deconfinement. ZiF, University of Bielefeld, Germany: Proceedings of Science, Jan. 8, 2015. arXiv: 1501.01895 (cit. on p. 5).

[HKK91] S. Hands, A. Kocić & J. B. Kogut. "Compositeness, anomalous dimensions and renormalizability in four-Fermi theories". In: *Physics Letters B* 273.1 (Dec. 12, 1991), pp. 111–117. DOI: 10.1016/0370-2693(91)90562-5 (cit. on pp. 33, 34, 46, 77).

[HKK93] S. Hands, A. Kocić & J. B. Kogut. "Four - Fermi Theories in Fewer Than Four Dimensions". In: *Annals of Physics* 224.1 (May 1993), pp. 29–89. arXiv: hep-lat/9208022. DOI: 10.1006/aphy.1993.1039 (cit. on pp. 6, 33, 34, 53, 55).

[HL99] S. Hands & B. Lucini. "The phase diagram of the three dimensional Thirring model". In: *Physics Letters B* 461.3 (Aug. 26, 1999), pp. 263–269. arXiv: hep-lat/9906008. DOI: 10.1016/S0370-2693(99)00843-6 (cit. on pp. 6, 7, 69, 71, 72).

[HS08] S. Hands & C. Strouthos. "Quantum Critical Behaviour in a Graphene-like Model". In: *Physical Review B* 78.16 (Oct. 2008). arXiv: 0806.4877. DOI: 10.1103/PhysRevB.78.165423 (cit. on p. 5).

[HK10] M. Z. Hasan & C. L. Kane. “Colloquium: Topological Insulators”. In: *Reviews of Modern Physics* 82.4 (Nov. 8, 2010), pp. 3045–3067. arXiv: 1002.3895. DOI: 10.1103/RevModPhys.82.3045 (cit. on p. 5).

[Her06] I. F. Herbut. “Interactions and phase transitions on graphene’s honeycomb lattice”. In: *Physical Review Letters* 97.14 (Oct. 2, 2006). arXiv: cond-mat/0606195. DOI: 10.1103/PhysRevLett.97.146401 (cit. on pp. 5, 32).

[Her07] I. F. Herbut. *A Modern Approach to Critical Phenomena*. Cambridge: Cambridge University Press, Jan. 4, 2007. 223 pp. ISBN: 978-1-139-46012-5. DOI: 10.1017/CBO9780511755521 (cit. on p. 4).

[HJV09] I. F. Herbut, V. Juricic & O. Vafek. “Relativistic Mott criticality in graphene”. In: *Physical Review B* 80.7 (Aug. 27, 2009). arXiv: 0904.1019. DOI: 10.1103/PhysRevB.80.075432 (cit. on p. 5).

[HW16] S. Hesselmann & S. Wessel. “Thermal Ising Transitions in the Vicinity of Two-Dimensional Quantum Critical Points”. In: *Physical Review B* 93.15 (Apr. 27, 2016), p. 155157. arXiv: 1602.02096. DOI: 10.1103/PhysRevB.93.155157 (cit. on pp. 6, 51, 55, 109).

[HNW02] F. Höfling, C. Nowak & C. Wetterich. “Phase transition and critical behavior of the d =3 Gross-Neveu model”. In: *Physical Review B* 66.20 (Nov. 27, 2002), p. 205111. arXiv: cond-mat/0203588. DOI: 10.1103/PhysRevB.66.205111 (cit. on pp. 53, 57).

[HP94] D. K. Hong & S. H. Park. “Large-N analysis of (2+1)-dimensional Thirring model”. In: *Physical Review D* 49.10 (May 1994), pp. 5507–5511. arXiv: hep-th/9307186. DOI: 10.1103/PhysRevD.49.5507 (cit. on pp. 7, 16, 69, 70).

[HKS99] I. Horváth, A. D. Kennedy & S. Sint. “A new exact method for dynamical fermion computations with non-local actions”. In: *Nuclear Physics B - Proceedings Supplements* 73 (1–3 Mar. 1999), pp. 834–836. arXiv: hep-lat/9809092. DOI: 10.1016/S0920-5632(99)85217-7 (cit. on p. 23).

[Hub59] J. Hubbard. “Calculation of Partition Functions”. In: *Physical Review Letters* 3.2 (July 15, 1959), pp. 77–78. DOI: 10.1103/PhysRevLett.3.77 (cit. on p. 18).

[HLY94] S. J. Hyun, G. H. Lee & J. H. Yee. “Gaussian approximation of the (2+1) dimensional Thirring model in the functional Schrödinger picture”. In: *Physical Review D* 50.10 (Nov. 1994), pp. 6542–6546. arXiv: hep-th/9406070. DOI: 10.1103/PhysRevD.50.6542 (cit. on pp. 7, 70).

[Ili17] L. Iliesiu, F. Kos, D. Poland, S. S. Pufu & D. Simmons-Duffin. “Bootstrapping 3D Fermions with Global Symmetries”. May 9, 2017. arXiv: 1705.03484 (cit. on pp. 5, 51, 53, 109, 110).

[Ili16] L. Iliesiu, F. Kos, D. Poland, S. S. Pufu, D. Simmons-Duffin & R. Yacoby. “Bootstrapping 3D Fermions”. In: *Journal of High Energy Physics* 2016.3 (Mar. 2016). arXiv: 1508.00012. DOI: 10.1007/JHEP03(2016)120 (cit. on p. 53).

[Ito95] T. Itoh, Y. Kim, M. Sugiura & K. Yamawaki. “Thirring Model as a Gauge Theory”. In: *Progress of Theoretical Physics* 93.2 (Jan. 2, 1995), pp. 417–439. arXiv: hep-th/9411201. DOI: 10.1143/PTP.93.417 (cit. on pp. 7, 69–71).

[Jan12] L. Janssen. “Critical phenomena in (2+1)-dimensional relativistic fermion systems”. PhD Thesis. Jena: Friedrich-Schiller-Universität, June 2012. 117 pp. URL: http://www.db-thueringen.de/servlets/DocumentServlet?id=20856 (cit. on pp. 17, 20, 70, 74, 87, 103).

[JG12] L. Janssen & H. Gies. “Critical behavior of the (2+1)-dimensional Thirring model”. In: *Physical Review D* 86.10 (Nov. 6, 2012). arXiv: 1208.3327. DOI: 10.1103/PhysRevD.86.105007 (cit. on pp. 7, 61, 69, 70, 74, 78, 87).

[JH14] L. Janssen & I. F. Herbut. “Antiferromagnetic critical point on graphene’s honeycomb lattice: A functional renormalization group approach”. In: *Physical Review B* 89.20 (May 6, 2014), p. 205403. arXiv: 1402.6277. DOI: 10.1103/PhysRevB.89.205403 (cit. on pp. 32, 33, 51–53, 109–111).

[Jeg96] B. Jegerlehner. “Krylov space solvers for shifted linear systems”. Dec. 15, 1996. arXiv: hep-lat/9612014 (cit. on p. 23).

[KKR91] K. Kajantie, L. Kärkkäinen & K. Rummukainen. “Tension of the interface between two ordered phases in lattice $SU(3)$ gauge theory”. In: *Nuclear Physics B* 357.2 (July 1, 1991), pp. 693–712. DOI: 10.1016/0550-3213(91)90486-H (cit. on p. 37).

[Kär94] L. Kärkkäinen, R. Lacaze, P. Lacock & B. Petersson. “Critical Behaviour of the 3d Gross-Neveu and Higgs-Yukawa Models”. In: *Nuclear Physics B* 415.3 (Mar. 1994), pp. 781–796. arXiv: hep-lat/9310020. DOI: 10.1016/0550-3213(94)90309-3 (cit. on pp. 6, 33, 34, 36, 37, 51, 54, 55, 98, 110).

[Kar81] L. H. Karsten. “Lattice fermions in euclidean space-time”. In: *Physics Letters B* 104.4 (Sept. 3, 1981), pp. 315–319. DOI: 10.1016/0370-2693(81)90133-7 (cit. on p. 24).

[KS78] L. H. Karsten & J. Smit. “Axial Symmetry in Lattice Theories”. In: *Nuclear Physics B* 144.2 (Nov. 13, 1978), pp. 536–546. DOI: 10.1016/0550-3213(78)90385-1 (cit. on p. 25).

[KS79] L. H. Karsten & J. Smit. “The vacuum polarization with SLAC lattice fermions”. In: *Physics Letters B* 85.1 (July 30, 1979), pp. 100–102. DOI: 10.1016/0370-2693(79)90786-X (cit. on pp. 6, 25).

[KS81] L. H. Karsten & J. Smit. “Lattice fermions: Species doubling, chiral invariance and the triangle anomaly”. In: *Nuclear Physics B* 183 (1–2 May 18, 1981), pp. 103–140. DOI: 10.1016/0550-3213(81)90549-6 (cit. on pp. 24, 25).

[Käs08] T. Kästner, G. Bergner, S. Uhlmann, A. Wipf & C. Wozar. “Two-Dimensional Wess-Zumino Models at Intermediate Couplings”. In: *Physical Review D* 78.9 (Nov. 5, 2008), p. 095001. arXiv: 0807.1905. DOI: 10.1103/PhysRevD.78.095001 (cit. on pp. 6, 25).

[Ken06] A. D. Kennedy. “Algorithms for Dynamical Fermions”. In: *Perspectives in Lattice QCD*. World Scientific, July 31, 2006. ISBN: 978-981-4477-20-8. arXiv: hep-lat/0607038. DOI: 10.1142/9789812790927_0002 (cit. on p. 23).

[KK96] S. Kim & Y. Kim. “Lattice Gauge Theory of Three Dimensional Thirring Model”. In: *Gravitation and Cosmology, Proceedings of the ICGC-95 Conference*. Pacific Conference on Gravitation and Cosmology. Seoul, Korea: World Scientific, May 16, 1996, pp. 261–269. arXiv: hep-lat/9605021. DOI: 10.1007/978-94-011-5812-1 (cit. on pp. 6, 7, 69, 71).

[KKK95] T. S. Kim, W.-H. Kye & J. K. Kim. “The Dynamical Behaviors in (2+1)-Dimensional Gross-Neveu Model with a Thirring Interaction”. In: *Physical Review D* 52.10 (Nov. 15, 1995), pp. 6109–6115. arXiv: hep-th/9509068. DOI: 10.1103/PhysRevD.52.6109 (cit. on p. 78).

[KLW05] A. Kirchberg, J. D. Länge & A. Wipf. “From the Dirac Operator to Wess-Zumino Models on Spatial Lattices”. In: *Annals of Physics* 316.2 (Apr. 2005), pp. 357–392. arXiv: hep-th/0407207. DOI: 10.1016/j.aop.2004.09.002 (cit. on pp. 6, 25).

[Kno16] B. Knorr. “Ising and Gross-Neveu model in next-to-leading order”. In: *Physical Review B* 94.24 (Dec. 1, 2016), p. 245102. arXiv: 1609.03824. DOI: 10.1103/PhysRevB.94.245102 (cit. on pp. 51, 53, 109, 110).

[KS75] J. Kogut & L. Susskind. “Hamiltonian Formulation of Wilson’s Lattice Gauge Theories”. In: *Physical Review D* 11.2 (Jan. 15, 1975), pp. 395–408. DOI: 10.1103/PhysRevD.11.395 (cit. on pp. 6, 26).

[Kon95] K.-I. Kondo. “Thirring model as a gauge theory”. In: *Nuclear Physics B* 450 (1–2 Sept. 11, 1995), pp. 251–266. arXiv: hep-th/9611198. DOI: 10.1016/0550-3213(95)00316-K (cit. on pp. 7, 69, 70, 77).

[Kos16] F. Kos, D. Poland, D. Simmons-Duffin & A. Vichi. “Precision Islands in the Ising and $O(N)$ Models”. In: *Journal of High Energy Physics* 2016.8 (Aug. 2016). arXiv: 1603.04436. DOI: 10.1007/JHEP08(2016)036 (cit. on pp. 5, 53).

[LB09] D. Landau & K. Binder. *A Guide to Monte Carlo Simulations in Statistical Physics*. 3rd ed. New York, NY, USA: Cambridge University Press, 2009. ISBN: 978-0-521-84238-9. DOI: 10.1017/CBO9781139696463 (cit. on p. 34).

[Li13] A. Li. “Fermion bag solutions to some sign problems in four-fermion field theories”. In: *Journal of Physics: Conference Series* 432 (Apr. 30, 2013), p. 012024. arXiv: 1211.0619. DOI: 10.1088/1742-6596/432/1/012024 (cit. on p. 30).

[LJY15] Z.-X. Li, Y.-F. Jiang & H. Yao. “Fermion-Sign-Free Majorana-Quantum-Monte-Carlo Studies of Quantum Critical Phenomena of Dirac Fermions in Two Dimensions”. In: *New Journal of Physics* 17.8 (Aug. 6, 2015), p. 085003. arXiv: 1411.7383. DOI: 10.1088/1367-2630/17/8/085003 (cit. on pp. 6, 51, 55, 109).

[Lie] T. Lienart. *Matrix Inversion Lemmas*. URL: https://www.stats.ox.ac.uk/~lienart/blog_linalg_invlemmas.html (visited on 08/29/2017) (cit. on p. 94).

[LR91] C. Luperini & P. Rossi. “Three-loop β function(s) and effective potential in the Gross-Neveu model”. In: *Annals of Physics* 212.2 (Dec. 1, 1991), pp. 371–401. DOI: 10.1016/0003-4916(91)90120-W (cit. on p. 52).

[Mac77] G. Mack. “Duality in Quantum Field Theory”. In: *Nuclear Physics B* 118.5 (Feb. 7, 1977), pp. 445–457. DOI: 10.1016/0550-3213(77)90238-3 (cit. on p. 5).

[MS00] N. E. Mavromatos & S. Sarkar. “Nodal Liquids in Extended T-J Models and Dynamical Supersymmetry”. In: *Physical Review B* 62.5 (Aug. 1, 2000), pp. 3438–3452. arXiv: cond-mat/9912323. DOI: 10.1103/PhysRevB.62.3438 (cit. on p. 78).

[Mih17] L. N. Mihaila, N. Zerf, B. Ihrig, I. F. Herbut & M. M. Scherer. “Gross-Neveu-Yukawa Model at Three Loops and Ising Critical Behavior of Dirac Systems”. Mar. 26, 2017. arXiv: 1703.08801 (cit. on pp. 51–53, 109, 110).

[Mir94] V. A. Miransky. *Dynamical Symmetry Breaking in Quantum Field Theories*. World Scientific, Feb. 1994. ISBN: 978-981-02-1558-3. DOI: 10.1142/9789814343336 (cit. on p. 112).

[MM97] I. Montvay & G. Münster. *Quantum Fields on a Lattice*. Cambridge: Cambridge University Press, Mar. 6, 1997. 512 pp. ISBN: 978-0-521-59917-7. DOI: 10.1017/CBO9780511470783 (cit. on p. 9).

[MZ03] M. Moshe & J. Zinn-Justin. “Quantum field theory in the large N limit: a review”. In: *Physics Reports* 385 (3–6 Oct. 2003), pp. 69–228. arXiv: hep-th/0306133. DOI: 10.1016/S0370-1573(03)00263-1 (cit. on pp. 5, 52).

[NJ61a] Y. Nambu & G. Jona-Lasinio. “Dynamical Model of Elementary Particles Based on an Analogy with Superconductivity. I”. In: *Physical Review* 122.1 (Apr. 1, 1961), pp. 345–358. DOI: 10.1103/PhysRev.122.345 (cit. on pp. 4, 12).

[NJ61b] Y. Nambu & G. Jona-Lasinio. “Dynamical Model of Elementary Particles Based on an Analogy with Superconductivity. II”. In: *Physical Review* 124.1 (Oct. 1, 1961), pp. 246–254. DOI: 10.1103/PhysRev.124.246 (cit. on p. 4).

[NR06] M. Niedermaier & M. Reuter. “The Asymptotic Safety Scenario in Quantum Gravity”. In: *Living Reviews in Relativity* 9.1 (Dec. 1, 2006), p. 5. DOI: 10.12942/lrr-2006-5 (cit. on p. 4).

[NN81a] H. B. Nielsen & M. Ninomiya. “Absence of neutrinos on a lattice: (I). Proof by homotopy theory”. In: *Nuclear Physics B* 185.1 (July 13, 1981), pp. 20–40. DOI: 10.1016/0550-3213(81)90361-8 (cit. on pp. 5, 24).

[NN81b] H. B. Nielsen & M. Ninomiya. “A no-go theorem for regularizing chiral fermions”. In: *Physics Letters B* 105 (2–3 Oct. 1, 1981), pp. 219–223. DOI: 10.1016/0370-2693(81)91026-1 (cit. on pp. 5, 24).

[NN81c] H. B. Nielsen & M. Ninomiya. “Absence of neutrinos on a lattice: (II). Intuitive topological proof”. In: *Nuclear Physics B* 193.1 (Dec. 21, 1981), pp. 173–194. DOI: 10.1016/0550-3213(81)90524-1 (cit. on pp. 5, 24).

[Nov04] K. S. Novoselov, A. K. Geim, S. V. Morozov, D. Jiang, Y. Zhang, S. V. Dubonos, I. V. Grigorieva & A. A. Firsov. “Electric Field Effect in Atomically Thin Carbon Films”. In: *Science* 306.5696 (Oct. 22, 2004), pp. 666–669. arXiv: cond-mat/0410550. DOI: 10.1126/science.1102896 (cit. on p. 5).

[Par16] Particle Data Group. “Review of Particle Physics”. In: *Chinese Physics C* 40.10 (2016), p. 100001. DOI: 10.1088/1674-1137/40/10/100001 (cit. on p. 3).

[Pel88] A. Pelissetto. “Lattice non-local chiral fermions”. In: *Annals of Physics* 182.1 (Feb. 15, 1988), pp. 177–187. DOI: 10.1016/0003-4916(88)90299-0 (cit. on p. 25).

[Per09] R. Percacci. “Asymptotic Safety”. In: *Approaches to Quantum Gravity: Toward a New Understanding of Space, Time and Matter*. Cambridge: Cambridge University Press, Apr. 2009. ISBN: 978-0-511-57554-9. arXiv: 0709.3851. DOI: 10.1017/CBO9780511575549.009 (cit. on p. 4).

[PS95] M. E. Peskin & D. V. Schroeder. *An Introduction To Quantum Field Theory*. Reading, Massachusetts: Addison Wesley, Oct. 2, 1995. 864 pp. ISBN: 978-0-201-50397-5 (cit. on p. 134).

[Pis91] R. D. Pisarski. "Fermion Mass in Three Dimensions and the Renormalization Group". In: *Physical Review D* 44.6 (Sept. 15, 1991), pp. 1866–1872. DOI: 10.1103/PhysRevD.44.1866 (cit. on p. 14).

[PB06] M. Plischke & B. Bergersen. *Equilibrium Statistical Physics*. 3rd ed. Singapore: World Scientific, Apr. 2006. ISBN: 978-981-256-048-3. DOI: 10.1142/5660 (cit. on p. 34).

[Pol74] A. M. Polyakov. "Nonhamiltonian Approach to Conformal Quantum Field Theory". In: *Journal of Experimental and Theoretical Physics* 39 (1974), pp. 9–18. URL: http://www.jetp.ac.ru/cgi-bin/e/index/e/39/1/p10?a=list (visited on 09/08/2017) (cit. on p. 5).

[QZ11] X.-L. Qi & S.-C. Zhang. "Topological Insulators and Superconductors". In: *Reviews of Modern Physics* 83.4 (Oct. 14, 2011), pp. 1057–1110. arXiv: 1008.2026. DOI: 10.1103/RevModPhys.83.1057 (cit. on p. 5).

[Rab81] J. M. Rabin. "Perturbation Theory for Undoubled Lattice Fermions". In: *Physical Review D* 24.12 (Dec. 15, 1981), pp. 3218–3236. DOI: 10.1103/PhysRevD.24.3218 (cit. on p. 25).

[RS12] M. Reuter & F. Saueressig. "Quantum Einstein Gravity". In: *New Journal of Physics* 14.5 (May 21, 2012), p. 055022. arXiv: 1202.2274. DOI: 10.1088/1367-2630/14/5/055022 (cit. on p. 4).

[RVW01] L. Rosa, P. Vitale & C. Wetterich. "Critical exponents of the Gross-Neveu model from the effective average action". In: *Physical Review Letters* 86.6 (Feb. 5, 2001), pp. 958–961. arXiv: hep-th/0007093. DOI: 10.1103/PhysRevLett.86.958 (cit. on p. 53).

[RYK93] B. Rosenstein, Yu, Hoi-Lai & A. Kovner. "Critical Exponents of New Universality Classes". In: *Physics Letters B* 314.3 (Sept. 23, 1993), pp. 381–386. DOI: 10.1016/0370-2693(93)91253-J (cit. on p. 52).

[RWP89] B. Rosenstein, B. J. Warr & S. H. Park. "Four-fermion theory is renormalizable in 2+1 dimensions". In: *Physical Review Letters* 62.13 (Mar. 27, 1989), pp. 1433–1436. DOI: 10.1103/PhysRevLett.62.1433 (cit. on p. 5).

[RS94] G. L. Rossini & F. A. Schaposnik. "Parity Violation in the Three Dimensional Thirring Model". In: *Physics Letters B* 338.4 (Nov. 1994), pp. 465–470. arXiv: hep-th/9406033. DOI: 10.1016/0370-2693(94)90801-X (cit. on p. 70).

[Rot05] H. J. Rothe. *Lattice Gauge Theories: An Introduction*. 3rd edition. Vol. 74. Lecture Notes in Physics. Singapore: World Scientific, 2005. 588 pp. ISBN: 978-981-256-168-8. DOI: 10.1142/8229 (cit. on pp. 9, 60).

[Saa03] Y. Saad. *Iterative methods for sparse linear systems*. 2nd ed. SIAM, 2003. ISBN: 978-0-89871-534-7. DOI: 10.1137/1.9780898718003 (cit. on p. 133).

[SSV11] S. Schaefer, R. Sommer & F. Virotta. "Critical slowing down and error analysis in lattice QCD simulations". In: *Nuclear Physics B* 845.1 (Apr. 2011), pp. 93–119. arXiv: 1009.5228. DOI: 10.1016/j.nuclphysb.2010.11.020 (cit. on p. 39).

[Sch09] S. Schäfer. *Simulations with the Hybrid Monte Carlo algorithm: implementation and data analysis*. Tutorial given at Les Houches summer school. Aug. 2009. URL: http://nic.desy.de/workshops__schools/les_houches_2009/tutorial/index_eng.html (visited on 03/02/2017) (cit. on p. 23).

[SBG13] D. D. Scherer, J. Braun & H. Gies. "Many-flavor Phase Diagram of the (2+1)d Gross-Neveu Model at Finite Temperature". In: *Journal of Physics A: Mathematical and Theoretical* 46.28 (July 19, 2013), p. 285002. arXiv: 1212.4624. DOI: 10.1088/1751-8113/46/28/285002 (cit. on p. 112).

[SWW15] D. Schmidt, B. Wellegehausen & A. Wipf. "Critical flavour number of the Thirring model in three dimensions". In: *PoS(LATTICE 2015)050*. The 33rd International Symposium on Lattice Field Theory. Kobe, Japan: Proceedings of Science, Nov. 2, 2015. arXiv: 1511.00522 (cit. on p. 8).

[SWW16] D. Schmidt, B. Wellegehausen & A. Wipf. "Four-Fermion Theories with Exact Chiral Symmetry in Three Dimensions". In: *PoS(LATTICE2016)247*. The 34th International Symposium on Lattice Field Theory. Southampton, England: Proceedings of Science, Nov. 1, 2016. arXiv: 1611.00275 (cit. on p. 8).

[Sch51] J. Schwinger. "On the Green's Functions of Quantized Fields. I". In: *Proceedings of the National Academy of Sciences* 37.7 (Jan. 7, 1951), pp. 452–455. pmid: 16578383. DOI: 10.1073/pnas.37.7.452 (cit. on p. 133).

[Sem84] G. W. Semenoff. "Condensed-Matter Simulation of a Three-Dimensional Anomaly". In: *Physical Review Letters* 53.26 (Dec. 24, 1984), pp. 2449–2452. DOI: 10.1103/PhysRevLett.53.2449 (cit. on p. 5).

[Smi02] J. Smit. *Introduction to Quantum Fields on a Lattice*. Vol. 15. Cambridge Lecture Notes In Physics. Cambridge: Cambridge University Press, Sept. 19, 2002. 287 pp. ISBN: 978-0-521-89051-9. DOI: 10.1017/CBO9780511583971 (cit. on p. 9).

[SO10] A. Stathopoulos & K. Orginos. "Computing and deflating eigenvalues while solving multiple right hand side linear systems in Quantum Chromodynamics". In: *SIAM Journal on Scientific Computing* 32.1 (Jan. 2010), pp. 439–462. arXiv: 0707.0131. DOI: 10.1137/080725532 (cit. on p. 28).

[Sto] C. Stover. *Generalized Gell-Mann Matrix*. From MathWorld–A Wolfram Web Resource. URL: http://mathworld.wolfram.com/GeneralizedGell-MannMatrix.html (visited on 01/22/2016) (cit. on p. 87).

[Sug97] M. Sugiura. "Fermion Mass Generation in the D-Dimensional Thirring Model as a Gauge Theory". In: *Progress of Theoretical Physics* 97.2 (Jan. 2, 1997), pp. 311–326. arXiv: hep-th/9611198. DOI: 10.1143/PTP.97.311 (cit. on pp. 7, 70).

[Thi58] W. E. Thirring. "A soluble relativistic field theory". In: *Annals of Physics* 3.1 (Jan. 1958), pp. 91–112. DOI: 10.1016/0003-4916(58)90015-0 (cit. on pp. 4, 11).

[TW05] M. Troyer & U.-J. Wiese. "Computational complexity and fundamental limitations to fermionic quantum Monte Carlo simulations". In: *Physical Review Letters* 94.17 (May 4, 2005). arXiv: cond-mat/0408370. DOI: 10.1103/PhysRevLett.94.170201 (cit. on pp. 6, 28, 29).

[Upp74] D. Upper. "The Unsuccessful Self-Treatment of a Case of "Writer's Block"". In: *Journal of Applied Behavior Analysis* 7.3 (1974), p. 497. DOI: 10.1901/jaba.1974.7-497a (cit. on p. 139).

[Urb06] C. Urbach, K. Jansen, A. Shindler & U. Wenger. “HMC Algorithm with Multiple Time Scale Integration and Mass Preconditioning”. In: *Computer Physics Communications* 174.2 (Jan. 2006), pp. 87–98. arXiv: hep-lat/0506011. DOI: 10.1016/j.cpc.2005.08.006 (cit. on p. 23).

[VZ15] G. P. Vacca & L. Zambelli. “Multimeson Yukawa Interactions at Criticality”. In: *Physical Review D* 91.12 (June 1, 2015), p. 125003. DOI: 10.1103/PhysRevD.91.125003 (cit. on pp. 53, 109).

[VL61] V. G. Vaks & A. I. Larkin. “On the application of the methods of superconductivity theory to the problem of the masses of elementary particles”. In: *Soviet Physics Journal of Experimental and Theoretical Physics* 13.1 (Jan. 1961), pp. 192–193. URL: http://www.jetp.ac.ru/cgi-bin/dn/e_013_01_0192.pdf (visited on 01/13/2017) (cit. on p. 12).

[Vas93] A. N. Vasil’ev, S. E. Derkachev, N. A. Kivel’ & A. S. Stepanenko. “The $1/n$ expansion in the Gross-Neveu model: Conformal bootstrap calculation of the index η in order $1/n^3$”. In: *Theoretical and Mathematical Physics* 94.2 (Feb. 1, 1993), pp. 127–136. DOI: 10.1007/BF01019324 (cit. on pp. 33, 52).

[VR06] M. K. Volkov & A. E. Radzhabov. “The Nambu–Jona-Lasinio Model and Its Development”. In: *Physics-Uspekhi* 49.6 (2006), p. 551. arXiv: hep-ph/0508263. DOI: 10.1070/PU2006v049n06ABEH005905 (cit. on p. 4).

[WCT14] L. Wang, P. Corboz & M. Troyer. “Fermionic Quantum Critical Point of Spinless Fermions on a Honeycomb Lattice”. In: *New Journal of Physics* 16.10 (Oct. 8, 2014), p. 103008. arXiv: 1407.0029. DOI: 10.1088/1367-2630/16/10/103008 (cit. on pp. 6, 51, 54, 109).

[Wan15] L. Wang, M. Iazzi, P. Corboz & M. Troyer. “Efficient Continuous-Time Quantum Monte Carlo Method for the Ground State of Correlated Fermions”. In: *Physical Review B* 91.23 (June 30, 2015). arXiv: 1501.00986. DOI: 10.1103/PhysRevB.91.235151 (cit. on p. 54).

[WBB14] T. O. Wehling, A. M. Black-Schaffer & A. V. Balatsky. “Dirac Materials”. In: *Advances in Physics* 63.1 (Jan. 2, 2014), pp. 1–76. arXiv: 1405.5774. DOI: 10.1080/00018732.2014.927109 (cit. on p. 5).

[Wei] E. W. Weisstein. *Confluent Hypergeometric Function of the Second Kind*. From MathWorld–A Wolfram Web Resource. URL: http://mathworld.wolfram.com/ConfluentHypergeometricFunctionoftheSecondKind.html (visited on 07/19/2017) (cit. on pp. 92, 115).

[WSW17] B. H. Wellegehausen, D. Schmidt & A. Wipf. “Critical Flavor Number of the Thirring Model in Three Dimensions”. In: *Physical Review D* 96.9 (Nov. 9, 2017), p. 094504. arXiv: 1708.01160. DOI: 10.1103/PhysRevD.96.094504 (cit. on pp. 8, 21, 69, 90, 99, 100).

[Wel12] B. H. Wellegehausen. “Phase diagrams of exceptional and supersymmetric lattice gauge theories”. PhD Thesis. Jena: Friedrich-Schiller-Universität, July 2012. URL: http://www.tpi.uni-jena.de/qfphysics/homepage/wipf/abschlussarbeiten/wellegehausen_diss.pdf (visited on 03/17/2017) (cit. on pp. 21, 23).

[Wip13] A. Wipf. *Statistical Approach to Quantum Field Theory*. Vol. 100. Lecture Notes in Physics. Berlin, Heidelberg: Springer Berlin Heidelberg, 2013. ISBN: 978-3-642-33104-6. DOI: 10.1007/978-3-642-33105-3 (cit. on pp. 23, 24, 26, 27, 33, 104).

[Wip16] A. Wipf. "Introduction to Supersymmery". Lecture Notes. Jena, 2016. URL: http://www.tpi.uni-jena.de/qfphysics/homepage/wipf/lectures/susy/susyhead.pdf (visited on 06/14/2017) (cit. on p. 104).

[WS86] B. de Wit & J. Smith. *Field Theory in Particle Physics, Volume 1*. 1st edition. Amsterdam; New York; New York, N.Y., U.S.A.: North Holland, Aug. 15, 1986. 502 pp. ISBN: 978-0-444-86999-9 (cit. on pp. 10, 17).

[Wol04] U. Wolff. "Monte Carlo errors with less errors". In: *Computer Physics Communications* 156.2 (Jan. 1, 2004), pp. 143–153. DOI: 10.1016/S0010-4655(03)00467-3 (cit. on p. 39).

[Wol07] U. Wolff. "Monte Carlo errors with less errors". In: *Computer Physics Communications* 176.5 (Mar. 2007), p. 383. arXiv: hep-lat/0306017. DOI: 10.1016/j.cpc.2006.12.001 (cit. on p. 39).

[WW12] C. Wozar & A. Wipf. "Supersymmetry Breaking in Low Dimensional Models". In: *Annals of Physics* 327.3 (Mar. 2012), pp. 774–807. arXiv: 1107.3324. DOI: 10.1016/j.aop.2011.11.015 (cit. on p. 6).

Abbreviations

γ_{45}-model (G45)

A four-fermion theory, where the reducible interaction includes the matrix $\gamma_{45} = \mathrm{i}\gamma_4\gamma_5$. In the irreducible formulation, it acquires the form of the *reducible* Gross-Neveu model (GN), so that we sometimes refer to it as the *irreducible* GN. The Lagrangian is defined in (2.8) and the bosonised version is given in (2.34).

chiral symmetry breaking (χSB)

Chiral symmetry is related to the handedness of fermions, see section 2.1.1 for a detailed introduction for three-dimensional four-fermion theories. It can break spontaneously at strong couplings which leads to a dynamically generated fermion mass (see (2.16)).

conjugate gradient (CG)

Standard iterative method to solve a system of linear equations. A good introduction can be found in the book of Saad [Saa03]. It is commonly used in the update of an HMC algorithm as well as in evaluations of observables. See section 2.3.1 and section 2.3.3.

Dyson-Schwinger-Equation (DSE)

Relations between Green's functions in a QFT, found by Dyson [Dys49] and Schwinger [Sch51], that can be used to perform non-perturbative studies of a theory.

Fierz matrix formulation (FM)

A four-fermion theory that was obtained by application of the Fierz identity (2.26a) to Th. It contains a GN term and a Hermitian matrix in flavour space after HS. The Lagrangian is given in (2.28a) and the bosonised version can be found in (2.37a).

Fierz vector-matrix formulation (FVM)

A four-fermion theory that was obtained by application of the Fierz identity (2.26b) to Th. It contains a GN term and a vector of Hermitian matrices in flavour space after HS. The Lagrangian was defined in (2.28b) and the bosonised version given in (2.37b).

Functional Renormalisation Group (FRG)

A non-perturbative approach to QFTs based on renormalisation group equations that allow integration over scales to interpolate between microscopic descriptions and macroscopic phenomena of physical systems. See [BTW02; Gie12] for introductory reviews.

Gross-Neveu model (GN)

The simplest four-fermion theory with a scalar-scalar interaction, well-known to show χSB for any number of flavours. It has a $\mathbb{Z}_2$-symmetry that breaks spontaneously. The acronym usually refers to the reducible verion, for which the Lagrangian is defined in (2.11). The bosonised version after HS is given in (2.32).

Gross-Neveu-Yukawa model (GNY)

An extension of GN, where the scalar field introduced by HS is a dynamical field with a fourth-power potential. It shares the chiral Ising universality class with GN and has the same critical exponents. See also section 3.3.

Hubbard-Stratonovich transformation (HS)

A method based on Gaussian integrals to transform four-fermion Lagrangians into Lagrangians bilinear in the fermion fields. For this purpose, additional auxiliary fields without kinetic term are introduced. See section 2.2.2 for details.

Hybrid Monte Carlo (HMC)

An algorithm that is commonly used to generate a new configuration from an old one in a Markov Chain Monte Carlo simulation. It combines an evolution of a fictious molecular dynamics system with a Metropolis update. See section 2.3.1 for details.

Nambu–Jona-Lasinio model (NJL)

A four-fermion theory with two auxiliary scalar fields. One of the four symmetry generators of Th is broken, but the remaining chiral symmetry is still continuous. Hence, some other authors call it $U(1)$ Gross-Neveu model. The Lagrangian is defined in (2.9) and the bosonised version is given in (2.35).

Quantum Chromodynamics (QCD)

The theory of the strong interaction describing the dynamics of quarks and gluons. It is strongly interacting at low energies, making studies with non-perturbative methods necessary for this regime. Lattice QCD is the most prominent example of a lattice gauge theory, see for example [GL10].

Quantum Field Theory (QFT)

A theory based on the quantisation of fields, usually used to describe fundamental interactions in particle physics. A good introduction can be found in the book of Peskin & Schroeder [PS95].

Quantum Monte Carlo (QMC)

Various approaches from condensed matter physics using Monte Carlo methods to investigate non-relativistic systems in a Hamiltonian formulation.

rational Hybrid Monte Carlo (rHMC)

A modification of the HMC algorithm that uses a rational approximation to calculate a rational power of the Dirac operator. See section 2.3.1 for details.

Thirring model (Th)

A four-fermion theory with a current-current interaction and a large, continuous chiral symmetry. It is usually believed to only show χSB for small flavour numbers $N_\mathrm{f} \leq N_\mathrm{f}^\mathrm{cr}$, although this is not in accordance with recent lattice simulations. The reducible version is defined in (2.7) and the Lagrangian with an auxiliary vector field is given in (2.33). The irreducible Lagrangian given in (2.20) has the same form as the reducible model. Main results for the Thirring model can be found in chapter 4,

but also chapter 5 and 6 address the question of the critical flavour number of this theory.

three-dimensional Quantum Electrodynamics (QED_3)

The QFT of electromagnetic interactions in three spacetime dimensions. It is sometimes discussed to share properties regarding chiral symmetry with Th.

List of Figures

List of Tables

Danksagung

Mein Dank gilt zunächst Prof. Andreas Wipf, der diese Arbeit durch die Finanzierung über das DFG-Graduiertenkolleg 1523/2 „Quanten- und Gravitationsfelder“ ermöglicht hat und mir Gelegenheit zu interessanten Konferenz- und Workshop-Besuchen gegeben hat. Außerdem danke ich Björn Wellegehausen, der mir während unserer engen Zusammenarbeit (fast) alles über Gittersimulationen vermittelt hat, was für das Entstehen dieser Arbeit notwendig war. Vielen Dank für die zahllosen Diskussionen!

Des weiteren möchte ich allen Mitgliedern der Quantenfeldtheorie-Arbeitsgruppen für viele interessante Gespräche auf Workshops, Konferenzen und in der Mittagspause danken. Dies betrifft insbesondere auch meine Bürokollegen und Gitter-Doktoranden Daniel August und Marc Steinhauser sowie Prof. Holger Gies, der immer großes Interesse an meiner Arbeit hatte und meine Untersuchungen mit Fierz-Identitäten angeregt hat. Für den guten überfachlichen Austausch möchte ich auch den anderen Doktoranden des Graduiertenkollegs aus der Gravitationstheorie und der Mathematik danken.

Ohne zahlreiche Computer-Resourcen wäre diese Arbeit nicht machbar gewesen. Daher möchte ich auch dem IT-Team des TPI und dem Uni-Rechenzentrum danken, die sich immer schnell um Probleme mit Clustern und Compute-Servern gekümmert haben. Ebenso danke ich Prof. Brügmann mit seiner Gravitations-Gruppe, deren Cluster `quadler` ich für eine Simulation des Gross-Neveu-Modells mit $N_\mathrm{f} = 4$ nutzen durfte, ebenso wie Björn Wellegehausen, der für mich alle $N_\mathrm{f} = 8$-Simulationen auf dem LOEWE-Cluster in Frankfurt durchgeführt hat.

Zahlreiche inhaltliche und sprachliche Fehler wurden von den fleißigen Korrektur-Lesern gefunden. Vielen Dank dafür an Benjamin Knorr, Björn Wellegehausen, Marc Steinhauser, Michael Fennen und Pascal Törek, dem ich ebenfalls für die Diskussionen über kritische Exponenten und deren Berechnung danke.

Auch meiner Familie und meinen Studienfreunden gebührt großer Dank für psychische Unterstützung und Ablenkung. In ganz besonderem Maße möchte ich daher auch meiner Freundin Maike danken, die bedauerlich viel von dieser Arbeit lesen musste.

Zum Schluss möchte ich noch auf die äußerst hilfreiche Arbeit von Upper [Upp74] hinweisen, die eine große Hilfe beim Schreiben dieser Doktorarbeit war.

Ehrenwörtliche Erklärung

Ich erkläre hiermit ehrenwörtlich, dass ich die vorliegende Arbeit selbstständig, ohne unzulässige Hilfe Dritter und ohne Benutzung anderer als der angegebenen Hilfsmittel und Literatur angefertigt habe. Die aus anderen Quellen direkt oder indirekt übernommenen Daten und Konzepte sind unter Angabe der Quelle gekennzeichnet.

Bei der Auswahl und Auswerung folgenden Materials haben mir die nachstehend aufgeführten Personen in der jeweils beschriebenen Weise unentgeltlich geholfen:

1. Andreas Wipf, Betreuung der Arbeit über die gesamte Dauer der Promotion als betreuender Hochschullehrer.

2. Björn Wellegehausen, enge Kooperation über die gesamte Dauer der Promotion, insbesondere bei allen Arbeiten über das Thirring-Modell (Kapitel 4, Kapitel 5 und Kapitel 6).

Weitere Personen waren an der inhaltlich-materiellen Erstellung der vorliegenden Arbeit nicht beteiligt. Insbesondere habe ich hierfür nicht die entgeltliche Hilfe von Vermittlungs- bzw. Beratungsdiensten (Promotionsberater oder andere Personen) in Anspruch genommen. Niemand hat von mir unmittelbar oder mittelbar geldwerte Leistungen für Arbeiten erhalten, die im Zusammenhang mit dem Inhalt der vorgelegten Dissertation stehen.

Die Arbeit wurde bisher weder im In- noch im Ausland in gleicher oder ähnlicher Form einer anderen Prüfungsbehörde vorgelegt.

Die geltende Promotionsordnung der Physikalisch-Astronomischen Fakultät ist mir bekannt.

Ich versichere ehrenwörtlich, dass ich nach bestem Wissen die reine Wahrheit gesagt und nichts verschwiegen habe.

Ort, Datum Unterschrift des Verfassers